Thermochemical Conversion of Agricultural-Biomass to Engineered Biochar and Composites for Environmental Applications

Thesis submitted in partial fulfilment

for the Award of Degree

Doctor of Philosophy

by

Harikeshvar Pandey

Rajiv Gandhi Institute of Petroleum Technology

Jais-229304

20CE0007 **2025**

CERTIFICATE

It is certified that the work contained in the thesis titled **"*Thermochemical Conversion of Agricultural-Biomass to Engineered Biochar and Composites for Environmental Applications"*** has been carried out under my supervision and that this work has not been submitted elsewhere for a degree.

It is further certified that the student has fulfilled all the requirements of Comprehensive, Candidacy, and SOTA.

Dr. Gunjan Kumar Agrahari

(Supervisor)

DECLARATION BY THE CANDIDATE

I, ***Harikeshvar Pandey***, certify that the work embodied in this thesis is my own bonafide work and was carried out by me under the supervision of ***Dr. Gunjan Kumar Agrahari*** from August 2020 to December 2025*,* at the *Department of Chemical and Biochemical Engineering,* Rajiv Gandhi Institute of Petroleum Technology, Jais. The matter embodied in this thesis has not been submitted for the award of any other degree. I declare that I have faithfully acknowledged and given credits to the research workers wherever their works have been cited in my work in this thesis. I further declare that I have not wilfully copied any other's work, paragraphs, text, data, results, etc., reported in journals, books, magazines, reports, dissertations, theses, etc., or available on websites and have not included them in this thesis and have not cited as my work.

Date:

Place: RGIPT, Jais, Amethi **Harikeshvar Pandey**

CERTIFICATE BY THE SUPERVISOR

It is certified that the above statement made by the student is correct to the best of my knowledge.

Dr. Gunjan Kumar Agrahari	**Dr Venkata Subbarayudu Sistla**
(Supervisor)	(Head of Department)

CERTIFICATE

CERTIFIED that the work contained in the thesis titled **"*Thermochemical Conversion of Agricultural-Biomass to Engineered Biochar and Composites for Environmental Applications"*** by **Mr. Harikeshvar Pandey** has been carried out under my supervision. It is also certified that he fulfilled the mandatory requirement of TWO quality publications that arose out of his thesis work.

It is further certified that the two publications (copies enclosed) of the aforesaid **Mr. Harikeshvar Pandey** have been published in the Journals indexed by -

(a) SCI

(b) SCI Extended

(c) SCOPUS

Dr. Gunajn Kumar Agrahari	**Dr. Vivek Kumar**
(Supervisor)	(Convener, DPGC)

COPYRIGHT TRANSFER CERTIFICATE

Title of the Thesis: Thermochemical Conversion of Agricultural-Biomass to Engineered Biochar and Composites for Environmental Applications.

Name of the Student: Harikeshvar Pandey

Copyright Transfer

The undersigned hereby assigns to the Rajiv Gandhi Institute of Petroleum Technology Jais all rights under copyright that may exist in and for the above thesis submitted for the award of the **"DOCTOR OF PHILOSOPHY".**

Date:

Place: RGIPT, Jais, Amethi **Harikeshvar Pandey**

Note: However, the author may reproduce or authorize others to reproduce material extracted verbatim from the thesis or derivative of the thesis for the author's personal use provided that the source and the Institute's copyright notice are indicated.

Dedicated to Amma-Papa, Mama, and all family members…

ACKNOWLEDGMENT

I express my deepest gratitude to the **"*Divine Supreme*",** the eternal source of all grace and wisdom, whose unseen hand has guided every step of life and this PhD journey. Equal gratitude fills my heart for my ***Amma*** *a*nd ***Papa*** (my parents), *my brothers* and all family members whose selfless sacrifices and unwavering prayers sustained me through every challenge and made me capable of reaching this stage. Thereafter, I profoundly express my gratitude to my *thesis supervisor* ***Dr. Gunjan Kumar Agrahari*** for his esteemed guidance throughout the PhD journey. I am thankful for his kindness and exemplary demeanor throughout. He always listened patiently to my ideas and concerns, provided thoughtful guidance, and never imposed his own views or decisions-instead encouraging independent thinking throughout this work. In most moments, he felt less like a supervisor and more like a friend and well-wisher. Being his first PhD student made our collaboration truly special.

I thank my research progress evaluation committee members, Dr. V.S. Sistla and Dr. Shivanjali Sharma, for their valuable suggestions. Gratitude also to Dr. V.S. Sistla and Dr. Arvind Singh for their generous offers of guidance without expecting acknowledgment; and to Prof. Amit Ranjan, Dr. Milan Kumar, Dr. Koushik Guha Biswas, Dr. Deepak Dwivedi, Dr. Karan Malik, Dr. Sweta Jatav, and Dr. Vivek Kumar for lab access and support. I thank to Dr. U. Ojha (former professor, at the institute) and Dr. Praveen Kumar Srivastav for equipment access; Mr. Arun Kumar and Mr. Mahesh for instrument assistance; and all the staff at the CCIS, CIF and department office. Thanks to the Department of Chemical Engineering and RGIPT.

I wish to mention my elder brothers, Vishnu and Anshuman, and my younger brothers, Dhirendra, Abhishek, and Shivanshu, for their constant love and support. My friends Himanshu Singh and Utkarsh Saxena kept me motivated through their constant encouragement and regular contact.

My PhD batchmates (roll number wise) - Aash Mohammad, Ajeet Prajapati, Amit Kumar Gomey, Niyamat Ullah Khan, Rohit Kumar Singh, Sujeet Kumar Pandey, Ms. Pragati Awasthi (part-time Ph.D.); - true friends who helped professionally and personally. Ms. Eram Anis (JRF) introduced me to lab work initially; Sujeet taught characterization (we co-authored papers); Niyamat Ullah Khan, my senior from bachelor's and batchmate here, was a close friend. I thank him for our engaging daily chats. Seniors like Dr. Yogendra Yadawa, Dr. Pooja Jaiswal, Dr. Vinamra Bhushan Sharma, Mr. Anil Verma, were generous. Dr. Maharshi Yadav, a post doc fellow (introduced Mendeley). Almost a year, we shared mess table with great conversations. Thanks to Ms. Alpana Singh for research collaboration. They were all kind and supportive companions during my five years at RGIPT.

Juniors and friends: Saurabh Mishra, Amrendra Uttam, Siddharth, Bhupendra, Wasim, Shikha, Swati, Akansha, Swapan, Prabodh; inter-department batchmates like Chandan Upadhyay (roommate), Arpan Tiwari, Amit Verma, Ashish, Shashank Shukla, Shayed, Saurabh Pandey, Aditya Mishra, Kaushal Kishor, Manish Srivastava, Himanshu, Divyanshoo, Darshan, Anil and B.Tech student Anshu Pandey (co-author). I acknowledge the humility and respect shown by several undergraduate students during our interactions. Thanks to Nagendra ji, Surjeet, chemical suppliers-Mukesh ji, hostel/mess staff, and security-all who crossed my path at RGIPT.

Though I name only a select few here, I gratefully acknowledge all at RGIPT who helped directly or indirectly.

Thank you everyone!

-Harikeshvar Pandey

PREFACE

Energy and environment are two interlinked pillars for sustainable growth of a nation and emphasize waste utilization, renewable energy, low emissions, circular economy, etc. In this context, it becomes important for an agrarian and developing economy like India to use agricultural biomass in a scientific and sustainable way. Agriculture is the most important part of India's economy and society. It provides livelihood opportunity for more than half of the people. India is one of the top producers of agricultural goods in the world since it has one of the greatest areas of land that can be farmed. Agricultural activity leaves behind a lot of biomass waste, which is one of the most common and underused renewable resources. This agro biomass waste generated amounts in millions of tonnes annually during harvesting, processing, and post-harvest operations. The improper management of this biomass-such as open-field burning, land dumping, or uncontrolled decomposition-leads to serious environmental challenges, such as air pollution, greenhouse gas (GHG) emissions, loss of soil's nutrients, and loss of potentially valuable carbon resources. In this context, the conversion of unutilized agricultural biomass waste into value-added materials such as biochar, activated carbon and biochar-based composite materials has gained significant attention due to their multifunctional applications in energy storage, environmental remediation, soil amendment, carbon sequestration, and sustainable material development.

Pyrolysis is a well-established thermochemical method of converting biomass waste into valuable materials such as biochar, bio-oil, and synthesis gas. It involves heating of biomass in the absence of oxygen at higher temperatures, typically in the range of 300°C to 800°C.

The key objective of this research is to transform different types of agricultural biomass waste into biochar using controlled pyrolysis or co-pyrolysis and to evaluate its

physiochemical characteristics and functional properties and explore its application potentials. The further work was carried out to develop activated carbon and biochar-based composite materials to enhance performance in targeted applications such as adsorption of dye from contaminated water, CO_2 adsorption, etc. By optimizing parameters such as temperature, residence time, heating rate etc. for the pyrolysis process and composite preparation method, the research seeks to improve properties such as yield, surface reactivity, porosity, etc.

Beyond laboratory-scale findings, this work has a broader implication for sustainable waste management, climate action, and the growth of a circular bioeconomy. Processing of agricultural residues for preparation of biochar, activated carbon and biochar based composite materials not only creates value-added products but also helps in minimizing adverse effect of unscientific and unsustainable way of its handling. More notably, biochar provides a pathway for long-term carbon sequestration by locking biomass-derived carbon in stable forms for years.

This research aims to connect the domains of material science, environmental engineering, and sustainability by offering a comprehensive understanding of biomass pyrolysis, optimization of biochar properties, and development of advanced composite materials. The findings have the potential to support cleaner production practices, encourage the circular use of agricultural residues, and provide scientific insights that can strengthen policies focused on reducing biomass waste and promoting renewable, eco-friendly materials.

The work in the thesis has been organized in the following eight chapters:

Chapter 1: Introduction

This talks about current energy and environment-related challenges by highlighting dependency on fossil fuel and greenhouse gas emission associated with its burning. It also

discusses the subject of energy security. It further discuss about renewable energy sources and the potential of agricultural biomass as a key renewable energy resource. It also presents the classification, key properties, and availability of biomass resources across the country. The chapter further describes the chemical composition of biomass-which typically consists of cellulose, hemicellulose, and lignin-and discusses the major technological methods used to convert biomass into value-added products, highlighting biomass pyrolysis, a thermochemical method for biomass utilization.

Chapter 2: Literature Survey

This chapter gives the detailed classification of biomass and presents a biomass atlas of India highlighting the total and surplus biomass generation of each state. It discusses in detail biomass pyrolysis, its product, and factors affecting biomass pyrolysis. It further discusses the previous works done by various researchers related to biomass pyrolysis and co-pyrolysis.

Chapter 3: Materials and methodology

This chapter discusses the instrument and procedure adopted for biomass processing, biochar preparation, and materials characterization. It discusses in detail the pyrolysis setup used for this study. The major characterization techniques discussed here are CHNS analyzer, calorific value determination using bomb calorimetry, thermogravimetric analysis (TGA), Fourier transform infrared spectroscopy (FT-IR), field-emission scanning electron microscope (FE-SEM), X-ray diffraction (XRD), X-ray photoelectron spectroscopy (XPS), Raman spectroscopy, UV-Vis (ultraviolet-visible spectroscopy), and the Brunauer-Emmett-Teller (BET) surface area analyzer.

Chapter 4: Pyrolysis of Rice Straw and Sugarcane bagasse for production of biochar

This chapter presents experimental work on biomass pyrolysis of rice straw, sugarcane bagasse, and their mixture at different temperatures ranging from 300 to 700°C. The biomass feedstocks used were in the form of both pellets and powder. The various physicochemical properties of the produced biochar were evaluated at different temperatures. The highest mass yield of 43.72 % was observed in the case of biochar produced from co-pyrolysis of rice-straw and bagasse at 300°C. The bagasse biochar produced at 700°C had the highest heating value of 23.01 MJ/kg and the lowest mass yield 20.13%. The pellet and powder forms of biochar were also compared for their properties.

Chapter 5: Pyrolysis of Rice straw and Mustard-Oil Residue for sustainable applications

This chapter discusses the pyrolysis of rice straw and mustard-oil residue, as well as their co-pyrolysis, to determine the optimal mixture ratio for achieving the best results. Combining de-oiled cake with less dense rice straw powder helped in quality pellet formation, having significant strength and durability. The pyrolysis was carried different temperature (300-600°C) and the different properties were evaluated to show its potential application for biochar gasification and energy application. The highest mass yield was for mustard-oil residue (MR) biochar (53.59%) produced at 300°C and the lowest for rice straw biochar (28.5%) produced at 600°C. The MR biochar has the highest energy content among all feedstock samples as reflected in its HHV results which were 18.35 and 26.19 MJ/Kg for biochar sample obtained at 300 and 600°C respectively.

Chapter 6: Green synthesis of biochar-graphene oxide composite for enhanced dye adsorption

In this chapter rice straw biochar was prepared following the earlier discussed method. Then graphene oxide was synthesized in the laboratory using the well-established modified

Hummer's method. Using mechanical stirring and ultrasonication, the GO and biochar were mixed properly. The mixture was further put under hydrothermal conditions to ensure the proper bonding of GO over biochar surfaces. The materials thus prepared were named as RS-GO-0.1 and RS-GO-1 depending on the biochar and GO compositions. These composites were characterized and tested for methylene blue dye adsorption. The result shows superior adsorption have adsorption efficiency of 99.29% for a 20-ppm methylene blue solution.

Chapter 7: Development of Nitrogen (N)-doped Activated Biochar (AB) using Mango Kernel Biomass for CO_2 Entrapment Application

This chapter discuss the preparation of biochar from mango kernal biomass and its activation using potassium hydroxide (KOH). The activated biochar was further treated with urea (NH_2CONH_2) to introduce nitrogen functionalities over the surfaces and improve its CO_2 capture potential. Its structural and surface analyses confirmed the successful activation and presence of additional functional groups that support entrapment capacity. Chemical activation increased BET surface area from 21.6 $m^2\ g^{-1}$ to 1882.1 $m^2\ g^{-1}$, while nitrogen doping leads to further enhancement to 2021.6 $m^2\ g^{-1}$ by introducing nitrogen functionalities. N-doped activated biochar was further combined with a suitable additive to improve the stability of entrapped CO_2 bubbles. This combined system was evaluated to understand its ability to retain CO_2 under controlled conditions. The overall aim of this chapter was to demonstrate how biomass-derived carbon materials can be engineered for efficient CO_2 entrapment.

Chapter 8: Conclusion and future scope

This chapter summarizes the work discussed above in all the chapters and outlines the future scope of this research work.

Table of Contents

List of Figures:

List of Tables:

List of important abbreviations

Å	Angstrom
AB	Activated biochar
Qt	Adsorption Coverage at time "t"
B.E.	Binding Energy
BC	Biochar
BET	Brunauer-Emmett-Teller
DI	Deionised
EDX	Electron Dispersive X-ray
EDR	Energy density ratio
Y_E	Energy yield
Q_e	Equilibrium Adsorption Coverage
FE-SEM	Field emission Electron Spectroscopy
FTIR	Fourier Transform Infrared
FWHM	Full Width Half Maxima
GO	Graphene oxide
HHV	Higher heating value
K.E.	Kinetic Energy
kN	Kilo Newton
kV	Kilovolts
Y_m	Mass Yield
M.K.	Mango Kernal
MPa	Mega Pascal
MB	Methylene blue dye
µm	Micrometre
mg	Milligram
mL	Millilitre
MR	Mustard-oil-residue
M.W.	Molecular weight
nm	Nanometer
RS	Rice-straw
RS-GO	Rice-straw-Graphene oxide composite
SB	Sugarcane Bagasse
TGA	Thermogravimetry Analysis
UV-Vis	Ultraviolet Visible Spectroscopy
XRD	X-Ray Diffraction
XPS	X-ray Photoelectron Spectroscopy

CHAPTER- 1

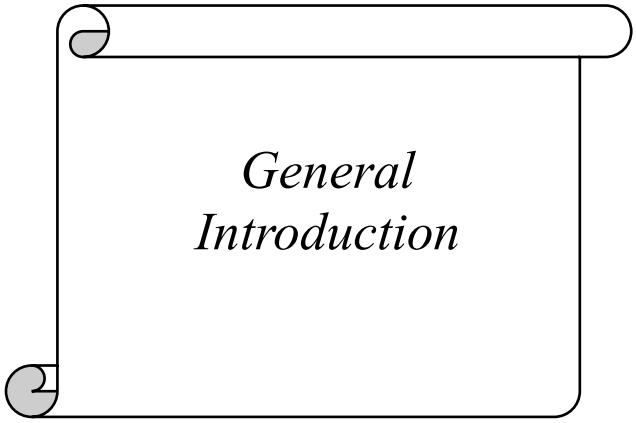

1.1. Introduction

Energy needs of modern nations have manifolded since the industrialization of society. The rising global population, urbanisation, and technological advancement are among the main reasons for the increased energy consumption. Almost all advanced economies of the world are heavily relying on conventional energy resources, i.e., fossil fuels, to meet their energy demands. As a result, the conventional energy sources have been depleted at accelerated rates over the past few decades. Apart from energy needs, climate change, global warming, and environmental degradation are also major concerns among scientists, researchers, and various governments worldwide, as conventional energy sources have also damaged the environment in some way or another. Limited conventional energy sources, price and supply chain risks, geopolitical tensions, and environmental concerns collectively threaten a nation's energy security. The concept of energy security has changed from just making sure there is enough supply to include things like accessibility, affordability, acceptability, and sustainability. These are termed as the 'four As' of energy security [1].Within this wider framework, the shift toward some kind of renewable energy sources has become essential to make sure that energy supply systems are stable and long-lasting. In several countries, dual goals of decreasing reliance on fossil fuels and ensuring energy security have led to a growing interest in the adoption of renewable energy sources. Although renewable energy has made significant progress in recent years, it still cannot meet global energy demands independently.

Renewable energy resources provide an opportunity to utilise native and low-carbon energy sources that can make the energy supply system more robust and less reliant on petroleum imports [2].The Paris Agreement (2015) and the United Nations Sustainable Development Goals (SDG 7) are a few examples of international agreements that stress the need for everyone to have access to affordable, reliable, and clean energy. Renewable energy

sources like solar, hydro, wind, geothermal, and bioenergy are some of the promising alternatives to fossil fuels that have the potential to lower greenhouse gas emissions in the environment [3].

Biomass is a renewable energy source that can make solid, liquid, and gaseous fuels. It acts as a link between old and new energy systems. Among all renewable energy sources, biomass is the oldest, which has been used for energy by humans. The primary reasons for their use of energy sources are easy and abundant availability, simple methodology to utilise for energy, e.g. combustion, carbon-neutral nature and easy storage [3] [4]. Biomass to bioenergy conversion becomes especially important because it can create diverse types of energy (solid, liquid, and gas). Biomass-based systems can also provide continuous and dispatchable energy, which helps keep the grid stable [5]. This is different from solar and wind, which have geographical and time constraints. Bioenergy also helps people in rural areas as a sector of new job opportunities, encourages circular waste management, and is also used in farm fields to improve soil fertility through by-products like biochar [6] [7].

India, being a highly populated and developing country, has faced a huge surge in energy demand over the last few decades. In its first Updated Nationally Determined Contribution (NDC) under the Paris Agreement, India committed to achieving 50% of its cumulative installed electricity capacity from non-fossil fuel-based energy sources. Also, with the two ambitious goals set for the future, i.e., 500 GW of energy from non-fossil sources by 2030 and achieving net-zero emissions by 2070, India is committed to accomplishing these goals by diversifying its energy sources such as solar, wind, hydro and bioenergy: thus, ensuring energy security for the nation.

1.2. Biomass as a renewable energy resource

Biomass is considered a renewable energy resource consisting of organic matter from plants, animals and microorganisms, formed when photosynthesis converts atmospheric CO_2 into sugars and lignocellulosic structures. Biomass-based fuels can be regrown on human timescales, whereas fossil fuels require millions of years to form in the geologic subsurface. When biomass is harvested sustainably and regrowth balances removals, the CO_2 released during combustion can be approximately offset by CO_2 taken up during plant growth, so the system can approach carbon neutrality over its life cycle, in contrast to fossil fuels that add geologic carbon to the atmosphere. Therefore, sustainably managed biomass can function as a low-carbon, long-term renewable energy option, although actual net emissions depend on full life-cycle management [8] [9].

It is predicted that the world's yearly biomass production is about 220 billion tons, which means there is a lot of room for making renewable fuel [10] [11]. It has been estimated that India produces more than 500 million tons of agricultural waste every year, including rice husk, wheat straw, sugarcane bagasse, and forest waste [12]. A significant portion of this biomass is either not used, or burned, or disposed of improperly, which leads to the transfer of harmful particulate matter and greenhouse gases into the air, causing serious health concerns and sometimes death as well. Conversion of these leftover biomass waste into bioenergy promises to diminish pollution, provide income opportunities in rural areas, and enhance the national energy portfolio [13].

Biomass can be classified based on its source of origin into several categories: woody biomass (from forestry waste, wood chips, etc.), agricultural biomass (lignocellulosic crop residues like rice straw, wheat straw, bagasse, and husks), animal-generated biomass (manure, poultry litter, and organic waste), industrial biomass (from agro- and wood-processing

industries like paper mills), aquatic biomass (seaweed, algae, and aquatic plants), and municipal biomass (sewage sludge, kitchen waste, yard waste, etc.) [14] [15]. Lignocellulosic biomass is different from other types of biomass since it has a good fraction of carbon and is available all around the world easily and abundantly, and doesn't compete much with food resources [16]. Its structure, which is particularly made up of cellulose, hemicellulose, and lignin, makes it a suitable carbon matrix for thermochemical conversion into fuels and value-added compounds like biochar, bio-oil and syngas [17] [18].

1.3. Lignocellulosic biomass: composition and characteristics

Biomass is considered a complex material because of its inherent complex structure resulted from its different chemical constituents based on its source of origin. Lignocellulosic biomass, which is the principal form of plant biomass, predominantly consists of three biopolymers: cellulose, hemicellulose, and lignin, along with some minor amounts of low molecular weight substances and inorganic minerals.

Cellulose stands out as the most abundant organic polymer in biomass, typically accounting for 40 to 50 percent of the biomass dry weight. It is made up of numerous linear chains of D-glucose units connected by β-1,4-glycosidic bonds. These linear chains make amorphous and crystalline regions stabilised by hydrogen bonding that influence the polymer's structural and reactive behaviours [19].

Hemicellulose, which makes up 25 to 30 percent of the biomass, is a heterogeneous polymer of pentoses, hexoses, and sugar acids with an amorphous structure. Its content varies depending on the type and source of the biomass.

Lignin is an amorphous aromatic polymer that creates a three-dimensional network of phenylpropane units and constitutes approximately 20 to 35 percent of biomass [20]. Lignin is rich in carbon and hydrogen, with oxygen making up the remaining fraction.

Biomass also contains organic extractives such as proteins, lipids, simple sugars, waxes, and resins. It also has minerals that are not organic, like calcium, potassium, salt, magnesium, phosphorus, silica, aluminium, and iron. The exact amount of these minerals depends on the source of the biomass and the state of the soil. We need to understand how this complicated composition works in order to get the most out of biomass conversion and valorisation processes [21].

The complicated biomass structure makes biochemical conversion difficult, but it works very well for thermochemical processing, especially using pyrolysis, where the various carbon-oxygen bonds get converted into solid, liquid, and gaseous bio-products. The proportions of cellulose, hemicellulose, and lignin in a biomass affect the quantities of bio-oil, biochar, and aromatics produced during pyrolysis [22]. Additionally, lignocellulosic biomass does not contribute carbon to the atmosphere, as plants absorb the CO_2 released during the conversion process and reutilise it in their subsequent growth cycle [23] [24].

1.4. Biomass conversion technologies.

Biomass conversion methods are various approaches to turn organic biomass feedstocks, like agricultural waste, forestry waste, or energy crops, into useful fuels, chemicals, and energy carriers. Depending on the operating conditions, the type of catalyst or microorganisms used, and the physical state of the biomass, the conversion process can occur in two main ways: via biochemical or thermochemical pathways [25] [26]. Biochemical routes depend on enzymatic or microbial reactions that usually occur at moderate temperatures, while thermochemical routes involve the use of heat and chemical reactions at significantly higher temperatures to quickly break down organic matter into solid, liquid and gases [27] [28].

1.4.1 Biochemical conversion methods

The biochemical conversion method is the process of breaking down any organic biomass using biological agents like bacteria, fungi, or some enzymes to obtain fuels like bioethanol, bio-gas, and bio-diesel. It works best with wet, carbohydrate-rich feedstocks like crop residues, food waste, and microalgae. Anaerobic digestion, fermentation, and enzymatic hydrolysis are the main processes. They all work at low temperatures (30-60 °C), so they don't need as much energy as thermochemical routes [27] [29].

Anaerobic digestion

Anaerobic digestion (AD) transforms organic matter into biogas, which is mostly CH_4 and CO_2, through a series of microbial reactions: hydrolysis, acidogenesis, acetogenesis, and methanogenesis. People use this method a lot to get rid of animal waste, agricultural waste, and sewage sludge [30]. The amount of biogas that can be made depends on the C/N ratio, the temperature (mesophilic or thermophilic), and the time it takes for the water to flow through the system. Digestate, the solid waste, can be used as a biofertilizer to close nutrient cycles [31]. Co-digesting biomass with food or industrial waste often increases methane production because it improves the balance of nutrients and the way microbes work together [32].

Fermentation

Fermentation transforms starches and sugars present in biomass into alcohols, primarily ethanol, by using bacteria or yeast. To obtain fermentable sugars from cellulose and hemicellulose, lignocellulosic biomass needs to first be pretreated and then broken down by some enzymes. The conversion of glucose molecules to ethanol through fermentation is one of the most developed biochemical processes for producing biofuels [29]. But the high cost associated with the enzymes and the reason that lignin is hard to break down easily are still

big problems. To make this conversion method more efficient and cheaper, scientists are looking into genetic engineering and consolidated bioprocessing methods [33].

Production of biodiesel (lipid conversion)

Transesterification is a well-known process that converts lipid-rich biomass like micro-algae or oil-bearing seeds into biodiesel. In this conversion process, triglycerides react with alcohol in the presence of acid, base, or enzyme catalysts to generate fatty acid methyl esters (FAMEs). Algal biodiesel is especially appealing because it grows quickly and can store CO_2 [34] [35]. But downstream processing-harvesting, drying, and oil extraction-still uses a huge amount of energy and makes the process costlier [36].

1.4.2 Thermochemical Conversion Methods

Thermochemical conversion uses pressure, heat, and chemical reactions to break down biomass into chemicals and fuels. It works with dry, lignocellulosic biomass and can quickly change it into something else at a high rate, which is not the case with biochemical routes. The leading thermo-chemical processes are combustion, pyrolysis, gasification, torrefaction, and hydrothermal processes such as hydrothermal liquefaction, hydrothermal carbonization and hydrothermal gasification. Each of these performs best depending on different thermal and oxidising conditions [28] [26].

Combustion

When biomass burns, it completely oxidises in the presence of excessive oxygen, generating CO_2, H_2O, and heat. It is the oldest and very well-known method of converting biomass waste into heat, electricity, and co-firing with coal to obtain energy. Combustion commonly occurs at significantly high temperatures between 800 and 1000 °C. For traditional grate furnaces, it has an overall thermal efficiency of 20 to 35%. For more advanced fluidised-bed systems, it can be as high as 40 % [37] [38].

The process has three steps: drying, devolatilization, and oxidation. How well it works depends a lot on the moisture and ash content of the feedstock. Biomass with a lot of moisture (more than 40%) lowers the flame temperature and energy recovery, so it needs to be dried first or mixed with drier fuels [26]. Alkali and chlorine compounds in ash can cause fouling and slagging on boiler surfaces, making it hard to run the boiler for a long time [39]. Fluidised-bed combustion and oxy-fuel combustion are two examples of new technologies that have made heat transfer, combustion stability, and emission control better [40] [38].

Gasification

Gasification converts solid biomass into a combustible gas mixture (syngas) consisting mainly of CO, H_2, CH_4, and CO_2 through partial oxidation at 700-1000 °C. In contrast to combustion, only a restricted oxidant (air, O_2, or steam) is provided to facilitate endothermic reactions, such as the Boudouard and water-gas shift equilibria. The syngas that is made can be used to make hydrogen [41] [26]; or to make synthetic fuels (vis Fisher-Tropsch synthesis). There are many different types of reactors. Fixed-bed gasifiers work best for small, decentralized units, while fluidized-bed and entrained-flow systems allow for even temperature distribution and scalability [26].The equivalence ratio (ER), the steam-to-biomass ratio, and the temperature all affect the gas composition and heating value. When air is used, a higher ER increases conversion but dilutes the syngas with nitrogen [42].

Using nickel, dolomite, or iron-based catalysts in catalytic gasification works well to lower tar formation and raise hydrogen yield [43]. Chemical-looping gasification also uses oxygen carriers to capture CO_2 on-site, making it a low-emission way to make hydrogen-rich syngas [44].

Pyrolysis

Pyrolysis is the process of breaking down biomass into bio-oil (liquid), bio-char (solid), and syngas (gas) without oxygen. The temperature of the process (300-700 °C), the rate of heating, and the residence time all affect the yield of the product. Slow pyrolysis (low heating rate, long residence time) is used mostly when the objective is char formation, while fast pyrolysis (~500 °C, >100 °C s^{-1}, short residence time< 2 s) is used when the desirable product is bio-oil [4] [28]. The composition of the feedstock has a profound effect on pyrolysis works. Cellulose and hemicellulose mostly make volatiles and bio-oil, while lignin makes char because it is stable in aromatic compounds [45]. Bio-oil usually has a lot of oxygen (about 35-40 wt. %), corrosive properties, and is unstable because it has water, acids, aldehydes, phenols, and furans in it. Catalytic upgrading (e.g., zeolites, $NiMo/Al_2O_3$) lowers the amount of oxygen and raises the amount of hydrocarbons [46]. Emerging co-pyrolysis of biomass with plastics or coal increases the amount of hydrogen available and works together to improve the quality of oil and the amount of energy that can be recovered [47] [48]. Biochar, which is a main by-product of the pyrolysis process and which is high in fixed carbon and mineral nutrients, can also be used to improve soil, adsorb, or store carbon [49].

The produced raw biochar through further modification can be converted into engineered biochar, activated carbon, composites material, etc., with enhanced properties for wider application in area of science and technology.

Torrefaction

Torrefaction is a mild thermal pretreatment process that takes place at 200-300 °C in an environment with little or no oxygen. It seeks to enhance the energy density, grindability, and hydrophobicity of biomass by breaking down hemicellulose while preserving the majority of the lignin and cellulose components [50].The resulting torrefied biomass, which is often

called bio-coal, has a higher heating value and a lower O/C ratio. This makes it easier to transport and store. This process lowers the overall mass yield (about 70%), but it raises the energy yield by getting rid of low-energy volatiles. Torrefied biomass can be burned with coal in power plants that are already built, which makes it a good solid fuel that can be added to existing plants [51]. Contemporary research has investigated reactive torrefaction that utilises steam or CO_2 environments to tailor product quality and reduce energy consumption [52].

Hydrothermal liquefaction

This is a wet thermos-chemical process known as hydrothermal liquefaction (HTL), which uses hot and compressed water conditions (usually 250-400 °C, 10-30 MPa) to transform biomass into bio-crude, an energy-dense liquid fuel [53]. HTL is considered more energy-efficient for high-moisture or wet biomass than the pyrolysis process because it can process high-moisture-containing feedstocks like algae or sewage-sludge without drying [54]. Subcritical water functions as a solvent, reactant, and catalyst all at once in HTL, facilitating the hydrolysis, dehydration, decarboxylation, and condensation reactions that depolymerise biopolymers and re-polymerise intermediates into compounds that resemble oil [55]. Biocrude (10-60 wt.%), an aqueous phase with soluble organics, a small gas fraction (primarily CO_2), and a small amount of solid residue, are the product of the process. Although oxygen, nitrogen, and sulfur impurities need to be hydrotreated before being used as fuel, HTL offers high carbon conversion and yields a biocrude with a heating value of 30-36 MJ kg^{-1} [53].

Direct conversion of wet feedstocks and the creation of liquid fuels are its primary benefits; high-pressure operation, corrosion, and the requirement for aqueous-phase management are its drawbacks [54].

Hydrothermal carbonization

Hydrothermal carbonisation (HTC) is a mild hydrothermal process that turns wet biomass into a solid, hydrochar, that is rich in carbon. It takes place at 180-260 °C under autogenous pressure for 0.5-6 hours [56]. It uses hydrolysis, dehydration, decarboxylation, and aromatisation reactions in subcritical water to make coal in a way that is similar to how it happens in nature [57]. The process makes hydrochar (50-80 wt.%), a small amount of gas (mostly CO_2), and an aqueous phase that is full of soluble organics.

Hydrochar has a higher heating value (22-30 MJ kg^{-1}), is hydrophobic, and is stable, which makes it good for solid fuels, adsorbents, and soil conditioners [58]. HTC's strong points are that it can process wet feedstocks without drying them out and make a stable carbonaceous solid [57]. However, the process produces wastewater that needs to be treated afterwards, and the properties of hydrochar depend on the feedstock and the conditions of the reaction [58].

It can be concluded that surplus agricultural biomass waste generation and its improper utilisation are a serious concern. Every harvesting season generates an enormous amount of surplus biomass waste that should be utilised in a sustainable manner. Also, the increasing trend of energy demand, energy supply-chain issues, global geopolitics and moreover environmental problems associated with conventional fuel and various other constraints associated with its availability, etc., are inspiring the researchers to utilise the low-cost, easily and abundantly available biomass waste toward energy generation or conversion into some kind of value-added materials.

Among the various methods of biomass utilization, pyrolysis which is a thermochemical conversion process of biomass into biochar, bio-oil and syngas; is a well-established, scientifically robust, economically viable and environment friendly route to

utilize biomass for conversion into biochar, bio-oil and syngas. This produce can further be tailored for specific and improved properties aiming to some specific application.

Overall, utilisation of agricultural biomass as a renewable energy source is essential to stop its open field burning and associated environmental problems and to meet the sustainability targets of clean energy and clean environment. Figure 1.1 shows crop residue burning in open fields and the resulting poor visibility.

By exploring the biomass utilisation for conversion into value-added materials, this thesis aims to contribute meaningful understandings towards waste utilisation, renewable energy, circular bioeconomy, low-carbon emissions, etc., for a sustainable future.

Figure 1.1: Crop residue burning in open field and a glimpse of its effect.

Next chapter consists of detailed literature survey on agricultural biomass, biomass pyrolysis and co-pyrolysis-mechanism, its products, affecting parameters, and its characterizations, knowledge gap and objective of the thesis.

CHAPTER 2

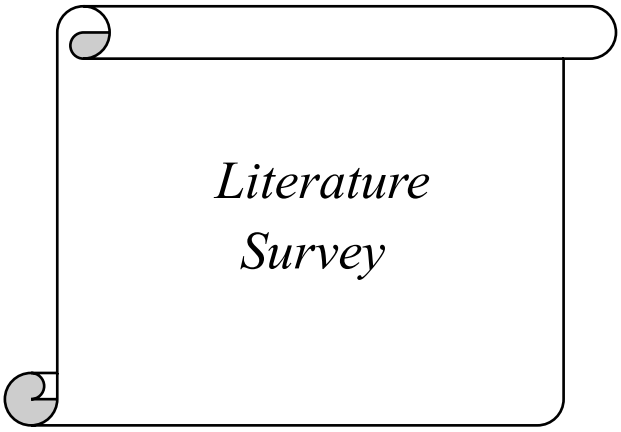

2.1. Biomass and its classification

Biomass has been one of the oldest and most foundational energy resources for human beings. Early civilisations relied on wood and plant residues for heating, cooking, and basic industry. Historical evidence indicates that the use of biomass for energy dates back hundreds of thousands of years, with archaeological findings supporting its consistent utilisation for warmth and food preparation. With the progress of societies, the development of advanced fuels and technologies took place, but biomass retained a critical role, especially in rural regions and during periods of resource scarcity [59].

Biomass can be defined as the organic matter that comes from plants and animals that have recently died. It can be used to make renewable energy and as a raw material for a number of industrial uses. It is frequently put into groups based on where it comes from (for example, land vs. water), what chemicals it has (for example, lignocellulosic vs. lipid-rich), and its physical qualities (for example, moisture content and particle size). This lets us make our own ways to manufacture energy and resources.

2.2. Defining biomass in renewable energy contexts

Biomass has emerged as one of the most significant and widely used forms of renewable energy worldwide. Its growing importance arises from the urgent need to reduce the environmental damage caused by fossil fuels, including greenhouse gas emissions, climate change, and air pollution-related health issues. The term *biomass* encompasses a broad range of materials-such as agricultural residues, forestry by-products, dedicated energy crops, and municipal wastes-all of which can serve as sustainable sources for fuel and chemical production. The increasing shift toward biomass utilisation is largely driven by its abundance and its potential to substitute non-renewable resources. However, the composition and characteristics of biomass vary greatly across

different sources and regions, posing challenges for consistent processing and efficient conversion. These differences make it essential to establish systematic classification methods that enhance both technological performance and economic feasibility [14].

2.3. Sources and origin-based classification

Biomass can be grouped according to its biological origin, since the environment in which it develops and the way it is harvested both influence its productivity and long-term availability. Figure 2.1 shows the major types of biomasses used for energy generation, classified by source of origin. The largest share of the world's biomass comes from land-based sources. Forest residues such as logs, twigs, and sawdust, together with herbaceous materials like crop stubble and grasses, make up this category. Several crops, including maize stover, switchgrass, and miscanthus, are often cultivated specifically for energy use because they grow quickly and adapt well to different soils. Biomass is also obtained from aquatic systems, although on a smaller scale. Algae and other water plants grow rapidly and contain significant amounts of natural oils, which makes them valuable raw materials for biodiesel and related biofuels [14].

Biomass is further divided based on the type of waste stream it originates from. Agricultural residues such as straw, husks, and stalks, forestry wastes like bark and thinnings, and municipal solid wastes that include food scraps and yard litter are common examples. Classifying biomass according to its source helps in assessing its environmental footprint. Terrestrial feedstocks often require proper land-use management to avoid problems like deforestation or soil nutrient loss, whereas waste-derived biomass supports a circular economy by turning discarded materials into usable energy or materials [60]. Economic studies suggest that using these residual sources can reduce dependence on raw natural inputs, but the availability of such feedstocks varies widely between

regions. In countries with strong agricultural activity, such as India, these materials are more abundant, making regional biomass potential mapping an important step for planning sustainable utilisation [61].

In the case of marine resources, biomass classification also considers ecosystems such as Antarctic waters, where krill and other pelagic species form massive standing stocks, estimated between 800 and 5,000 million tonnes. Here, classification is often linked to trophic levels and patterns of biological productivity. These distinctions help in monitoring ecosystem health and ensuring that harvesting practices remain sustainable, particularly in high-biomass regions that are vulnerable to overexploitation [62].

Figure 2.1: Type of biomass used for energy generation.

2.4. Chemical Composition and Structural Classification

At the molecular level, biomass can be categorised according to its major structural components, which largely determine its conversion behaviour and the types of

products obtained. Among these, *lignocellulosic biomass* is the most abundant form, accounting for roughly 50-70% of all plant matter. It is primarily composed of three polymers: cellulose (40-50%), a glucose-based polymer that provides structural rigidity to plant cell walls; hemicellulose (20-35%), a heterogeneous polysaccharide responsible for flexibility and porosity; and lignin (15-30%), a complex phenolic polymer that confers strength and resistance to microbial degradation. The relative proportions of these components differ among plant species-hardwoods typically contain about 20-30% lignin, whereas softwoods may reach 25-35%, and these variations significantly affect the pretreatment requirements and efficiency of biofuel and biochemical production processes [60].

Biomass can also be classified based on its dominant biochemical composition, which determines its most suitable conversion pathway. Figure 2.2 shows biomass classification based on its chemical composition. *Starch-rich feedstocks*, such as corn grains containing roughly 70% carbohydrates, are primarily utilized for ethanol production through fermentation. *Lipid-rich_sources*, including oilseeds like soybeans with about 15-20% oil content, serve as raw materials for biodiesel synthesis via transesterification. Similarly, *proteinaceous biomass*, such as certain species of microalgae, may contain up to 50% protein and can be effectively converted to biogas through anaerobic digestion.

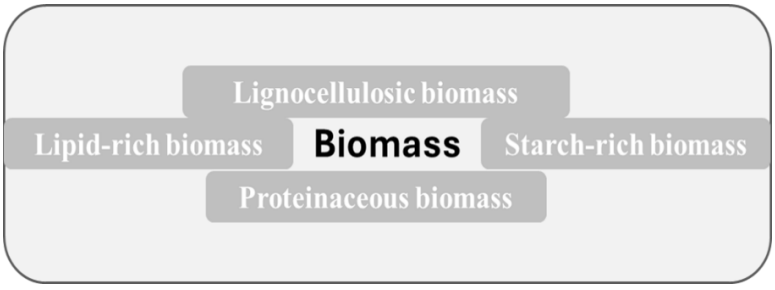

Figure 2.2: Chemical composition-based classification of biomass.

In addition to these major components, extractives (such as resins and tannins) and volatile compounds-typically comprising 5-10% of total biomass-introduce further complexity to thermochemical processes, as they can inhibit reactions like pyrolysis or lead to unwanted by-products. The ash fraction (1-15%), composed mainly of inorganic minerals such as silica and potassium, also plays a crucial role by influencing combustion efficiency, slagging, and fouling tendencies in thermal systems [14] [60].

This type of compositional classification forms the basis for selecting appropriate conversion technologies for biomass utilization. Depending on the dominant constituents, biomass can undergo thermochemical, biochemical, or physicochemical transformations. In thermochemical routes such as gasification, biomass is converted into syngas, while in biochemical pathways, processes like enzymatic hydrolysis break down carbohydrates into fermentable sugars. Physico-chemical methods, including solvent extraction, are often applied to recover lipids or other valuable compounds. The composition also influences the preferred conversion process: high-lignin feedstocks are better suited for pyrolysis, where they yield stable biochar, whereas low-lignin, herbaceous biomass is more amenable to fermentation, producing bioethanol and other biochemicals efficiently. Advanced characterization techniques, such as Fourier-transform infrared (FTIR) spectroscopy, provide detailed insights into the molecular structure of biomass. These analyses can detect subtle differences, such as variations in the syringyl-to-guaiacyl (S/G) ratio of lignin, that serve as key indicators of feedstock reactivity and processing behavior. Incorporating such molecular-level classifications has been shown to enhance conversion efficiency and improve product yields by approximately 20-30% in pilot-scale operations.

2.5. Agricultural Biomass

Agricultural waste is the leftover material from farming activities, such as growing and processing crops, fruits, vegetables, dairy products, and other foods. Agro-waste biomass is made up of plant wastes and their parts, like cellulose, hemicellulose, and lignin. It can be broken down into several types, such as paper waste, wood residues, grass, and so on. The potential of these resources is immense due to India's agrarian economy, making agricultural biomass a vital component for sustainable energy, environmental management, and rural economic development [63] [64].

2.5.1 Agricultural biomass availability in India

The Ministry of New and Renewable Energy (MNRE) of India did research in 2017-18 and found that the country had over 230 million metric tons of surplus biomass from agricultural waste each year. This is enough to generate about 28 GW of power. This additional waste is a valuable resource that could be used to make sustainable energy [63].

A national biomass atlas has been prepared under the supervision of the Biomass and Energy Management Division, MNRE, which graphically shows state-wise and crop-wise data of the total biomass production, surplus biomass and power generation capacity of surplus biomass. *Figure 2.3 and 2.4* present total biomass available in India and surplus biomass available in India respectively.

2.5.2 Challenges with biomass management

Turning agro-residues, forest residues, and organic waste into reliable feedstocks is far from a simple looking challenge. One central challenge is feedstock variability: species, growing conditions, harvest timing and plant parts produce wide swings in moisture, composition and energy content. That variability complicates conversion performance and makes it hard to define a single, repeatable processing recipe for pyrolysis, gasification or biochemical routes. Understanding and characterizing this

heterogeneity is therefore a necessary first step for any project [65]. Closely linked are seasonality and supply uncertainty. Many biomasses are produced in pulses (post-harvest residues, seasonal pruning), so supply is concentrated in a few months and scarce at other times. This forces projects to invest in large storage, drying and handling systems or to design supply networks that aggregate across many small producers, both of which raise costs and logistics.

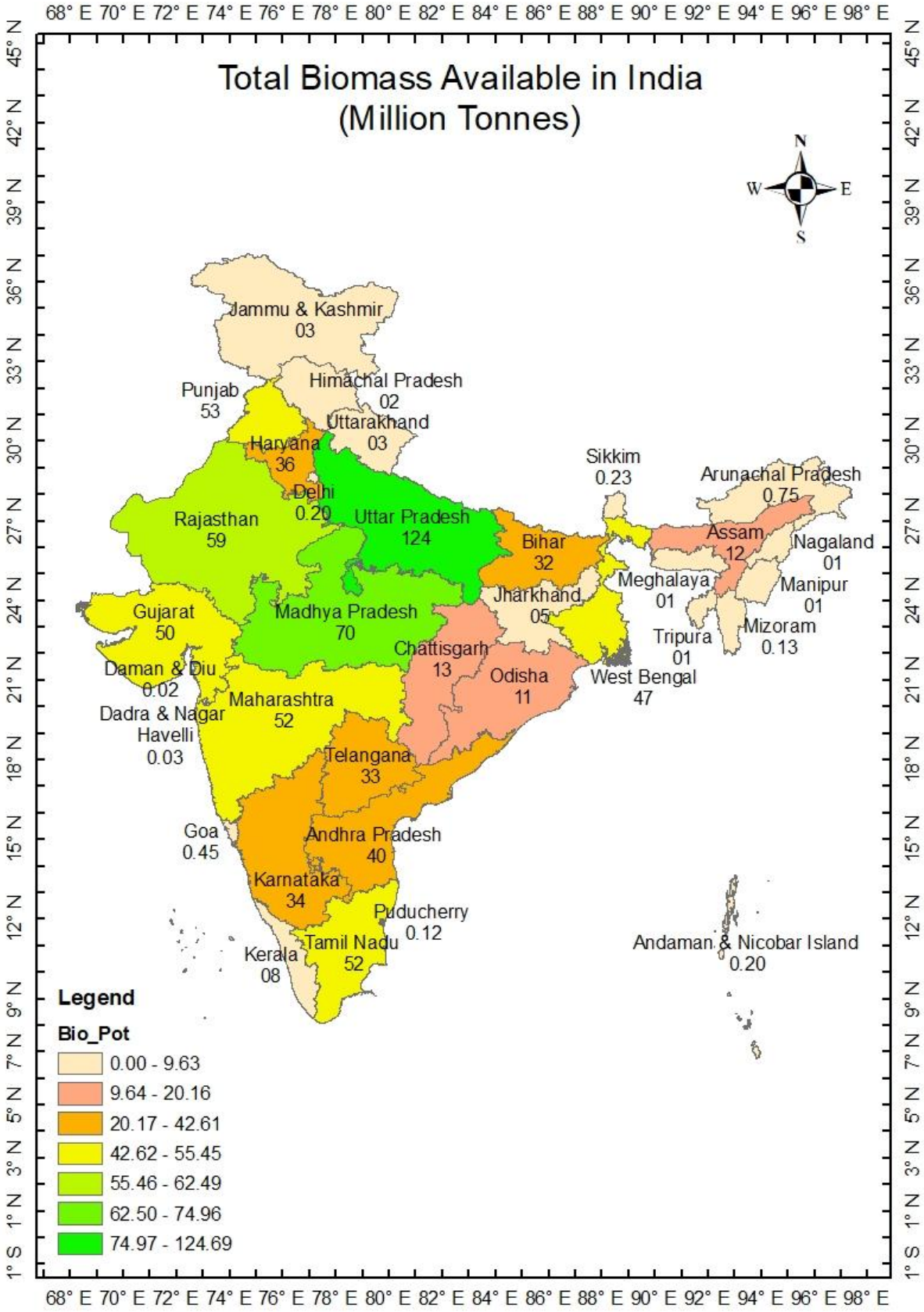

Figure 2.3: Total biomass available in India [66].

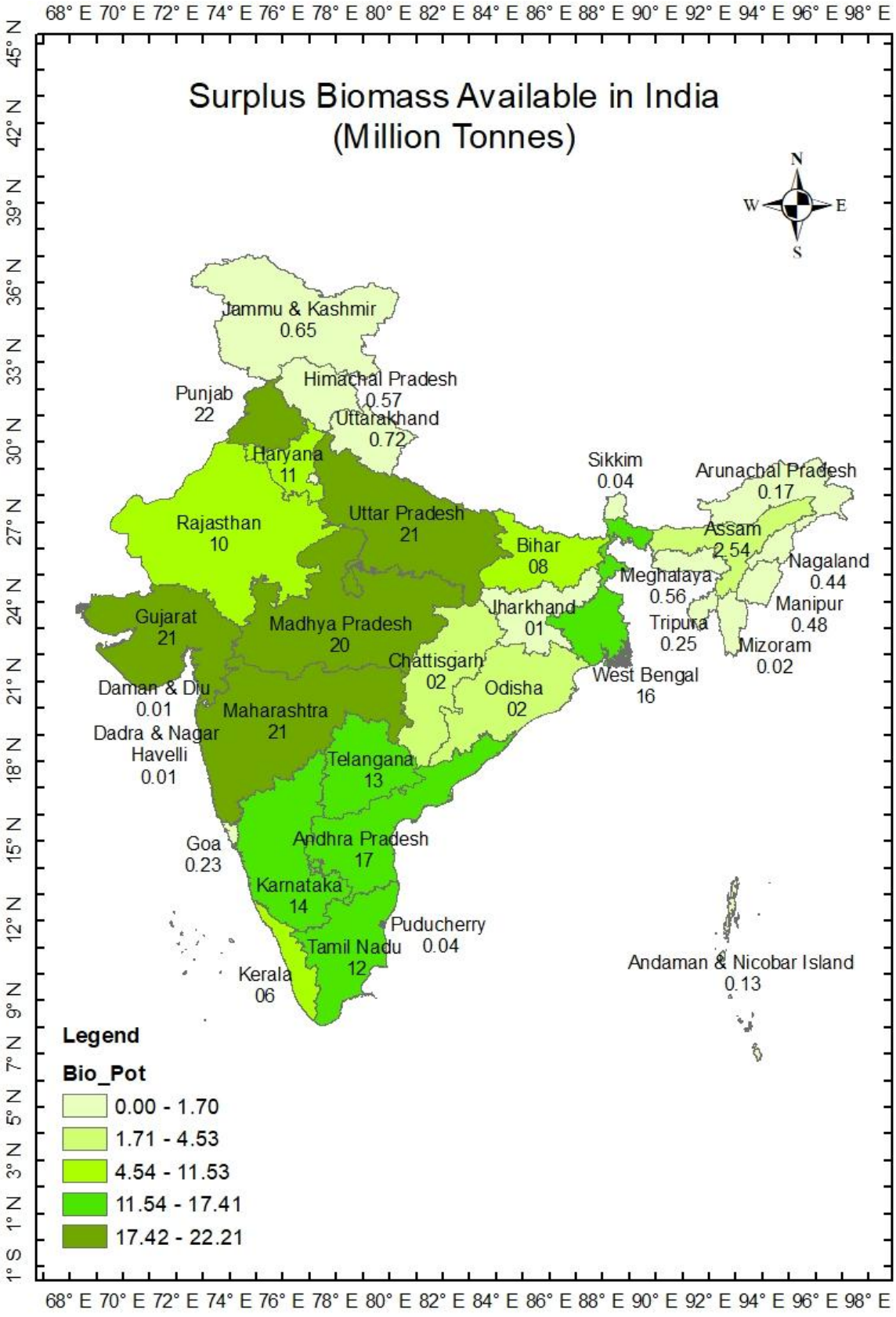

Figure 2.4: Surplus biomass available in India [66].

complexity. Seasonal surges also raise risks of quality loss (biological degradation) during storage unless careful protocols are followed. Logistics and scale economics present another set of hurdles. Biomass sources are dispersed across landscapes, often far from processing plants; transport costs per unit energy are high relative to fossil fuels.

Achieving economies of scale, therefore, depends on hub-and-spoke collection, consolidation terminals and optimized routing-solutions that require capital, coordination and local buy-in. In many regions, the lack of established aggregation infrastructure discourages investors [67]. The quality of biomass and its contamination with dirt, stones, plastics, or agrochemical residues are again a big concern that may damage reactors, may cause fouling or produce harmful emissions. Ash and high alkali metal contents of some biomass can cause slagging and corrosion in thermal systems, which may reduce plant availability and finally increase repairs costs. Pre-treatment (screening, washing, torrefaction) helps but adds cost and process steps. The technical, logistical, economic and governance-related challenges of biomass management are connected. Addressing them requires integrated solutions: better feedstock characterization, investment in aggregation and storage infrastructure, practical pre-treatments, robust sustainability standards, and policies that create predictable markets while protecting land and communities [68] [69].

2.6. Thermochemical characterization of biomass

Thermo-chemical characterization of lignocellulosic biomass is a key step in deciding on a suitable feedstock for producing sustainable fuels and other high-value products. By examining these properties, it could be decided whether a given biomass is worth exploring further for thermochemical conversion pathways. Over the years, many

investigations have reported detailed proximate, ultimate, and fiber analyses for a broad spectrum of biomass materials.

We have referred a number of research articles to compile the important findings of thermochemical characterization, which is presented in *table 2.1*, the reported moisture contents span roughly from 1.2 to 25 wt.%, volatile matter generally falls between 32.2 to 83 wt.%, ash contents was around 0.2 wt.% in cleaner, low-mineral biomasses up to about 42.3 wt.% in some biomass such as cattle manure. Fixed carbon values vary roughly 0.1 to 29.45 wt.%. Elemental analysis shows similarly broad ranges. Hydrogen contents vary from about 2.94 to 38.6%, while carbon from roughly 6.5 to 77%, highlighting the diversity from low-carbon wastes to energy-dense feedstocks. Nitrogen values range from essentially 0 up to around 35 %, oxygen from about 0.1 to 63%, and sulfur from 0.0 to 2.5%. Together, these wide intervals underscore how heterogeneous lignocellulosic biomass can be and why careful characterization is essential before selecting conversion technologies or designing downstream processes.

Table 2.1: Thermochemical characterization data of different types of biomasses from the literature.

Sr.	*Biomass Feedstock*	*MC*	*VM*	*FC*	*Ash*	*Hem*	*Lig.*	*Cell.*	*C*	*H*	*N*	*O*	*S*	*Ref.*
1	Banana leaves	8.4	73.05	11.26	7.26	34.34	15	43.35	43.28	6.83	1.28	48.31	0.3	[70]
2	Rice hull	5.92	58.55	-	12.78	18.12	24.65	36.23	39.65	5.21	1.02	53.92	0.02	[71]
3	Rice straw	7.2	62.4	14.9	15.4	20.4	14.1	60.3	44.8	5.1	0.9	49.2	0.6	[72]
4	Sorghum bagasse	7.6	81	1.9	9.5	24	10	41	68.33	8.64	0.08	22.81	0.14	[73]
5	Sugarcane leaves	5.67	77.33	10.67	3.38	42	17	44	76.83	8.19	0.59	14.39	0	[74]
6	Sunflower-extracted bagasse	5	78.4	10.5	6.1	-	-	-	53.2	7.1	8	31.7	-	[75]
7	Tomato peel	4.67	78.12	12.34	4.87	-	-	-	55	7.9	2.8	34	0.3	[76]
8	Walnut shells	6.98	76.45	15.99	0.58	26.2	36.89	32.19	47.52	6.71	0.21	45.56	-	[77]
9	Wheat straw	7.41	80.98	7.52	4.09	36	18	35	48.24	5.64	0.56	45.55	-	[78]
10	Black cumin seed cake	-	70.9	19.2	4.8	10.4	26.7	37.1	51.2	7.9	5.3	35.1	0.5	[79]
11	Cottonseed cake	5.8	79.3	9.7	5.2	-	-	27.6	52	5.9	1.3	40.8	-	[80]
12	Grape seeds	7.67	67.31	22.47	2.55	18.7	49.2	13.83	51.51	6.39	1.77	40.33	-	[77]
13	Jatropha cake	10	72.5	10.9	6.5	-	-	-	44.4	6.2	4.3	44.5	0.5	[72]
14	Linseed seed	6.7	77	10.7	5.6	-	-	14.1	61	8.5	2.3	28.2	-	[81]
15	Moringa cakes	10.4	75.1	8.3	6.3	1.9	24.9	17.9	45.6	6.5	6.5	41.5	-	[72]
16	Pomegranate seed	5.4	78.7	14.1	1.8	25.5	39.7	26.9	49.7	7.5	4	38.1	0.7	[82]
17	Safflower seed	5.7	80.8	11.3	2.2	18.6	28.9	27.2	60.5	9.1	3.1	27.4	-	[83]
18	Canola residue	6.88	81.85	13.32	4.82	-	-	-	50.22	5.41	3.18	41.19	-	[84]
19	Cocoa pod	10.3	68.5	10.4	10.8	-	-	-	43.9	4.9	2.2	47.3	0.8	[72]
20	Empty fruit bunch	2.88	75.61	16.42	5.36	26.9	25.4	26.6	46.83	6.28	0.66	45.99	0.24	[85]
21	Olive residue/waste	10.6	70.4	15.3	3.7	-	-	56	44.8	5.1	0.9	49.2	-	[86]

22	Palm empty fruit bunch	8.8	79.7	8.7	3	-	-	-	48.8	7.3	0	40.2	-	[87]
23	Peach stones	6.88	72.42	19.84	0.86	25.1	39.3	29.5	49.28	6.65	0.34	43.73	-	[88]
24	Soybean straw	1.8	75.5	19.8	4.7	-	-	-	47.8	6.9	1	44.3	0.1	[89]
25	Para grass	7.23	79.45	-	9.32	-	-	-	44.73	6.88	0.98	46.84	0.24	[90]
26	Saccharum munja	4.5	80.7	10.91	3.89	38.9	17.7	35.1	63.29	7.84	2.34	27.19	-	[91]
27	Timothy grass	5	77.9	16	1.1	33.1	28.9	38	42.4	6	1	50.4	0.2	[92]
28	C. pilulifera	10.5	32.2	18.4	38.6	-	-	-	-	-	-	-	-	[93]
29	Polysiphonia elongata	11.6	48.2	12.8	27.45	-	-	-	35.81	5.93	6.86	51.4	-	[94]
30	Wolffia arrhiza	4.76	72.6	-	10.4	-	-	-	35.55	6.36	5.25	35.87	1.16	[95]
31	Horse manure	8.2	70.4	11	10.5	23.8	56	6.3	43.3	5.9	0.9	49.2	0.8	[96]
32	Corrugated cardboard	-	-	13.1	4	-	13.2	-	43.24	5.8	0.12	-	-	[97]
33	Kitchen garbage	-	63.5	8.8	27.8	-	-	-	-	4.4	2.3	5.3	0.6	[98]
34	Rice husk	12.1	60.6	15	12.4	31.6	24.6	43.8	45.5	4.5	0.5	36.1	0.1	[99]
35	Sugarcane bagasse	16.1	79.6	8.1	4.3	33.1	24.2	42.7	58.1	6.1	0.7	34.5	0.2	[100]
36	Sunflower stalks	12.4	-	-	14.4	18	23	33	49.9	6.3	0.9	42.9	-	[101]
37	Tobacco stalk	8.5	65.5	16	9.9	32.9	30.2	21.3	39.6	4.9	3.2	52.3	0.1	[102]
38	Vine shoots	-	-	-	-	72.5	13.3	14.2	48.2	6.9	1	-	0.07	[103]
39	Wheat bran	7.78	64.66	23.87	3.69	38.56	20.24	20.36	42.2	7.89	3.64	45.42	0.85	[104]
40	Wheat straw	5.9	74.2	13	6.9	45.2	18.1	31.2	52.9	6.3	0.4	40.4	-	[105]
41	Cherry seed kernel shell	5.5	77.6	15.7	1.2	28.6	29.1	32.1	52.5	7.6	4.5	35.3	0.1	[106]
42	Date palm seed	4.9	76.6	7.7	10.8	55	23	20	45.3	5.6	1	47.2	0.8	[107]
43	Guarana seed residue	-	78.34	16.06	5.59	59.37	13.49	7.82	41.55	6.44	1.51	44.91	-	[108]
44	Jatropha seed cake	8.1	43.6	4.4	-	-	-	-	49.3	6.1	3.4	-	-	[109]
45	Pine sawdust	6.09	78.03	13.96	2.07	15.35	10.55	55.92	50.03	6.0	0.69	42.99	-	[110]

46	Neem seed	16	71	8.1	4.9	-	-	-	38.4	8.3	7.5	45.1	0.7	[111]
47	Rapeseed residue	4.9	81.7	7.9	5.5	-	-	-	62.1	9.1	3.9	24.9	-	[112]
48	Safflower seed cake	6	83	14	3	16	26.7	40	49.5	6.9	3	40.6	-	[113]
49	Castor residue	11.16	74.3	9.16	5.4	22.4	20.2	38.42	43.59	5.56	4.69	46.16	-	[114]
50	Corn cob	6.3	80.7	7.6	2.1	31.7	3.4	31.7	42.9	6.4	0.6	45.5	0.3	[72]
51	Olive kernel	-	73.1	19.8	7.1	-	-	-	49	6.7	2	34.8	0.3	[115]
52	Olive stone	-	-	-	-	50.5	23.8	25.7	49.9	6.1	0.51	-	-	[103]
53	Acacia nilotica	6.46	79.08	13.68	0.78	28.64	24.2	41.66	43.69	7.54	0.47	48.3	-	[103]
54	E. rigida	3.02	75.05	15.21	6.72	29.5	37.92	19.17	54.17	5.7	1.3	38.3	-	[116]
55	Miscanthus	5.7	72.9	25	2	29.6	21.9	40.8	46	6	0.5	47.5	-	[117]
56	Reed canary grass	5.7	74.9	15.8	3.6	28.3	9.4	42.9	44.9	6.1	0.04	39.1	-	[118]
57	Switchgrass	7.9	72.6	16.4	3.1	31.9	10.2	39	44.8	5.7	0.2	38.2	-	[118]
58	C. humicola	3.42	55.6	14.18	26.8	-	-	-	33.16	5.58	4.8	27.54	2.42	[119]
59	Microalgae chlorella	6.8	72.2	15.1	5.9	9.5	-	7.1	6.7	38.6	-	-	47.5	[120]
60	Reeds	5.89	72.12	13.52	8.47	30.68	20.34	43.05	42.78	5.17	1.33	50.51	0.21	[121]
61	Cattle manure	24.6	53.1	4.6	42.3	24.5	42.8	32.7	21.9	3.6	2.3	20.8	1.1	[100]
62	Rice	-	80.42	16.72	2.86	-	-	-	44.28	7.85	1.24	42.99	0.78	[122]
63	Incense sticks	6.08	65.98	13.12	14.82	-	-	-	35.63	4.51	0.32	38.62	0.023	[123]
64	Paper waste pulps	-	-	-	-	17.1	8.6	74.3	-	-	-	-	-	[100]

2.7 Kinetic analysis of biomass

Comprehensive estimation of the kinetic parameters that influence the thermal decomposition of a biomass is essential for designing an efficient biomass pyrolysis system and forecasting the performance of biomass conversion processes. The thermal degradation behavior of any lignocellulosic biomass involves a highly complex decomposition mechanism affected by the composition of cellulose, hemicellulose, and lignin components. Thermogravimetric analysis (TGA) and differential thermogravimetric analysis (DTG) are two important methods that serve as fundamental analytical methods for investigating the thermal decomposition pathways and kinetic properties of various biomass feedstocks. The TGA data can be found using non-isothermal and isothermal conditions. The obtained results can be evaluated using suitable kinetic models, including two famous approaches- model-fitting approaches and model-free iso-conversional methods such as the Kissinger-Akahira-Sunose (KAS), Flynn-Wall-Ozawa (FWO), and Friedman (FM) methods. The iso-conversional methods are generally preferred over others. These are simple, give accurate results, and they have the ability to handle complicated multi-stage degradation process data without requiring prior knowledge of reaction mechanisms. The kinetic parameters resulting from these analyses, primarily activation energy (E_a) and the pre-exponential factor (A), are very useful in knowing the thermal stability of various biomass types and their potential suitability for specific thermochemical conversion processes. A comprehensive compilation of findings from published studies presented in *table 2.2*. The changes in activation energy values across different waste biomass feedstocks are indicative of the differences aroused from inherent variations in composition of biomass, moisture levels, ash content, and elemental content, all these together influence decomposition behavior during heating. These variations in values highlight the necessity for doing detailed kinetic characterization of specific biomass materials prior to its use in pyrolysis, process design and optimization of pyrolysis operations.

Table 2.2.: Kinetic analysis data of different types of biomasses.

Sr.No.	*Biomass*	*Temperature Range*	*Heating Rate (°C/min)*	*HHV (MJ/kg)*	*Kinetic Models*	*Ea (kJ/mol)*	*Ref.*
1	Eucalyptus leaves, bark & sawdust	Room temp–800°C	10, 40	—	Continuous DAEM, Modified discrete DAEM	141.15, 215.65, 149.21, 264.76, 175.79, 150.66	[124]
2	Para grass (Urochloa mutica)	Room temp–1000°C	10, 30, 50	15.04	KAS, FWO	163, 175	[90]
3	Chlorella vulgaris, Kitchen waste	Room temp–900°C	20, 30, 40, 50	22.82 ± 0.044, 18.74 ± 0.040	FWO, KAS	206.67, 198.94, 237.00, 230.92	[125]
4	Corrugated cardboard	30–900°C	5, 10, 15, 20, 25	259	FWO, KAS	180.9	[97]
5	Tomato peel	Ambient–1000°C	5, 10, 15, 20, 25	22.50	Kissinger, KAS, FWO	112.7, 113.85, 234.27	[76]
6	Straw, Sawdust, Cellulose	Room temp–800°C	20, 30, 40, 50	—	FWO, KAS, ST, DAEM	193.3, 141.05, 145.65	[126]
7	Horse manure	Room temp–900°C	1, 2, 5, 10	—	FWO, KAS, FM, Kissinger	199.3, 200.2, 194.6, 149	[96]
8	Sugarcane leaves (Saccharum officinarum L)	30–1000°C	5, 10, 15, 20, 30, 40	18.08	VZK, V.AIC, FM, FWO, KAS, ST, TM	215.11, 214.89, 239.58, 226.97, 226.75, 226.94, 226.91	[74]
9	Musa balbisiana	35–900°C	5, 10, 20	16.35	KAS, FWO, FM	137.94, 136.76, 133.36	[127]
10	Rice straw	298–973 K	5, 10, 15	—	FWO, KAS, Kissinger	192.66, 193.60, 172.62	[128]
11	Potamogeton crispus	Ambient–800°C	10, 30, 50	—	FWO, KAS, Popescu	145.3, 143.2, 131.7	[129]

12	Mustard oil residue	Ambient–900°C	10, 20, 30	19.4	FWO, KAS, ST, TM, VZK, FM, V.AIC	155.64, 152.94, 152.15, 153.29, 153.52, 163.53, 159.01	[130]
13	Cynodon dactylon grass	Ambient–900°C	10, 30, 50	17.96	KAS, FWO, FM, ST, DAEM, VZK	208.89, 220.43, 211.90, 213.66, 214.28, 192.30	[131]
14	Grape bagasse	6.2°C–800°C	5, 10, 15, 20	18.08	Differential method	440.85	[132]
15	Corn cobs & Sugarcane bagasse	Room temp–700°C	10, 20, 30, 40, 50	17.2, 17.5	FM	102.5, 197.5	[133]
16	Banana leaves biomass	Ambient–900°C	10, 20, 30	17.8	FWO, KAS, ST, TM, FM, Kissinger	84.02, 79.36, 92.12, 73.89, 70.75	[70]
17	Soybean straw	Room temp–1173 K	5, 10, 20, 30	—	KAS, FWO	154.15, 156.22	[89]
18	Pine sawdust, Sal sawdust, Areca nut husk	25–900°C	5, 10, 15, 20, 25	18.44, 18.20, 18.21	KAS, FWO, FM, DAEM	171.66, 179.29, 168.58, 206.62, 148.44, 156.58, 181.53, 171.63, 171.24, 179.47, 184.61, 160.45	[110]
19	Sewage sludge	25–800°C	5, 10, 20	11.5	Coats-Redfern	—	[134]
20	Banana peel	Ambient–800°C	10, 20, 30, 40	18.87	FM, KAS, FWO	9417, 9411, 942	[135]
21	Eucalyptus leaves, bark & sawdust	Room temp–800°C	10, 40	—	Continuous DAEM, Modified discrete DAEM	141.15, 215.65, 149.21, 264.76, 175.79, 150.66	[124]
22	Chlorella vulgaris, Kitchen waste	Room temp–900°C	20, 30, 40, 50	22.82 ± 0.044, 18.74 ± 0.040	FWO, KAS	206.67, 198.94, 237.00, 230.92	[125]

2.8 Pyrolysis and co-pyrolysis of biomass

Using the fundamental information obtained from TG/DTG results of the biomass, several studies conducted by researchers across the world discuss the pyrolysis behavior of different types of biomasses in fixed or fluidized bed reactors for production of biofuels. Kumar et al. (2026) did pyrolysis studies on a few biomasses and their blend comprising rice husk, sugarcane bagasse and wood chips, using TGA data and curie point pyrolizer. The study details the pyrolysis kinetics and product distribution of individual biomass and their blend. They used a Distributed Activation Energy Model (DAEM) to get the activation energies of individuals and blended feedstocks. The decomposition behavior of lignin, cellulose and hemicellulose was interpreted using DAEM. It was observed that the hemicellulose and cellulose degraded in a broadly additive manner across the feedstock blends, indicating minimal mutual influences. However, lignin exhibited pronounced variability, with activation energy values strongly dependent on blend composition. Wood-chip lignin showed the highest resistance to thermal breakdown (265.9 kJ mol^{-1}), whereas higher proportions of bagasse reduced the energy barrier, demonstrating that lignin-lignin interactions significantly shape the kinetic behavior of blended biomass systems. A pyrolysis temperature of 590°C exhibited significantly higher selectivity to phenolic compounds, 56.30 %, particularly for wood chips biomass, followed by 34.1 % for rice husk and 17.30% for sugarcane bagasse biomass. Blended feedstock's behavior also differed markedly. Rice husk-bagasse mixtures followed nearly linear additive trends, with deviations remaining within ±2 %, while rice husk-wood chip blends displayed substantial non-linear deviations in phenolics, furans and sugar-derived volatiles, signaling strong synergistic or antagonistic interactions during co-pyrolysis. The study clearly demonstrates that the thermal and chemical behavior of biomass cannot be inferred solely from individual components and that blend composition plays a decisive role in determining product distribution. The results give a valuable insight into the pyrolysis behavior of blended feedstock [136].

Biswas et al. (2022) conducted pyrolysis to examine the effect of temperature on the structural and physicochemical properties of rice straw biochar produced at 300-450°C temperature under slow pyrolysis conditions. The results obtained showed that carbonization of biomass increases with the increase in the pyrolysis temperature, which is reflected in a rise of carbon concentration from 42.20% to 45.33% and a corresponding reduction in H/C and O/C ratios, signifying greater aromaticity and thermal stability. Structural characterization of the biomass and biochar, as depicted by XRD, showed a clear transition from the crystalline structure of raw biomass feedstock to a predominantly amorphous carbon structure in the produced biochar. This change was more pronounced in biochar produced at a higher temperature. FT-IR spectra showed that aliphatic and oxygenated functional groups slowly disappear, which indicates that biochar at higher temperature have less surface functionality. BET results showed an increase in surface area from 1.17 m^2/g at 300°C to 6.60 m^2/g for biochar produced at 450°C. SEM images showed pore development and matrix degradation with an increase in temperature, which also supports the porosity enhancement findings. Overall, the work summarizes that higher pyrolysis temperature helps in better carbonization of biochar, reduces functional groups and improves structural stability. These observations provide valuable guidance for deciding pyrolysis conditions depending on the targeted application with specific biochar characteristics of stability, porosity or surface functionalities [137].

Kapoor et al. in a co-pyrolysis study of Lantana camara and spent coffee grounds to examine a way to produce renewable liquid fuels and value-added char. The experiments were carried out in a fixed-bed reactor, where temperature, residence time and blend ratio were adjusted systematically using a Box-Behnken design. The resulting data were analyzed through ANOVA and fitted into a quadratic model so that the individual and combined effects of the variables could be understood more precisely. A blend ratio of 2:8 and a residence time of 10 minutes at 500 °C temperature was found highly optimum condition for the pyrolysis that produced the highest liquid yield, reaching slightly above 40%. This increase in bio-oil yield from 23% obtained at 400° C temperature shows

the sensitivity of the system to temperature and holding time. This bio-oil obtained at these optimum pyrolysis conditions was evaluated for its fuel properties. It indicated a cloud point of around 11 °C, a pour point near −4°C and flash and fire points around 130 °C and 151 °C, respectively. The calorific value of this obtained bio-oil was close to 8100 cal/g, which indicates its suitability to be used for practical bio-oil applications. Further, the kinetic study using TGA data showed that the activation energies for the two biomasses used were found to be ~ 3.1×10^4 J/mol for Lantana camara and about 5.7×10^4 J/mol for spent coffee grounds - reflecting the distinct thermal stability of each component of biomass. A catalyst, ZnO, was also used to observe its effects that reduced rich oxygen compounds in vapor phase and increased the formation of lighter volatiles. Apart from the bio-oil, the bio-oil obtained under the optimal conditions exhibited strong adsorption potential when it was tested for the adsorption of heavy metals from wastewater. It achieved Cu removal efficiencies over 90%, along with Pb, Cd and Ni removal, following in descending order. The findings of this work indicate that the co-pyrolysis process for the selected biomass not only improves bio-oil yield but also generates a functional biochar that is suitable for environmental applications, adding further value to the process [138].

Gautam et al. examined the thermal degradation behavior of lignocellulosic biomass, teak sawdust, to understand how its structural polymers decompose over temperature rise during the pyrolysis process. This study highlights that biomass does not behave as a uniform material; instead, its thermal response results from the distinct decomposition characteristics of cellulose, hemicellulose and lignin content. The hemicellulose usually begins to break down at relatively low temperatures, typically in the range of 200-260 °C, while cellulose follows with a much sharper and more intense decomposition zone centered around 315-400 °C due to its highly ordered structure. However, lignin shows a completely different behavior, degrading slowly over a broad range of temperature, i.e. from 250 -500 °C, which contributes to the biochar yield and explains why lignin-rich biomass feedstocks generally yield more solid carbon. Also, it shows that each component of

biomass generates volatiles in its own temperature range of decomposition, and the combined behavior of all these polymers forms the overall TG-DTG profile of biomass. The cellulose decomposition, driven mainly by depolymerization, results in a rapid release of volatiles, whereas lignin produces a more complex mixture due to its aromatic structure. Overall, the understanding of these individual decomposition patterns is essential for predicting char yield, designing pyrolysis processes and optimizing conditions for biochar or bio-oil production from biomass [139].

2.9 Pyrolysis mechanism

The thermal decomposition of lignocellulosic biomass proceeds through a sequence of overlapping physical and chemical events that collectively define the mechanism of pyrolysis. Its decomposition pathway is governed by the distinct behavior of its major constituents-hemicellulose, cellulose and lignin-each reacting within a characteristic temperature range. As heating begins, the initial stage is simple drying, where free and bound moisture evaporate below approximately 150-200 °C, leaving behind a matrix ready for chemical breakdown [140]. Primary decomposition follows as the temperature increases. Hemicellulose, which contains a heterogeneous and branched polysaccharide structure, decomposes first, typically between 200 and 300 °C. This leads to the release of light oxygenated volatiles such as acetic acid, CO, etc. Celluloses decompose more sharply, with a narrow and intense mass-loss usually occurring around 300-380 °C. Its crystalline chains undergo polymerization, forming significant quantities of anhydro sugars, mainly levoglucosan, which is a principal precursor in bio-oil formation [141].

Lignin shows the broadest decomposition range, spanning roughly 250-500 °C or higher, due to its complex aromatic chains. This slow breakdown produces phenolics and aromatic compounds but also leaves behind a considerable fraction of solid carbon, justifying the higher char yields in lignin-rich biomass [142].

As volatiles escape from the solid matrix, secondary reactions start to shape the final product distribution. Vapor-phase cracking, which becomes more apparent at higher temperatures during the pyrolysis process, converts heavy oxygenated vapors into lighter smokes such as H_2, CO and CH_4. On the other hand, if vapors are retained within the hot zone, repolymerization and condensation reactions may occur, increasing tar or secondary char development. The balance between these competing reactions is extremely sensitive to heating rate, vapor residence time and reactor design. Fast heating and rapid vapor removal usually favor liquid formation, while slow heating encourages char formation and extensive secondary reactions [28]. Figure 2.5. shows a proposed pyrolysis reaction pathway: (a) cellulose, (b) hemicellulose, and (c) lignin.

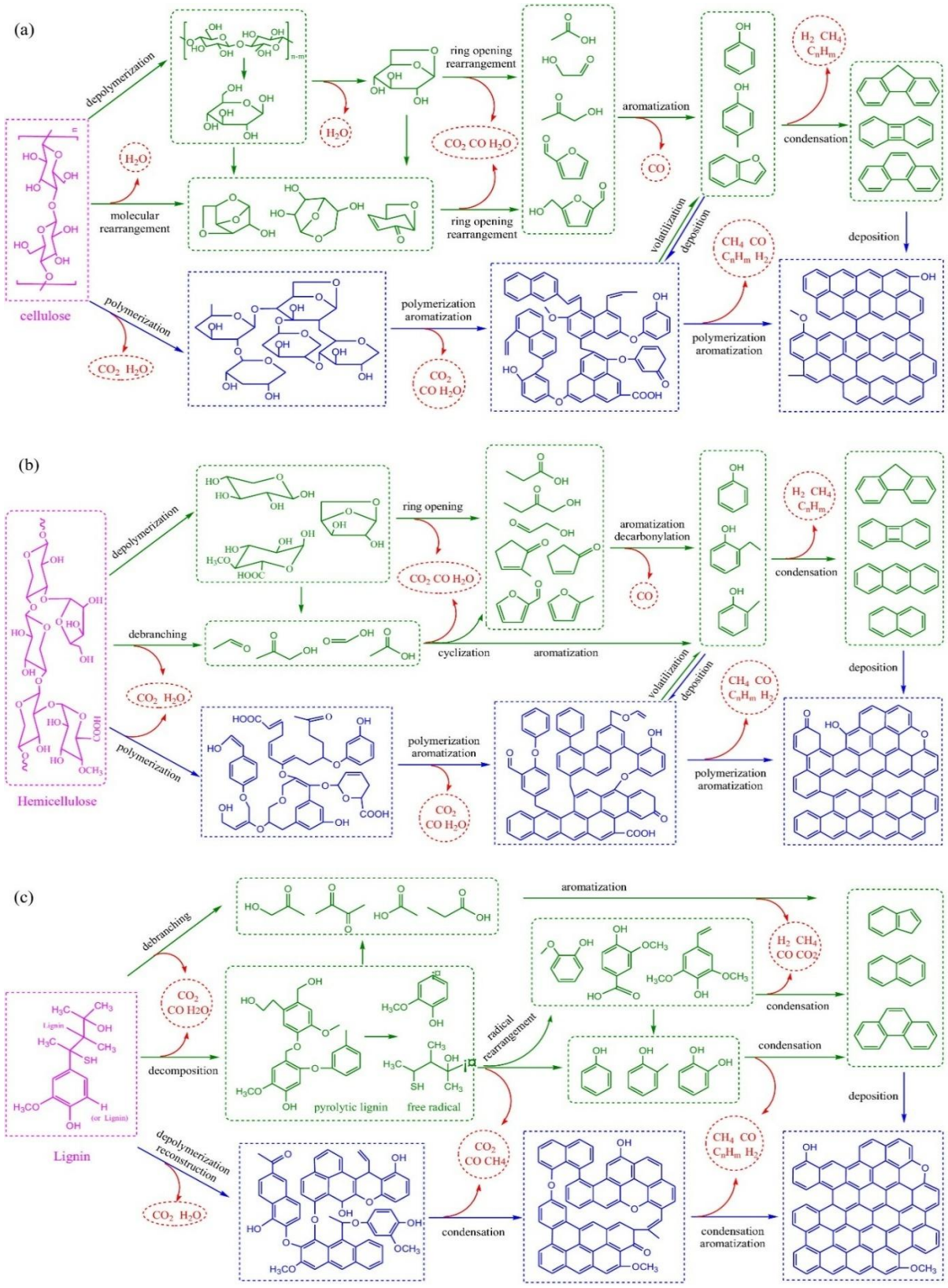

Figure 2.5: The proposed pyrolysis reaction pathways: (a) cellulose, (b) hemicellulose, and (c) lignin [142]*.(open access journal).*

2.10 Pyrolysis products

Pyrolytic Liquid (Bio-oil)

The liquid fraction generated during pyrolysis is a dark, viscous mixture commonly termed bio-oil. It originates from the thermal polymerization and fragmentation of the three major biopolymers-cellulose, hemicellulose and lignin during the pyrolysis process. The resulting liquid is chemically complicated, usually containing a combination of water, light carbonyl compounds, sugar-derived intermediates and phenolic fragments. Also, a significant portion of water in bio-oil comes from dehydration reactions of cellulose and hemicellulose, while lignin contributes additional water through the loss of hydroxyl groups from the biomass.

The high amount of water and oxygen content (often 30-40 wt.%) lowers the heating value of bio-oil, while also imparting a polar nature that reduces miscibility with other hydrocarbon fuels. The presence of organic acids, particularly acetic and formic acids, decreases bio-oil pH to around 2-3, posing corrosion and storage challenges. These qualities, combined with instability arising from reactive oxygenated compounds, indicate that raw bio-oil needs upgrading before it can be directly used in engines. Despite these limitations, bio-oil remains an important renewable intermediate and can be used to produce phenols, resins, flavoring chemicals and value-added fine chemicals [143] [144].

Pyrolytic Gases

The gaseous stream produced during pyrolysis consists mainly of CO, CH_4, H_2 and light hydrocarbons (C_1-C_4). The composition depends strongly on pyrolysis temperature and the composition of the biomass. Decarboxylation and cleavage of carboxyl groups generate CO_2, whereas bond scission reactions in carbohydrate structures form CO. Hydrogen content generally increases at higher temperatures due to the cracking of aromatic or aliphatic fragments, while methane formation becomes more prominent during lignin degradation [145].

At low temperatures, CO and CO_2 formation dominate because of dehydration and decarboxylation, but as the process proceeds into the secondary cracking regime, hydrocarbon gases and H_2 generation become more prominent. Depending on process design, these gases can be burned for process heat, incorporated into syngas applications, or purified for catalytic upgrading [146].

Solid Product (Biochar)

Biochar is the carbon-rich solid residue obtained after devolatilization of biomass in a pyrolysis process. Its formation is greatly linked to the lignin content of biomass and the severity of pyrolysis conditions. Under slow pyrolysis conditions or temperatures below 500 °C, biochar yield is generally higher, and the material usually contains a significant amount of fixed carbon with varying degrees of aromaticity. The morphology and porosity of biochar depend on biomass feedstock composition and heating rate, but the material commonly exhibits a porous structure with substantial specific surface area, making it suitable for environmental and catalytic applications [147] [148].

Biochar applications in water purification, soil amendment, carbon sequestration and as a precursor for activated carbon are very common. Its stability in soil and ability to immobilize contaminants make it valuable in environmental remediation. With some kind of chemical or physical activation, the biochar can be transformed into highly porous activated carbon suitable for adsorption processes, energy storage electrodes, catalytic supports or some other specific application. Moreover, due to its carbon stability, biochar offers a sustainable route for long-term carbon sequestration, contributing to greenhouse gas mitigation when compared to direct biomass combustion [149].

2.11 Factors affecting the pyrolysis process

Figure 2.6 shows the various factors affecting biomass pyrolysis.

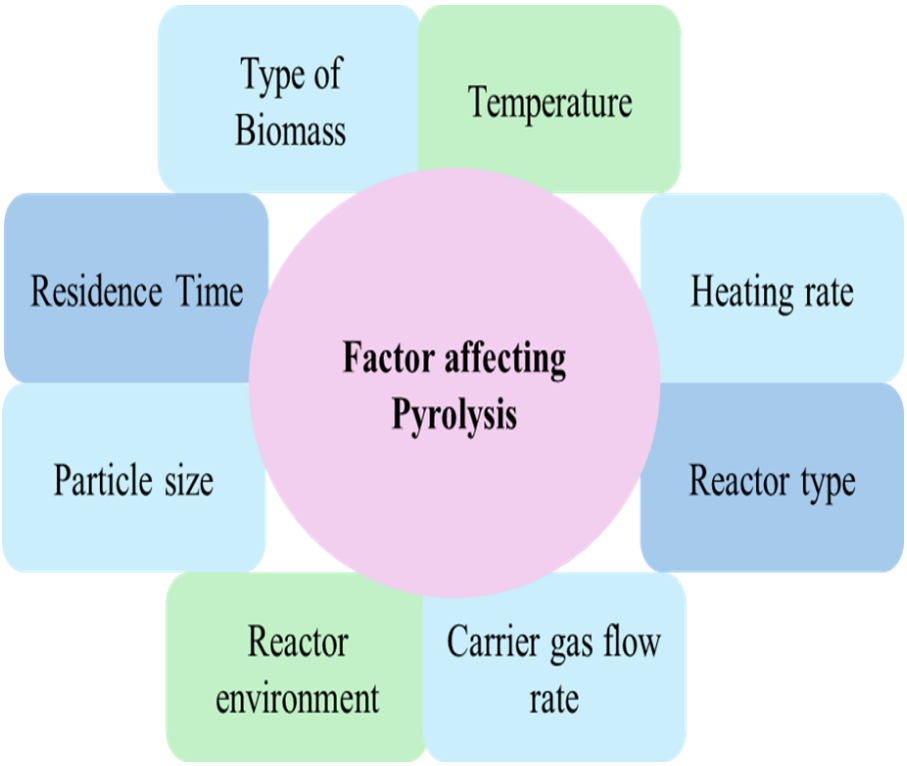

Figure 2.6.: Factors affecting the pyrolysis process.

2.11.1 Effect of Biomass Type

The feedstocks for biochar production are the materials that are available abundantly, low-cost and considered waste. Generally, feedstocks for biochar production are biomass collected from forest or agricultural fields that may include woody biomass, crop residues, animal manure or some other organic biomass. The composition of feedstock, such as lignin, cellulose and hemicellulose, depends on the source of its origin. The composition significantly affects the biochar formation and its properties [150]. Feedstocks used for biochar preparation can potentially influence biochar production with several degrees of stability and control its properties. It also influences the surface reactions that are responsible for the change in surface

charges [151]. The quality of biomass feedstock that may influence the pyrolysis products is moisture content, particle size and shape, density, elemental composition, chemical constituents, protein, extractives, lipids, energy content, bulk density, etc. [152]. Tag et al. compared biochar obtained from several feedstocks over a range of pyrolysis temperatures and showed that feedstock type significantly affects fixed carbon content, ash fraction and heating value, thereby determining suitability for energy use versus soil amendment. Higher lignin woody materials generated chars with greater carbon stability and calorific value, whereas herbaceous residues produced higher ash, lower energy density materials, more appropriate for agronomic applications than for combustion. This work underpins the common practice of classifying feedstocks into energy-oriented and soil-oriented sources [153] [154]. Gai et al. conducted pyrolysis experiments using three agricultural residues (wheat straw, corn straw, and peanut shell) and demonstrated that feedstock identity influenced both yield and nitrogen sorption capacity, even at identical pyrolysis temperatures. All three materials showed decreasing yield and increasing ash and pH with rising temperature, but absolute values of cation exchange capacity and ammonium sorption differed among feedstocks, reflecting their initial mineralogy and organic structure [155]. AL-Rumaihi et al. observed the effect of feedstock on key properties such as surface area, porosity and pH. It was found that lignocellulosic feedstocks (wood, straw, husks) generally favour high surface area and microporosity, whereas sludge and manure tend to yield mesoporous, mineral-rich chars that are more reactive but less persistent [156]. Mishra et al. discuss how animal-manure-based biochar exhibits high nutrient content and is potentially risky because of trace metals, so there is a need for careful feedstock screening for biochar preparations. Similarly, physical-chemical characterization of rice husk and rice straw-derived biochar showed that silica-rich feedstocks retain mineral bands and higher ash, which strongly affects pH and limits potential application in acidic soils [154].

Briefly, biochar cannot be treated as a single material because feedstock chemistry imprints strongly on its properties. Woody feedstocks favour stable, carbon-dense chars, while nutrient-rich residues and manures produce more reactive, agronomically potent but less persistent materials. Therefore, rational biochar design now begins with deliberate feedstock selection, prior to optimization of temperature and reactor conditions.

2.11.2 Effect of Temperature

Temperature is the most significant factor controlling biochar formation and carbonization during pyrolysis. At lower temperatures, a large fraction of biomass polymers, especially cellulose and hemicellulose-undergo only partial decomposition, which results in higher solid residue in the form of biochar. As the temperature increases, devolatilization intensifies, resulting in a progressive reduction in char yields due to enhanced breakdown of oxygenated functional groups and the evolution of volatile intermediates from the biomass. Higher temperatures favor secondary cracking and aromatization reactions during the pyrolysis, which convert reactive fragments into more ordered carbon structures. This leads to biochar with higher fixed-carbon content, lower volatile matter, and increased aromatic stability [157].

However, high-temperature regimes also foster the formation of heavy polycyclic aromatic hydrocarbons (PAHs). These compounds are produced during secondary gas-phase reactions and may condense on the biochar surface if vapor escape is restricted. Their accumulation increases the toxicological risk associated with the resulting char. Thus, temperature controls not only the mass of biochar obtained but also its chemical safety and suitability for soil or environmental applications [158].

Putun et al., during the pyrolysis of hazelnut shells between 400-700° C, observed that the biochar yield decreased by 10 % [159]. Similarly, Ates et al observed 17% reduction in biochar yield during the pyrolysis of sesame stalk [160]. Williams et al. recorded a decrease in biochar yield from

33 to 25.5% when the temperature was changed from 400 to 600°C during the pyrolysis of rice husk [161]. Sakhiya et al. (2022) produced biochar from rice straw biomass under slow pyrolysis conditions and reported the biochar yield as 57.8 % at 300°C, 42.9% at 400°C and 37.2% at 500°C [162]. In a pyrolysis study of sugarcane bagasse biomass, Valenga et al. reported a decrease in biochar yield from 44 % at 300°C to 23% at 700°C [163].

2.11.3 Effect of heating rate

The heating rate during the pyrolysis process influences the composition of products and the morphology of the biochar surface, similar to the temperature. Pore volume and surface area of biochar usually decrease with increasing heating rate due to the higher evaporation of volatile matter from the biomass. Lower heating rates usually promote secondary pyrolysis steps and the production of biochar, while higher heating rates help in fragmentation that increases oil and gas yield from the biomass. The effect of heating rate and temperature on product distribution during pyrolysis of wood biomass exhibits that temperature is the dominant operating parameter, whereas heating rate plays a relatively minor role. When the temperature increased from 300 to 720 °C at a slow heating rate of 5 °C/min, the bio-oil proportion increased only reasonably, rising from about 10.6 wt.% to 13 wt.%. Under process conditions where both heating rate and temperature were high, the liquid yield attained a slightly higher amount of around 15.9 wt.%. In contrast, the solid residue demonstrated a great sensitivity to temperature. Biochar yield fell sharply by nearly 20-25 wt.% as the temperature increased across the experimental range, whereas variations in heating rate produced only a minute difference of roughly 2-3 wt.%. Gas formation showed a similar trend: changing heating rate alone formed only a minor rise of around 1-2 wt.%, but increasing temperature led to a much larger change, with gas yields rising by approximately 5-15 wt.%. At higher temperatures combined with high heating rates, the concentrations of major pyrolysis gases, particularly CO, CO_2, H_2, CH_4 and C_2H_6, also increased, indicating more extensive cracking and volatile release under such conditions [164].

Angin et al. observed that increasing both the pyrolysis temperature and the heating rate leads to a consistent decline in biochar yield. At higher temperatures, this drop arises from more extensive primary devolatilization concurrently with secondary decomposition of the char residue. In contrast, the relatively higher char yields observed at lower temperatures suggest that the biomass has undergone only partial pyrolysis. The effect of heating rate is more noticeable within the lower temperature range. For instance, at 400 °C, when the heating rate was raised from 10 to 50 °C min-1, the biochar yield decreased from 34.18% to 29.70%, representing a change of about 4.48%. At higher temperatures, however, the influence of heating rate becomes less significant. At 600 °C, the same increase in heating rate resulted in only a small reduction of roughly 1.76%, suggesting that temperature becomes the dominant factor controlling char formation once high-temperature pyrolysis conditions are reached [165].

Simler observation by many other authors during the pyrolysis of different biomass have been observed and reported. Al-Rumaihi et al. observed that the increase in the rate of heating biomass from 0.5-180°C per second and maintaining the constant pyrolysis temperature of 765°C, the biochar yield from the feedstock used declined from 25% to 17%, which resulted in increased tar formation and total volatile contents [156] [166] [167].

Angin, Aysu and Kucuhk, and Sensoz and Augin also have reported a decline in the biochar yield obtained from pyrolysis of safflower seed, Ferula orientalis and Carthamus tinctorius L., respectively, when the heating rate was increased from 30 to 50 °C per min between a temperature range of 400-600°C [168] [165] [169] [170].

2.11.4 Effect of residence time

Like temperature and heating rate, residence time is also an important operational factor shaping the characteristics and yield of biochar and its characteristics during pyrolysis. Residence time is the duration for which the biomass solids and intermediate char remain exposed to the peak

pyrolysis temperature inside the reactor atmosphere. Short residence times generally help retain a higher portion of the solid fraction by limiting secondary decomposition reactions during pyrolysis. On the other hand, long residence rises continued devolatilization, aromatization, and cracking of the partially formed biochar, which is generally responsible for the formation of reduced biochar yield and richer carbonization of the final product.

Wang et al., who investigated the co-pyrolysis behaviour of sewage sludge and cotton stalks, noted that biochar yield decreased markedly when residence time was increased from 30 to 90 min at 600 °C; however, beyond 90 min, the change in yield became minimal, signifying that secondary pyrolysis reactions predominantly occur during the initial residence window. At 600°C, when the residence time was 30 min, the produced biochar yield was approximately 52-54%. At the same pyrolysis temperature, when the residence time was changed to 60 min and 90 min, the obtained biochar yield was 48% and 46%, respectively. Beyond 90 min, the decrease in yield was minimal, indicating that a major portion of primary devolatilization and char break-down happened during the initial hour of heating. Apart from the yield, there had been an increase in ash content from approximately 38 wt.% to 45% for a residence time of 30 min and 90 min, respectively, and pH also increased due to progressive removal of acidic oxygenated functional groups [171].

Zhao et al. in a slow pyrolysis work of rapeseed stem between 200-700°C, and residence time of 10, 20, 40, 60, 80, and 100 min, found that biochar yield shows a slightly negative pattern when the residence time was increased. This negative trend is logical as a major portion of biomass volatilizes during higher residence time, leaving behind less biochar. However, the observation of this study was that there is a minimal effect of residence time on biochar yield of rapeseed stem, indicating that an approximate maximum biochar mass yield can be obtained in a relatively shorter residence time [172].

Suresh Babu et al. and co-workers, in pyrolysis work using mixed wood husk, concluded some findings related to the effect of residence time on biochar yield. At a temperature of 400°C, the biochar yield was approximately 37, 36 and 35 wt.% for a residence time of 30 min,45 min, and 60 min, respectively. At a temperature of 600 °C, the yield was 24.5, 23.5, 22.8 wt.% for 30 min, 45 min and 60 min, respectively. At a temperature of 800°C, the biochar yield was 22.8, 22.2, and 22 wt.% for residence times of 30 min, 45 min and 60 min, respectively [173].

Chandra et al. conducted pyrolysis of rice straw at 400,500,600 and 700°C and a residence time of 60 min, 90 min and 120 min. The biochar yield at 400°C was approximately 45.4,44.94,44.82 for a residence time of 60 min, 90 min and 120 min, respectively. A similar trend of yield decrease with an increase in residence time was observed at other pyrolysis temperatures also [174].

2.11.5 Effect of biomass particle size

The size of biomass particles significantly influences pyrolysis; a sit governs the rate of heat transfer within the material. When particle size increases, the distance between the outer surface and the core of the biomass expands, slowing down heat conduction from the hot exterior to the cooler interior. This temperature difference encourages higher char formation [175]. Additionally, larger particle forces the volatile vapors produced during thermal degradation to travel farther through the char layer, promoting more secondary cracking reactions, ultimately yielding more biochar. Demirbas et al. [176]; examined the impact of particle size on the pyrolysis behaviour of olive husks, corncobs, and tea waste at 677°C. An increase in particle size from 0.5 mm to 2.2 mm improved biochar yield from 19.4 % to 35.6% for olive husks and from 5.7% to 16.6% for corncobs, while a similar trend was recorded for tea waste also. Similar results were reported by Ates et al. [160] and Zhang et al. [177]; who also observed higher char yields with increasing particle size of the biomass. Mani et al. [178]; also found that wheat straw pyrolysis led to an increase in char yield from 11.85% to 23.28% as particle size grew from 0.25 mm to 0.475 mm. However, further increase in size up to 1.35 mm produced no notable change. Despite these generally consistent results, a few studies have reported

the opposite trend- where increasing particle size reduced biochar yield [179] [180]. In the work by Onay and Kockar [181]; during pyrolysis of rapeseed at 550°C (Heating rate-30°C/min; gas flow-100 cm3/min), a decrease in biochar yield was observed as the particle size rose from 0.425 mm to 0.85 mm, but beyond 0.85 mm, the yield began to rise again. Other researchers, such as Gonzalez [175] and Aysu and Kusuk [168]; noted minimal or no variation in yield across different particle sizes. These divergent findings imply that the influence of particle size on biochar production during pyrolysis remains complex and not yet fully understood.

2.11.6 Effect of reactor type

Reactor configurations have a profound effect on pyrolysis products. It impacts biochar yield in pyrolysis by controlling heat transfer rates, residence time, and vapor-solid interactions. Fixed-bed reactors, which are characterized by static biomass packing, facilitate slow heating and longer residence times (often >10 min), which help in the development of secondary reactions needed for more char formation and result in elevated biochar yield to 30-50wt.% at a pyrolysis range of 450-600°C. This happens because of longer exposure of volatiles to heat that foster re-polymerization over volatilization. On the other hand, fluidized- bed type of reactor uses high velocity gas to achieve rapid heating and short vapor residence (< 1 sec), suppressing development of secondary reactions and so biochar yield lowers 15-30 wt.% and result into higher yield of bio-oil [182] [183] [184] .Augur or screw reactors bridge the limitations; it maintains continuous supply of biomass, ensuring uniform heating and moderate residence time (2-5) min, and usually have a char yield of 35-42 wt.% from lignocellulosic biomass feedstocks. Comparative studies show that fixed-bed reactors are suitable for obtaining maximum char yield via vapor retention, whereas fluidized-bed reactors may be preferred when the objective is to obtain a higher yield of bio-oil. For feedstocks with a larger particle size fixed bed is recommended for better biochar yield [185] [184] [186] [184].

2.11.7 Effect of reactor environment

During the pyrolysis of biomass, the reactor's environment has a profound influence on the product properties and distribution. Usually, an inert atmosphere is created with the help of nitrogen for biomass pyrolysis to avoid the influence of oxygen on the process. However, it can also be conducted in the environment of other gases such as carbon monoxide, carbon dioxide, helium, steam, hydrogen, etc.

Properties of biochar vary noticeably with the surrounding gas atmosphere during pyrolysis. Guizani et al. showed that beech woodchips pyrolyzed at 850 °C in a CO_2 rich environment produced less char than under N_2, the CO_2 atmosphere also generated biochar with a higher surface area and an altered chemical profile compared with its N_2-derived counterpart [187]. Studies on steam-assisted pyrolysis report that steam behaves as a mild oxidant and induces partial gasification of the solid matrix. This environment has been found beneficial for enhancing the formation of oxygenated organics and for suppressing unwanted secondary cracking of vapors in the gas phase [188]. Other investigations indicate that CO_2 promotes more effective thermal breakdown of lignocellulosic biomass and reduces the formation of several aromatic hydrocarbons. In contrast, conducting pyrolysis in a hydrogen atmosphere increases the formation of hydrocarbon species. The generation of reactive hydrogen radicals in such conditions facilitates the deoxygenation of pyrolysis vapors, thereby enriching the product stream with various hydrocarbons [189] [190] [191].

Premchand et al. found that using a CO_2 atmosphere strongly alters both yields and char properties compared with inert gas. Their review of experimental studies reports that CO_2-promoted pyrolysis (especially in the 400-600 °C range) often increases char yield and surface area and enhances aromatic carbon content, because CO_2 participates in mild gasification and surface activation reactions that etch and enlarge pore structure while promoting secondary condensation. They also note trade-offs: excessive reactive gas or high temperature shifts reactions toward gasification, lowering yield and changing O/C and H/C ratios [192].

2.11.8 Effect of carrier gas flow rate

The interaction between evolving pyrolysis vapors and their surrounding atmosphere often promotes secondary reactions that add to char formation. Rapid removal of these vapors is therefore important to suppress such reactions. In most systems, nitrogen is used to maintain an inert ambience, and its flow helps carry freshly formed vapors away from the hot reaction zone, reducing their chance of condensing back on the solid or undergoing repolymerization. Effective quenching of these thermally cracked vapors is equally critical, as prolonged exposure to high temperatures encourages further transformation that alters product distribution. Consequently, an appropriate sweep-gas flow becomes a key operational parameter in controlling both the extent of secondary reactions and the final yields of pyrolysis products [193] [194].

Somerville et al. found that increasing the flow of an inert carrier gas through a packed biomass sample reduces charcoal/biochar yield by accelerating volatile removal and suppressing secondary vapor-solid reactions. Their thermo-gravimetric and bench-scale work on radiata pine showed faster decomposition rates and lower char yields as purge flow increased, and they link this to shorter vapor residence time that prevents re-polymerization on the solid surface [195].

Tripathi et al. found in their broad review that carrier-gas flow rate is one of the under-appreciated but reproducible levers controlling char formation: low flows favour retention of reactive vapors and promote secondary char formation (higher fixed-C), while higher flows sweep vapors away, producing lower char yields and cleaner char chemistry. They emphasize that the magnitude of the effect is feedstock- and reactor-dependent and must be interpreted alongside heating rate and particle size [157].

Buss et al. (and co-workers) found that carrier-gas flow has an important role in controlling polycyclic aromatic hydrocarbon (PAH) contamination of biochar. Their systematic analyses show that raising inert purge flow markedly reduces PAH concentrations in chars across feedstocks: for

straw-derived chars, PAHs dropped from tens of mg-kg^{-1} at zero flow to single-digit mg-kg^{-1} at moderate flows (order 0.5-0.7 L min^{-1}). They conclude that rapid vapor evacuation mitigates PAH formation and re-adsorption onto the solid [196].

Shrivastava et al. found that carrier gas flow also influences product quality and surface properties in agitated/bench reactors: moderate increases in nitrogen flow can increase specific surface area and total pore volume by reducing vapor condensation and pore blockage, but excessive flow combined with high temperature can trigger partial gasification and mass loss, so the BET response is non-monotonic. Their comparative reactor study underscores the need to optimize flow with temperature and heating profile for desired char properties [197].

2.12 Knowledge gap

A number of reported research works are related to biomass pyrolysis and biochar production, still knowledge gap, scope for qualitative research, and improvement are still there. Most studies focus on single biomass feedstock for pyrolysis, while systematic investigations on the co-pyrolysis of blended agricultural residues such as rice straw with sugarcane waste or mustard de-oiled cake are limited. The influence of blending biomass for co-pyrolysis on biochar for its energy characteristics and thermal behaviour is not yet well established.

Furthermore, while biochar modification has gained attention in the recent past, limited reported work is available on integrating rice straw-derived biochar with graphene oxide using environmentally benign synthesis routes and evaluating its performance for dye removal. The relationship between synthesis conditions and adsorption performance remains inadequately explored. In addition, although various chemical activation method of biochar using different chemicals is widely reported, studies combining activated biochar with surfactants for CO_2 entrapment are scarce.

The synergistic function of activation and surfactant addition in improving gas capture performance has not been comprehensively addressed. These research gaps highlight the need for an integrated study linking feedstock blending, biochar engineering, and exploring multifunctional applications for energy generation and environmental remediation.

2.13. Objectives of this thesis

- To investigate the pyrolysis behaviour of rice straw, sugarcane bagasse and co-pyrolysis of their blends for producing biochar and investigating its potential for energy applications.
- To study the pyrolysis of rice straw and mustard de-oiled cake and its co-pyrolysis to evaluate the influence of blending on biochar properties and explore its energy characteristics.
- To synthesize and characterize a rice straw biochar-graphene oxide composite following a green route and assess its efficiency for methylene blue dye adsorption.
- To develop activated biochar from agro-waste using KOH and nitrogen doping steps to investigate its physicochemical properties significant to gas adsorption.
- To evaluate the influence of surfactant addition on the prepared activated biochar for enhanced CO_2 entrapment performance.

Next chapter discuss about biomass feedstock collection and its processing for further use. Also, details about all the methodology adopted for material preparation including pyrolysis setup and characterization techniques used throughout the thesis work.

CHAPTER- 3

3.1. Introduction

Biomass feedstocks for the planned pyrolysis work were collected from the agricultural fields, industrial mills or local sellers and shops. The collected biomass was processed through various steps, including washing, drying, grinding, etc., to convert in usable form. The biomass and the prepared materials from it, through various experimental work, were analysed using various characterisation techniques to evaluate properties and explore potential applications of the various synthesised materials. The characterisation methods used were FT-IR, FE-SEM, TGA, Raman Spectrocopy, XRD, XPS, BET analyser, Bomb Calorimetry and UV-Vis spectroscopy.

This chapter consists of a discussion on experimental and analytical methods adopted to complete the objective of the thesis.

3.2. Collection of biomass feedstocks

Rice straw, sugarcane bagasse, mustard de-oiled cake, groundnut shell, banana peel, sweet lemon peel, lychee seed and mango shell were a few of the biomasses that were used during the various experimental works. However, the majority of the research in this thesis is based on the rice straw, sugarcane bagasse, mustard de-oiled cake and mango shell.

Rice straw was collected from the agricultural fields of a village named Mubarakpur Mukhatiya (26.272766 °N, 81.510594 °E) situated in Amethi district of Uttar Pradesh, India. Sugarcane bagasse was collected from a sugar mill (Kisan Sahkari Chini Mill Sultanpur; 26.296552 °N, 82.098879 °E) situated in Sultanpur district of Uttar Pradesh, India. Mustard de-oiled cake was bought from a local oil mill situated near our institute (RGIPT, Jais). The mango shell used was collected from a Juice shop in the nearby market (Bahadurpur) of the institute. Lychee seed, groundnut shell collected from local seller shops. Banana peel and sweet

lemon peel were collected from our institute's mess. *Figure 3.1* shows the collection of different types of biomass feedstock.

Figure 3. 1: Collection of different type of biomass feedstocks

3.3. Biomass processing for experimental use

The collected biomasses were washed rigorously to remove all kinds of dirt or any form of contaminant from the surface. For washing, tap water was used for initial washing, and the final washing was done by DI water. Thereafter, the washed biomass was oven-dried in a hot air oven at 105°C for more than 24 hours. After drying, all biomass was chopped into smaller sizes and ground using a kitchen grinder to make powder form for making pellets as per the requirements of the experiment. This usable form of biomass feedstocks was stored in airtight

containers to save it from a humid environment. *Figure 3.2* shows the pictorial representation of various stages of biomass processing.

Figure 3. 2: Various stages of biomass processing

3.4. Lab-scale pyrolysis procedure

Lab-scale pyrolysis of the biomass feedstock was carried out using a horizontal tube furnace, a muffle furnace and a developed pyrolysis and gasification setup during various planned research projects.

3.4.1. Pyrolysis using a tube furnace

The pyrolysis and co-pyrolysis experiments were conducted in a horizontal quartz tube located inside a tube furnace (Lindberg®, USA). The inner diameter of the used tube was 22 mm, and the outer diameter was 25 mm. The length of the tube was 500 mm. The quartz tube was selected for pyrolysis because it is a stable material at higher temperatures, as compared to glass, in which softening starts at a lower temperature. The material softening makes the glass tube unsuitable for pyrolysis in the temperature range of 300°C to 700°C or higher. Hence, the quartz tube was selected for experiments in the required range, as its melting point is approximately 1500°C, which makes it appropriate for high temperature pyrolysis. The maximum operational temperature of the furnace was 1200°C. A PID temperature controller, connected to the furnace, maintained the desired operating environments such as temperature, heating rate, and dwell-time as per the requirements. The schematic diagram of the tube furnace used in this experiment is shown in *Figure 3.3*. The feedstock samples were prepared as mentioned earlier and placed inside the quartz boat. The sample weight kept in the boat in each

run was approximately 3-4 grams. The quartz boat loaded with the sample was placed inside the quartz tube approximately in the centre of the tube. The centre position was preferred to ensure proper heating of the biomass. Thereafter, the nitrogen gas supply and the furnace controls were turned on and set at the operating conditions. Nitrogen gas of 99.99% purity was constantly supplied at a flow rate of 100 mL min^{-1} using a rotameter through the tube to maintain the inert atmosphere required for the pyrolysis. Nitrogen gas was supplied to the reactor to maintain an inert atmosphere during the pyrolysis process.The nitrogen gas flow also swept the product gases from the quartz tube, thus preventing the pressure build-up inside the tube. After the desired duration of the experiment, the system was left to cool up to room temperature. *Figure 3.3* shows the real image of tube furnace used and a schematic representation of biomass pyrolysis process using tube furnace.

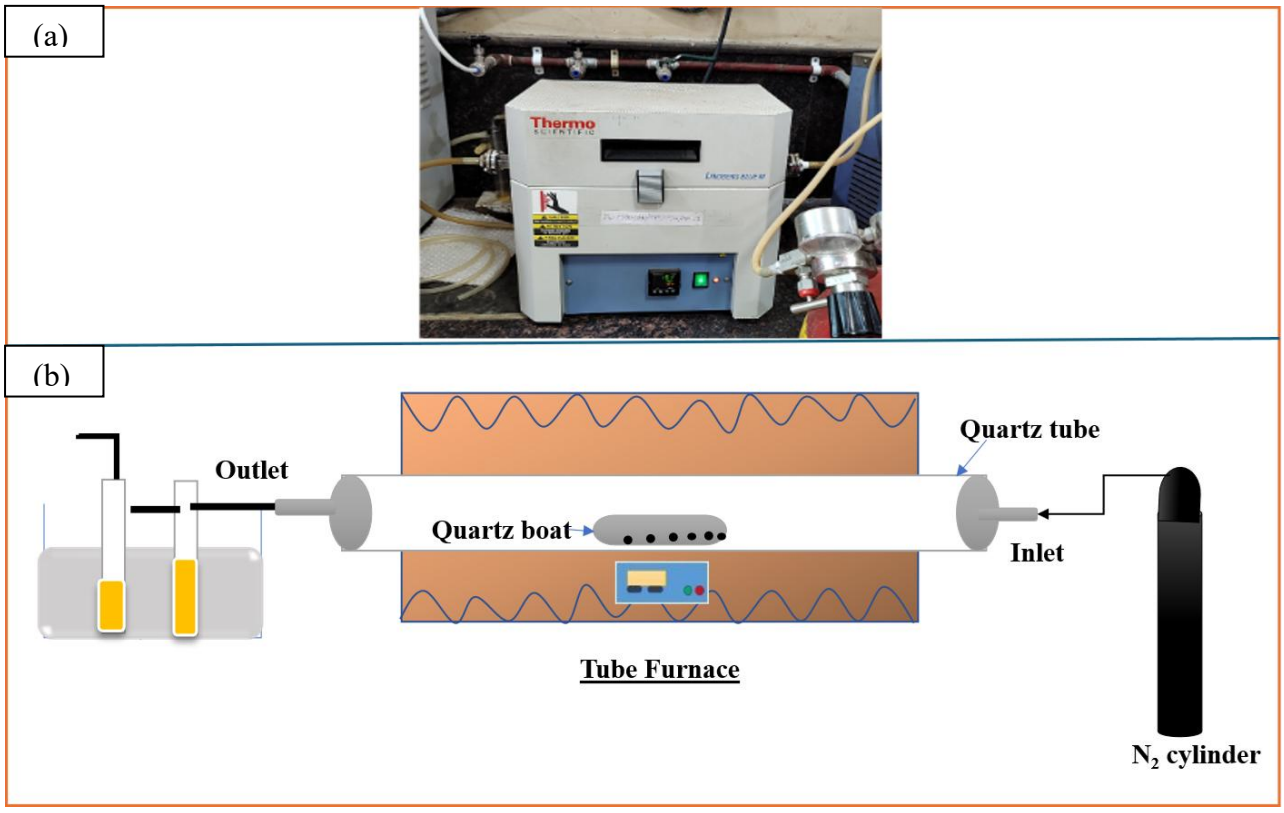

Figure 3. 3: (a) Real image of tube furnace ;(b) Schematic representation of biomass pyrolysis process using a tube furnace.

3.4.2. Pyrolysis in a modified muffle furnace

A muffle furnace in the laboratory was modified to make it suitable for pyrolysis. Since the existing muffle furnace has no arrangement for making an inert atmosphere inside it, it was modified with the help of a local shop named Gulab Engineers, located in Jais, Amethi, Uttar Pradesh, India. Along with it, a reactor was developed to fit inside the furnace, which was the actual pyrolysis chamber inside the furnace. This modified furnace was a scale-up version of the tube pyrolysis work. Here, up to 100-200 grams of biomass, depending upon its density, could be pyrolyzed which was 5-6 grams in the case of the tube furnace. A schematic diagram of this setup is being presented in *figure 3.4*.

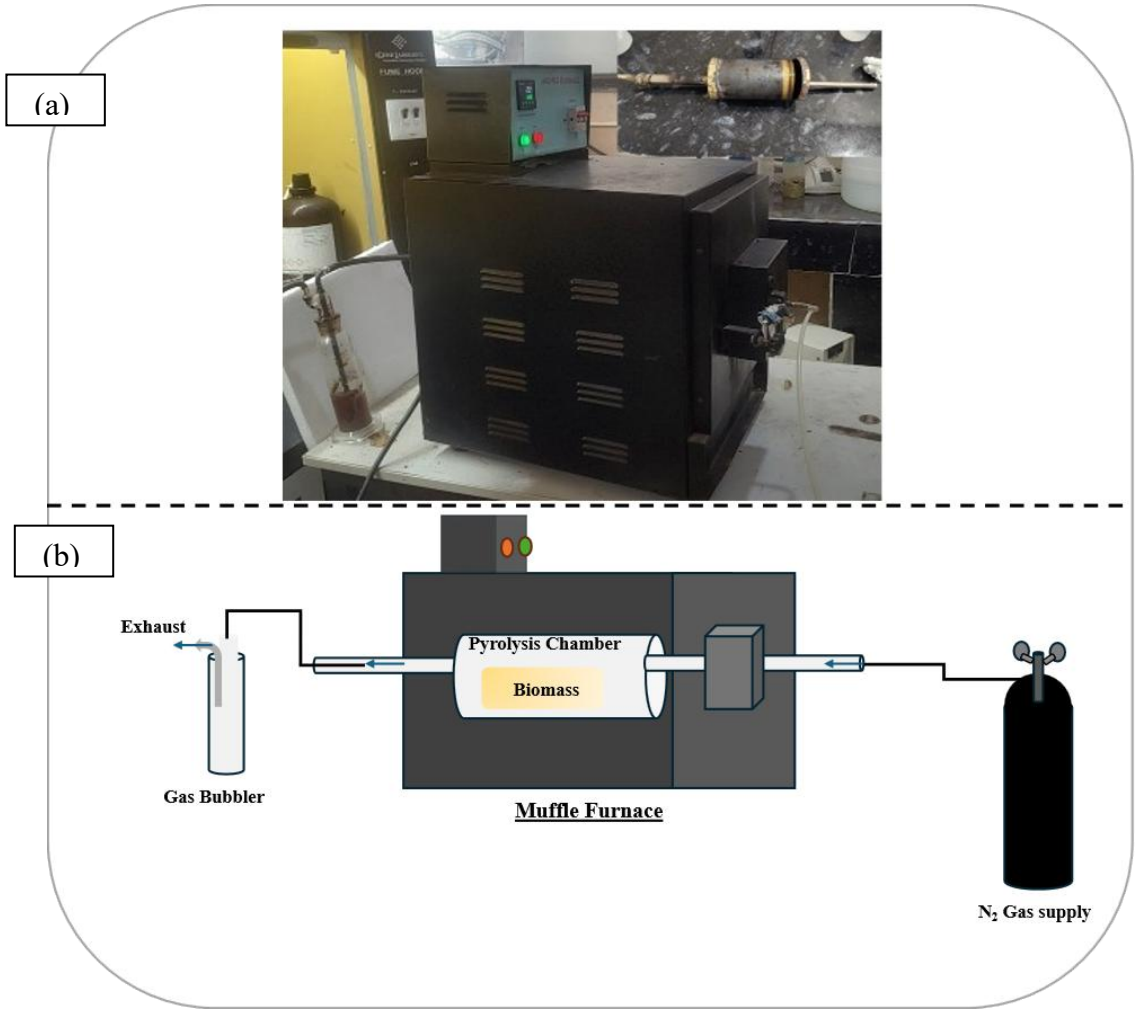

Figure 3. 4: (a) Real image of muffle furnace and reactor; (b)Schematic representation of pyrolysis process using modified muffle furnace.

3.4.3. Design and fabrication of a pyrolysis and gasification reactor

A hybrid reactor for gasification and pyrolysis was designed and fabricated for lab scale work. This reactor consist of a hopper for biomass feeding, a heating furnace equipped with a vertical heating tube, a thermocouple to measure the inside temperature of the tube, a sample holder to position and hold the sample during reaction process, an arrangement to supply the gas to make N_2, CO_2, NH_3 or steam or any other gas environment inside the heating tube as per the experiment requirement. Below the heating furnace, there is a reactor vessel in which the produced gas from the tube may further react with any gas or material to improve or change the gas quality and composition. Then there is a condenser situated below it. The condensable gases, after passing through the condenser, are converted into liquid form and can be stored in the collection vessel along with the non-condensable gases. The designed setup facilitated us for further gasification of biochar produced from the pyrolysis process. *Figure 3.5* shows a schematic representation and a real image of the designed setup for biomass pyrolysis and gasification.

3.5. Experimental procedure for biochar activation

The biochar obtained from the pyrolysis process can be further enhance its properties via physical activation or chemical activation methods. Physical activation involves heating the carbonised material in the presence of activating gases like steam or carbon dioxide at high temperatures (typically 600-1200°C). Chemical activation involves impregnating the raw material with chemicals (e.g., phosphoric acid, zinc chloride, potassium hydroxide) before or during carbonisation, followed by heating. In this thesis work, chemical activation using potassium hydroxide has been done, and the activated biochar was further activated with urea for nitrogen, doing to incorporate addition functional groups useful for CO_2 adsorption applications. The procedure involves the required chemicals, a vacuum oven for drying, a muffle furnace for pyrolysis and some other laboratory glassware and consumables for washing

and filtering. The detailed experimental procedure has been discussed in the respective chapters. *Figure 3. 5* shows schematic representation of pyrolysis and gasification setup; and real image of fabricated set-up being used in laboratory.

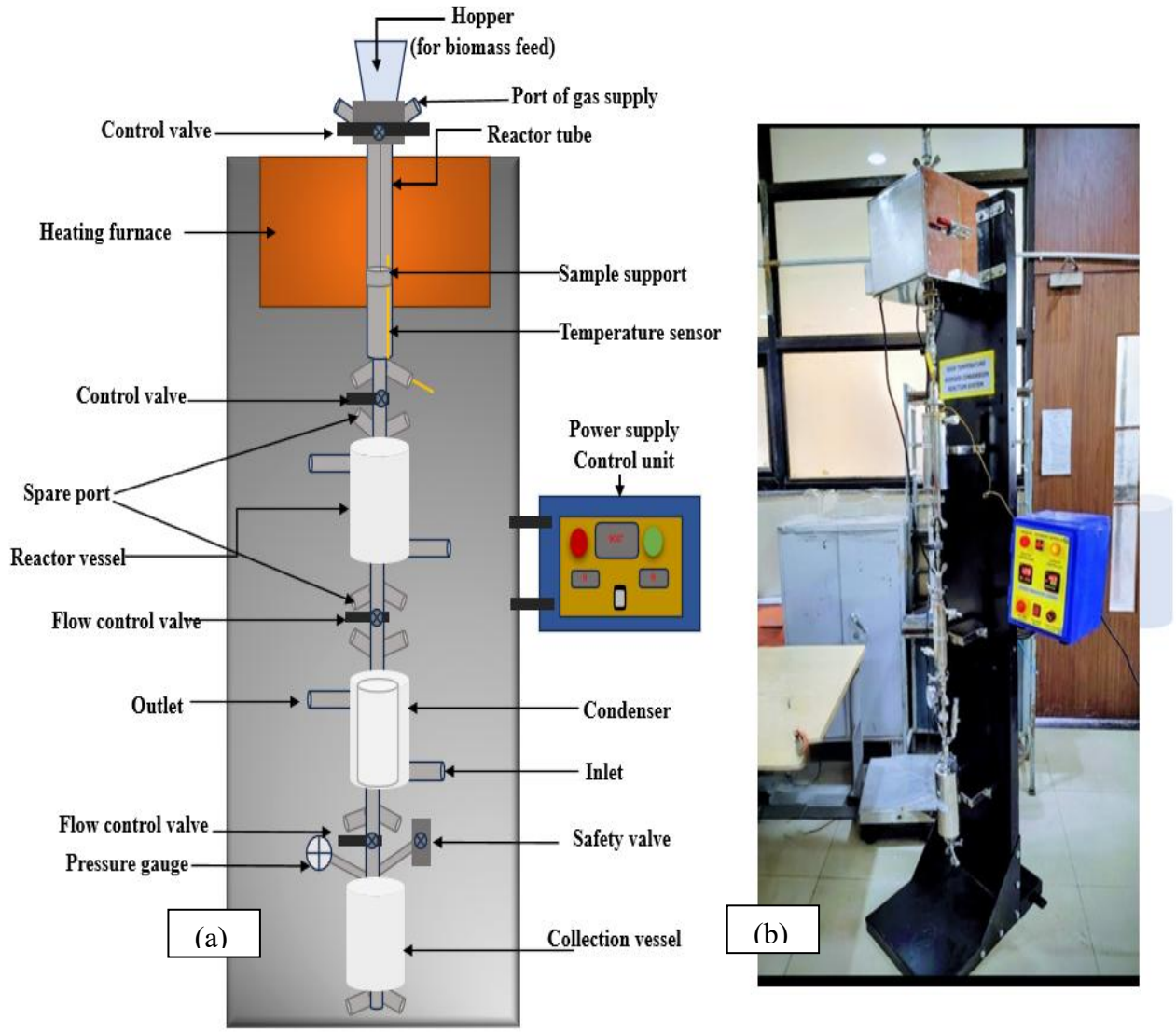

Figure 3. 5: (a) Schematic representation of pyrolysis and gasification setup; (b) Real image of fabricated set-up.

3.6 Experimental procedure for composite preparation

This involves three major steps: preparation of biochar, preparation of GO and, preparation of biochar-GO composites. (i) muffle furnace, pyrolysis temperature -400°C. The biochar was washed and stored (ii)GO was synthesize following the well-established procedure (Modified Hummer's method) and then GO suspension was made and biochar was mixed. The mixture was continued stirring followed by ultrasonication and hydrothermal treatment for composite preparation. The respective chapter discuss the process in detail.

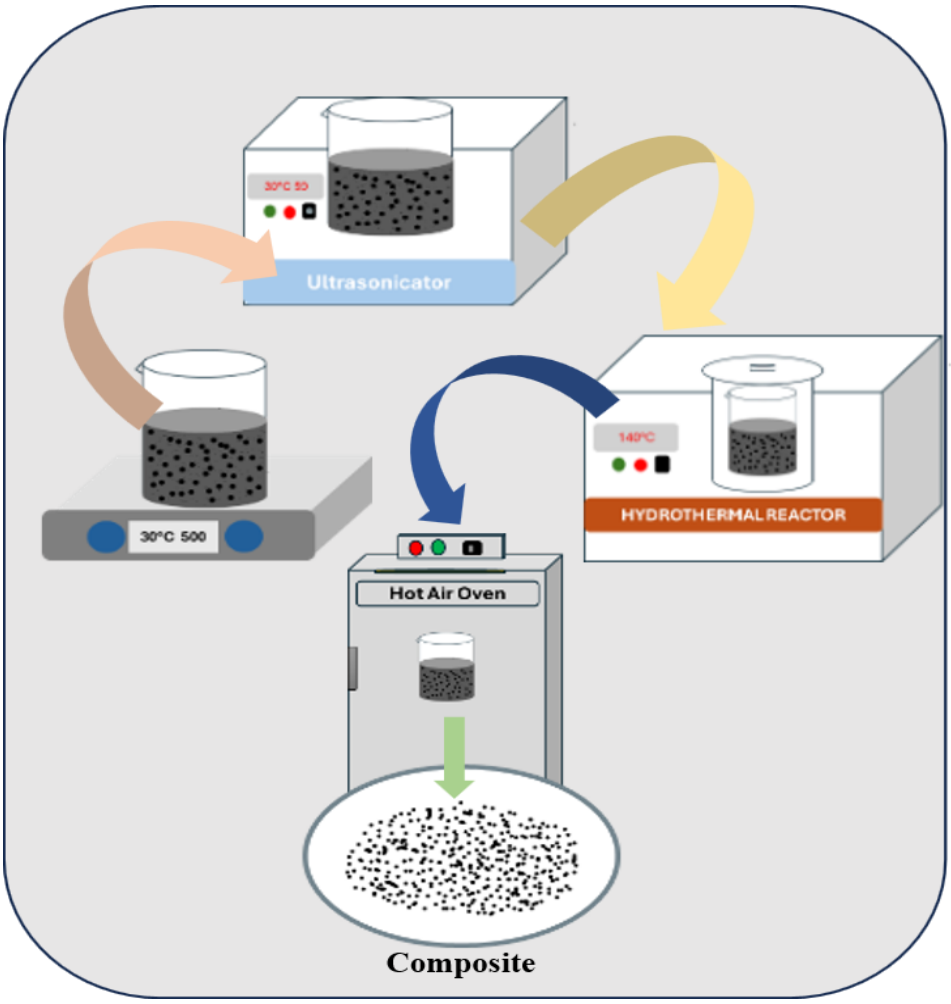

Figure 3. 6: Schematic diagram of composite preparation steps.

3.7. Experimental procedure for adsorption studies

The adsorption study was done for prepared biochar-graphene oxide composites. Aqueous MB solution was prepared by dissolving MB reagent (98% purity, RANKEM™, USA) in DI

water. Initially, the pH of the solution was kept constant throughout the experiment. The synthesised composite of a particular dosage was mixed in the MB solution of known concentration and pH. The experiments were also done using rice-straw biochar (non-composites). The adsorption testing was carried out using different doses of composites. The MB dye solutions of varied concentrations were prepared and contacted with the synthesised samples in a batch experiment, and UV-VIS spectra for all samples were regularly collected and recorded to monitor the adsorption kinetics.

3.8. Characterization methods

3.8.1. Ultimate analysis (Elemental analysis)

The compositions of elements present in the biomass sample were mostly carbon, hydrogen, nitrogen, and sulfur (C-H-N-S), which were determined using an organic elemental analyser (UNICUBE®, India). The oxygen content in the sample can then be obtained by subtracting the overall percentage of CHNS from 100.

3.8.2. Higher heating value determination (HHV)

The higher heating value (HHV) of biomass is a key indicator of its energy potential for value-added applications. HHV of the biomass samples were obtained using a Bomb Calorimeter (HAMCO® India). A pellet of approximately one gram was made using a hand pelletizer, and this pellet was placed inside the bomb calorimeter. The experiment was completed following the standard procedure. Oxygen supply was given inside the instrument for the combustion of the sample.

3.8.3. Thermogravimetric analysis (TGA)

Thermal analysis of biomass samples such as rice straw (RS), sugarcane bagasse (SB), rice straw-sugarcane bagasse mixture (RB), mustard-oil residue (MR) and rice-straw & mustard-oil residue mixture was performed using a thermogravimetric analyser (PerkinElmer®, UK). Crushed biomass (near about 10-12 milligram weight) was taken and

placed inside the crucible fitted to the weighing balance in the TGA furnace. The system was purged with nitrogen gas continuously at a flow rate of 50 mL/min to maintain oxygen free inert condition within the reaction chamber. Finally, the samples were heated from ambient to 1000°C at heating rates of 5, 10, 20, or 40°C/min. When the temperature reached 1000°C, the sample was held for 10 minutes to confirm complete conversion. The obtained data were plotted using Origin-Lab® graphic and analysis software.

3.8.4 Fourier transform infrared (FTIR) spectroscopy

Fourier transform infrared (FTIR) spectroscopy is a non-destructive analytical technique that is suitable for analysing a wide range of sample including solids, liquids, gases, fibres and powders. Within the instrument, enhanced functionality is recorded using an attenuated total reflectance (ATR) accessory equipped with a ZnSe crystal [198]. FTIR has extensive applications in research and the industrial sector for the identification of functional groups of any sample. It works on the principle of the Michelson Interferometer experiment in which infrared light gets split, recombined after hitting the sample, and captured as an interferogram that's then converted via Fourier transform into a readable spectrum. Those peaks in the mid-IR range reveal specific molecular vibrations, pinpointing organic and inorganic functional groups [199].

FTIR analysis can be used to observe the distribution of various functional groups in the feedstock and the biochar. Five milligrams of biomass samples were weighed and mixed with potassium bromide. The resulting mixture was compressed to form a very thin pellet, which was placed inside the FTIR-analyser (Nicolet™ iS20 FTIR Spectrometer, Thermofisher®, USA), and scanned through a 400 cm^{-1} to 4000 cm^{-1} wavelength range in the IR region. Various functional groups present in the feedstock and biochar were observed after plotting the transmittance intensity with respect to variations in the wavenumber.

3.8.5. X-ray diffraction (XRD)

X-ray diffraction (XRD) is a standard, non-destructive method used to probe how atoms are arranged in crystalline materials. When a monochromatic X-ray beam (commonly Cu Kα, λ= 1.5406 Å) strikes regularly spaced atomic planes, the scattered waves interfere constructively at specific angles that satisfy Bragg's law (equation 3.1).

$$n\lambda = 2d \sin\theta \qquad (3.1.)$$

Where d is the interplanar spacing, n is an integer. By recording the diffracted intensity as a function of 2θ, the resulting pattern of peaks is used to identify phases, determine lattice parameters and estimate crystallite size and macrostrain [200].

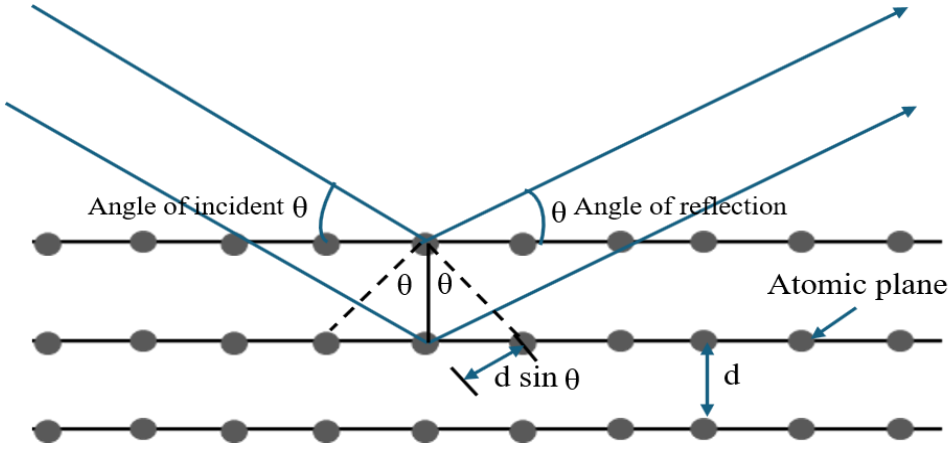

Figure 3.7: Braggs law of diffraction.

3.8.6. X-ray photoelectron spectroscopy (XPS)

X-ray photoelectron spectroscopy (XPS) or electron spectroscopy is widely used to determine the elemental composition, chemical bonding, and electronic states of materials. XPS work on the principle of the photoelectric effect, in which electrons are emitted from a material when it is exposed to radiation of sufficient energy. During the sample analysis, the surface of the sample is irradiated with monochromatic X-rays, which are commonly produced using magnesium (Mg Kα, 1253.6 eV) or aluminium (Al Kα, 1486.6 eV) sources. When the

incident X-rays interact with atoms at the surface of the sample, core electrons are ejected from the surface and produce photoelectrons. The kinetic energy of these emitted electrons is measured, and hence the binding energy can be calculated, which provides details about the elements present and their corresponding chemical environments. As XPS is very surface sensitive, it is a very useful and powerful tool for analysing the modification and functional groups of a maceral's surface [201].

3.8.7. Raman spectroscopy

Raman spectroscopy is a commonly used non-destructive chemical analysis method to study phase and morphology, chemical structure, crystallinity and molecular interaction. It works on the light scattering phenomenon in which light is scattered from the materials when high intensity laser is incident on it. Some of the scattered light differs in wavelength from the incident laser due to interaction with molecular vibrations within the material. This is called Raman Scatter.

A Raman spectrum consists of several peaks demonstrating the intensity of the scattered light as a function of wavelength or Raman shift. Each peak corresponds to a specific vibrational mode of a molecular bond or group of bonds, such as C-C, C=C, C-H, or N-O stretching, as well as more complex vibrations including ring breathing modes, polymer chain motions, and lattice vibrations. As a result, Raman spectroscopy serves as a powerful tool for identifying molecular structures and bonding characteristics [202].

3.8.8. Scanning electron microscopy (SEM)

Scanning electron microscopy (SEM) create images by passing a finely focused electron beam through a sample's surface. When these electrons hit atoms near the top layer, they generate some signals that show the morphology of the sample surface. The beam outlines a raster pattern, and detectors depict signals point-by-point to build the image. Standard SEM generally needs a high vacuum. SEM instruments are generally equipped with energy-

dispersive X-ray spectroscopy (EDS/EDAX) for elemental mapping. The beam excites characteristic X-rays from sample atoms; their energies and strengths tell us the presence and composition of various elements.

In this work, the biomass and biochar were analysed using FE-SEM. The devolatilization process during thermal cracking can affect the char-surface, forming voids. SEM-images can provide insight into the apparent surface morphology of biomass. The morphological studies were performed using a high-resolution scanning electron microscope (JSM 7900F, JEOL® Ltd., Japan) [203] [204].

3.8.9. Brunauer-Emmett-Teller (BET)

Specific surface area was determined using N_2 adsorption-desorption isotherms analysed by the Brunauer-Emmett-Teller (BET) method. Since smaller particles have higher surface area per unit mass, this property strongly influences the reactivity and performance of nanostructured materials in adsorption and catalysis. The adsorption–desorption data, plotted as adsorbed gas volume versus relative pressure (P/P_0), reveal characteristic isotherms that classify pore structure (IUPAC types I-VI) and provide quantitative textural parameters essential for materials optimisation [205] [206].

3.8.10. UV-VIS

UV-visible (UV-Vis) spectroscopy is a very common instrument used to evaluate dye adsorption performance from aqueous solutions of various dyes. The instrument passes the ultraviolet or visible light, which is then adsorbed by dye molecules in the solution due to electronic transitions within their chromophoric groups. Generally, most organic dyes show absorption maxima (λ_{max}) in the UV-visible region, which are directly related to their molecular structure. During adsorption experiments, a certain dosage of adsorbent is mixed in known concentration of dye solution and contacted for a specific time. After the adsorption time is over, the solution is separated using a centrifuge and its absorbance is measured using a UV-

Vis spectrophotometer at the dye's λ_{max}. According to the Beer-Lambert law, absorbance is directly proportional to the dye concentration within a certain range. By using the absorbance values before and after adsorption, the remaining dye concentration in the solution can be found. The difference between the two, the initial and final concentration values, is then used to calculate the adsorption capacity and removal efficiency.

UV-Vis spectroscopy is specifically suitable for adsorption studies because it is a quick, sensitive, and non-destructive method. It helps in continuous monitoring of adsorption kinetics and is often used to analyse isotherms, rate mechanisms, and equilibrium behaviour of dye adsorbent systems [207] [208] [209].

Next chapter is about pyrolysis and co-pyrolysis work of two biomass- rice straw and sugarcane bagasse for biochar production in pellet and powder form and evaluation of its properties for various application.

CHAPTER- 4

Pyrolysis of Rice Straw and Sugarcane bagasse for production of biochar

Abstract

The thermochemical conversion of agricultural wastes has been carried out to produce biochar. Rice-straw, sugarcane bagasse and their mixture in 1:1 weight ratio was used as feed for pyrolysis experiments carried out in a tube furnace. The processing temperature varied over 300°C-700°C, heating rate at 10°C/min. Analysis was carried out to determine elemental composition, higher heating value, thermal stability, functional groups, and surface morphology. The results demonstrated a synergic effect of co-pyrolysis on the mass and energy yield. The highest mass yield of 43.72 % was observed in the case of biochar produced from co-pyrolysis of rice-straw and bagasse at 300°C. The energy yield also increased slightly for the mixed biomass feed, compared to individual rice-straw and bagasse feeds. The pyrolysis of individual biomass showed that bagasse biochar produced at 700°C had the highest heating value of 23.01 MJ/kg and the lowest mass yield 20.13%. The low pyrolysis temperature was favorable for higher mass yield while higher temperature was favorable for higher energy yield. The thermogravimetric analysis was carried out at a single heating rate-10°C/min for rice-straw, bagasse, and mix feeds. The Coats-Redfern model was used to evaluate the activation energy for different feeds.

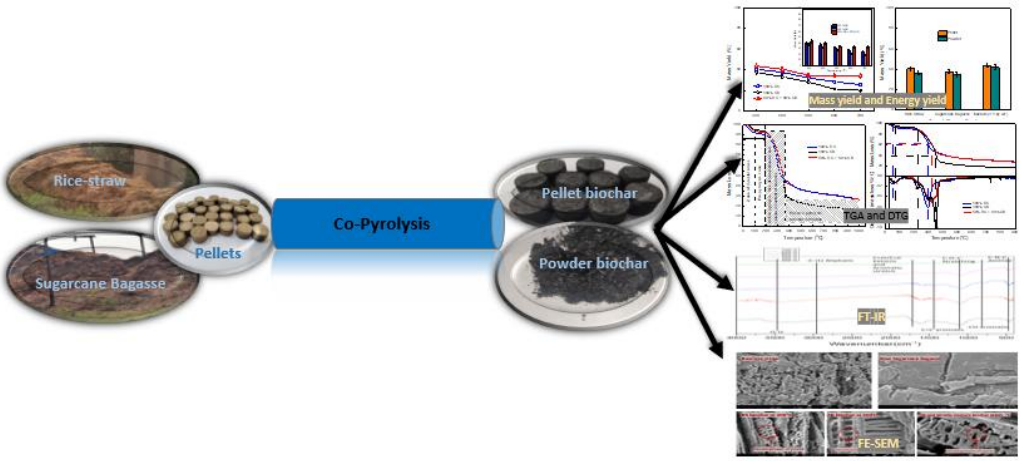

Figure 4.1a: Graphical Abstract.

4.1. Introduction

Agricultural activities produce large quantities of organic waste, or biomass, which can be a useful source of energy. The conversion of agricultural waste to produce energy is predominantly based on open combustion, which leads to undesirable emissions of carbon dioxide in air Advanced thermochemical conversion techniques such as gasification, and pyrolysis can be employed to extract energy from different biomass waste such as agricultural leftovers, agro-industrial waste, forest residues, garden waste, sewage sludge etc., with reduced CO_2 emissions [210]. Such a process that utilizes biomass waste materials as fuels, can potentially replace hydrocarbons combustion for energy generation. Furthermore, agricultural biomasses are composed of lignin, cellulose, and hemicellulose, which can be converted to useful chemicals through thermal conversion processes for further industrial applications. The development of a sustainable agri-waste management technology, however, depends on many factors; few of them include - (i) type of biomass feedstock, (ii) the industrial applications of the end-products, (iii) environmental standards, and (iv) the economic viability. The conversion of agricultural waste to energy and other value-added products has been considered as significant with respect to associated environmental and economic aspects. Thermochemical conversion techniques are preferred over biochemical processes because of their ability to process large quantities of feed at higher product yield. Among, thermochemical process, combustion, pyrolysis, and gasification have been employed widely [210] [160] [211].

Biomass pyrolysis and gasification have attracted significant interest in recent years for converting waste to useful products. Compared to combustion, pyrolysis is a process that can reduce emissions of harmful compounds in the environment. The products of pyrolysis such as CO_2, CH_4, and volatiles are often subjected to further conversion through gasification [160]. A

study of pyrolysis plant in China observed that ~41% of the total produced biochar is returned to the field leading to the net emission of greenhouse gas becoming zero -thus the complete carbon cycle can be considered renewable [212]. The economic potential and feasibility of commercialization of pyrolysis are under investigation by various researchers. The overall cost of the pyrolysis unit can be higher than the economic value of the product in few cases; however the upgradation of the overall process can result in attractive economic benefits by employing low-cost raw materials and transportations, and innovations in technology, as demonstrated by several studies[213] [214] [215]. Other than pyrolysis, available waste-to-energy technologies include biochemical conversion routes, torrefaction and hydrothermal carbonization [215]. Pyrolysis process is preferred technology due to higher yield, higher processing quantities of waste, and improved properties of product [216].

Gasification, which is another thermochemical waste-to-energy conversion technology, can also be employed for synthesis gas production which is used as a raw material for producing methanol and ethanol through Fischer-Tropsch process [217]. These alcohols can be further used as additives in motor-fuels. The gasification mainly consists of two steps - (i) devolatilization of biomass through pyrolysis resulting in the formation of char, and (ii) the reaction of char with a gas such as steam or carbon dioxide [218]. Biochar has been identified as one of the significant feedstocks for improved process efficiencies and enhancements in synthesis gas production through gasification [219]. It is obtained from biomass through the pyrolysis of pelletized or powdered raw material. Compared to raw biomass, biochar exhibits improved properties such as heating value and grindability which can subsequently lead to improvements in the synthesis gas production through the gasification [220]. Co-pyrolysis process involves heating simultaneously, two or more different raw materials mixed in varying weight ratios, at different temperatures - the temperature playing a crucial role in influencing the mass yield of produced biochar [221] [222]. In this study, the pyrolysis of rice-straw and

bagasse has been performed to produce biochar. The synergistic effects of co-pyrolysis were investigated under different experimental conditions.

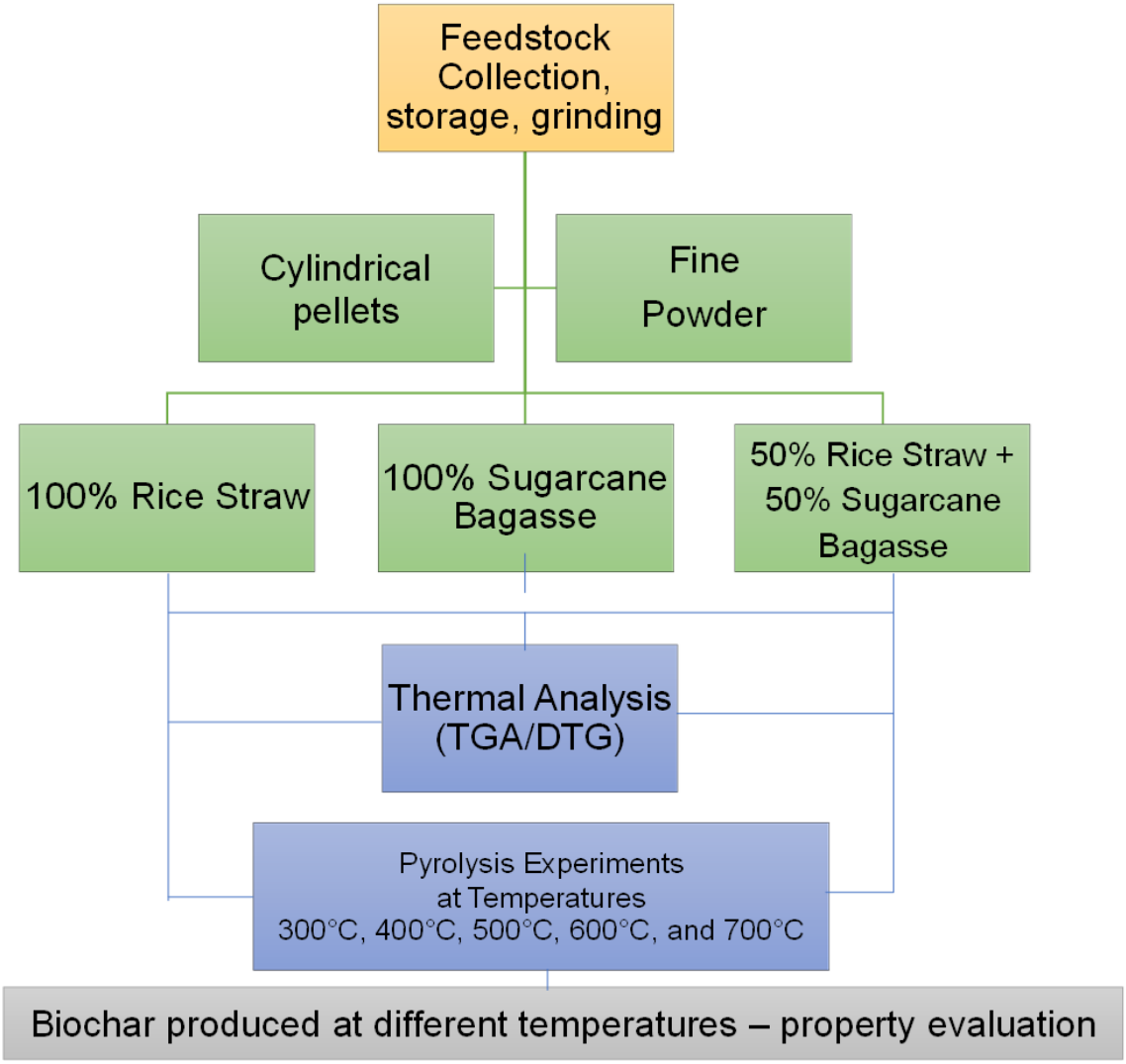

Figure 4. 1 : schematic diagram outlining the experimental methodology.

Figure 4.1 shows a schematic diagram outlining the methodology. The produced biochar was characterized for mass and energy yield, heating values, surface morphology, functional groups, and the presence of carbon, hydrogen, nitrogen, and sulfur elements. The results provide insight into the characteristics of biochar produced from rice-straw and bagasse waste obtained from farm areas in Northern India. Moreover, the results provide guidance for

the utilization of biochar obtained from rice straw and sugarcane bagasse biomass for gasification to produce synthesis gas.

4.2. Experimental methodology

4.2.1. Collection and preparation of feedstock

Rice straw was collected from the agricultural field in Amethi District, India. The sugarcane bagasse was obtained from a nearby sugar factory (KSCM Ltd., Sultanpur). The feed was dried to lower the moisture content to ~15 wt.%, ground and sieved in an RO-TAP® sieve shaker (85 mesh). The powder was stored in container to prevent it from absorbing excess moisture. Following samples were prepared- (i) rice-straw particles (100% RS), and (ii) sugarcane bagasse (100% SB). The prepared stock samples were mixed in 1:1 weight ratio (50% RS + 50% SB). Throughout this work the1:1 mixing ratio was kept constant to ensure an equal contribution of both biomass feedstocks and to investigate their synergistic interaction during co-pyrolysis under balanced conditions. If the biomass mixing ratio will be changed, the relative contribution of individual biomass components such as cellulose, hemicellulose and lignin will also change which may significantly influence product distribution, biochar yield, pore structure, and surface chemistry. The experiments were performed as follows - (i) in one process the feed was used in the powdered form without additional processing, and (ii) in the second process the feed was converted into cylindrical pellets of height and diameter of one centimetre using pelletizer *(Figure 4.2(a))*. Pelletization leads to the compaction of biomass of low mass density, which is also convenient for handling, storage, and transportation of the raw rice-straw. Both the pellet and powder forms of feedstock were prepared in sufficient quantity and kept in Ziploc® bags.

4.2.2. Pyrolysis of biomass

The pyrolysis and co-pyrolysis experiments were conducted in a quartz tube placed inside a tube furnace (Lindberg®, USA). The inner diameter of tube was 22 mm and outer

diameter was 25 mm. The length of the tube was 500 mm. The quartz tube was used for pyrolysis because it is a stable material at higher temperature as compared to glass, in which softening starts at lower temperature. The maximum operating temperature of furnace was 1200°C. A PID temperature controller, attached to the furnace, maintained the desired operating conditions. The schematic diagram of the tube furnace is shown *Figure 4.2(b)*.

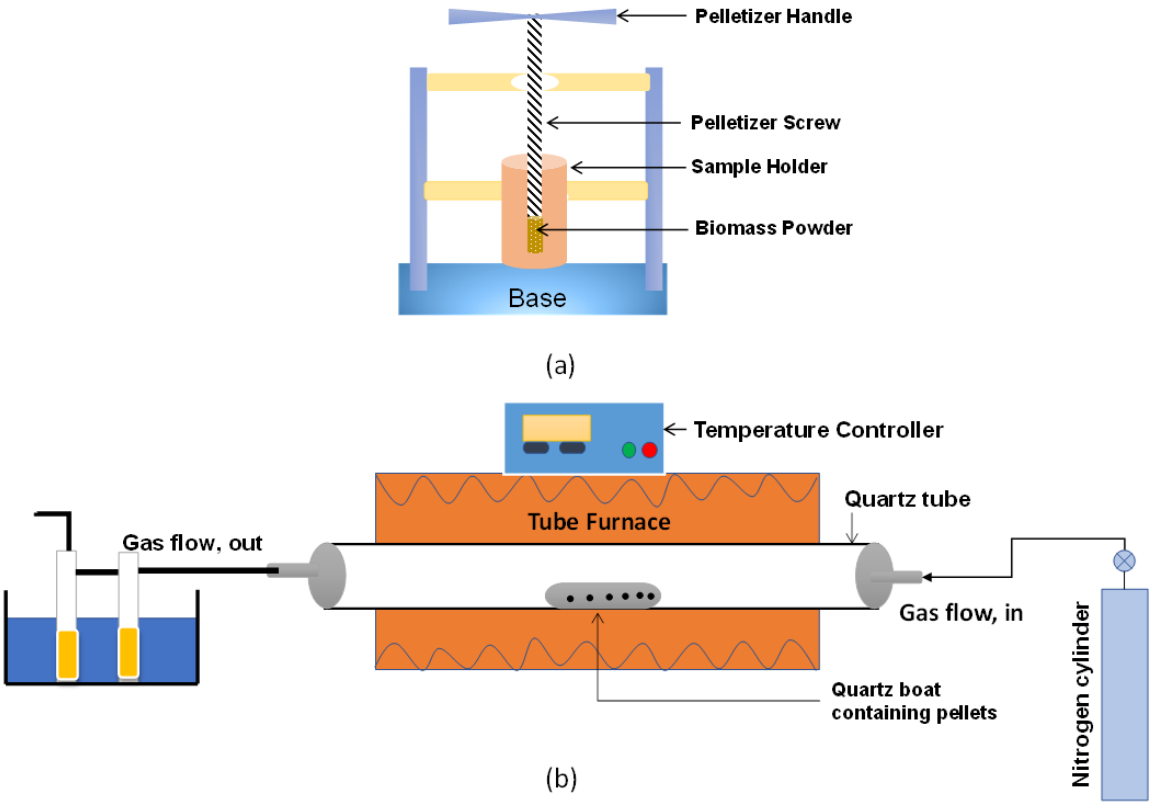

Figure 4. 2: (a) Schematic diagram of a hand pelletizer; (b) Schematic diagram of tube furnace pyrolysis.

The feedstock sample were taken in a boat and placed inside the quartz tube. Nitrogen gas of 99.99% purity (flow rate 100 mL min^{-1}) was continuously supplied to maintain the inert atmosphere. The gas flow also swept the product gases from the quartz tube thus avoiding the pressure build-up inside. All experiments were conducted in the range of 300°C-700°C at a fixed ramp-heating rate of 10°C/min and for a fixed duration (30 minutes). Literature data also show that residence time within the range of 10 to 100 min have only slight effect on biochar yield, thus short duration is sufficient to achieve high yield from pyrolysis [172].

The products obtained were - (i) liquid bio-oil, (ii) non-condensable gases, and (iii) the solid biochar. The gases- both condensable and non-condensable, were passed through a condenser kept at outlet. The produced solid biochar was taken out from the tube for further analysis.

4.2.3 Characterization and analysis

Mass yield, energy yield, and energy density ratio

The values of parameters -mass yield (Y_m)and energy yield (Y_E)for produced biochar, and the energy density ratios (EDR) of biochar were determined using relations given in equations 4.1 to 4.3 [223]:

The EDR is calculated using the Higher Heating Values, or HHV described in section 4.2.3.2. In equation (4.1), m_b is mass of biochar produced, and m_f is the mass of feedstock used for pyrolysis. In equation (4.2), H_b is the HHV of produced biochar, and H_f is the HHV of corresponding feed.

$$Y_m\% = \frac{m_b}{m_f} \times 100 \tag{4.1}$$

$$EDR = \frac{H_b}{H_f} \tag{4.2}$$

$$Y_E = Y_m \times EDR \times 100 \tag{4.3}$$

Higher heating value (HHV)

Calorific value of the biomass samples was obtained using a Bomb Calorimeter (HAMCO® India). A pellet of approximately one gram was made using a hand pelletizer and this pellet was placed inside the bomb calorimeter. The experiment was completed following

the standard procedure. Oxygen supply was given inside the instrument for combustion of the sample.

Elemental analysis

The compositions of elements such as carbon, hydrogen, nitrogen, and sulfur (CHNS) were determined using an organic elemental analyzer (UNICUBE®, India). The oxygen content in the sample can then be obtained by subtracting the overall percentage of CHNS from 100.

Morphology study through field emission scanning electron microscopy (FE-SEM)

Devolatilization process during thermal cracking can affect the char-surface, forming voids. SEM-images can provide insight to the apparent surface morphology of biomass. The morphological studies were performed using a high-resolution scanning electron microscope (JEOL® Ltd. Japan).

Fourier-transform infrared spectroscopy (FTIR)

FTIR analysis can be used to observe the distribution of various functional groups in the feedstock and the biochar. Five milligrams samples were weighed and mixed with potassium bromide. The resulting mixture was compressed to form a very thin pellet and placed inside the FTIR-analyzer (Nicolet™ iS20, Thermofisher®, USA), and scanned through 400 cm-1 to 4000 cm-1 wavelength range in the IR region. Various functional groups present in the feedstock and biochar were observed after plotting the transmittance intensity with respect to variations in the wavenumber.

Thermogravimetric analysis (TGA/DTG)

Thermal analysis of RS, SB, and their mixture, RB was performed using thermogravimetric analyzer (PerkinElmer®, UK). Crushed biomass (near about 10-12 milligram weight) was taken and placed inside the crucible fitted to the weighing balance in the TGA furnace. The system was purged with nitrogen gas continuously at a flow rate of 50 mL/min to maintain

oxygen free inert-condition within the reaction chamber. Finally, the samples were heated from ambient to 1000°C at a heating rate of 5, 10, 20, and 40°C/min. When the temperature reached 1000°C, the sample was held for 10 minutes to confirm complete conversion.

4.2.4. Kinetic modelling

Thermal degradation of biomass under pyrolytic conditions is a complex process because at high heating rate, the decomposition is a non-equilibrium process; the devolatilization of biomass to form solid char and gaseous matters may be written as [224]:

$$\underset{\text{solid}}{\text{Feedstock}} \xrightarrow{k} \underset{\text{solid}}{\text{char}} + \text{volatile matter} \tag{4.4}$$

Considering that the biomass-decomposition during thermal degradation can be represented by a single model and activation energy, the disappearance of feedstock is expressed as [224] [225]:

$$\alpha = \frac{m_0 - m_i}{m_0 - m_f} \tag{4.5}$$

where α is the decomposition factor representing the degree of mass-conversion, m0 is the initial mass of biomass, mi is the mass at some instant, and mf the final mass present in the reaction chamber. Coats and Redfern have developed a simple kinetic expression to relate the kinetics of mass-decomposition of a solid, i.e, α with respect to time, given by the following rate-expression [224]:

$$\frac{d\alpha}{dt} = k.(1-\alpha)^n \tag{4.6}$$

where t is time and α is the model representing the kinetics of decomposition and n is the reaction-order. In equation (6), k is the temperature-dependent rate constant term given by the following expression [224]:

$$k = Ae^{(-E_a/RT)} \tag{4.7}$$

where E_a is the activation energy term, A is the pre-exponential factor, R is the universal gas constant, and T is the reaction temperature in Kelvin. The term β is the constant heating rate and is given by:

$$\beta = \frac{dT}{dt} \tag{4.8}$$

Thus, equation (4.6), (4.7), and (4.8) can be rearranged and integrating as follows:

$$\int_0^{\alpha} \frac{d\alpha}{(1-\alpha)^n} = \int_0^{T} \frac{A}{\beta} e^{(-E_a/RT)} dT \tag{4.9}$$

The equation (4.9) has been integrated for n=1 and n≠1 , as follows [224]:

for n = 1,

$$\mathbf{log}_{10}\left[\frac{-\mathbf{log}_{10}(1-\alpha)}{T^2}\right] = \mathbf{log}_{10}\left[\frac{AR}{\beta E_a}\left(1-\frac{2RT}{E_a}\right)\right] - \frac{E_a}{2.3RT} \tag{4.10}$$

For n≠1,

$$\mathbf{log}_{10}\left[\frac{\left(1-(1-\alpha)^{1-n}\right)}{T^2(1-n)}\right] = \mathbf{log}_{10}\left[\frac{AR}{\beta E_a}\left(1-\frac{2RT}{E_a}\right)\right] - \frac{E_a}{2.3RT} \tag{4.11}$$

For lower temperature ranges for example, 200 - 350°C where most of the degradation of biomass was observed, it can be considered that $\frac{2RT}{E_a} \ll 1$, and therefore the logarithmic term can be assumed to be nearly constant [224]. With this simplification, the LHS of equations

(4.10) and (4.11) can be plotted with respect to $\frac{1}{T}$, and from the slope of the resulting line, the value of activation energy can be determined.

4.3. Results and discussions

4.3.1 Mass Yield

Figure 4.3(a) shows the mass yield of biochar at different temperatures. The pyrolysis results of feedstock samples shows that the mass yield of produced biochar varied for each sample at a given pyrolysis temperature. For all samples, the maximum value of mass yield was obtained at 300°C. The observed values were 40.65%, 43.72% and 37.5 % for RS, RB and SB samples respectively. The biochar yield of RS varied from 40.65% at 300°C to 25.78% at 700°C. In the same temperature range, the biochar yield of SB and RB decreased from 37.50% to 20.13% and 43.72 to 34.40.

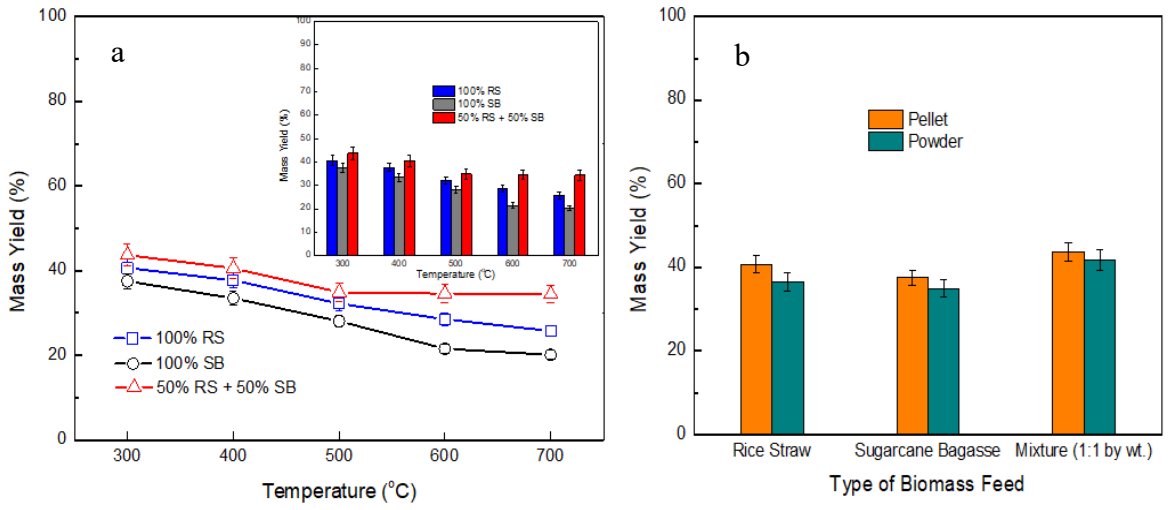

Figure 4. 3 : (a) Variations in mass yield of biochar with temperature for three different feeds (pellet form); inset shows comparative yields at a particular temperature; (b) Changes in mass yield of biochar at 300°C for pellet feed and powder feed.

The mass yield for SB showed the maximum decrease of 46.32% when the pyrolysis temperature increased from 300°C to 700°C. The inset of Figure 4.3(a) shows the comparative analysis of respective mass-yields. It is important to note here that when the RS and SB were

mixed in weight ratio of 1:1, the biochar yield was the highest among all the three feedstocks at all the pyrolysis temperatures, whereas the same was the lowest for SB feed. The results indicate that there could be a synergetic effect of mixing rice straw and sugarcane bagasse for biochar formation.

The reduction in the mass yield values with temperature has also been reported in the literature [226]. The results show that the higher pyrolytic temperatures negatively affect the mass yield of biochar. The loss of more volatile matter at higher temperatures, dehydration, and thermal decomposition of lignin and cellulose into lower molecular weight gaseous and liquids (bio-oil) could be the reason behind the decrease in the respective mass yield of biochar [226]. Literature shows higher lignin content in the biomass leads to more solid biochar after pyrolysis, whereas cellulose and hemicellulose result in the production of volatile chemicals [227]. In our biomass the lignin, cellulose and hemicellulose concentrations were respectively 21.7%, 35.2% and 27.3% respectively for RS and the respective concentration for SB were 20.9%, 43.2%, and 26.5%. The typical values of lignin, cellulose and hemicellulose range from 15-25%, 30-49% and 20-30% in biomass, as reported by various authors [228] [229] [230] [231].

Pelletization of rice straw leads to the densification of feed, which should increase its mass yield value when subjected to pyrolysis [232]. Both the pelletized, and powdered rice-straw feed were therefore subjected to pyrolysis to observe its effects. Figure 4.3(b) shows that the RS, SB and their mixture RB when pyrolyzed in loose powder form for biochar production, resulted in relatively lower mass yield than their pellet form of biochar. For example, SB pellet biochar mass yield at 300°C was 37.5 % while at the same temperature the mass yield of powder biochar was 34.90%. The reason for this decrease in the mass yield of powder form of biochar might be the larger gap between the particles which would have facilitated the escaping of volatiles thus lowering the condensation of condensable gases inside the particles.

4.3.2 Higher heating value (HHV) and EDR

The HHV and the EDR values are given in Figure 4.4 (a). The heating values for raw feedstocks and their respective biochar produced at different pyrolysis temperature are presented on left-y-axis against the temperature plotted on the bottom-x-axis. The EDR values are calculated using equation (4.2) and plotted on right-y-axis against the common bottom-x-axis for temperature.

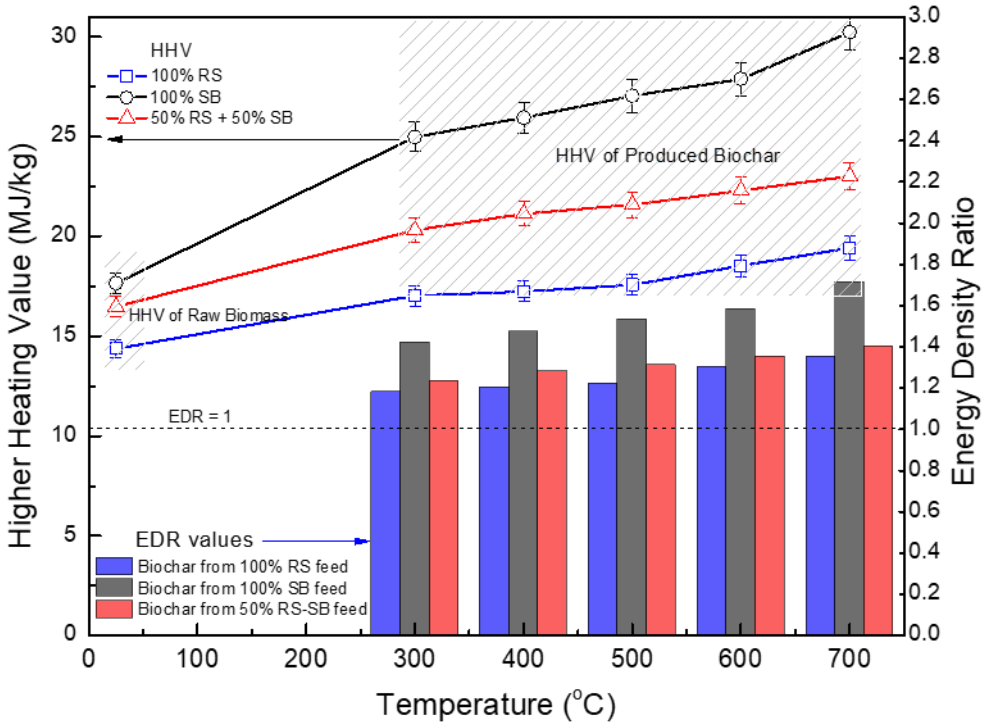

Figure 4. 4 (a).: Variations in HHV and EDR of produced biochar with temperature.

The HHV of the three feedstock samples were 14.37, 17.66 and 16.49 MJ/kg respectively. For SB, the HHV are highest among the three feeds - it was 17.66 MJ/kg for raw feed which increased to 24.99 and 30.24 MJ/kg for its biochar produced respectively at 300°C and 700°C. Thus, from energy vector point of view SB shows excellent results among all.

Table 4.1: Elemental compositions of different types of biomass feed.

Sample	Element Composition (%)				Ratio of Carbon to Hydrogen
	Carbon	Hydrogen	Nitrogen	Sulfur	
RS	36.27	5.27	1.04	0.14	6.88
SB	44.06	6.41	0.39	0.16	6.87
RB (50% RS + 50% SB)	39.37	6.04	0.52	0.12	6.52

It can be further observed that the HHV of biochar produced for all three feedstocks increased with respect to the rise in the pyrolysis temperature. This trend could be because of the higher C/H ratio of the biochar as high C/H ratio is linked with higher energy content of the material. The C/H ratios are shown in Table 4.1 and discussed in Section 4.3.4 in the subsequent text. The significant observation from the EDR calculations was that the SB biochar produced at all temperatures had the highest values among all the biomass samples – which could be attributed to the higher HHV of sugarcane bagasse feedstock.

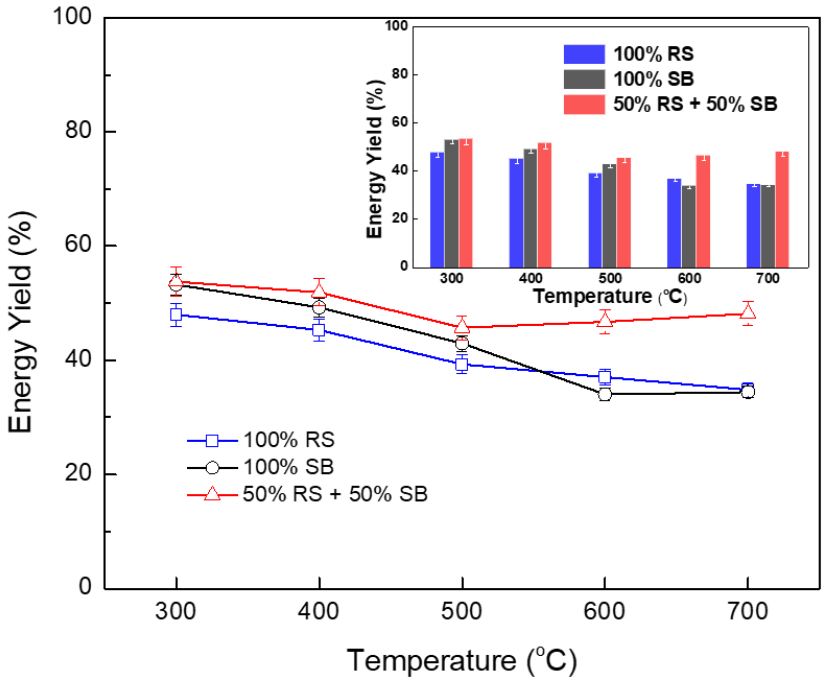

Figure 4.4 (b).: Variations in the energy yield with temperature for three different feeds; inset shows comparative energy yields for different feeds at a particular temperature.

4.3.3 Energy yield

The energy yield of the biochar is given in Figure 4.4(b); calculated using equation (4.3). For RS samples, the energy yield decreased with the increase in pyrolysis temperature throughout. The SB and RB (mixture) feed samples also exhibited the decreasing trend at lower temperatures, however, the energy yield remained almost unchanged for the two samples at higher temperatures. For SB, the energy yield was observed to decrease till the temperature reached 600°C and remained nearly constant with further rise in temperature to 700°C. For mix feed RB slightly increasing trend in energy yield was observed in the temperature range of 500-700°C - it was ~54% at 300°C which decreased to ~46 % at 500°C and then increased slightly to ~48% at 700°C. The slight increase in the energy yield of RB biochar in the mentioned temperature range (500-700°C) may be attributed to the much higher values of EDR of SB compared to the EDR of RS sample.

At a particular pyrolysis temperature, the energy yield was highest for RB biochar produced at 300°C while it was lowest for RS and SB biochar produced at 700°C. The highest decrease in energy yield was observed for SB samples (from ~53% to ~35%) in the pyrolysis temperature range of 300 -700°C, whereas for the same temperature range, the RB samples had the lowest decrease of ~10.5% in the reported values. The decrease in energy yield of biochar with increase in temperature could be because of the devolatilization, and thermal decomposition of lignin and cellulose from the biomass at higher temperatures, which is consistent with the earlier reported results [148]. Further, the decrease in the mass yield of biochar with increasing pyrolysis temperature is also responsible for the decreased energy yield [223].

4.3.4 Elemental composition of raw feed and produced biochar

The elemental composition with respect to carbon, hydrogen, nitrogen, and sulfur of biomass feedstock and their biochar were determined using the organic elemental analyzer

(refer Section 4.2.3.3). The values are presented in Tables 4.2. The primary constituent elements of biomass are carbon and hydrogen. Nitrogen and sulfur are also presented in very low amounts, in addition to some trace elements. Expectedly, the values of carbon composition were observed to be highest -respectively at 36.27%, 44.06%, 39.37% for the three raw feeds (Table 4.2(a)).

The effect of pyrolysis on elemental composition in the RS feed was determined. When the raw RS feed was pyrolyzed at 300°C, the carbon composition of the produced biochar increased up to 52.68. It was further observed that when the pyrolysis temperature was increased, the carbon composition in the produced biochar also showed an increasing pattern. For different temperatures of 400, 500 and 600°C, the carbon composition in the rice straw (RS) feed was measured to be 54.45%, 56.12%, 60.09% respectively, after the pyrolysis. Thus, the pyrolysis process enhances the carbon concentration in produced biochar. The increasing trend of carbon percentage with increase in pyrolysis temperature has been reported [172]. The increase in temperature slightly affects the hydrogen composition which shows a decreasing trend, whereas there is negligible effect on nitrogen and sulfur compositions.

Table 4.2 (a): Effect of temperature on the elemental composition (RS).

Sample	**Pyrolysis Temperature (°C)**	**Elemental Composition (%)**				**Ratio of Carbon to Hydrogen**
		Carbon	Hydrogen	Nitrogen	Sulfur	
Raw RS	--	36.27	5.27	1.04	0.14	6.88
Biochar from RS feed	300	52.68	4.15	1.04	0.21	12.71
	400	54.45	3.40	1.17	0.18	16.06
	500	56.12	2.50	0.84	0.13	22.44
	600	60.09	2.12	0.81	0.15	28.42

Table 4.2 (b): Elemental composition in the SB biochar at 400^{0}C (powder and pellet).

Sample	Elemental Composition (%)				Ratio of Carbon to Hydrogen
	Carbon	Hydrogen	Nitrogen	Sulfur	
Raw SB	44.06	6.41	0.39	0.16	6.87
Biochar from SB Pellet	56.21	3.36	0.94	0.21	22.44
Biochar from SB Powder	70.35	3.38	0.6	0.11	28.42

The higher carbon concentration in biochar produced at relatively higher pyrolysis temperature may possibly be due to the higher carbonization rate as well as formation of new stable aromatic carbon rings. The biochar obtained at higher temperatures has higher number of C-C bonds compared to C-O and C-H bonds, thus increasing the C/H and C/O ratios due to decarboxylation and dehydration of lignocellulosic components. The biochar produced from the co-pyrolysis of RB mixture shows the increasing pattern of C/H ratio with the rise in co-pyrolysis temperature. This can be attributed to the increased aromatic and stable carbon as a result of some transformation reactions of unsaturated carbon at higher temperatures. Higher C/H ratio is linked with the greater energy content of the materials that also reflects the loss of low energy bonds like C-H & C-O, and formation of high energy bonds like C-C [174]. This can be observed in FTIR results of the biochar. Moreover, the biochar of mixture (RB) produced at 700°C pyrolysis temperature, has the highest HHV which also confirms the presence of high energy bonds in biochar produced at higher temperature. Besides the increase in carbon content the decrease in hydrogen composition in the biochar produced at higher temperatures might be because of the loss of more hydrocarbons, water vapors, H_2, CO_2, and CO through the formation of synthesis gas during the pyrolysis process [223]. Further, the nitrogen percentage did not show specific pattern with the increase in co-pyrolysis temperature for all the samples.

The elemental compositions of all the produced biochar from pellets as well as from powdered feed for sugarcane-bagasse pyrolyzed at a temperature of 400°C were also determined (Table 4.2(b). The carbon percentage was found to increase after pyrolysis. The higher concentration of carbon in biochar might be linked with well-developed transformation

reactions of unsaturated carbon that results in increased aromaticity and stability of carbon in biochar [174].

It may be noted here that carbon concentration is higher in the biochar produced from powder feed, than in the biochar produced from the pelletized feed. Literature shows that the surface area per unit mass of the biochar produced from crushed biomass is higher compared to the pelletized biomass [232]. This may lead to higher release and subsequent more loss of volatile matter in powder than in pellets, thus increasing the final carbon composition after the pyrolysis [232]. Further studies on this aspect of biochar are important with respect to the utilization of biochar for gasification. It is also noteworthy that, as mentioned earlier in Section 4.3.1, the mass yield of powder feed when subjected to pyrolysis was lower compared to that from the pelletized feed. It is important to mention here that pellets may have other advantages over powdered biomass. The loosely structured rice-straw biomass as received from the farms, may not be suitable for further uses in thermochemical conversion processes employing large-size equipment. Densification process leads to increase in the energy density and thermal stability, and makes the feed suitable for bulk applications in high temperature gasification process [148].

4.3.5 Thermogravimetric analysis (TGA)

The thermal degradation of RS, SB, and RB biomass under inert gas atmosphere are shown in Figures 4.5(a) and 4.5(b), as a function of temperature, at the heating rate of 10°C/min. Heating rate can influence the pyrolysis of biomass- as the rate is increased, the onset temperature of devolatilization also increases. However, beyond the rate of 10°C/min the shift in devolatilization onset temperature is confined within a narrow range - heat and mass transfer effects are also minimized at slow heating rates [233].

Under pyrolytic conditions, biomass degradation consists of three main steps-(i) moisture loss, (ii) active pyrolysis, and (ii) passive pyrolysis [233]. From Figure 4.5(a), the

observed mass loss for RS is approximately 10% when the temperature reaches slightly above 100°C, whereas for SB and the RB feeds, the mass losses are in the range of approximately 6-7%. This loss corresponds to the evaporation of moisture content in the feed.

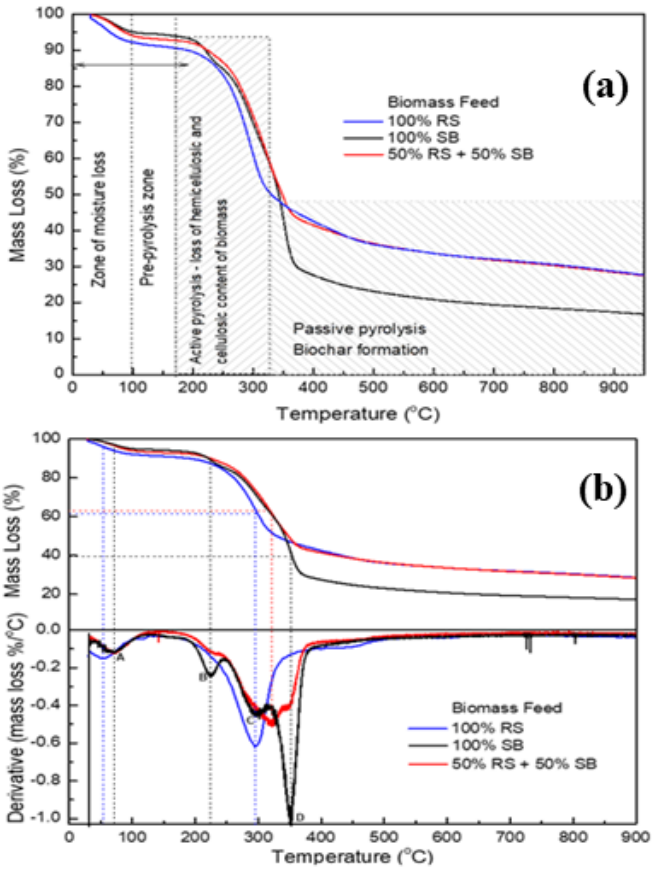

Figure 4. 5: ***(a):*** *TGA under non-isothermal conditions.* ***(b)*** *:DTG analysis for three biomass feeds.*

In the temperature range 100-210°C, the losses for all samples were observed to be approximately 12% of the initial weight. In this pre-pyrolysis zone, the remaining bound moisture within the biomass is lost. Thereafter, with further rise in temperature to 322°C the mass loss for RS was observed to be approximately 49% for RS. Similarly, for SB feed the mass loss was nearly 70%, whereas it was approximately 57% for SB feed, as the temperature reached 369°C. Thus maximum mass loss in all the samples was confined within the temperature range 200-400°C (active pyrolysis zone [233]. Beyond 400°C, the remaining biomass is converted to biochar with high carbon. The decomposition of lignin content of

biomass begins after the moisture loss is complete, i.e. beyond 200°C and continues till the end. The derivative thermogravimetry (DTG) analysis for all the feed samples are presented in Figure 4.5(b). For rice straw feed, the first trough occurs at approximately 55°C indicating the highest rate at which moisture is lost from the biomass. The maximum rate of mass loss for RS occurs around 300°C, beyond which the rate decreases. Thus, it may be concluded that at approximately 300°C, the decomposition rate of cellulose and hemicellulose content is maximum, indicating active pyrolysis.

On the other hand, four numbers of distinct troughs are observed for sugarcane bagasse. The two troughs designated by letters "B" and "C" for SB curve may be attributed to the decomposition process of hemicellulose and cellulose - the two components degradation does not occur simultaneously but sets at different temperatures during the active pyrolysis. The rate of mass loss again shows a local maximum at approximately 300°C (shown by letter "C"), indicating a sudden increase in the volatilization rate because of prevailing physical condition of the SB biomass. This may be attributed to local high mass transfer rates during the formation of porous structures within the decomposing biomass. At point "D", the maximum rate of mass-decomposition for SB occurs at around 350°C during the active pyrolysis process. Literature suggests that at higher heating rates, the separate troughs may disappear because of simultaneous decomposition of hemicellulose and cellulose, and the temperature of biomass can increase much quickly than the rate of devolatilization, thus overlapping the separate troughs [225].

The co-pyrolysis of RB feed shows a similar trend as shown in figure 4.5(b). One important observation is that co-pyrolysis of rice straw and sugarcane bagasse results in much lower mass loss compared to that observed for pure bagasse feed. This observation is also supported by the mass-yield results shown in figure 4.3 (a).

4.3.6. Kinetic analysis

From the thermogravimetric data, the extent of conversion given by equation (4.5) is plotted with respect to the temperature, as shown in figure 4.6(a). The rates of conversion for SB and mix biomass feeds show a similar trend within the narrow temperature range 200-380°C. For RS feed, slightly higher decomposition rates of conversion are observed compared to the other feeds. The Coats-Redfern (C-R) model given by equation (4.10) for reaction order n = 1, and equation (11) for n = 0.5, and 1.5 are plotted in Figure 4.6(b) for the corresponding TGA data for different feeds. The values are plotted with respect to the reciprocal of temperature multiplied by a factor of 1000, where Y represents the corresponding right hand side expressions within the parenthesis as given in the equations (4.10) and (4.11). The temperature range in the model analysis was chosen from approximately 230°C to 300°C during which the RS feed demonstrated the highest conversion rates.

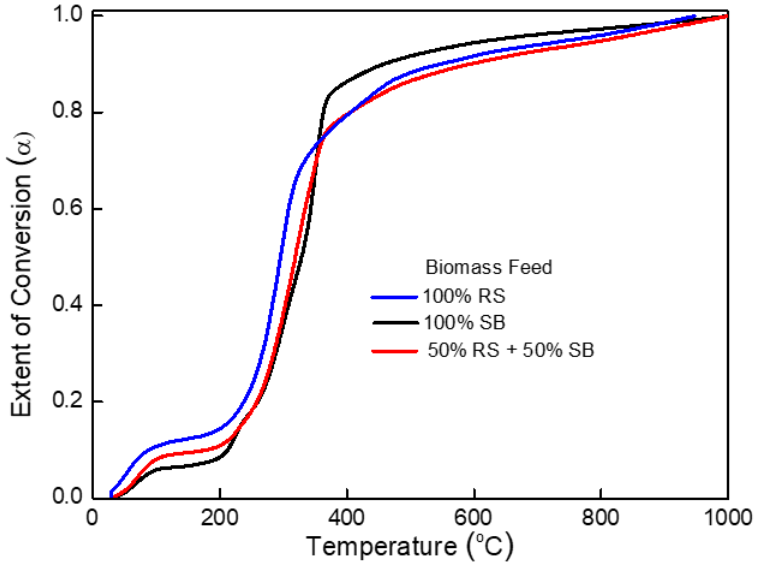

Figure 4. 6(a): Variations in the extent of conversion (α) of biomass with respect to temperature, at heating rate of 10°C/min.

Thus, for comparative analysis, the same range was chosen for other feeds as well. In this study, the feed type used in TGA analysis was powder (for all samples) However, the activation energy, E_a and the pre-exponential factor, A are understood to vary respectively, with

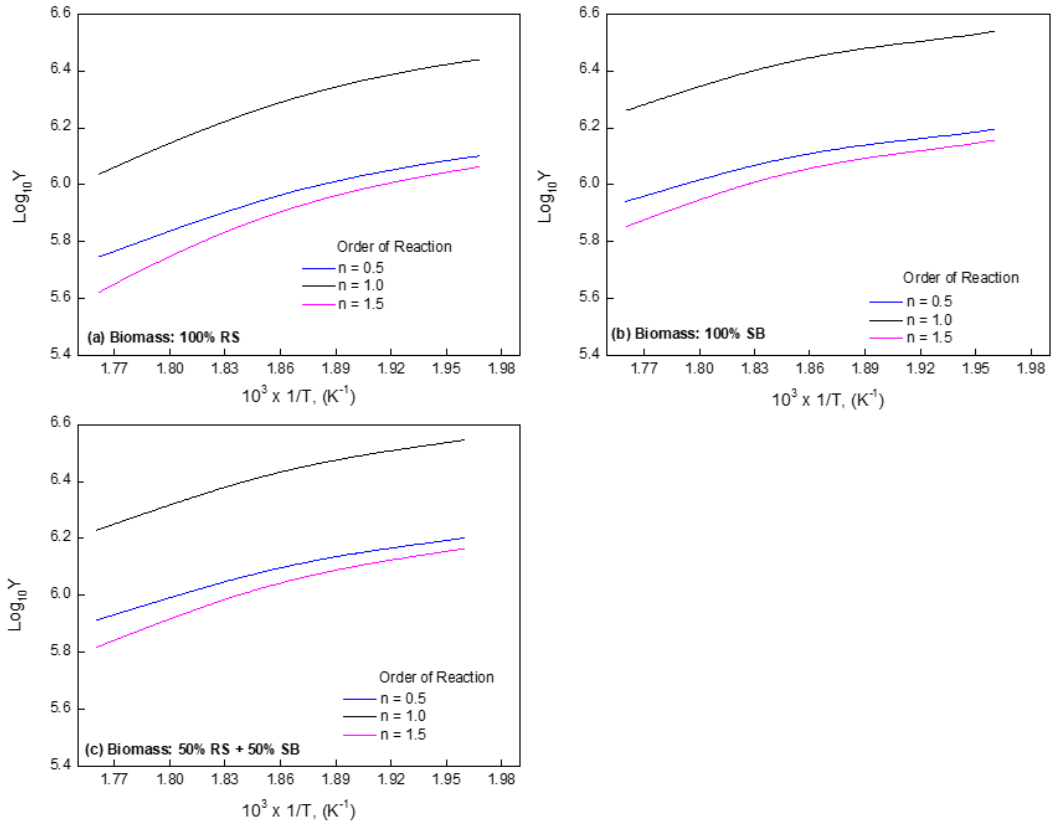

Figure 4. 6(b): Kinetic Analysis - Fitting of Coats-Redfern equations for different values of reaction order. [The Y-values on y-axis are given by equations (4.10) and (4.11).

Table 4.3: Calculation of E and A by Coats-Redfern Model during Thermal Degradation of Feed.

Biomass	**Selected Parameters**	**Order of Reaction, *n***	**Activation Energy, *E*** **(kJ mol^{-1}**	**Pre-exponential Factor, *A*** **(min^{-1})**
100% RS	• Temperature Interval: 238-295°C • Heating Rate: 10°C/min	0.5	33.24	20582.00
		1.0	37.52	18679.23
		1.5	40.57	4170.66
100% SB		0.5	23.77	172498.32
		1.0	26.02	246636.32
		1.5	28.37	64632.94
50% RS + 50% SB		0.5	30.52	102540.64
		1.0	27.91	78138.71
		1.5	33.27	24540.86

the physical structure of biomass feeds and their reactivity behavior; literature suggests that pelletization process can increase both E and A values significantly [30]. The values of E and A calculated from the C-R model for the powdered feed are given in *table 4.3.*

4.3.7. FT-IR analysis

The IR spectra demonstrate the different functional groups present on the surface of the produced biochar. In Figure 4.7, the band until wavenumber 3435 cm^{-1} is due to the -OH group stretching, and the band gap between 2945 to 2916 cm^{-1} is because of the -CHn stretching [174]. The increase in temperature can lead to the occurrence of decarboxylation and dehydration during pyrolysis, thus may decrease OH and C=O vibrations.

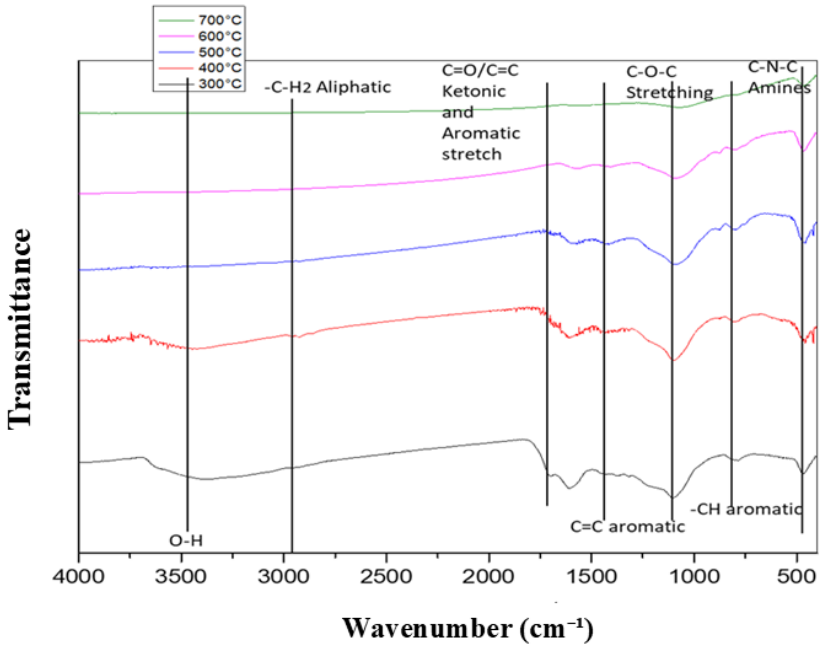

Figure 4. 7: FT-IR spectra of biochar (RB) at different temperature.

The presence of ketones and carboxylic stretching is within the spectra range of 1740-1700 cm^{-1}. The presence of aromatic hydrocarbons was indicated by C=O and C=C stretching in the band gap of 1650-1600 cm^{-1}. Strong presence of C=C in the aromatic ring was observed in biochar produced at lower temperature which is consistent with hydrogen-to-carbon ratio result. This vibration almost disappeared when the pyrolysis temperature was above 600°C.

The absence of aromatic C=C vibration in the FTIR spectra of biochar obtained at increased temperatures was in accordance with their low hydrogen-to-carbon ratio. The C -O -C stretching observed, can be recognized in the range of wavenumbers from 1300 cm^{-1} to 1100 cm^{-1}.

4.3.8. Field emission scanning electron microscopy (FE-SEM)

The morphological analysis of raw feedstock and the produced biochar produced after pyrolysis at different temperatures were carried out to investigate the corresponding changes in the surface topography (figure 4.8). The morphology of raw RS and SB (feedstock materials) are highly disordered. However, in the biochar the pores are clearly developed. The surface of material becomes rough as volatiles escape and remarkable increase in the number of pores on the surface is observed. BET surface area analyser is generally used to investigate the pore structure and adsorption characteristics of biochar materials in details. could act as an ideal nutrient adsorption site when biochar is used for soil application.

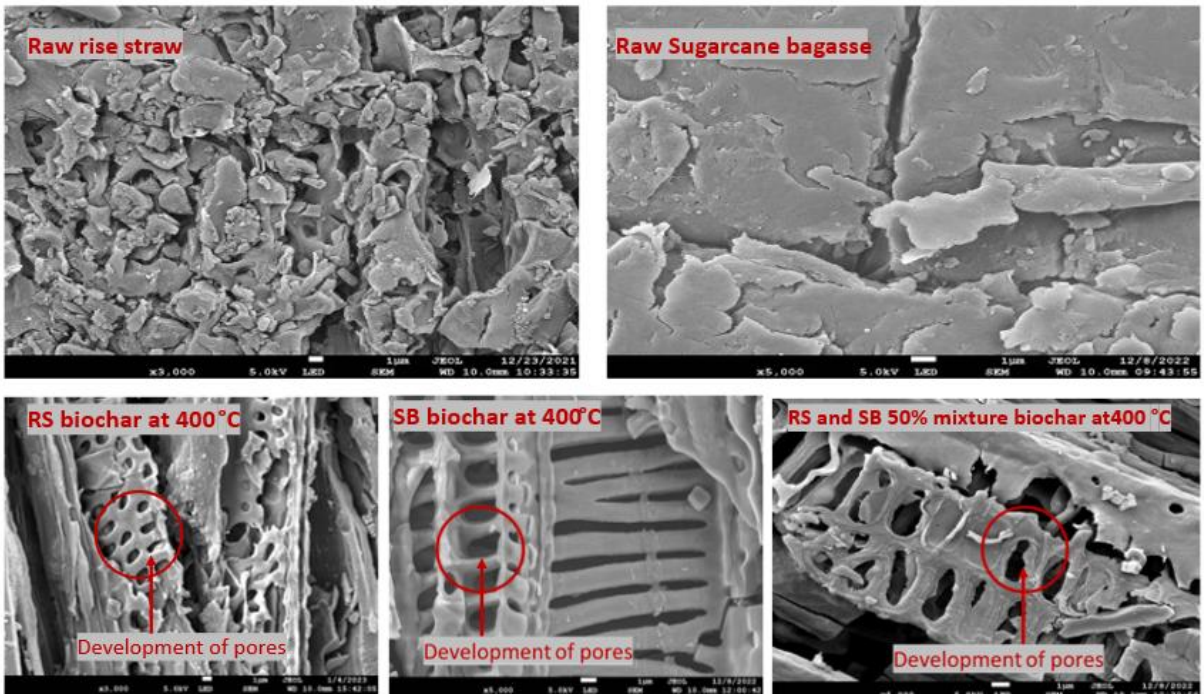

Figure 4. 8: FE-SEM images of different raw feeds and their biochar produced at 400°C.

The formation of porous char is highly desirable during thermochemical conversion processes - when char is used to produce synthesis gas through gasification process at elevated temperatures [220]. Porous structure of biochar is also desirable for agricultural applications, and in the production of useful material through biochemical conversion routes. The well developed and enlarged pores

4.4. Conclusions

Rice straw and sugarcane bagasse biomass are the waste generated during the processing of agricultural produce. In the context of generating useful products by harnessing the waste resources through technological intervention, the development of a conversion process is necessary. The objective of this work was to study the development of a thermochemical conversion route to convert the otherwise menacingly agricultural waste into some form of usable entity. Pyrolysis and gasification routes can be potentially employed to produce synthesis gas from rice-straw and bagasse. However, the large material volume, low density, loose structure, and associated cost for collection and feedstock preparation are some of the challenges that should be addressed prior to a high temperature conversion route for rice straw biomass. In this work, the loose rice-straw feed was used in powder, as well as in pelletized form. When subjected to pyrolysis, the mass yield of low-density rice-straw should be high for the produced biochar to be used in gasification. The feed was also mixed with the sugarcane bagasse, to evaluate the enhancements in the quality of produced biochar. A few of the important outcomes that can be drawn from this study are summarized below:

1. The maximum mass yield of biochar was obtained at 300°C. A decreasing trend in mass yield and energy yield was observed with the rise in pyrolysis temperature. This tendency of decreased mass and energy yield can be attributed to more decomposition of macro-components of biomass at a higher temperature.

2. The mass yield of biochar produced from individual biomass was the lowest for SB and the highest yield was obtained in the case of a mixture of RS and SB. In the case of SB, the lower yield was due to the easy emission of CO_2 from the surface and lower lignin content than the rice straw as lignin help to decelerate the pyrolysis which may be a reason for higher mass yield. The RS and SB mixture pyrolysis gave the highest biochar yield that reflects the synergic effect of mixing the two biomasses.

3. The pyrolysis of powdered form or loose biomass shows lower mass yield, but higher carbon content compared to the pelletized form. Rice straw, powdered and mixed with bagasse, was easier to convert into pellet form. Subsequently, produced biochar was also in pellet form which appeared stable enough through visual observation. A mix-feed, instead of pure rice straw feed, should therefore be a better option for subsequent applications in the gasification process.

Similar pyrolysis work has been discussed in next chapter. The feedstock used is rice straw and mustard-oil-residue, pellet form of biochar was prepared, and calorific value have been highlighted for energy use. First time here, mustard-oil-residue is being used for co-pyrolysis with rice straw.

CHAPTER- 5

Pyrolysis of Rice straw and Mustard-Oil-Residue for sustainable applications

Abstract

This work presents an insight into the biochar properties of rice straw (RS), mustard-oil residue (MR) and its blended feedstocks obtained from pyrolysis. Pyrolysis experiments for these feedstocks have been conducted between 300-600°C in a tube furnace for a fixed residence tie of 30 minute and resulted biochar has been analyzed for its thermal and physio-chemical properties such as mass yield, energy yield, higher heating value, surface morphology, functional groups and thermogravimetric analysis. The low pyrolysis temperature was favorable for higher mass yield and the high pyrolysis temperature was favorable for higher heating value of the biochar. Among the selected feedstocks MR showed comparatively higher mass yield and higher heating values for any particular pyrolysis temperature. The feedstock blending (RS:MR) in 7:3 (wt./wt.) was optimal as depicted in the results. Highest mass yield was for MR biochar (53.59%) produced at 300°C and the lowest for RS biochar (28.5%) produced at 600°C. The MR biochar has the highest energy content among all feedstock samples as reflected in its HHV results which were 18.35 and 26.19 MJ/Kg for biochar sample obtained at 300 and 600°C

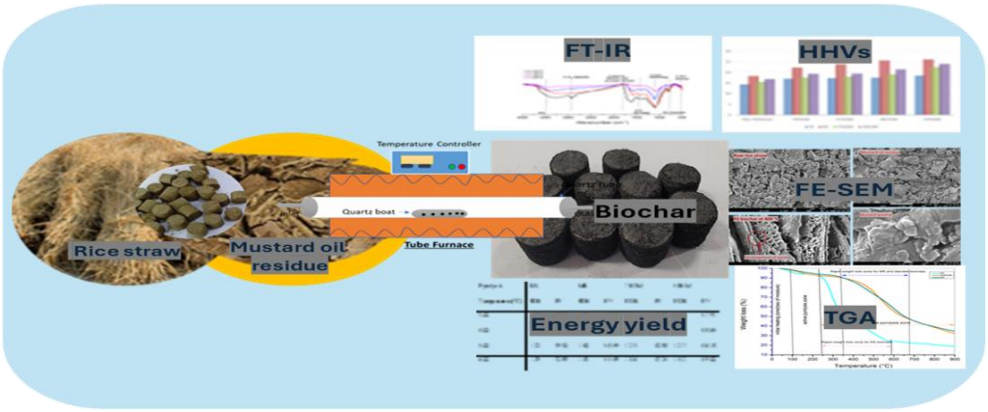

Figure 5.1: Graphical abstract.

5.1 Introduction

Clean and sustainable energy is one of the most important goals as outlined by United Nation's SDG 7. Biomass has always been considered as a potential source of renewable and sustainable energy that can be utilized to produce energy and various value-added materials and chemicals[137]. The need for diversification in energy sources is necessary because it diminish reliance on fossil fuels as well as reduces the associated greenhouse gas emissions [234] [235].Approximately 140 billion metric tons of biomass waste are produced annually on a global scale [236] [237]. Notably, within this category, agricultural residues play a pivotal role as a significant portion of lignocellulosic biomass. These residues are prominently featured in the sustainable energy systems of agricultural economies worldwide, India being a notable example [238] [239]. In most of the developing economies, significant amounts of agricultural residues are generated which often remains unused and become waste material. Most of the time they are burned in open fields, leading to noteworthy environmental issues. Scientific research, innovation and technological advancement are paving sustainable and eco-friendly ways for the utilization of these biomass waste and thus helping to limit the adverse effects of burning it openly. Agricultural biomass residues consist of cellulose, hemicellulose, and lignin, showcasing a substantial energy content [240] [16].Conversion techniques can encompass physical, chemical, thermal, or biological processes to yield solid, liquid, or gaseous fuels [241] [242] [243].

Rice and mustard are two important crops among India's agricultural produce. Rice cultivation spans 44 million hectares, with the northwestern Indo-Gangetic Plains. The northwestern region of India heavily relies on rice-centric cropping systems, with over 80% of its agricultural activities encompassing rice-based cultivation. India also cultivates various oil-bearing fruits and seed-producing crops, including peanuts, coconut, sesame seeds, mustard seeds (or rapeseeds), sunflower, and more. Mustard seed or rapeseed (Brassica spp.) stands as

the second most vital oilseed yielded in India, following groundnut, and it caters to approximately 27.8% of the nation's vegetable oil needs [244]. Generally, due to their initially elevated calorific value, de-oiled cakes are well-suited for thermochemical conversion processes [130]. This byproduct contains roughly 50% of the plant's total energy and has the potential to be utilized as an energy source [245].

Usually, thermochemical processes are used for utilization of lignocellulosic biomass. Biomass combustion for bioenergy generation is currently the dominant process for biomass utilization. However, it is not a green process as it emits gaseous pollutants in the environment. Pyrolysis is another promising thermochemical technique that can be used to produce bioenergy from biomass [28].Biofuels obtained through thermochemical processes, like pyrolysis, may have lower energy yield than petroleum products. However, they contain less amount of sulphur, nitrogen, and ash, which means they release lower levels of harmful gases (such as NO_X and SO_2) and other particulate matter when burned [246]. Rajnish et al. [130] has done a kinetic and thermodynamic investigation of mustard oil residue at a heating rate of 10,20 and 30°C/min using TGA instrument and concluded that 234-417°C is the best suited temperature range for the pyrolysis of mustard oil residue. Through his observations he also concluded that mustard oil residue could be a suitable source for biofuel. Although his study is focused on one biomass type that is mustard oil residue alone but is a new work in this domain. However, his study is only based on the data obtained from TGA instrument and kinetic modelling unlike this article which involve the actual pyrolysis work of selected biomass in the laboratory conditions.

Boateng et al.[247] has explored the fast pyrolysis of two varieties of mustard oil seed cake (camelina and pennycress) and observed the production of liquid fuel with notably elevated heating values, reaching up to 34.7 MJ/kg and 29 MJ/kg from the fast pyrolysis of these mustard de-oiled cakes. The carbon conversion efficiency in this process was determined

to fall within the range of 60% to 80%. The focus of his study was liquid fuel unlike the solid byproduct i.e. biochar in our study. In another notable work by Jinje et al. on slow pyrolysis of rice straw (300-700°C) it was found that above 500°C the mass yield was about 25% and the biochar was primary product of the pyrolysis which has nearly 40% energy of straw [223]. In a co-pyrolysis work of paper waste (PW) and mustard press cake (MPC), Aparna et al. has outlined the obtained bio-oil's properties. She optimized the results using RSM technique which suggest that the maximum bio-oil yield of 46.95% is obtained at pyrolysis temperature of 874.75 K and maximum energy yield of 56.51% is obtained at temperature of 812 K [248]. Most of the work done so far on pyrolysis or co-pyrolysis highlight either work on mustard oil residue or rice straw alone and few authors also discuss co-pyrolysis of another biomass with either of these biomasses selected here. However, none of them explored the co-pyrolysis work using these two selected biomasses. In the aspect of selection of biomass also the presented work is novel.

This experimental work involved subjecting the biomass feedstocks -RS, MR and its blend to pyrolysis, which is a controlled thermal decomposition process that occurs in the absence of oxygen. This process breaks down the biomass into different components, including gases, liquids (such as bio-oil), and solid residues (like biochar). The biomass feedstocks used were converted into pellets. The size of the pellets used in the experiments was consistent across all runs. This standardization ensures that the size of the starting material is not a variable affecting the outcome of the pyrolysis process. The pellets were subjected to pyrolysis at different temperatures from 300-600°C at an interval of 100°C. This variation in temperature allows us to study how the temperature affects the composition and properties of the resulting biochar. Before conducting the pyrolysis experiments, the feedstock samples (the material from which the pellets were made) were characterized in raw form for their properties to evaluate the properties enhancement after the pyrolysis of the same. This likely involved analysing the

chemical composition, moisture content, and other relevant properties of the feedstock to understand its initial characteristics. After the pyrolysis process, we performed various analytical investigations on the biochar samples that were produced. This co-pyrolysis of *the chosen biomass combination is a novel work* and aimed to evaluate biochar properties for its potential sustainable energy applications. The subsequent sections of our work likely detail the specific methods and techniques we used for these analytical investigations. The schematic diagram representing the experiment methodology has been shown in *figure 5.2*.

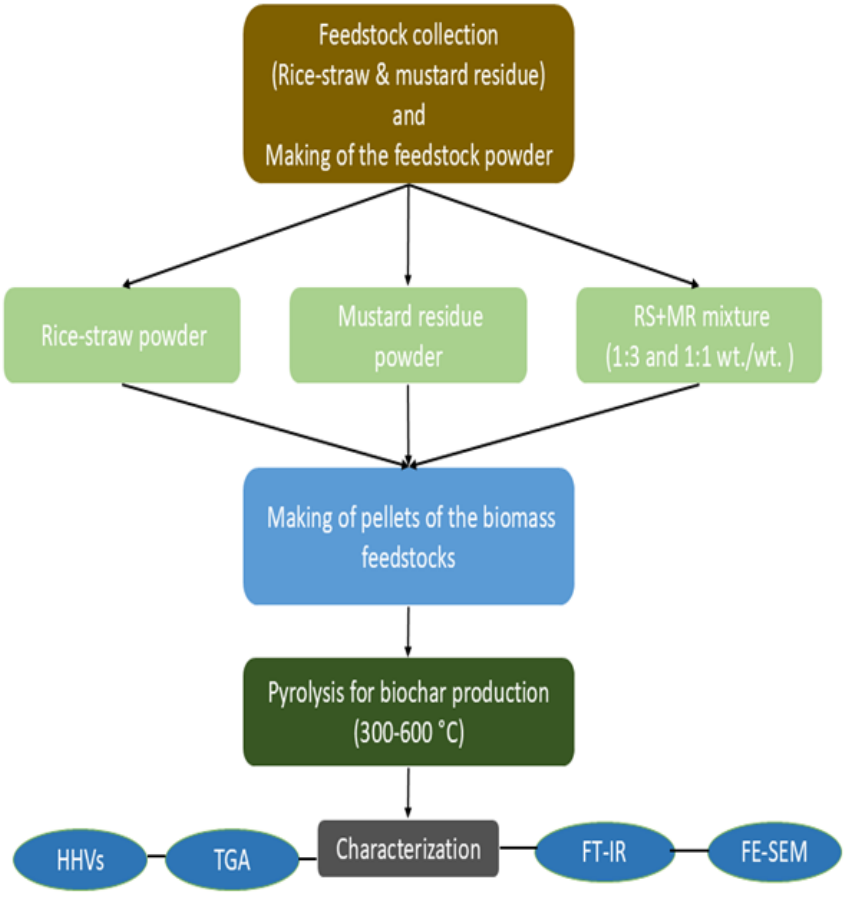

Figure 5.2: Schematic diagram of the experimental methodology

5.2 Materials and Methodology

5.2.1 Collection and preparation of feedstock

The rice straw biomass utilized in this study was gathered from agricultural fields situated in the Amethi District of Uttar Pradesh, India. The mustard oil residue was bought from an oil-expelling mill of Ayodhya district of Uttar Pradesh, India. Section 4.2.1 of the previous chapter discusses the feedstock preparation method that was followed for this work as well. Two distinct types of powdered stock samples (of mess size 100) were meticulously prepared and categorized as (1) 100%RS feedstock and (2) 100 %MR feedstock. For the purpose of pyrolysis four types of feedstock samples were prepared using the RS and MR feedstock. The sample were named as (i) RS i.e.,100%RS, (ii) MR i.e.,100% MR, (iii) 7R3M i.e.,70% RS &30% MR (wt./wt.) and (iv) 5R5M i.e.,50% RS & 50% MR (wt./wt.). All feedstocks were stored in Ziplock bags to save it from the environmental influence.

The feedstocks prepared were converted into pellet form using a hand pelletizer shown in *figure 5.3* The experiment utilized consistently sized pellets for all trials. These pellets, composed of a specific feedstock, underwent pyrolysis at varying temperatures to generate biochar.

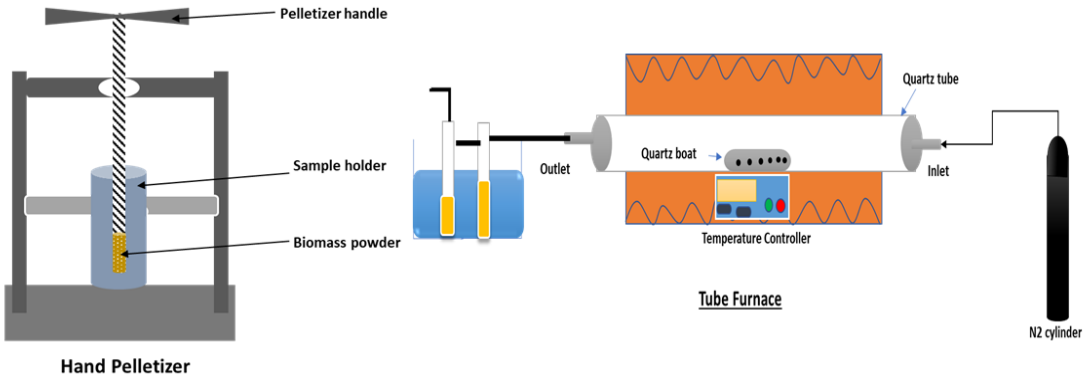

Figure 5.3: Schematic representation of Hand pelletizer and Tube furnace.

Before initiating the pyrolysis process, thorough characterization of the initial feedstock samples was conducted. The subsequent sections elaborate on the diverse analytical inquiries performed on the resultant biochar samples, aimed at assessing the impacts of the pyrolysis process.

5.2.2 Pyrolysis procedure for biochar production

Pyrolysis experiments were carried out within a quartz tube positioned inside a tube furnace (Lindberg®, USA). The detail pyrolysis procedure has been discussed in section 4.2.2 of previous chapter. Approximately 6-8 grams of the sample were placed within the quartz boat for each run. The experimental runs were consistently conducted within a temperature spectrum of 300°C to 600°C. The heating rate was fixed at 10°C/min, and the duration of each run was set at a constant 30 minutes as dwell time. At the culmination of the 30-minute dwell time, the nitrogen supply and furnace controls were automatically deactivated, initiating the cooling process of the furnace until it reached ambient temperature.

The outcome of the pyrolysis process consisted of three distinct products: (i) Condensed gases that subsequently formed liquid bio-oil, (ii) non-condensable gases, also known as biogas and (iii) Solid biochar, that is the subject of our study.

Both condensable and non-condensable product gases underwent passage through a condenser situated at the outlet. In this setup, condensable gases condensed within the condenser and outlet pipe, while incondensable gases were expelled into the atmosphere by the continuous supply of nitrogen gas on one side of the quartz tube. The solid biochar generated was retrieved from the tube only after the furnace had cooled down to ambient temperature, a process that typically took around 6-8 hours, contingent on the specific pyrolysis temperature employed.

5.2.3. Characterization and analysis

A series of analytical assessments were conducted to elucidate the properties and attributes of both the feedstocks employed in the pyrolysis experiments and the resulting biochar. The methods for these analytical procedures are delineated in Sections 4.2.3.1 to 4.2.3.6, of the previous chapter, with the corresponding outcomes discussed in Section 5.4. The main studies include:

- Mass yield, energy yield, and energy density ratio
- Higher Heating Value (HHV)
- Elemental Analysis
- Field Emission Scanning Electron Microscopy (FE-SEM)
- Fourier-Transform Infrared Spectroscopy (FTIR)
- Thermogravimetric Analysis (TGA)

5. 3 Results and discussions

5.3.1 Mass yield

Table 5.1 depicts the variation in biochar mass yield across different temperatures during pyrolysis. The outcomes of the pyrolysis trials on the various feedstock samples highlight the diverse mass yield of produced biochar at each specific pyrolysis temperature. Among all the samples, the peak mass yield was achieved at 300°C. Specifically, the recorded values were 40.65%, 53.59%, 46.48% and 48.26% for RS, MR,7R3M and 5R5M samples respectively.

The biochar yield originating from RS exhibited a fluctuation, ranging from 40.65% at 300°C to 28.50% at 600°C. Similarly, within this temperature range, the biochar yield from MR, 7R3M and 5R5M decreased from 53.59% to 38.81%, 46.48% to 32.36% and 48.26% to

34.50%, respectively. Notably, the substantial decrease in mass yield occurred in the case of MR as compared to RS when the pyrolysis temperature escalated from 300°C to 400°C however when temperature increased from 400-500°C both MR and RS registered a rapid decrease in mass yield.

Table 5.1: Mass yield (%) of biochar (M.V.-mean value of mass yield and S.D.- Standard deviation).

Pyrolysis Temperature(°C)	**Mass Yields (%) of Produced Biochar**							
	RS		**MR**		**7R3M**		**5R5M**	
	M.V.	S.D.	M.V.	S.D.	M.V.	S.D.	M.V.	S.D.
300	40.65	±5.44	±53.59	±6.62	±46.48	6.20	48.26	±6.09
400	37.70	±4.91	±48.02	±5.95	±40.69	5.58	42.30	±5.49
500	32.21	±3.94	±41.85	±4.77	±34.83	4.47	36.36	±4.40
600	28.5	±3.15	±38.81	±3.84	±32.36	3.58	34.50	±3.52

The highest mass yield was obtained for MR and the lowest for RS for a particular pyrolysis temperature. It's noteworthy that when RS and MR were blended in a weight ratio of 7:3 and 1:1, the resulting biochar yield at each pyrolysis temperature was in between the RS and MR mass yield. These mass yield findings of blended feedstock are notable that increasing the weight proportion of MR in the blended feedstock from 30% to 50% by weight does not have remarkable increase in mass yield as expected from the higher mass yield result of the MR for a particular temperature.

The biochar yield for RS as reported by Wang et al., 2020 at 600 °C was approximately 30 % which is comparable to our RS biochar yield at the same temperature which is 28.5%. In a RS pyrolysis experiment Chandra & Bhattacharya, 2019 between 400 °C -700°C the biochar yield was obtained as 45.36 % at 400 °C and 33.04 % at 700 °C. Also, the pyrolysis in [174].was done for the different heating duration and no significant effect of duration on the biochar yield

was observed however in our case the heating duration was kept fixed for 30 min. Higher pyrolytic temperatures are known to negatively affect the mass yield of biochar [249].

The decrease in the mass yield of biochar with the increase of pyrolysis temperature may be associated with the loss of more volatile at higher temperatures, dehydration, and thermal decomposition of lignin and cellulose into lower molecular weight gaseous and liquids *(bio-oil)* [250].The biochar yield of MR was higher than the yield of RS biochar; that most likely because of higher lignin of higher lignin in MR that decelerates the pyrolysis process [130] [251].Additionally, CO_2 is weakly bound on the biochar surface through physisorption so emitted easily during RS pyrolysis that may be a reason for lower yield of RS biochar. Moreover, the mass yield results of RS, MR and its mixture 7R3M and 5R5M in this experiment suggest that RS and MR blending in 7:3 ratio is optimal for co-pyrolysis of these feedstock as no such remarkable increase in yield had been found with further increase in the weight proportion of MR.

5.3.2 Elemental Analysis

The biomass pyrolysis process enhances the carbon concentration in produced biochar [246].As a consequence, the biochar gets converted into a well carbonaceous biochar. The elemental analysis results of biomass feedstock and their biochar are presented in *table 5.2.*The biomass feedstock RS and MR in their raw form had been found to have C% as 36.27 and 44.01 respectively. At a pyrolysis temperature of 300 °C the C % in RS and MR biochar increased up to 52.68 and 59.07 respectively.

Table 5.2: Elemental compositions of raw biomass and its biochar.

Feedstock	C%	H%	N%	S%	H/C
RS	36.27	5.272	1.04	0.143	0.145
RS biochar	46.92	3.128	1.06	0.244	.067
MR	44.01	6.638	5.19	1.338	0.151
MR biochar	59.07	5.489	7.16	1.199	0.093

The higher carbon concentration in biochar produced may possibly be attributed to the increase in carbonization as well as development of new stable aromatic carbon rings [155] [252].The biochar obtained has greater C-C bonds compared to C-O and C-H bonds, thus decreasing the H/C and O/C ratios due to decarboxylation, dehydration and decarbonization of lignocellulosic components [142] [253]. Lower H/C ratio is linked with the greater energy content of the materials that also reflect the declination of low energy bonds like C-H &C-O and increment of high energy bonds like C-C [254].This can be observed in FTIR results of the biochar. Apart from the increase in C %, the H % decrease in the biochar produced at higher temperatures that might be due to loss of more hydrocarbons, water vapors, H_2, CO_2, and CO through formation of syngas during the pyrolysis process [155].

Table 5.3: Higher heating values of different biomass and its biochar produced at different pyrolysis temperatures.

Pyrolysis Temperature (°C)	**Higher Heating Value (HHV)**			
	RS	MR	7R3M	5R5M
Raw feedstock	14.37	18.35	15.50	16.91
300	17.03	22.29	18.03	19.37
400	17.34	23.87	17.70	19.49
500	17.58	25.64	19.12	21.48
600	18.53	26.19	22.60	24.02

5.3.3 Higher heating values (HHVs), energy yields and energy density ratio (EDR)

The HHV of raw biomass feedstock i.e., RS, MR, its mixtures, and biochar produced at different pyrolysis temperature have been presented in *table 5.3*. The HHV of RS, MR,7R3M and 5R5M mixture in their raw form were 14.37, 18.35,15.50 and 16.91 MJ/kg respectively. It can be observed that that the HHV of biochar produced at higher pyrolytic temperature was higher that might be because of lower H/C ratio of the biochar as low H/C ratio is linked with higher heating values.

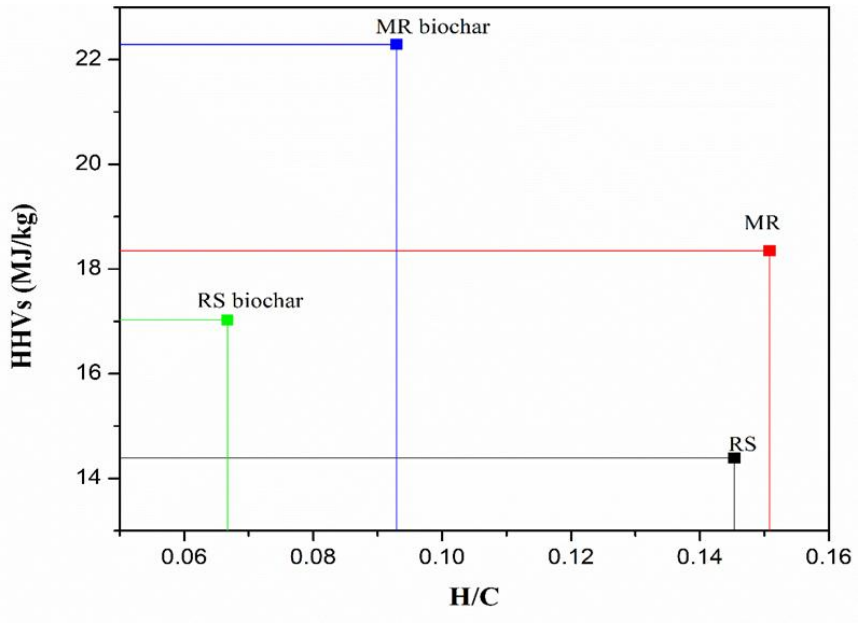

Figure 5.4(a): HHVs vs H/C representation of raw biomass and its biochar @300°C.

The HHV of MR in raw form was 18.35 MJ/kg and its biochar produced at 300 °C and 600°C had HHV of 22.29 and 26.19 MJ/kg respectively which was 21.47 % and 42.67 % higher as compared to HHV of raw MR. Thus, from energy vector point of view MR shows excellent results among all. Moreover, the HHVs of blended feedstock were also in between both prime feedstocks i.e., RS and MR. The mixture with RS and MR weight ratio 7:3 can be considered as optimal proportion for blending these biomasses to obtain greater energy from the biochar as the increase in the weight ration of MR does not so remarkable increase in HHV. The HHVs results of our research findings were in line with the earlier reported results [255] [256].

The EDR and energy yield of biochar produced from different feedstock at different pyrolysis temperatures are given in *table 5.4;* that were calculated using equations 4.2 and 4.3 (mentioned in section 4.2.3). From table *5.4* it could be observed that the energy yield of biochar decreases with the increase in pyrolysis temperature. This trend was followed by biochar of all feedstocks except the blended feedstock sample 7R3M and 5R5M in temperature range of 500-600°C. The reason for this increase in the energy yield of these biochar samples

in the mentioned temperature range might be the higher EDR and mass yield values as energy yield is dependent on both parameters. The energy yield was maximum for MR biochar produced at 300 °C while it was minimum for RS biochar produced at 600 °C. The energy yield of RS was 48.37 % at 300 °C which decreased to 32.89 % at 600 °C. The highest decrease in energy yield was observed for RS which was 32% in the pyrolysis temperature range of 300 - 600°C whereas for the same temperature range 7R3M had the lowest decrease in energy yield that was 12.30%. The MR biochar produced at all temperatures had the highest EDR value among all that was because of its greater HHVs and the blended feedstock 7R3M was found showing optimum energy yield as compared to 5R5M.

The decrease in energy yield of biochar may be because of the removal of volatiles, and thermal decomposition of lignin and cellulose from the biomass at higher temperatures, which is consistent with the earlier reported results [257]. Additionally, the decrease in the mass yield of biochar with an increase in pyrolysis temperature is also responsible for this decreased energy yield and which is consistent with the earlier reported results [258].

Table 5.4: Energy yield (EY) and energy density ratio (EDR) of biochar produced at different pyrolysis temperature.

Pyrolysis Temperature(°C)	RS		MR		7R3M		5R5M	
	EDR	EY	EDR	EY	EDR	EY	EDR	EY
300	1.19	48.37	1.21	64.84	1.16	53.92	1.20	57.91
400	1.21	45.62	1.30	62.43	1.14	46.39	1.15	48.65
500	1.22	39.30	1.40	58.59	1.23	42.84	1.27	46.18
600	1.29	32.89	1.43	55.49	1.46	47.25	1.42	49.00

3.3 Field emission scanning electron microscopy (FE-SEM)

The morphological examinations of raw materials and produced biochar reveal alteration in the biochar surface topography as influenced by the pyrolysis temperature. *Figure 5.5*, illustrating a noticeable transformation in the morphology of RS and MR biochar as compared to its raw form. It is clear from the *figure 5.5* that in the biochar distinct pore

structures become evident. The escape of volatile substances during pyrolysis contributes to a roughened surface, accompanied by a significant increase in pore density as depicted in the FE-SEM images. The development of a porous char is particularly advantageous in thermochemical conversion processes, such as the production of synthesis gas through the gasification process at elevated temperatures, as highlighted by Pena et al. [259].A porous biochar structure is also sought after in agricultural applications and in the creation of valuable materials through biochemical conversion routes.

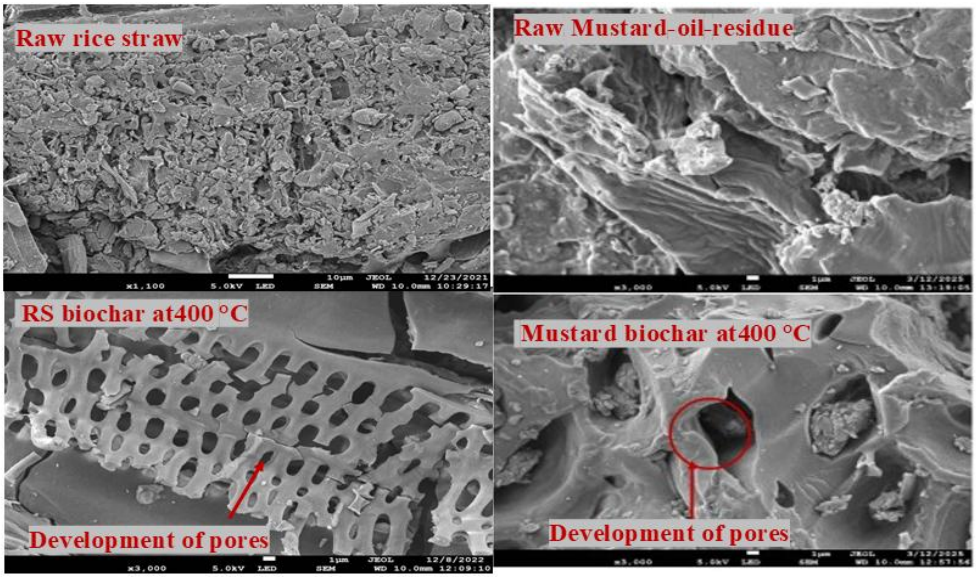

Figure 5.5: FE-SEM image of raw biomass and its biochar.

These well-developed and expanded pores serve as effective sites for nutrient adsorption when biochar is applied to soil. Additionally, such biochar pores typically exhibit enhanced redox-active characteristics and a variable surface charge, fostering the methanogenesis activity during anaerobic digestion. This, in turn, leads to an increase in methane production, thereby enhancing the overall efficiency of the methane generation process [37] [38].

5.3.4 Fourier transform infrared spectroscopy (FT-IR)

The results of the FT-IR analysis of the RS and MC mixture biochar are presented in *figure 5.6.* The IR spectra demonstrate the different functional groups present on the biochar surface. In the shown spectra, the wavenumber up to 3435 $cm^{-1}$is corresponds to the presence of hydroxyl -OH stretching, and the band gap between 2945-2916 cm^{-1} is attributed to the existence of aliphatic groups (-CHn stretching) [260].The increase in pyrolysis temperature resulted in a decrease in O-H and C=O vibrations that might be because of decarboxylation and dehydration during pyrolysis. The existence of ketones and carboxylic stretching is within 1740-1700 cm^{-1} [261].

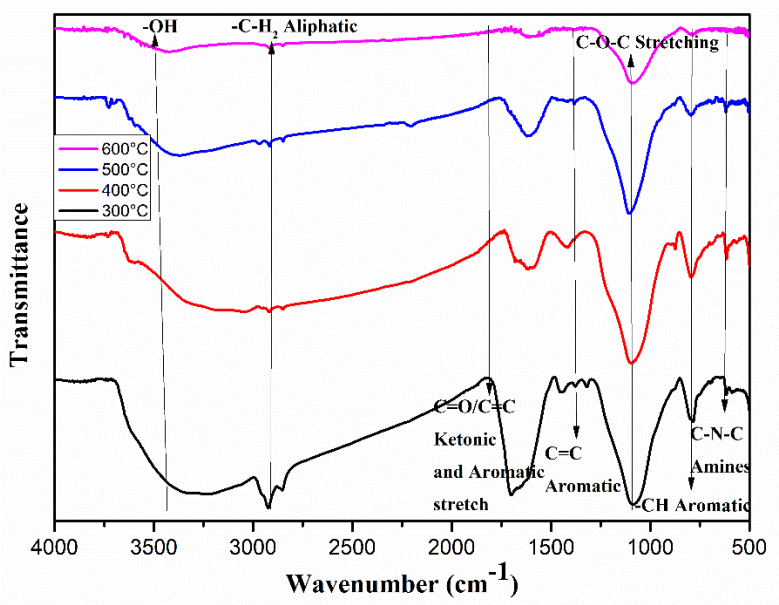

Figure5.6: *FT-IR spectra of biochar produced at different pyrolysis temperatures.*

Aromatic hydrocarbons are indicated by C=O and C=C stretching in the band gap of 1650-1600 cm^{-1}. Strong existence of C=C in aromatic ring was observed in biochar produced at comparatively low temperatures. The C=C vibration was absent when the pyrolysis temperature was above 500°C. The absence of C=C vibration in the FTIR spectra of biochar obtained at higher temperature is because of their low H/C ratio. The occurrence of C-O-C stretching is identified in the band range of 1300-1100 cm^{-1}.

5.3.5 Thermogravimetric analysis (TGA)

The thermal degradation of RS, MR, and its blended biomass under inert gas atmosphere has been shown in *figures 5.7* , as a function of temperature, at the heating rate of 10°C/min. Heating rate can influence the pyrolysis of biomass -as the rate is increased, the onset temperature of devolatilization may also increases [233].

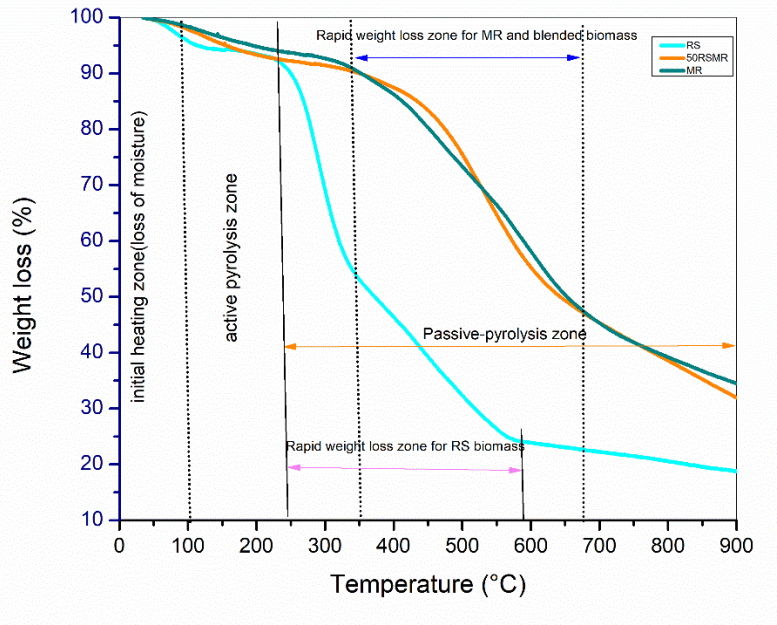

Figure 5.7: Thermogravimetric analysis of three different biomass feeds under non-isothermal conditions.

In a pyrolytic condition, biomass degradation mainly consists of three steps -(i) moisture loss, (ii) active pyrolysis, and (iii) passive pyrolysis [233].From *figure 5.7*, it is clear that when the temperature reaches slightly above 100°C, the mass losses of feed are in the range of approximately 6-7%. This loss corresponds to the evaporation of moisture content in the feed. In the temperature range 100-210°C, the losses for all samples were observed to be approximately 12% of the initial weight. In this pre-pyrolysis zone, the remaining bound moisture within the biomass is lost. Thereafter, with further rise in temperature the observed mass loss for RS is rapid after 200°C till approximately 600°C. However, the rapid weight loss for MR and blended biomass starts approximately after 350°C and continues till 700°C. Thus,

maximum mass loss in all the samples was confined within the temperature range 250-700°C (active pyrolysis zone). The decomposition of lignin continues as it usually starts degrading after content of biomass begins after the moisture loss is complete, i.e. beyond 200°C and continues till the end [130].

5.4. Conclusions

This study explores the thermochemical conversion of rice straw (RS) and mustard-oil residue (MR) into biochar, which is a valuable byproduct. The pyrolysis process was carried out at temperatures between 300°C and 600°C, with a heating rate of 10°C/min and a duration of 30 minutes. The findings indicated that the highest biochar mass yield was achieved at 300°C, with yields decreasing at higher temperatures due to increased biomass decomposition. When examining the individual feedstocks, MR produced the highest biochar yield, while RS yielded the least. This difference is attributed to RS's lower lignin content, which allows for quicker pyrolysis. Additionally, MR biochar exhibited the highest heating value, making it a promising fuel source. Combining RS and MR in a 7:3 ratio resulted in optimal outcomes, with only slight variations in biochar properties between the blends. The MR particles contributed to binding the RS particles, enhancing the strength of the feedstock pellet, which may facilitate easier transport and storage. Overall, the pyrolysis of RS, MR, and their blend proves to be an effective method for producing biochar, with MR biochar particularly notable for its high energy potential as a sustainable fuel.

Next chapter is about application of biochar for synthesis of composite material and its use for dye adsorption study. This gives a dimension for application of biochar in water remediation.

CHAPTER - 6

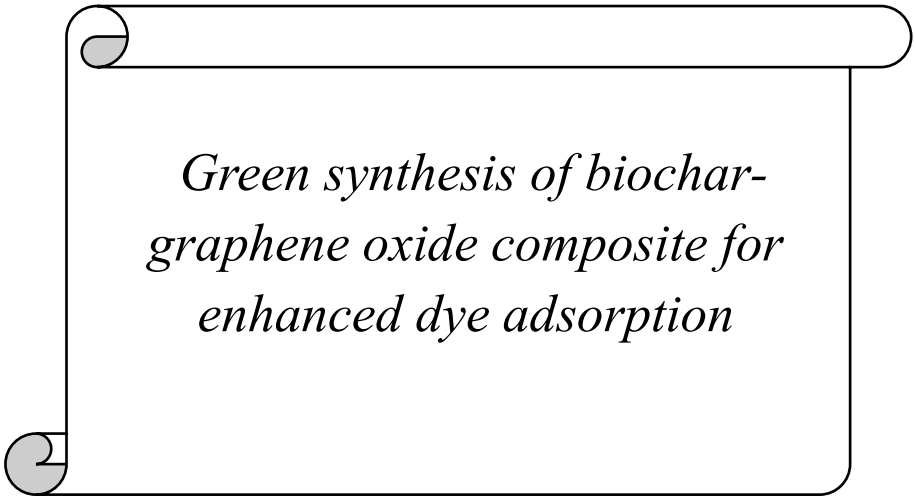
Green synthesis of biochar-graphene oxide composite for enhanced dye adsorption

Abstract

Biochar, produced from waste rice-straw biomass, was prepared and modified with graphene oxide (GO) to enhance the surface properties. The GO was synthesized using modified Hummer's method, and fabrication of biochar-GO composites was carried out through hydrothermal treatment to strengthen GO bonding over biochar surfaces. The mass percentage of GO in the composite material was varied to see its effect on the properties. The prepared materials were characterized by analyzing their properties. It was found that GO was well-coated over the biochar surface. The BET results show enhancement in surface area that was found to be 20.00 m^2/g for biochar, and 59.68 m^2/g , 66.64 m^2/g for two biochar-GO composite-RS-GO-0.1 and RS-GO-1 respectively. All three synthesized materials were tested for their adsorption behavior towards methylene blue dye from aqueous solution under batch adsorption conditions. The absorption time for this experiment was two hours. The GO composites exhibited superior adsorption performance compared to pristine biochar. The adsorption efficiency of biochar, and two composites were found to be 48.05 %, 87.90 % and 99.29 % respectively, for an initial concentration of 20 ppm solution. One of the composites (RS-GO-1) demonstrated removal efficiency of 90.20% for a 30 ppm MB dye solution. The simplicity of the synthesis process, environmental friendliness, and adsorption effectiveness provide strong and convincing grounds for its future application in sustainable waste management and water purification.

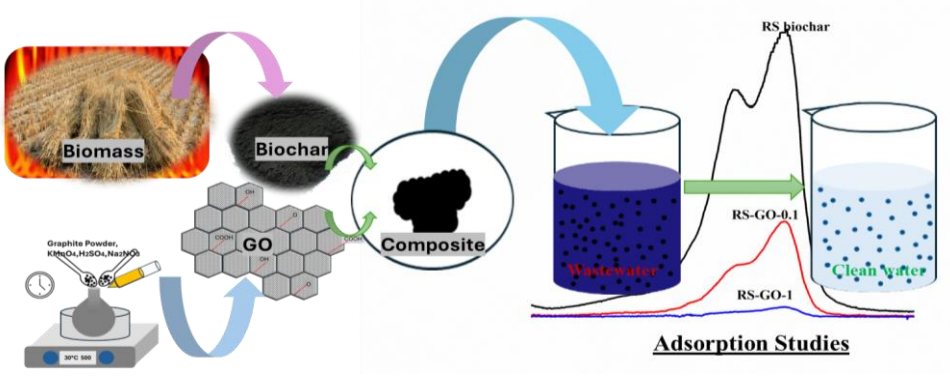

Figure 6.1: Graphical abstract.

6.1 Introduction

The scientific utilization of waste biomass has become essential for sustainable future through emerging concept of bio-circular economy. Accumulation of industrial effluents, municipal waste, agricultural leftovers, and other hazardous materials in air, soil, and water cause serious challenges to sustainable life. Rising pollution levels in natural systems adversely affects marine ecosystem and leads to the non-availability of clean environment. Within the context of sustainable development goals to build a robust circular economy, the effective waste management practices should consider reduction, recycling, and reuse of materials. One of the major causes of air pollution is the open burning of biomass waste which has become a huge concern in several countries. The agricultural biomass, which are abundantly available after each crop cycle, often remain unutilized for its full potential and are burnt or discarded in a casual manner which affects the environment through increased emissions of greenhouse gases. Adsorbing materials produced from biomass waste through thermochemical conversion process, can synergistically reduce agricultural residues significantly, as well as lead to the development of advanced methodologies for water pollution control. Biochar, which contains recalcitrant carbon in high concentrations, is the solid byproduct of slow pyrolysis of agricultural biomass. One of the widely adopted applications of biochar is its use as an adsorptive material for removing water contaminants. Its high percentage of carbon content, porosity, extensive surface area, and abundant surface functional groups, along with other beneficial physicochemical properties, make biochar an excellent candidate for adsorbing organic or inorganic pollutants from soil or wastewater [262], [263], [264].

The contaminated effluent from textile and garment manufacturing industry contains high concentrations of organic dye methylthioninium chloride, or methylene blue (MB) [265]. MB is frequently used as a coloring material for various types of fibers. Because of associated toxic effects, MB-loaded effluents are hazardous to aquatic ecosystem, as well as human health. Advanced treatment methods such as ion exchange, electrochemical treatment, photocatalysis,

ozonation, chemical oxidation, membrane-based separation have been studied and reported to achieve dye-adsorption from industrial wastewater [266], [267], [268], [269]. All such advanced methods, although efficient in dye removal, are energy and/or capital intensive [270]. Alternatively, the adsorption based treatment systems are relatively inexpensive and simple to construct and operate, and most often require natural and abundantly available materials as adsorbents [271] .

Adsorption performance of pristine biochar can be further enhanced by inducing modifications in its physicochemical properties. These modifications, also known as activation of biochar, are necessary to tune the porosity, specific surface area (SSA), surface wettability as required, and to attach functional groups on the surface [272]. One of the widely adopted method is to tune its physicochemical properties by attaching oxygenated functional groups (OFGs), which provide active sites to adsorbing contaminating agents through the mechanism of interfacial reactions [270] .In a reported work, Cable and his-co-researchers used $KMnO_4$ and steam to activate biochar produced from bean pods [273]. The authors reported that the specific surface area of biochar activated by $KMnO_4$ was 1580 m^2/g, whereas the steam activated biochar had a specific area of 258 m^2/gram; i.e. approximately six times enhancement in SSA was observed by using $KMnO_4$ as compared to steam activation. Accordingly, the $KMnO_4$-activated biochar demonstrated a significantly higher (~3.5 times) adsorption capacity for the targeted application. In another study, Regkouzas et al. produced sewage sludge biochar at different temperatures (300, 500 and 700°C) and concluded that high temperature is favorable of high SSA and pore volume which further showed high adsorption capacity for drugs in water [274]. Activation procedures such as these may often consume harmful substances or are energy intensive because of high-temperature applications. Literature studies report that biochar properties can be enhanced through functionalization methods, by attaching oxygenated functional groups (e.g. hydroxyl, carboxyl, ketone, lactone etc.), that form

chemical bonds with *C*-atom within the matrix [275] [270].Several functional materials, such as carbon nanotubes, metal oxides and graphene, have been reported as an effective functional groups for water pollution control strategies [272].Because of its remarkable thermal, mechanical and physicochemical properties, graphene and graphene-oxide have become a research hotspot - several recent studies report the use of graphene-oxide and its composites for controlling water pollution [276] [277] [278].

In this study we have adopted a hydrothermal method for graphene oxide coating over biochar particles obtained from rice straw biomass pyrolysis unlike previous research which mostly involve graphene coating over biomass particle followed by pyrolysis to obtain biochar-graphene composite. The biochar, GO and BG composites have been studied for its characteristics using SEM, FTIR, XRD, XPS and Raman spectroscopy. The absorption performance of these materials for methylene blue adsorption has been tested using UV-VIS instrument. The dye adsorption experiments were carried out for batch adsorption under various process conditions. However, a few studies have been done previously by some authors to prepare biochar and graphene composite but the synthesis method of preparing biochar-graphene oxide composite using hydrothermal reactor is rare [279] . Through its methodology of preparation and application for enhanced methylene blue adsorption, it represents a novel aspect for the field of waste management and water pollution remediation.

6.2 Materials and methods

6.2.1 Materials used

All the used reagents and chemicals were of Analytical Reagent (AR) grade with purity > 98%, and procured from SRL®, India and TCI®, Japan. The waste rice straw was sourced from the agriculture farms located in the District Amethi, India (26.263460, 81.506625). The waste straw material was washed and sun-dried and used as the raw material for biochar preparation.

6.2.2 Preparation of biochar

The collected rice straw after washing, drying and cutting into small pieces was powdered using grinder and stored in Ziplock bags after sieving for 100 mesh size following the standard procedure. The powder form of rice straw was pyrolyzed at 400°C inside a tube furnace with a 10°C/min of heating rate and a residence time of 1 hour. The obtained biochar was washed to remove any dissolvable content and stored for further use. The detailed method of biochar preparation is described in earlier studies carried out by our research group [280] [281].

6.2.3 Synthesis of graphene oxide (GO)

Modified Hummer's method which is a well-established method, was adopted to make GO sheets [282]. In a round-bottomed flask, 230 mL of 98% pure sulfuric acid (H_2SO_4) was taken, and 5-gram graphite powder was added to it. The mixture was then placed in an ice bath. To this mixture, 5 g of $NaNO_3$ and 30 g $KMNO_4$ were added gradually one after another and continuously stirred for a period of 2 hours. After 2 hours, the temperature was gradually increased to 98°C and 300 mL of de-ionized (DI) water (18 MΩ-cm) was added to the content in the flask. The stirring continued. After 1 hour, the stirring and heating were stopped, and mixture was left to be cooled to the room temperature. Next steps involved the addition of 2.5 ml of 30% H_2O_2 to the cooled mixture to remove excess $KMNO_4$. To separate the precipitate that developed, this liquid mixture was centrifuged. The resulting precipitate was cleaned first with a 5% aqueous HCl solution and then repeatedly with DI water. Thereafter, the solid was placed for 48 hours at 80°C in an air oven to obtain dried GO sheet. The dried GO sheet that was eventually produced after 48 hours of drying was utilized to create a GO suspension for coating over biochar particles in this experiment.

6.2.4 Preparation of biochar-GO composite

The dried GO-sheets were used to prepare GO-suspension in deionized water (ultrapure or DI-water of 18 MΩ-cm resistivity). The GO-sheets were crushed in mortar and pestle to form powder and then added to DI-water to make two different suspensions of 1% and 0.1% weight-to-volume ratios. The first suspension of 1% w/v ratio was obtained by adding 400 milligrams of crushed GO-sheets in 40 mL of water. The second suspension (0.1% w/v) was prepared by adding 40 milligrams of crushed GO-sheets in 40 mL of water. Both the suspensions were then ultrasonicated for one hour. Next, the suspensions were continuously stirred for ~2 hours to obtain a uniform suspension. To this unform suspension, 1.6 grams of rice straw biochar (described in section 6.2.2) was mixed under continuous stirring of 6 hours to obtain uniform coating of graphene oxide over biochar particles. Thereafter, the mixture was placed in a hydrothermal reactor at 140°C for 12 hours to finally prepare the desired hydrothermally processed biochar -graphene composites. The composites prepared using 1% (w/v) were denoted by the term RS-GO-1, whereas the second one was denoted by RS-GO-0.1. The methodology scheme of preparation of GO, biochar, and biochar-GO composite is summarized in figure 6.2 (a), (b), and (c).

6.2.5 Characterization studies

The biochar and its composites were characterized to study their structural and surface morphology using scanning electron microscope (*JEOL*®, Japan) and X-ray diffractometer (*Malvern Panalytical Ltd.*, UK). Raman spectra for the prepared composites were recorded using Raman microscope (*JASCO*® NRS-5500, Japan) using 514 nm excitation wavelength. Functional groups analysis for the samples was completed by Fourier transform infrared (FT-IR) spectroscopy instrument (*Thermo-Fisher*®, USA). The elemental composition over the surface was recorded by X-ray photoelectron spectroscope (*Thermo-Fisher*®, USA) using Al-Kα radiation.

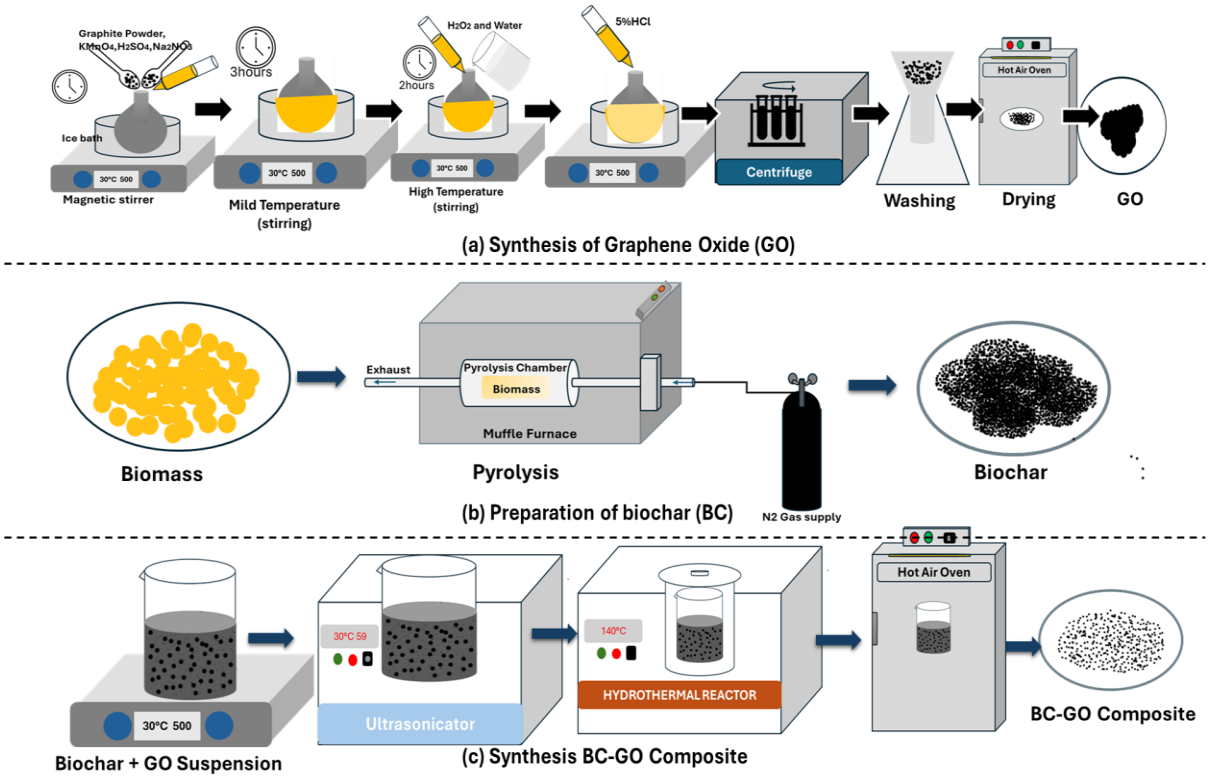

Figure 6.2: Schematic representations of preparation methods of (a) graphene-oxide, (b) biochar, and (c) biochar-GO composite

The N_2 adsorption/desorption measurements using BET method (*MicrotracBEL, Max II,* Japan) were measured by nitrogen adsorption at 77 K. The degassing of all the prepared samples was done under vacuum at 150°C temperature for 10 hours prior to the analysis. The specific surface area and the pore size distributions were investigated using the nonlinear density functional theory (NLDFT) model (incorporated within the instrument) based on the adsorption branch isotherms.

6.2.6 Adsorption of methylene-blue dye (MB)

The adsorption experiments were carried out using a batch adsorption setup under constant stirring to maintain uniform contact between the adsorbent and dye molecules. Aqueous MB solution (30 ppm) was prepared by dissolving MB reagent (98% purity, RANKEM™, USA) in DI water. The pH of the solution was maintained neutral (pH~7) throughout the experiment. Initially 50 mg of RS-GO composites were used for adsorption

studies using 100 mL of 30 ppm-MB solution. The experiments were also conducted using rice-straw biochar (non-composites). The adsorption experiments were carried out using different doses of composites. The MB dye solutions of varied concentrations were prepared and contacted with the synthesized samples in a batch experiment, and UV-VIS spectra for all samples periodically collected, were recorded to monitor the adsorption kinetics. The absorption spectra of methylene blue were initially recorded in the wavelength range of 400-800 nm to identify the maximum absorption peak (λ_{max}).

6.3 Results and discussion

6.3.1 Structural and surface morphology

6.3.1.1 X-ray diffraction (XRD)

XRD analysis results for graphene powder (GP), GO, RS and both composite samples (RS-GO-1, and RS-GO-0.1) are shown in Figure 6.3(a) and Figure 6.3(b). A sharp and intense diffraction peak is observed at approximately $2\theta = 26.5°$, corresponds to the (002) plane of graphite. This diffraction peak is indicative of highly ordered crystalline graphitic structure, with well-aligned graphene layers. A broad and less intense peak appears at 2θ=12°, corresponding to the (001) plane of graphene oxide. This shift to lower 2θ and the broadening of the peak indicates, firstly increased interlayer spacing, due to the addition of oxygen-containing functional groups such as hydroxyl, epoxy, carboxyl. And secondly reduced crystallinity, caused by the oxidation and disruption of the regular graphite lattice. Absence of the sharp peak at 26.5° confirms successful oxidation of graphite to GO, as the regular stacked structure is disrupted. Figure 6.3(b) shows broad and weak peaks, mainly around 2θ=27°, corresponding to amorphous cellulose and lignocellulosic content. This pattern suggests a largely amorphous structure with minor crystalline cellulose regions. RS-GO- 0.1 shows improved peak definition, particularly near 2θ = 27°, suggesting slight ordering due to the incorporation of GO. The appearance of minor peaks suggests interaction between rice straw

matrix and GO, improving structural features. RS-GO-1 exhibits further sharpening of peaks, especially at 2θ=27°, indicating enhanced crystalline behavior. Increased GO content contributes to improved graphitic stacking or partial restoration of graphitic domains within the composite. The presence of new or intensified peaks confirms better interaction and dispersion of GO in the RS matrix.

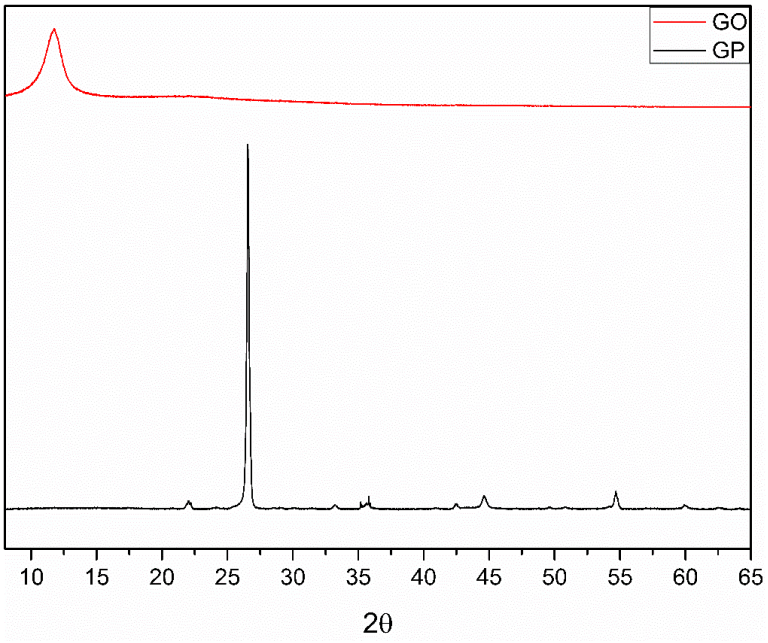

Figure 6.3(a): XRD pattern of Graphite Powder (GP) and Graphene Oxide (GO).

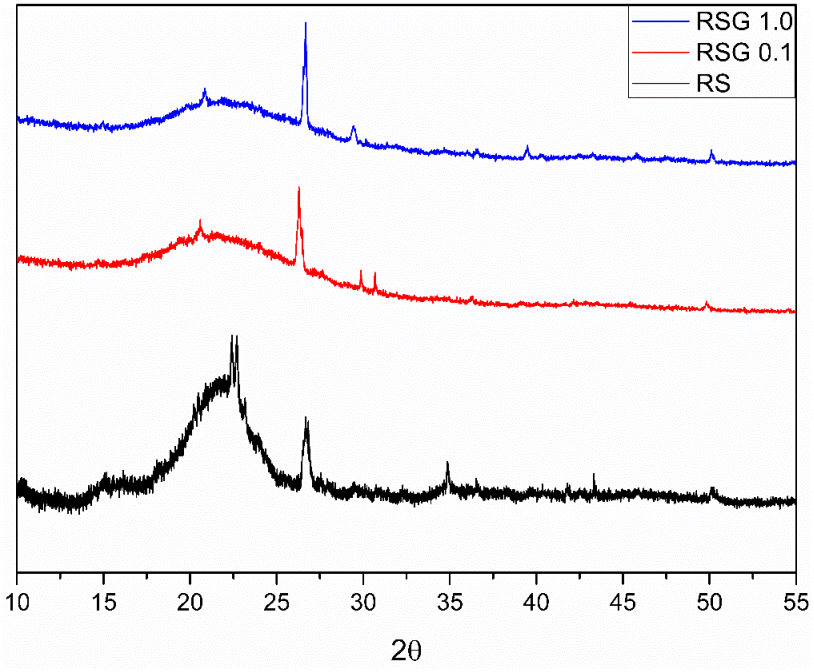

Figure 6.3(b): XRD pattern RS biochar, RS-GO- 0.1, and RS-GO-1 composites.

6.3.1.2 FE-SEM analysis

The surface morphology of RS biochar and RS-GO composites were examined through SEM analysis. From the images presented in Figure 6.4, it may be observed that the RS biochar has typically rough surfaces. The roughness observed in the biochar samples is the characteristic feature of carbonized biomass. Images also show that the biochar has well developed micro and mesopores which is the reason for its high surface area and adsorption capacity. The SEM image of RS-GO-0.1 composite shows that the surface has slightly different appearance due to the addition of GO. The pores are partially covered with thin layer of GO nanosheet indicating the successful incorporation of GO over biochar surface. The overall structure remains porous with more layered and flaky textural appearance over surface. The SEM image of RS-GO-1 shows a more pronounced GO coating on the biochar surface. The GO sheets appear as smooth, wrinkled layers which cover a large portion of the surface which indicate a high degree of composite formation. At some sites, the GO layer coating may block some pores and reduce surface area but could also increase the surface interaction due to oxygenated functional groups of GO. The enhancement in surface area of the samples are further supported by results of BET (described later in section) which shows improved surface area of both RS-GO composites, this indicates that GO has contributed additional surface area with the interaction of biochar matrix. The increased surface area supports grater active sites for adsorption and thus enhanced adsorption potential of the composites [283] [284].

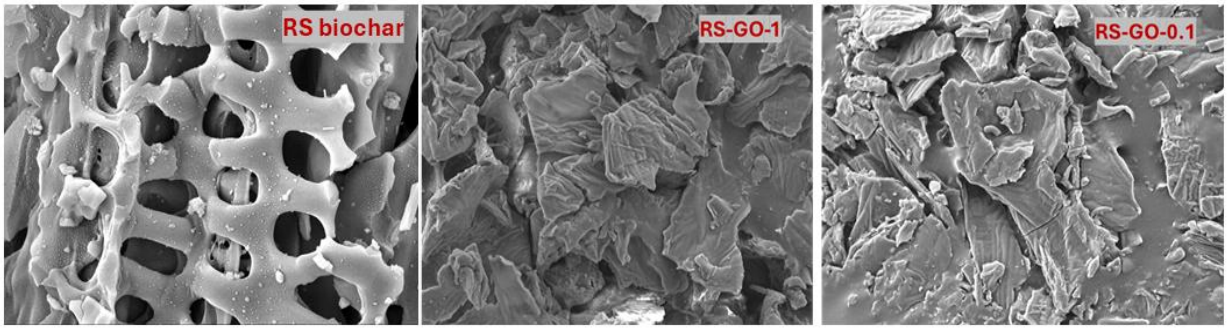

Figure 6.4: FE-SEM image of RS biochar, RS-GO-1 and RS-GO-0.1 composites

Structure and surface morphology of the prepared BC, GO and its composite was observed using SEM images of the respective samples.

6.3.1.3 FTIR analysis

FT-IR spectra of the RS biochar, RS-GO-1 and RS-GO-0.1 composites were shown in Figure 6.5. For RS biochar the bands at 3371 cm^{-1} is corresponding to *O-H* stretching, peak around 2980 cm^{-1} is associated with C-H stretching of aliphatic group, peak at 1700 cm^{-1} corresponds to *C=O* stretching, 1590 cm^{-1} is *C=C* stretching vibration in aromatic rings, peak between 1200-1000 cm^{-1} is related to *C-O* stretching of alcohols, eithers or carboxylic acids. Upon addition of GO notable changes have been observed in FTIR results. The peak at 3371 cm^{-1} became broader and more intense for RS-GO-1 composite which indicated increased hydroxyl groups by GO addition however the corresponding peak for RS-GO-0.1 is less pronounced as compared to RS-GO-1 composite which is indicative of limited GO incorporation in RS-GO-0.1. The C=C peak around 1700 cm-1 is not much pronounced in RS biochar spectra is appearing more distinctively in RS-GO composite indicating the presence of carboxylic groups from GO. Overall FTIR spectra confirms the successful introduction of GO into RS biochar matrix [284] [276].

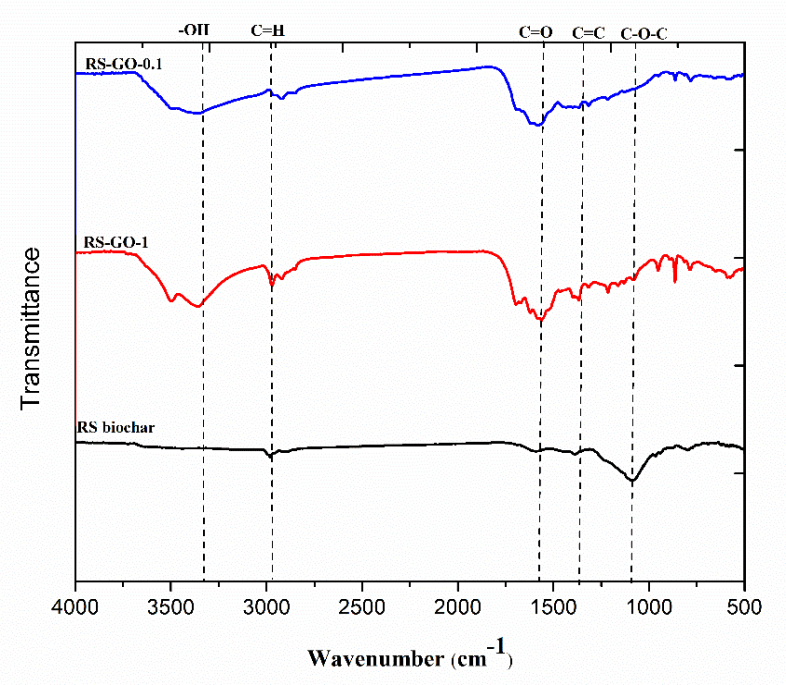

Figure 6.5: FTIR spectra of the RS biochar, RS-GO-1 and RS-GO-0.1 composites.

6.3.1.4 Surface area analysis

As shown in figure 6.6, all three samples exhibit Type IV adsorption isotherms, which are characteristic of mesoporous materials with pore diameters typically between 2-50 nm. The Type IV isotherm is distinguished by its hysteresis loop, indicating the presence of mesopores and demonstrating capillary condensation and evaporation phenomena. This classification is consistent with all samples that undergo monolayer-multilayer adsorption followed by capillary condensation in mesopores [285]. There is increase in BET surface area from 20.00 m^2/g (rice straw) to 59.68 m^2/g (RSGO-0.1%) and further in increased to 66.64 m^2/g (RSGO-1%). There is nearly 233.2% increase in surface area when comparing RS to RSGO-1%. The successful transformation of rice straw from a low-surface-area material (20 m^2/g) to a significantly enhanced adsorbent (66.64 m^2/g) through graphene oxide modification represents a sustainable approach to value-added material development from agricultural waste.

6.3.2 Adsorption experiments

The adsorption behavior of three different adsorbents i.e. RS (biochar), and RS-GO-1, and RS-GO-2 composites with respect to adsorption of methylene blue (MB) dye from the aqueous phase were carried out for MB solutions of varying concentrations. The kinetic analysis and the adsorption equilibrium studies have also been carried out for the three adsorbents. Further, the feed conditions had been varied with respect to feed concentration, and feed pH and the adsorption behavior have been compared against this condition to investigate their effects.

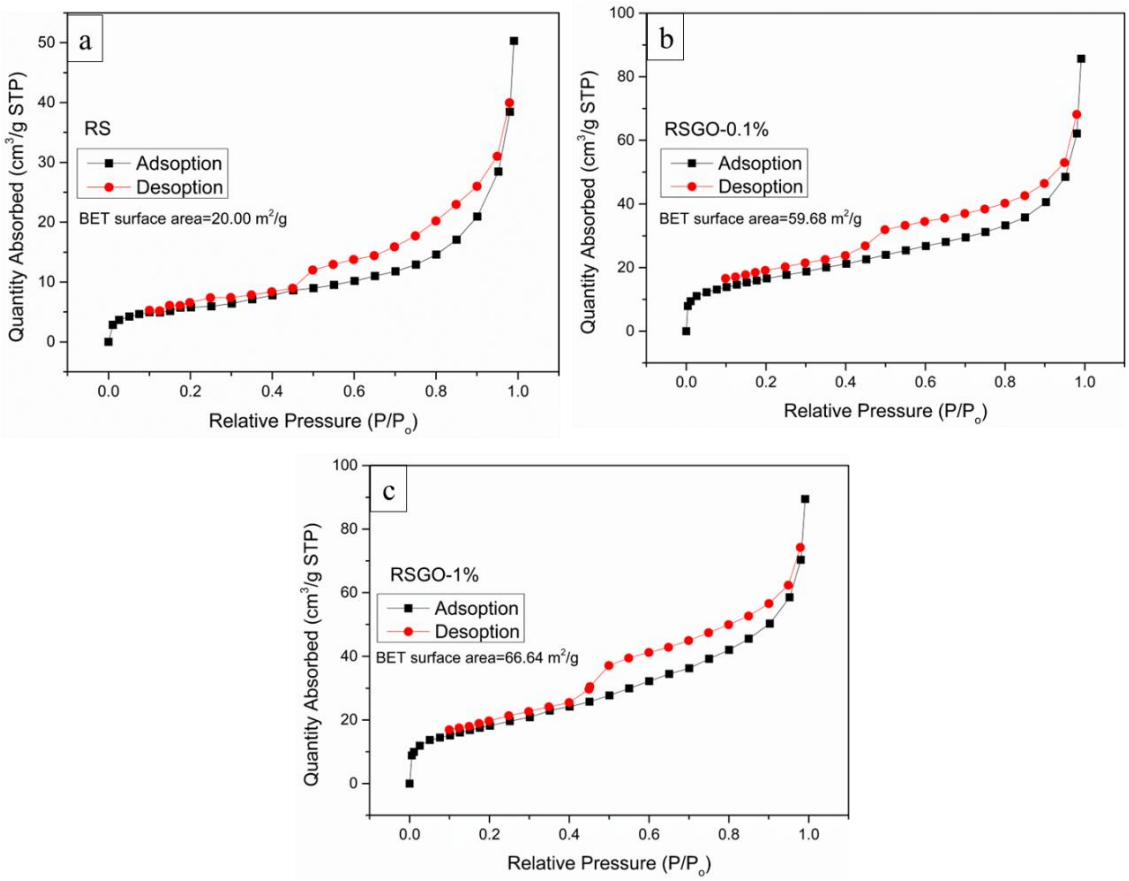

Figure 6.6: Nitrogen adsorption -desorption isotherms of RS, RS-GO-1 and RS-GO-0.1.

The measured and observed kinetics are governed by two main processes: first, the adsorbate diffuses from the bulk solution inside the particles and second, the actual adsorption on the particles' surfaces. At greater dye concentration, the diffusive process possibly masks the effect of the true adsorption kinetics. Thus, it becomes important to study kinetics using

different dye concentration solutions, so we have performed kinetics experiments using three different MB dye concentrations (10, 20 and 30 mg L^{-1}). Periodically, the samples were collected and analysed using UV-Vis spectroscopy to obtain the removal efficiency.

6.3.2.1 Adsorption kinetics

Figure 6.7, shows the kinetics observation of the experiments performed using these solutions. Other parameters such as pH of the solution, temperature and adsorbent dosage were kept constant during this experiment, which was adjusted to 7, 25°C and 50 mg/100 mL respectively. The adsorption experiment was observed for 120 min and samples were collected at every 15 min for UV-VIS analysis.

The adsorption capacity, Q_t against time, t of all the samples were calculated using following eqn(6.1) [286] :

$$Q_t = \frac{(C_0 - C_t)V}{m} \tag{6.1}$$

Here C_0 and C_t are the initial and remnant (at time t) dye concentration in mg/L in its aqueous, V and m are volume of solution the adsorbent mass in liter and gram respectively. The obtained Q_t and Q_e data in each case were employed to analyze the adsorption kinetics using two different models-pseudo first and second order model. The pseudo first-order model equation (6.2) can be presented as:

$$\ln(Q_e - Q_t) = \ln Q_e - k_1 t \tag{6.2}$$

Where k_1 is the rate constant of the pseudo-first-order model of adsorption (min^{-1}); and q_e and q_t are the adsorbed amount of MB dye at equilibrium and at different times respectively. The values of k_1 and q_e can be calculated from the intercept and slope of linear fittings of $\ln(Q_e - Q_t)$ versus t [15] [285].

The pseudo second order model is presented by eqn (6.3):

$$\frac{t}{Q_t} = \frac{1}{k_2 Q_e^2} + \frac{t}{Q_e} \tag{6.3}$$

where k_2 is the rate constant of the pseudo second order model of adsorption.

The Q_t was plotted with respect to time to observe the adsorption behavior as shown in Figure 6.7. From the graph it can be observed that for the biochar sample the adsorption capacity does not show significant improvement with an increase in contact time and was the lowest among all three samples tested. However, the adsorption capacity of RS-GO-0.1 and RS-GO-1 was much higher than the biochar sample. Both the samples show rapid adsorption behavior in the beginning up to 20 min; thereafter, no rapid adsorption behavior was shown with an increase in contact time. It is clear from the graph that the adsorption coverage of RS-GO-1 was the best among all three samples.

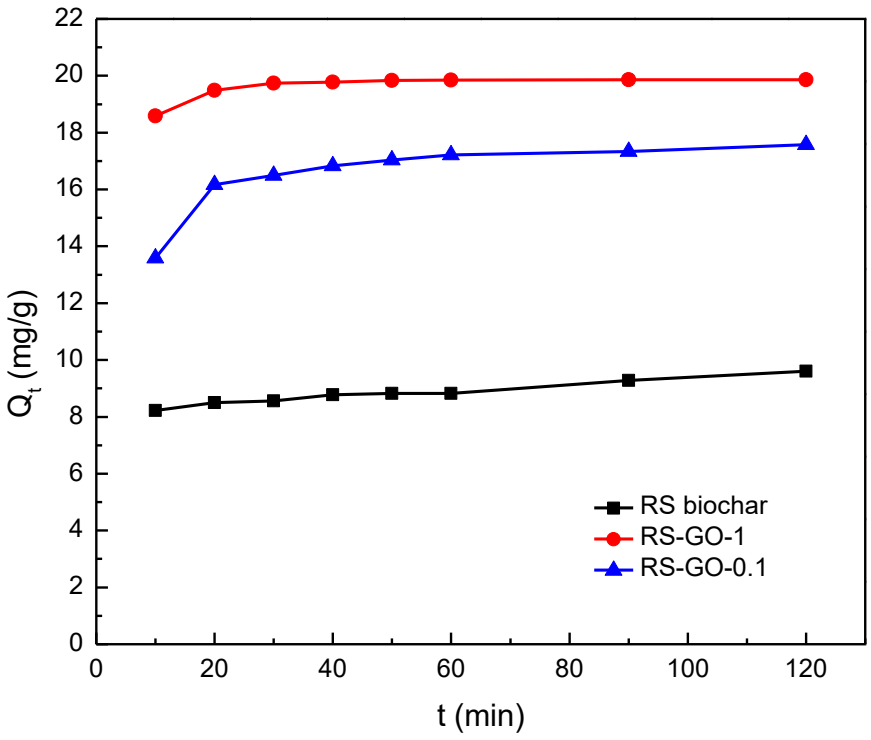

Figure 6.7: Variation of adsorption capacity (Qt) with respect to time (t) for an initial methylene blue (MB) concentration of 20 ppm.

We have fitted the data obtained from the RS biochar, RS-GO-1, and RS-GO-0.1 for PFO and PSO kinetics equations. These adsorption kinetics of all three samples are presented in Figures 6.8(a) and 6.8(b). From the slope and interception of the plot, the related correlation coefficients and kinetic parameters have been calculated and are listed in Table 6.1. For the biochar sample value, or k1, Q_e and R^2 are 0.0165, 1.68, and 0.92, respectively, which have been obtained using the PFO model fittings, and the corresponding values for the RS-GO-0.1 and RS-GO-1 samples were 0.032, 3.28, 0.871 and 0.1, 3.71, and 0.972, respectively.

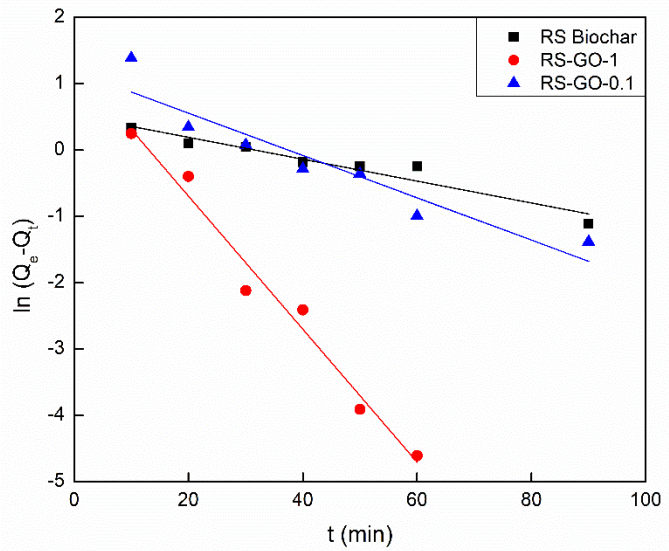

Figure 6.8(a): Linear fitting of pseudo-first order (ln (Q_e-Q_t vs t) for an initial methylene blue (MB) concentration of 20 ppm.

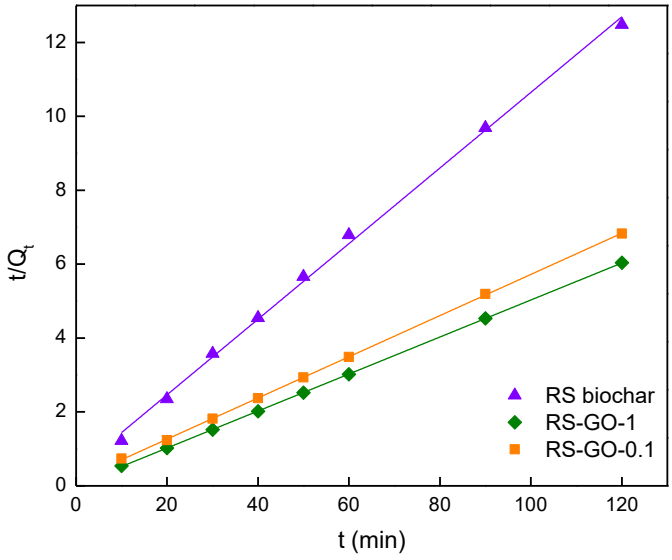

Figure 6.8(b): pseudo-second-order ($\frac{t}{Q_t}$ vs t) kinetics for RS biochar. RS-GO-1 and RS-GO-0.1.

However, the value of R^2 for the RS-GO-1 sample was 0.972, which shows an acceptable fitting of the PFO model for this sample, but the equilibrium adsorption capacity was far lower than the experimental value and PSO values. For all three samples, PSO fits better with $R^2 > 0.99$ and the higher rate constant values. The equilibrium adsorption capacity (Q_e) values using the PSO model are closer to experimental results. The superior fitting of the PSO model illustrates that it describes the experimental results well. It is consistent with the other reported results, which discuss that the adsorption kinetics of different dye compounds can be explained using the PSO model [287].

Table 6.1: Kinetic parameters and correlation coefficients for pseudo-first-order and pseudo-second-order fittings for an initial methylene blue (MB) concentration of 20 ppm.

	RS biochar	*RS-GO-0.1*	*RS-GO-1*
Pseudo-first order			
k_1 (g min^{-1}/mg) Q_e (mg/g)	0.0165 1.68	0.032 3.28	0.100 3.71
R^2	0.920	0.871	0.972
Pseudo-second order			
k_2 (g min^{-1}/mg?) Q_e (mg/g)	0.026 9.76	0.021 17.95	0.111 20
R^2	0.997	0.999	0.999

Percent removal efficiency, *R* for the removal of MB using RS biochar, RS-GO-0.1, and RS-GO-1 were calculated using eqn (6.4), which was 48.05 %, 87.90 % and 99.29 % respectively, for an initial concentration of 20 ppm solution.

$$R = \frac{C_0 - C_e}{C_0} \times 100 \tag{6.4}$$

The best-performing composite sample, RS-GO-1, was tested for different concentrations of 10, 20, and 30 ppm to observe the effect of varying concentration on the adsorption behavior. The well-fitting PSO model was fitted for this sample to see the variation in kinetic parameters.

From ***Table 6.2*** it can be observed that the value of Q_e increases with the increase in initial concentration as expected because the higher initial concentration offers a greater driving force for mass transfer and increases the availability of dye molecules for interaction with the active surfaces on the adsorbate molecule. However, the general trend in the values of k_2 is that it decreases with the increase in concentration. The inverse relationship indicates that at higher concentrations, though more adsorbate is taken up, the adsorption rate per unit driving force reduces. This observation can commonly be attributed to the progressive saturation of active sites over material molecules and the limited potential of intraparticle diffusion at increased concentrations. In order to further understand the adsorption dynamics, the initial adsorption rate using $h = k_2 Q_e^2$ was calculated, which was approximately 499.85, 44.40 and 6.94 mg min^{-1} g^{-1} for 10, 20, and 30 ppm solutions, respectively. Higher initial adsorption implies that mass transfer resistance or site saturation becomes more prominent for higher dye concentration solutions. These observations of adsorption behavior are an indication that the adsorption process for the synthesized materials follows the PSO kinetic model and is affected by the availability of active sites and mass transfer limitations for higher dye concentrations [288].

Table 6.2: Pseudo-second-order parameters for RS-GO-1 at different initial concentrations of methylene blue dye solution.

		Pseudo-second order equation parameters (RS-GO-1)		
C_0 *(ppm)*	C_e *(ppm)*	*Qe (mg/g)*	k_2 *(g* min^{-1}*/mg)*	R^2
10	0.142	9.90	5.10	0.999
20	0.142	20.00	0.111	0.999
30	2.94	27.77	0.009	0.999

We further examine the diffusive kinetics component of the adsorption process. There are three steps involved in the proposed diffusive transport model: (i) A liquid film carries the solute from the bulk solution to the adsorbent's outer surface during the *film diffusion step*, (ii)

Intra-particle diffusion step-during this the adsorbate moves from the outer surface to inside the adsorbents' pores, and (iii) During adsorption process on active sites, accumulation of adsorbate occurs on some specific sites of the inner or outer adsorbent surface. The final step of diffusive behavior will not be observable if the adsorption is very fast and the measured kinetics is diffusion limited. Here, we have utilized the Weber Morris model (eqn (6.5) to identify the diffusive steps and their timescale variations.

$$Q_t = k_i t^{1/2} + C \tag{6.5}$$

When Q_t is plotted against square root of time ($t^{1/2}$), and linear fitting is done then the intercept of the plot will be C which represents the initial coverage and slope will be k_i which is the diffusion rate constant in $\mathrm{mg\,min^{-1/2}\,g^{-1}}$ [276].

Usually, the linear fitting results of the graph show three distinct regimes with three distinct slopes. First regime is related to the film diffusion process, next regime represents the intra-particle diffusion, and the last regime corresponds to the adsorption saturation. Figure 6.9 (a) shows the adsorption spectra of all three samples recorded after 2 hours of adsorption for an initial methylene blue (MB) concentration of 20 ppm. From the figure 6.9 (b), it can be observed that for lower initial concentration the adsorption was very quick and efficient, so all three regimes are not observable separately. However, at higher concentrations all the three regimes are clearly observable as shown in figure 6.9(c) and 6.9(d).

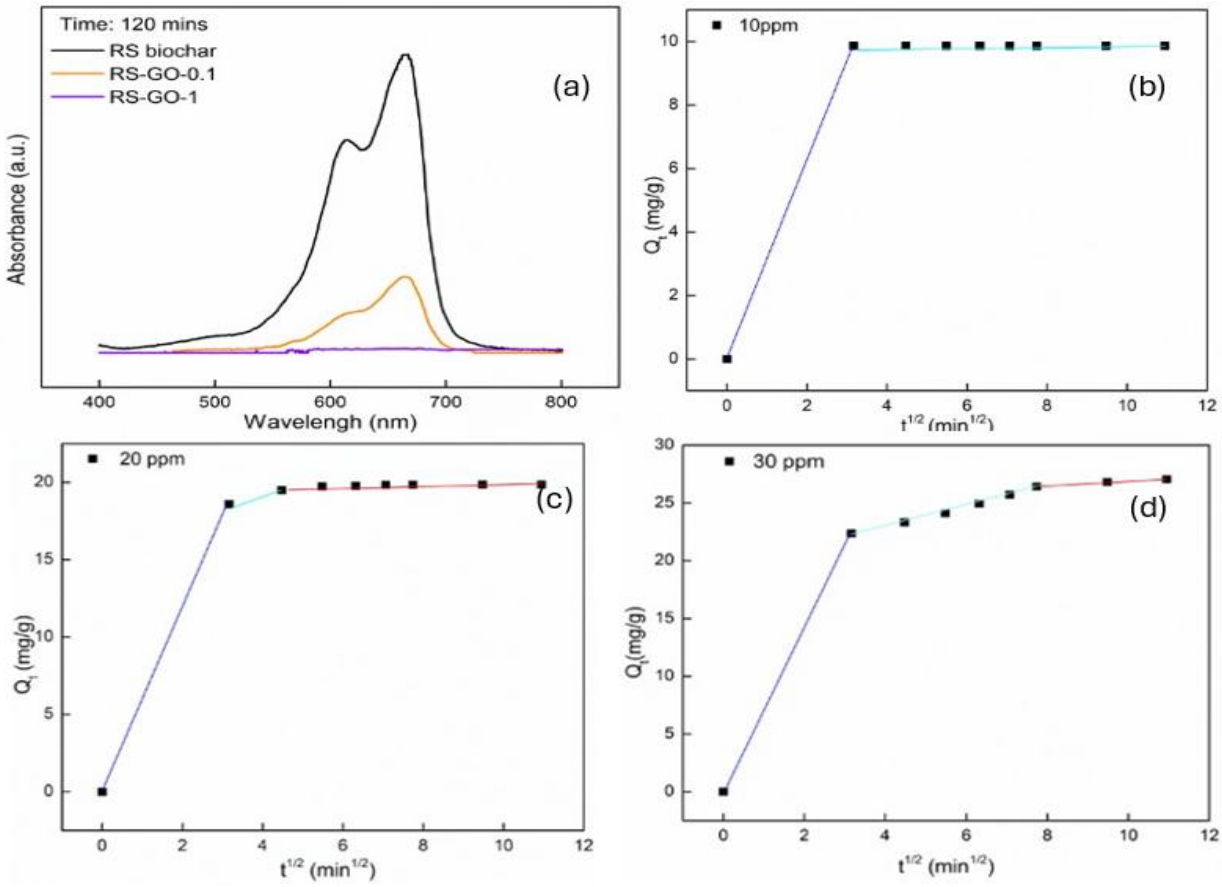

Figure 6.9: (a) Adsorption spectra of all three samples after 2 hours for an initial methylene blue (MB) concentration of 20 ppm. (b), (c), and (d) Intra particle diffusion plots (Q_t vs $t^{1/2}$) for RS-GO-1 at three different concentrations.

To understand synthesized composite and MB dye interaction, the batch study data was fitted to the classical *Langmuir* and *Freundlich models* to obtain the adsorption isotherms. The RS-GO-1 was selected to analyze the complete isotherm using the Langmuir and Freundlich models, which are represented by eqns (6.6) and eqn (6.9):

$$\frac{C_e}{Q_e} = \frac{1}{bQ_m} + \frac{C_e}{Q_m} \tag{6.6}$$

Here Q_m and Q_e are maximum monolayer adsorption and equilibrium adsorption, C_e is the equilibrium concentration, and b is the Langmuir constant that is associated with the free energy of adsorption. The values of C_e and Q_e are listed in *Table 6.2,* which were obtained from the kinetics data fittings. The value of Q_m and b can be obtained from the slope and intercept

of linear fittings of the C_e/Q_e vs. C_e plot. From the linear fittings, the obtained values of Q_m and b from the Langmuir isotherm model are 29.41 mg/g and 0.166 mg/g, respectively.

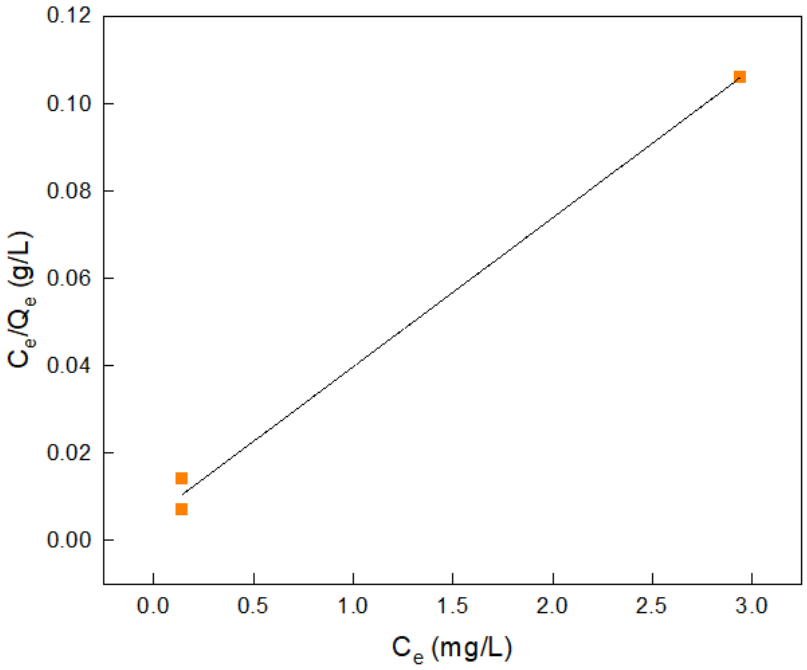

Figure 6.10(a): Langmuir isotherm model for RS-GO-1 samples.

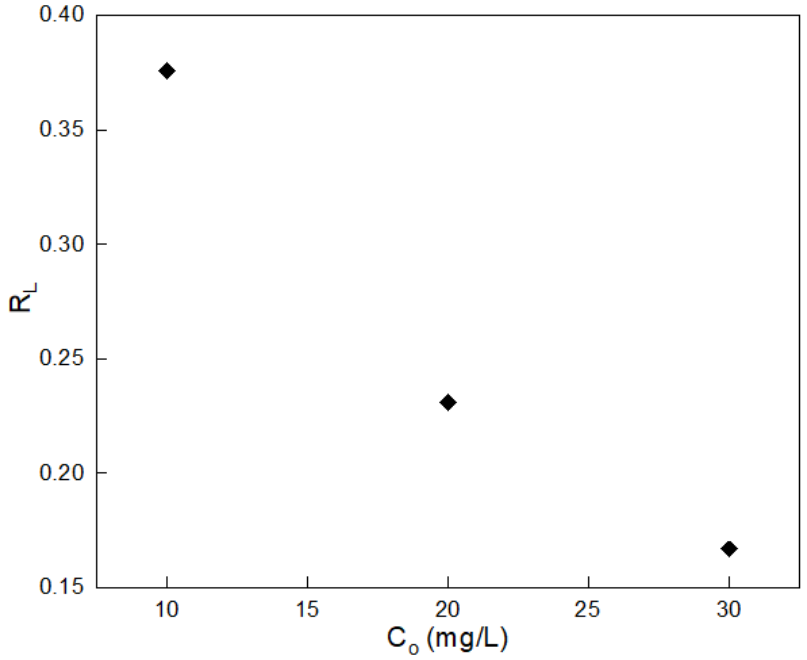

Figure 6.10(b): Separation Factor (RL) vs. initial concentration C0 for the adsorption of MB dye onto RS-GO-1.

An important characteristic of the Langmuir model is the separation factor (R_L), which is related to the feasibility and strength of the adsorption and is described by the following eqn (6.7) [289].

$$R_L = \frac{1}{1 + bC_0} \tag{6.7}$$

Here, C_0 is the initial concentration of MB dye, and b is obtained from the Langmuir model equation, which was described earlier. The value of R_L can be used to decide the feasibility of materials for adsorption as favorable ($0 < R_L < 1$), linear ($R_L = 1$), and unfavorable ($R_L > 1$) [290] [279]. For RS-GO-1, The calculated value of R_L at different initial concentrations was between 0 and 1, which have been presented in the figure 6.10(b), indicates that the adsorption is favorable for the MB dye using the synthesized biochar-GO composite.

Adsorption isotherm using the Freundlich model can be obtained using the following eqn (6.8):

$$Q_e = K_F C_e^{1/n} \tag{6.8}$$

Which can be written in linearized form as (eqn (6.9)

$$\mathbf{log}\, Q_e = \mathbf{log}\, K_F + \frac{1}{n}\mathbf{log}\, C_e \tag{6.9}$$

where K_F **(L g^{-1})** is the Freundlich adsorption coefficient and n is an isotherm nonlinearity index, which is associated with the heterogeneity of adsorption sites. Q_e and C_e are equilibrium adsorption and concentration in mg g^{-1} and mg L^{-1}, respectively. The values of n and K_F can be obtained by the slope and intercept of linear fitting to the $\mathbf{log}\, Q_e$ vs. $\mathbf{log}\, C_e$ plot.

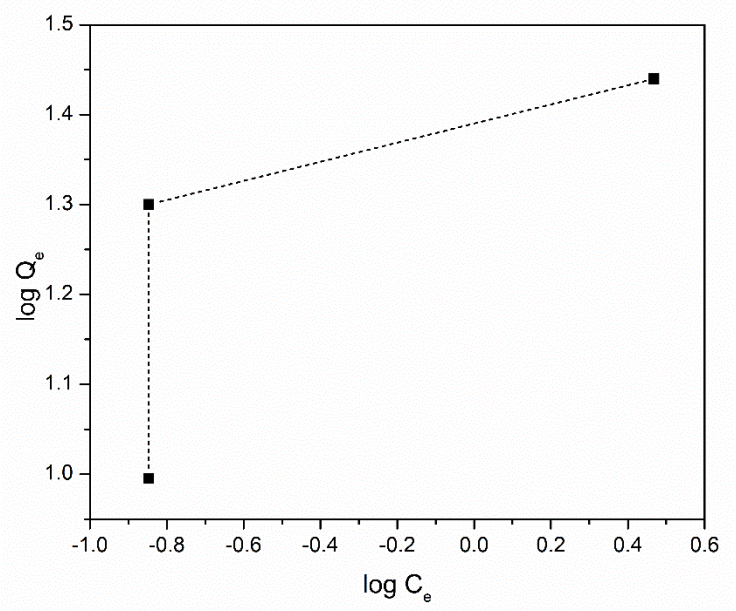

Figure 6.11: Freundlich isotherm model for RS-GO-1 sample.

From the figure 6.11, It can be observed that the experimental data does not fit well to the Freundlich isotherm model. The equilibrium concentration obtained was the same for the 10 and 20 ppm initial concentration solutions. Such adsorption behavior shows that the adsorption sites at the surface were saturated at lower concentrations. Since this model is used to observe adsorption behavior having a heterogeneous surface, the poor fit for adsorption in the selected system could be attributed to the adsorption occurring on a relatively homogeneous surface with monolayer adsorption behavior [291]. The comparison of material synthesized towards MB dye adsorption is presented in

Table 6.3: Performance comparison table for dye adsorption.

Adsorbent	**Q_{max} (mg/g)**	**Reference**
Coal fly ash	0.74	[292]
PDADMAC Modified ZSM-5 Zeolite	4.31	[293]
Activated carbon-apricot shell	4.11	[294]
RS-GO-1	19.86	This work

6.4 Conclusions

The three adsorbents, rice straw biochar and GO-modified biochar (RS-GO-0.1 and RS-GO-1), were synthesized and evaluated for their adsorption potential of methylene blue dye from aqueous solution under batch adsorption conditions with initial dye concentrations of 10, 20, and 30 ppm. The observation of this study indicated that the biochar-graphene oxide composites have superior adsorption potential for the methylene blue dye, with the best performance exhibited by RS-GO-1. The hydrothermal treatment during the synthesis process was done to ensure a strong bonding of graphene oxide over biochar surfaces. The adsorption of the low-concentration dye was almost 100% using the RS-GO-1 composite. The enhancement of adsorption by composites may be attributed to the increased surface area, as observed in the BET results, and the GO-induced interaction and functional groups over the biochar surface. The adsorption kinetics analysis confirmed that the pseudo-second order model was best followed by the adsorption process for all samples, which is an indication of chemisorption. The Weber-Morris model to interpret intraparticle diffusion further added clear insights into the adsorption behavior for the chosen system. The Langmuir isotherm model successfully fitted the collected adsorption data, while the Freundlich model was less suitable for the obtained experimental data set. In conclusion, the use of GO for the synthesis of biochar composite improved the adsorption capacity of raw biochar, so it could be a good alternative adsorbent for sustainable industrial uses.

The use of agricultural crop residue for biochar preparation and synthesis of biochar-graphene oxide composites is indeed an environmentally beneficial and sustainable route for obtaining a low-cost adsorbent for wastewater treatment.

The next chapter talk about enhancing biochar functionalities through activation, nitrogen doping and surfactant modification to further explore its application potential. This study added another new dimension of biochar-based material for use in CO_2 entrapment application.

CHAPTER- 7

Development of Nitrogen (N)-doped Activated Biochar (AB) using Mango Kernel Biomass for CO_2 Entrapment Application

Abstract

Development of sustainable and efficient carbon capture materials is critical for mitigating anthropogenic CO_2 emissions. In this work, mango kernel biomass was transformed into high performance carbon material through sequential process of activation, nitrogen doping and surface modification by using natural surfactant extracted from fenugreek seeds. Chemical activation increased BET surface area from 21.6 m^2 g^{-1} to 1882.1 m^2 g^{-1}, while nitrogen doping leads to further enhancement to 2021.6 m^2 g^{-1} by introducing nitrogen functionalities. Surfactant plays a vital role in surface modification, where partial decrease in BET surface area was observed along with significant alteration in surface chemistry and pore level interaction. Structural and surface characterization ensures the formation of microporous carbon framework enriched in nitrogen functionalities. CO_2 entrapment performance was monitored by pressure decay studies, shows progressive increase in pressure drop demonstrating combined advantages of porosity and surface functionalization. Enhanced performance of surfactant modified nitrogen doped activated biochar (SNMKAB) may be attributed to synergistic effects of micropore formation, nitrogen functionalities and surfactant assisted CO_2 interaction. This study introduces novel, fully bio-based surface modification strategy that integrates agricultural waste derived carbon with plant-based surfactant, offering environment friendly and low cost alternative to conventional material for CO_2 entrapment.

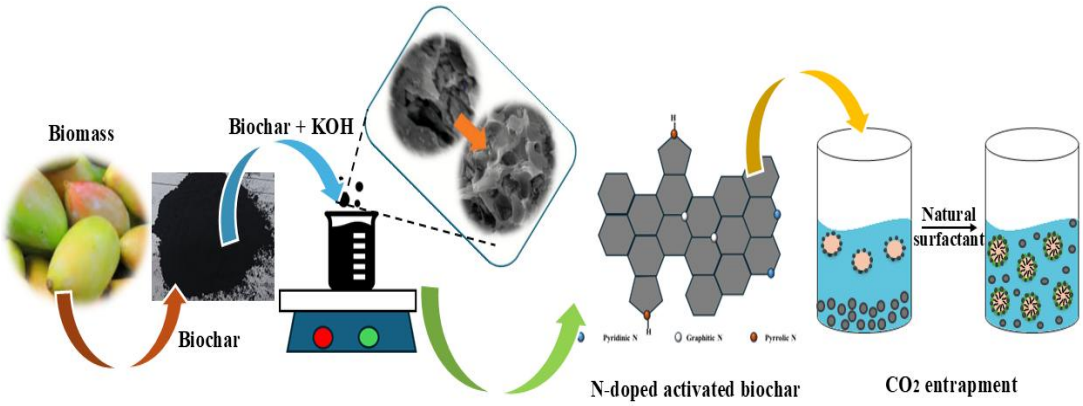

Figure 7.1a: Graphical abstract.

7.1 Introduction

Rapid increase in concentration of carbon dioxide (CO_2) in atmosphere has become one of the major drivers of climate change, thereby shows the path for intensive research towards the development of negative-emission and low-carbon technologies. Significant efforts have been made in developing economical and sustainable methods that leads in efficient CO_2 capturing and storing to limit its emission in the atmosphere. The principal methods for CO_2 capturing rely on processes such as adsorption, absorption, cryogenic distillation and membrane separation[295] [296] [297]. Among these, adsorption by amine is most widely used and effective method for CO_2 capture. However, it has several technical and economic disadvantages such as high energy consumption, quick corrosion in the equipment, the release of toxic amine vapours etc. which lead to high capital and operational costs. Among various mitigation strategies, solid based CO_2 entrapment using porous carbon materials has gained significant attention due to its operational simplicity, chemical stability and potential for large scale deployment. How ever, the performance of conventional carbon materials is often limited by insufficient surface functionality and poor affinity towards CO_2 molecules, which shows the need of further material modification and innovation.

Biochar derived from agricultural waste has emerged as a promising precursor for the preparation of low cost as well as environmentally friendly carbon materials. Biomass-derived carbons materials offer several advantages, that is, high surface area, tunable porosity and abundant surface functional groups with low cost and renewability. Utilization of biomass residue not only addresses waste valorization but also contributes in circular economy principles. Biochar, obtained by thermochemical conversion of biomass under oxygen-limited conditions, provides a versatile scaffold for designing CO_2 sorbents. Its pore structure, surface chemistry and mineral content depend strongly on feedstock and pyrolysis conditions, which can be optimized for gas adsorption rather than soil amendment. To enhance the adsorption

capability of biochar, physical or chemical activation is commonly employed to enhance surface area, pore volume and active sites. Among various activating agents, potassium hydroxide (KOH) activation has gained significant attention in generating well developed micro as well as mesoporous structures. KOH activation promotes extensive pore formation and introduces surface defects, thereby improving gas adsorption capacity. Kaya et al. prepared KOH activated biochar from pine cone for CO_2 capture. The pyrolysis temperature was 600°C and activation with KOH (mixed in1:4 wt./wt.) was done at 800°C for 1 hour. The BET surface area of biochar was 259.74 m^2/g and that pf activated biochar was found to be 1714.5 m^2/g. The CO_2 holding ability of KOH activated biochar was investigated by using the thermogravimetric analysis method. The activated biochar showed a 160 mg/g of CO_2 adsorption capacity at 25 °C temperature [298].

Rouzitalab et al. and the group had prepared biochar from walnut shell using pyrolysis temperature of 600°C. Then nitrogen doping was done by mixing the urea in different mass ratio and heating the mixture at 400°C. Thereafter, the N-doped sample was mixed with KOH in 1:4 mass ratio and activated at 900°C for 1 hour. The final prepared material showed a CO_2 adsorption capacity of 7.42 mmol/g under a pressure of 1 bar. It was concluded that N-doping improved adsorption of CO_2 and due to its high porosity, N-containing functional groups, high stability, simple regeneration process, and low cast make it a promising CO_2 adsorbent [299].

In another work by Nazzal et al. used banana peel for development of porous carbon. First the banana peel was dipped in aqueous solution of KOH and dried at 200°C. After drying and subsequent grinding it was heated in furnace at 700-900°C to obtain activated carbon. Again, to prepare another sample urea was mixed with KOH and similar procedure was followed. The activated carbonous sample exhibited specific surface area in the range of 2700-2800 m^2/g. The KOH activated materials were found to have CO_2 adsorption capacity of 5.75 mmol/g and 3.74 mmol/g at 1 bar pressure and 0 °C and 25°C temperature respectively[300] .

In a recent study by Zhang et al. employed machine learning models to predict the CO_2 adsorption capacity of KOH activated biochar. It was reported that CO_2 adsorption predominantly governed by micropore and nitrogen-containing surface functionalities and it increases when the nitrogen content increase at usually low adsorption temperature, (less than 20°C) as for CO_2 affinity to N-containing functional groups on activated biochar surface a lower temperature is more favourable [301].

Among various reported biomass, mango kernel biomass has been less explored as precursor for activated biochar for carbon capture application. Mango kernels are one of the widely available agro-industrial by-product, high carbon content and remain largely underutilized. Converting mango kernel biomass into value added carbon materials offers an attractive pathway for sustainable material development while reducing environmental burden. In addition, biochar and activated carbon materials derived from agricultural waste have been widely investigated for CO_2 capture applications, but most reported studies focus primarily on pore structure development through activation. Limited attention has been given to surface functional modification. Thus, there is need of sustainable and bio-based additives as surface modifiers, which can offer a practical and environmentally safe approach to improve CO_2 affinity while eliminating toxic chemical additives.

In recent years, increasing emphasis has been placed on modifying surface chemistry of carbon-based materials to improve their affinity towards CO_2 molecules. Introduction of eco-friendly functional additive has emerged as an effective strategy to enhance gas-solid interaction while maintaining environmental compatibility. Natural surfactant obtained from plant sources offers sustainable alternative to conventional modifiers, as they are biodegradable, non-toxic and derived from renewable resources. These bio-based surfactants typically contain oxygen and nitrogen containing functional groups, which can promote stronger interaction with CO_2 through surface adsorption mechanism. When bio-based

surfactants incorporated onto activated biochar surfaces, these biomolecules can alter surface chemistry and create additional active sites for CO_2 interaction. Such surface functionalization not only improves accessibility of adsorption sites but also enhances both physical adsorption and weak entrapment of CO_2.As a result, combination of activated biochar and natural surfactant represents a promising and sustainable approach for improving CO_2 entrapment performance. Thus, novelty of present work lies in the development of sustainable composite materials by integrating KOH- activated biochar derived from mango kernels with natural surfactant extracted from fenugreek seeds. This approach introduces an eco-friendly route to enhance surface functionality and CO_2 interaction without relying on synthetic modifiers.

In this study, biochar was synthesized from mango kernel biomass and subsequently activated using KOH activation followed by nitrogen doping using low-cost urea to obtain high surface area activated biochar. Prepared biochar and activated biochar were characterized using X-Ray Diffraction (XRD), Raman Spectroscopy, X-Ray Photoelectron Spectroscopy (XPS), Brunauer-Emmett-Teller surface analysis (BET) and Field Emission Scanning Electron Microscopy (FESEM) to understand structural as well as surface modifications. A sustainable composite was then developed by combining activated biochar with natural surfactant extracted from fenugreek seeds. CO_2 entrapment capability of developed composite material was evaluated through pressure decay studies, providing insights into its gas interaction behaviour under pressurized conditions. This work highlights a sustainable approach that combines agricultural waste-derived carbon material and bio-based surfactant for efficient and environmentally responsible CO_2 entrapment applications.

7.2 Materials and methods

7.2.1 Materials

Mango kernels were collected from local market and used as raw biomass for biochar synthesis. Initially kernels were washed thoroughly with distilled water and dried in hot air oven to remove surface impurities and moisture. Potassium hydroxide (KOH, purity 85%) used for activation was purchased from chemical supplier. Urea (purity 99.5%) used for nitrogen doping was also from the same supplier. Fenugreek seeds were procured from local outlet at Amethi and used for extraction of natural surfactant. Extraction of natural surfactant was done by using Soxhlet apparatus obtained from Jain Scientific Glassworks, India. High purity CO_2 gas (purity~99.95%) used for pressure decay studies was supplied by Sigma gases India [302]. Deionized water was used throughout the experimental work.

7.2.2 Synthesis of Surfactant modified nitrogen doped activated biochar

Synthesis of surfactant modified nitrogen doped activated biochar was carried out through a four-step process, as schematically illustrated in *figure 7.1*. The process involves four major steps; obtaining biochar from pyrolysis, activation of biochar, addition of nitrogen to the activated biochar and finally surfactant modification of nitrogen doped activated biochar.

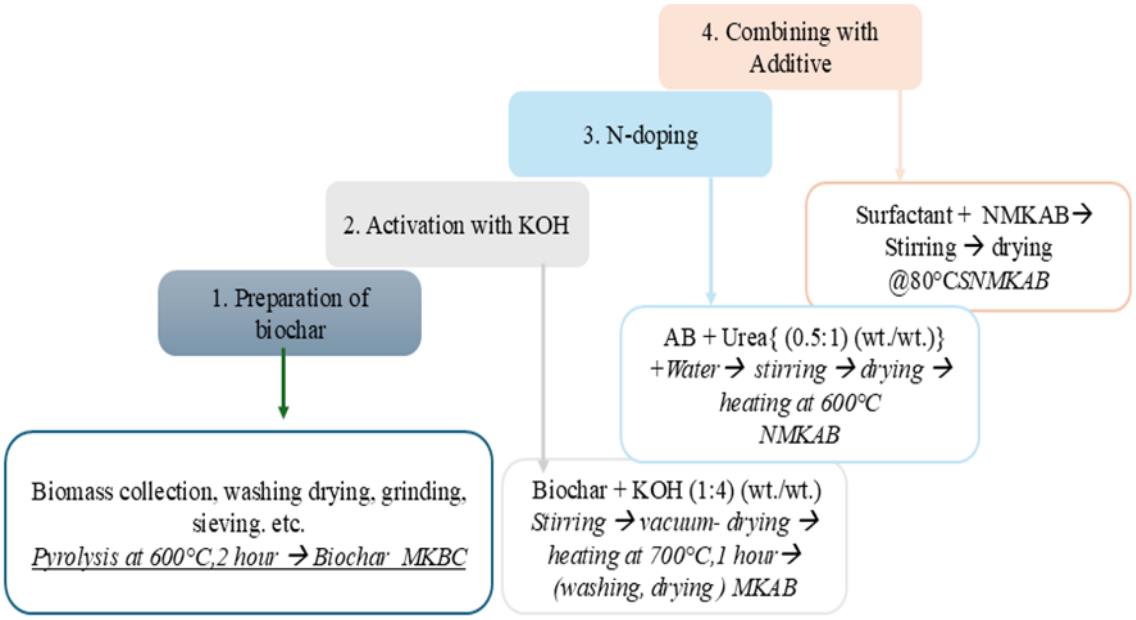

Figure 7.1: Schematic representation of the methodology used.

7.2.3. Preparation of activated biochar from Mango Kernal

Shells of Totapuri mango were collected from a fruit juice shop located in the local market of Jais, a town in the Amethi district of Uttar Pradesh, India. *Totapuri mango* or *Ginimoothi* is a cultivar of mango which is widely grown in southern states of India and is available throughout the year at fruit shops in the local market. The mango shells were washed thoroughly multiple times with tap water and DI water. After washing the mango shells were dried in an air oven at 80 °C for 48 hours. Thereafter the shells were broken, and mango kernel were separated. The mango kernel was then crushed and grounded using a kitchen grinder to obtain powder form. The mango kernel powder was sieved using 100 mesh size sieves to obtain uniform particle size for this experiment. Thus, obtained sample was stored in an airtight container to save it from atmospheric moisture. This sample was further used for pyrolysis at 550°C in a muffle furnace under nitrogen environment to convert it into biochar as shown in figure 7.2. Detailed procedure for pyrolysis process has been discussed in section 4.2.2. of the thesis and also reported in our previous works [280] [281]. For the preparation of activated

biochar, this mango kernel biochar was then mixed with potassium hydroxide in the ratio1:4 (wt./wt.) and a minimal amount of DI water and stirred continuously for 2 hours using a magnetic stirrer for uniform mixing. Thereafter, this mixture was kept in a vacuum oven at 80°C for 48 hours to remove excess moisture from the mixture. This mixture was then calcined at 650°C for 1 hour in a muffle furnace under nitrogen environment to obtain activated biochar and this was named MKAB.

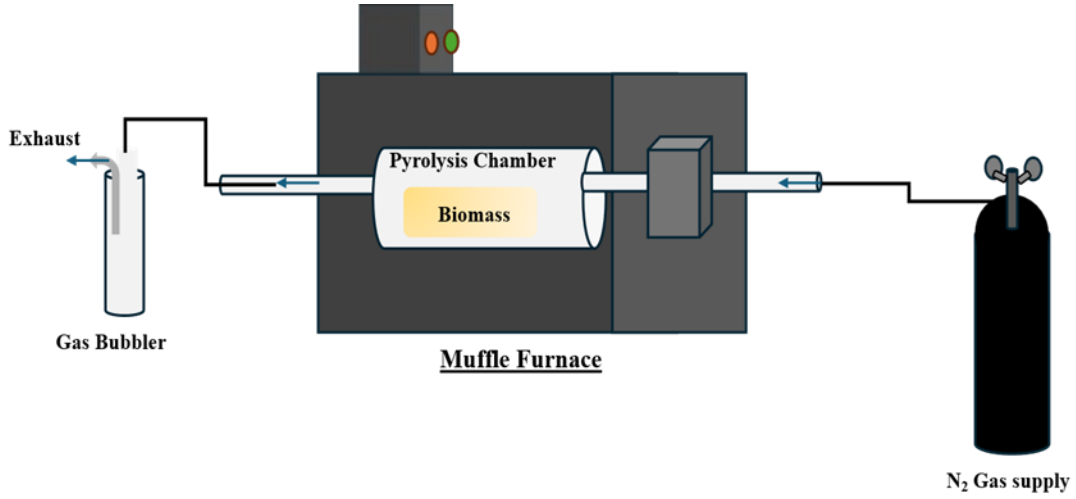

Figure 7.2: Schematic diagram of biomass pyrolysis using a modified muffle furnace.

7.2.4. Preparation of N-doped activated biochar

Thus, obtained MKAB was washed with 0.1 M diluted HCl solution and DI water to remove excess potassium or other impurities from the activated biochar. After washing, again the MKAB was kept in an air oven at moderate temperature (80°C) for 48 hours to remove excess moisture. After drying carefully stored for further uses.

This experiment was further carried out to obtain nitrogen doped activated biochar. For nitrogen doping urea was mixed with MKAB in the ratio 0.5:1 (wt./wt.) with minimal amount of water and stirred continuously for one hour. Thereafter, the mixture was dried in an air oven for 24 hours at 105°C to remove excess moisture. After drying the mixture was heated in a muffle furnace at 550°C for one hour under inert atmosphere. The temperature was desirably

kept lower than the activation temperature of 650°C so that it does not alter the structure of MKAB. After cooling to room temperature, the sample was collected and washed with DI water to remove impurities. This was again kept in air oven for drying. This dried sample was named NMKAB which is nitrogen doped activated biochar.

7.2.5. Surfactant modification of NMKAB

Natural surfactant was extracted from fenugreek seeds using Soxhlet extraction method. Fenugreek seeds were sun-dried for 10 days and then oven-dried at 50 °C for 0.5 h to remove excess moisture. The dried seeds were ground in an industrial grinder (Oster, India) at 2000 rpm. For extraction, ~50 g of the powder was wrapped in muslin cloth and placed in the Soxhlet extraction chamber containing vapor and siphon tubes. A round-bottom flask was positioned in the heating mantle below the chamber, and a condenser was fitted above it. Methanol was used as the solvent. During extraction, condensed solvent accumulated in the chamber until it reached the siphon level, after which the extract flowed back into the round-bottom flask. The Soxhlet extraction was continued for ~48 h to obtain the concentrated surfactant. The collected extract was then dried in a hot-air oven at 70 °C for 24-48 h. Using 100 g of fenugreek seeds as raw material, the surfactant yield was found to be 12.76 ± 11 % (w/w) [299]. Finely ground seed powder was continuously extracted with methanol as solvent for ~48 h to ensure complete extraction of surface-active compounds. Extracted solvent was then placed in hot air oven for drying and followed by crushing and sieving to obtain desired surfactant residue. Surfactant was used at critical micelle concentration (CMC), that is, 0.2 wt.%. Surfactant was dissolved in 20 ml of DI water and the 3 grams of NMKAB was added and stirred for absorbance of surfactant over activated biochar particles. After the stirring, the sample was dried in oven at 80°C for 48 hours. The dried sample was collected a stored for further uses. This surfactant modified sample was named as S-NMKAB.

7.2.6. Characterization

The crystal structure of all the sample prepared was studied by powder X-ray diffraction (XRD) with (Panalytical, EMPYREAN-QTY1) using Cu Kα monochromatic radiation at a voltage and current of 40 kV and 30 mA respectively. The diffraction angle was in the range of 2θ= 5-80°, with intervals of 0.5/min and 2.4 s integration. Total pore volume and specific surface area (SSA) of all the samples were analysed using Brunauer-Emmett-Teller (BET) instrument (MicrotracBEL, Max II). Before the analysis, the samples were degassed at 180° C for 8 hours in a vacuum. Raman spectra were recorded using Raman spectroscopy (JASCO NRS-5500) with a 514 nm laser excitation source. It was done to evaluate degree of structural disorder as well as graphitic nature of carbon samples by anlyzing D and G bands. Multiple scans were averaged for improved signals to noise ratio. The surface morphology of the samples was analysed using FESEM (JEOL, JSM-7900F). XPS instrument (Thermo Fisher SCIENTIFIC K-Alpha) was used to analyze the surface elemental composition and chemical states of the samples. It also provides details if successful incorporation of nitrogen functionalities surfactant related groups on the carbon surface.

7.2.7. CO_2 entrapment by pressure decay method

CO_2 entrapment performance of prepared materials was evaluated using pressure decay technique as shown in *figure. 7.3.* Experiment was conducted in stainless steel pressure cell with a known internal volume (~50 ml). To prepare the sample for CO_2 entrapment a 50 mg of synthesised material was mixed to 25 ml water. This mixture (~25 ml) was placed inside the cell. The pressure cell was sealed and purged to remove air. High purity CO_2 gas was introduced into pressure cell up to predetermined initial pressure at room temperature. Pressure inside the cell was monitored continuously using digital pressure sensor. When CO_2 starts interacting with the sample, a gradual decrease in pressure was observed with time. Change in pressure

was recorded until equilibrium was reached. The extent of CO_2 entrapment was estimated from the pressure drop, which shows the gas interaction and storage capability of the materials.

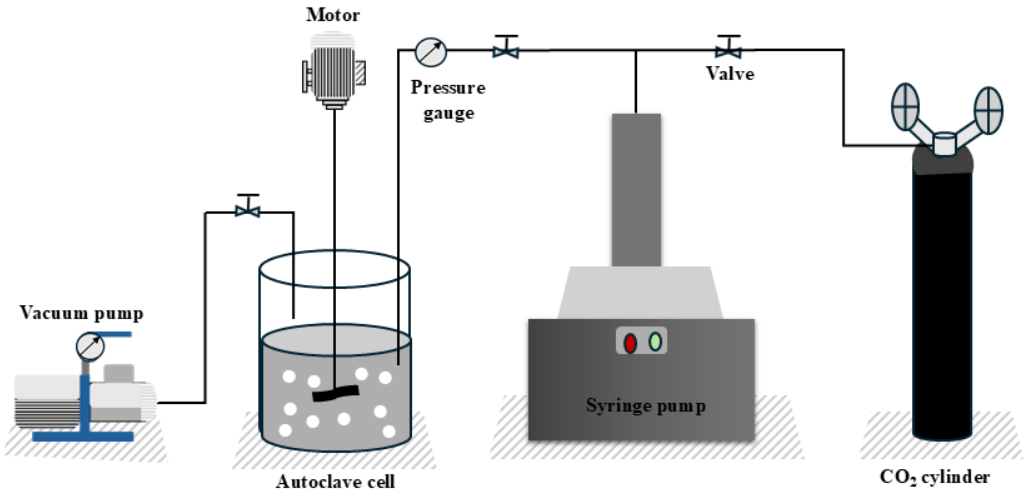

Figure 7.3: Experimental setup used for CO_2 entrapment observation.

7.3 Results and discussions

7.3.1 X-ray Diffractometer (XRD)

The XRD pattern as shown in *figure 7.4*; mango kernel-derived biochar (MKBC) shows almost flat profile with few low-intensity diffraction feature around 2θ =~26-30° which are broad humps and shoulders that indicates a highly disordered aromatic carbon structure. This region commonly corresponds to the reflection of turbostratic, rather than well-crystallized graphite. In biomass-derived biochar, such reflections are often observed that are typically broad and weak due to small crystallite size, random stacking of graphene layers, and a high density of structural defects formed during pyrolysis [303]. These peaks may also arise from the residual of inorganic or mineral phases that are often naturally present in biomass, such as SiO_2, K_2CO_3,$CaCO_3$ etc [304].

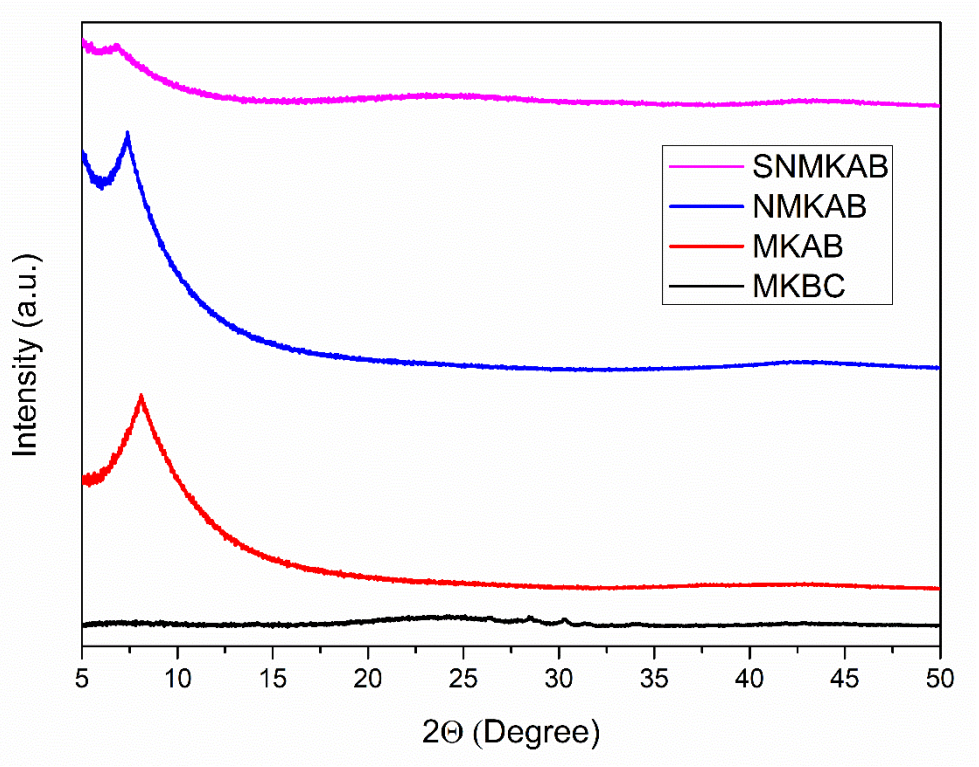

Figure 7.4: XRD pattern for all the samples.

After activation of biochar with KOH, the activated biochar (MKAB) shows low-angle diffraction peak around 2θ = ~8 °. This shift in peak may be attributed to expanded interlayer spacing which is due to chemical activation with KOH. During KOH and carbon reaction at higher temperature metallic potassium intercalates between carbon layers. This leads to lattice expansion and disruption of original carbon framework [305] [306]. However, the appearance of this peak in activated biochar is due to development of ordered micropore-mesopore network and partial alignment of carbon layers around pores. This does not represent graphitic crystallinity, instead it reflects pore-induced structural ordering, which is typical of chemically activated biochar [307].

Further modification through nitrogen doping of activated biochar (NMKAB), exhibit relatively sharp diffraction peak at 2θ = ~7°. This shift may be attributed to additional structural rearrangement, which may be due to addition of nitrogen doping into carbon matrix. Nitrogen doping may promote localized ordering altering electronic structure and inducing defects that

influence pore wall organization. Despite this increase in peak sharpness, overall structure remains non-graphitic as well as disordered. Moreover, in surfactant modified nitrogen doped activated biochar (SNMKAB), a weak diffraction profile was observed in lower angle value, that is in range of $2\theta = \sim 4 - 6°$. This shift towards lower angle may be attributed to additional increase in interlayer spacing between carbon layers. This may be due to surface coating as well as interfacial interaction between molecules of natural surfactant and carbon framework. The presence of surfactant is expected to influence the packing of carbon layers near the surface without affecting crystallinity.

Overall, XRD pattern observation confirms that pristine biochar MKBC is highly amorphous, and subsequent chemical activation, nitrogen doping and surfactant modification successfully modified the carbon structure by expanding interlayer spacing and enhancing pore-related ordering without forming crystalline graphite. The appearance of structural disorder across all samples is advantageous for application like gas adsorption, as it provides abundant site defects and accessible pores. This makes all these carbon materials highly suitable for CO_2 entrapment [308] [309].

7.3.2. Surface Area (BET) Analyzer

The nitrogen adsorption-desorption isotherms of MKBC, MKAB, NMKAB and SNMKAB clearly demonstrate the progressive development of highly microporous carbon framework tailored for post-combustion CO_2 capture. Distinct changes in isotherm shape and textural parameters confirm strong influence of chemical activation, nitrogen doping and surface modification on pore formation as well as surface characteristics.

MKBC, pristine mango kernel biochar, shows a low BET surface area of about 21.6 $m^2 g^{-1}$ (figure 7.5 a) and a gently rising type-II isotherm, which is typical for raw biochar with poorly developed microporosity and significant macropore contribution. Such small surface

areas are consistent with the general observation that non-activated biochar often exhibit low area when assessed by N_2-BET, despite their relatively high sorption capacities in aqueous systems [310].

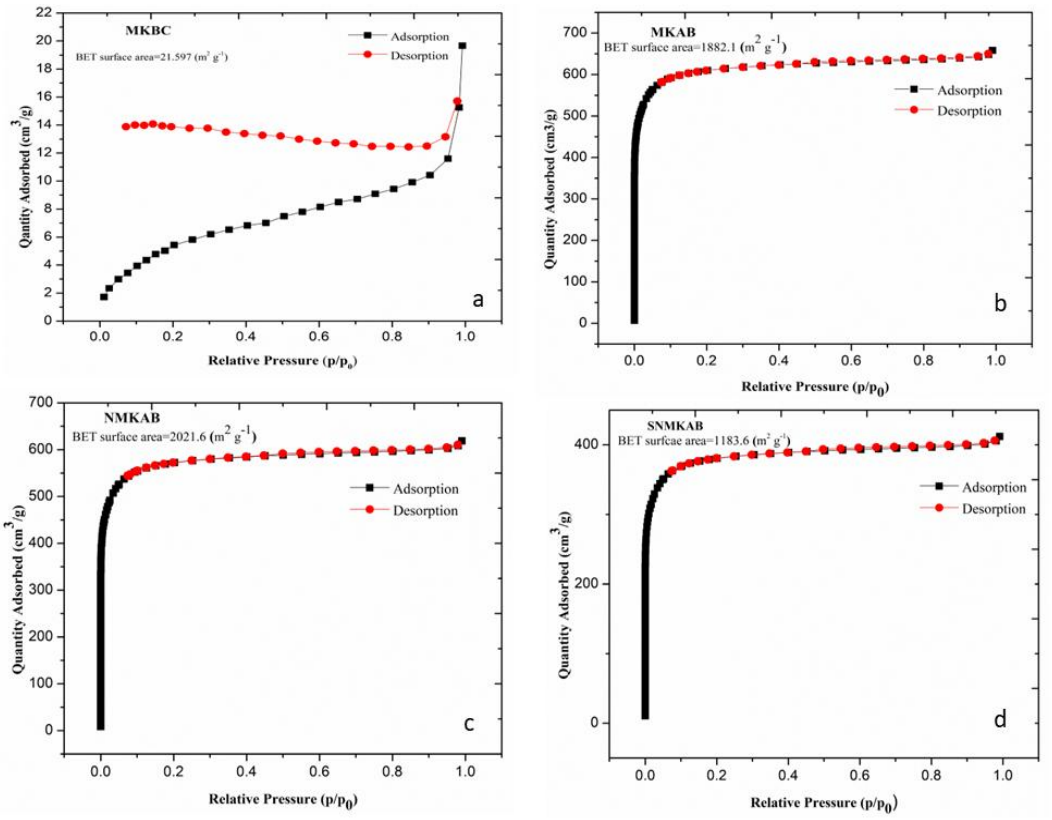

Figure 7.5: BET nitrogen adsorption-desorption isotherms of (a) MKBC, (b)MKAB, (c) NMKAB and (d) SNMKAB.

In addition, MKBC exhibit broader hysteresis loop between adsorption and desorption, suggesting the predominance of inter-particle voids and larger pores, as commonly observed for non-activated biochars. Gotre et al. also obserevd simler loop pattern for corn-derived biochar [311]. Simler BET isotherm for biochar reported by Yang Sun et al for corn stalk derived biochar [312].

Upon chemical activation with KOH, MKAB shows considerable enhancement in textural properties, reaching BET surface area of 1882.1 m^2 g^{-1} (figure 7.5b) which is roughly eighty-seven times as of MKBC surface area. The isotherm transforms into type-I (b) profile

as classified by IUPAC [313], indicating predominance of micropores with narrow pore size distribution. This considerable increase in surface area may be attributed to the reaction between KOH and carbon at elevated temperature, which further promotes pore etching, carbon framework expansion and removal of volatile species. This behaviour is accordance with earlier reported studies for KOH activated biochar derived from lignocellulosic biomass [314] [315]. Introduction of urea during activation to form NMKAB further increases the surface area to around 2021.6 m^2g^{-1} (figure 7.5 c). Improvement in surface area and microporosity can be attributed to thermal decomposition of urea, which releases gaseous species during heat treatment and promotes formation of additional micropores. Nitrogen doping via urea decomposition is expected to introduce basic surface functional groups (pyrrolic, pyridinic nitrogen) that modify the carbon matrix without effecting the pore structure [316] [317]. Hisse et al. showed that urea-aided nitrogen-doping of K_2CO_3-activated corn-husk biochar produced with surface areas around 1200 m^2 g^{-1} and substantially improved CO_2 uptakes compared with non-doped precursors, as a result of the combined effects of increased micropore volume (<1 nm) and basic nitrogen functionalities over the surface [318].

In contrast, surfactant modified NMKAB sample i.e., SNMKAB shows reduced BET surface area of 1183.6 m^2/g (figure 7.5 d) that is lower than activated biochar samples. The corresponding isotherm remains type-I, suggesting that the surfactant treatment partially blocks or reorganizes some micropores while maintaining a dominant microporous network. Similar reduction in BET surface area after surface modification have been reported in literature, where modifiers preferentially occupy narrow pores while enhancing surface chemistry. In addition to this, surfactant modification NMKAB is expected to influence the CO_2 entrapment behaviour through interfacial effects within porous carbon matrix. Adsorption of surfactant molecule on internal pore surfaces may lead to partial filling of micropores, as a result formation of organic coated environment is expected rather than open carbon surface. Similar

pore surface modification effects have been reported in literature showing modified porous carbon, where changes in gas uptake were attributed to altered surface chemistry instead of increased surface area. This surfactant lined pores are expected to provide favourable condition for CO_2 retention by enhancing local interaction and restricting gas mobility within confined pore spaces. The presence of organic layers may also reduce interfacial energy and thereby promotes stabilization of CO_2 within the pore structures. Although this modification may result in decrease in BET surface area, but it may simultaneously improve CO_2 entrapment efficiency due to stronger interfacial interaction and enhanced surface affinity. Therefore, surfactant modification is likely to contribute to CO_2 entrapment through combined mechanism involving pore confinement and surface chemical interaction rather than pure physical adsorption.

Therefore, BET results confirms the high surface area and increased microporosity of MKAB and NMKAB. While surfactant modification (SNMKAB) slightly reduces accessible surface area, but it maintained microporous framework, which remains favourable for CO_2 entrapment through surface interaction.

7.3.3. Raman spectroscopy

Raman spectroscopy was employed to investigate the effect of activation, nitrogen doping and surfactant modification on the carbon structure of prepared samples, that is, MKBC, MKAB, NMKAB and SNMKAB. All the prepared sample exhibit two prominent Raman bands at ~1344 cm^{-1} and 1587 cm^{-1}, (as shown in figure 7.6), corresponds to D and G band respectively. G- band is known to be associated with ideal graphitic lattice while D-band is associated with the vibration of mostly disordered graphitic lattice [319].

The ratio of corresponding intensity (I_G/I_D) gives a quantitative estimation of defects present in a material [320] [321]. I_D/I_G ratios increase systematically from MKBC (0.39), MKAB (0.60), NMKAB (0.67) and SNMKAB (0.71), showing that activation and subsequent

modifications progressively increase defect density and structural disorder in the carbon framework. This increase may be attributed to chemical activation followed by surface modification which introduces additional defects as well as reduced the size of aromatic domains.

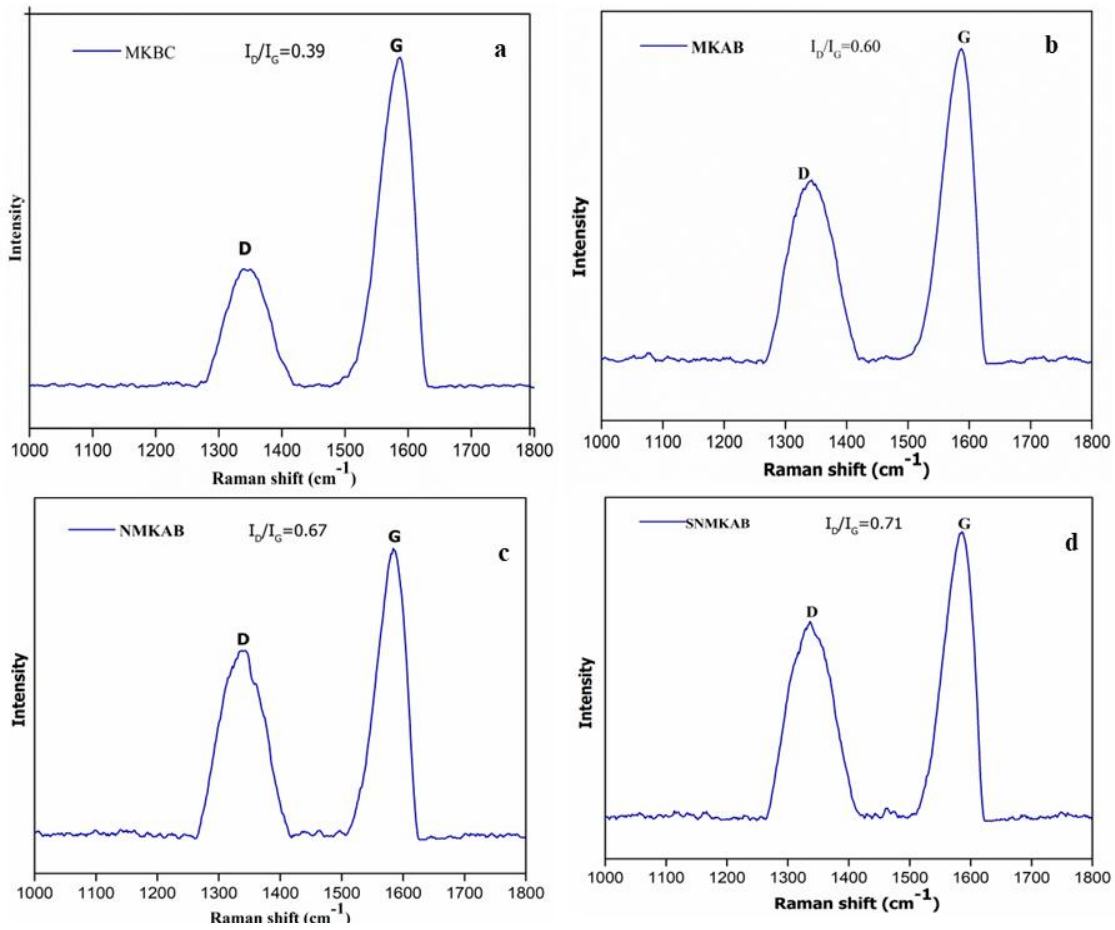

Figure 7.6: Raman spectra for (a)MKBC, (b)MKAB, (c) NMKAB, and (d) SNMKAB.

MKBC, with I_D/I_G =0.39, has a relatively intense G band (~1587cm-1) and a much weaker D band (~1345 cm-1), indicating comparatively large sp^2 domains and fewer in-plane defects; this pattern is typical of non-activated biochar produced at moderate temperature. After KOH activation, MKAB shows noticeable increase in D and I_D/I_G rises to 0.60, suggesting KOH activation might have introduces more defects, edges and small aromatic clusters into the carbon matrix. Further modification through nitrogen doping, NMKAB (I_D/I_G = 0.67) and

surfactant, SNMKAB (I_D/I_G = 0.71) show even more intense D bands relative to the G band, implying that N-doping and surfactant modification further enhance disorder and the number of defect sites, while maintaining an sp^2-dominated framework [322] [323].

This defect generation is consistent with the large increase in BET surface area and microporosity reported for KOH-activated and N-doped biochar.

In summary, consistent increase in structural defects were observed in Raman spectra which also aligns with the significant increase in BET surface area and microporosity of activated and modified biochar. These defect-rich carbon structure facilitates abundant active sites, which can be beneficial for CO@ interaction and entrapment. Similar increases in I_D/I_G after chemical activation and N-doping have been reported for biomass-derived biochar and are associated with the creation of microporosity and heteroatom-distorted graphitic layers that might be useful in enhance CO_2 adsorption or entrapment applications [324].

7.3.4 X-Ray Photoelectron Spectrometer (XPS)

XPS analysis was employed to observe composition and chemical functional group changes at various stages of material synthesis (figure 7.7 A, B and C). Evolution of carbon (C1s), nitrogen (N1s) and (O1s) spectra provides detail regarding surface chemistry responsible for enhanced CO_2 interaction.

The O1s spectra of materials (figure 7.7A) have C=O peaks around 531-532eV and 532-534 eV is corresponding to C-O and O-C=O groups. Peak around 531-533 eV in activated samples may be assigned to -OH groups [314]. The strong appearance of peak around 531 eV in MKAB can be attributed to effect of -OH activation and insertion of -OH bond while peak around 532.5 eV is broader in prismatic biochar MKBC due to more aliphatic groups and it diminishes further with activation because of aromatization [325]. All samples show multiple oxygen-containing species with BE values ranging from 530-535 eV. The presence of multiple

peaks indicates different oxygen functionalities (likely C=O, C-O, and O-H groups from different structural environments).

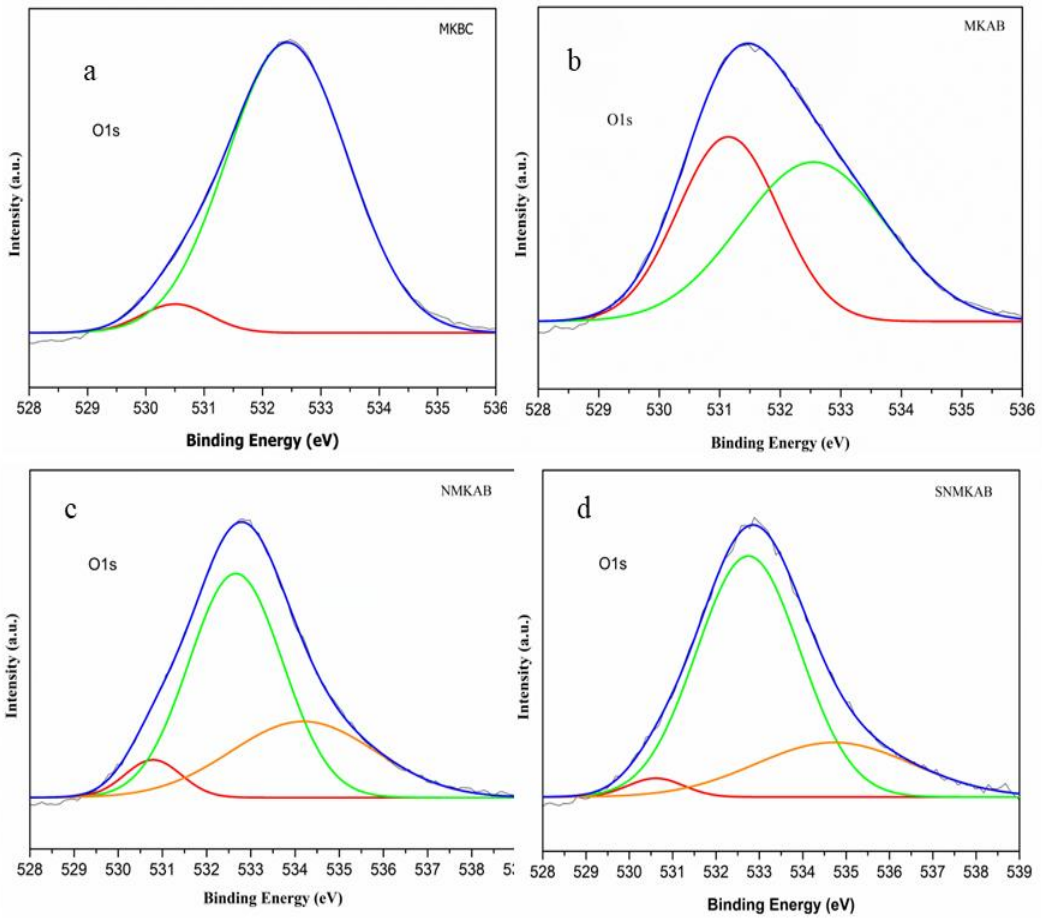

Figure 7.7(A): XPS spectra of O1s regions for (a) MKBC, (b) MKAB, (c) NMKAB and (d) SNMKAB.

The C1s spectra (figure7.7B) shows appearing in the 284-295 eV range, consistent with sp^2 hybridized carbon (aromatic), sp^3 hybridized carbon (aliphatic), and carbon bonded to heteroatoms. The multiple peaks suggest a complex carbon matrix with varying degrees of oxidation.

The N1s spectra (figure 7.7C) further reveal nitrogen incorporation in the modified materials. The introduction of nitrogen via urea treatment produces significantly broadened carbon and nitrogen peaks. This dramatic increase in C1s FWHM (from 1.8 eV to 4.43 eV at the 284.5 eV peak) suggests that urea incorporation creates a more chemically diverse carbon

matrix, possibly through formation of carbon-nitrogen bonds and increased surface oxidation. NMKAB showing an extremely broad peak at 9.27 eV. This exceptional broadening suggests that urea-derived nitrogen exists in multiple chemical states within the material, possibly including pyridinic-N, pyrrolic-N, and quaternary-N species.

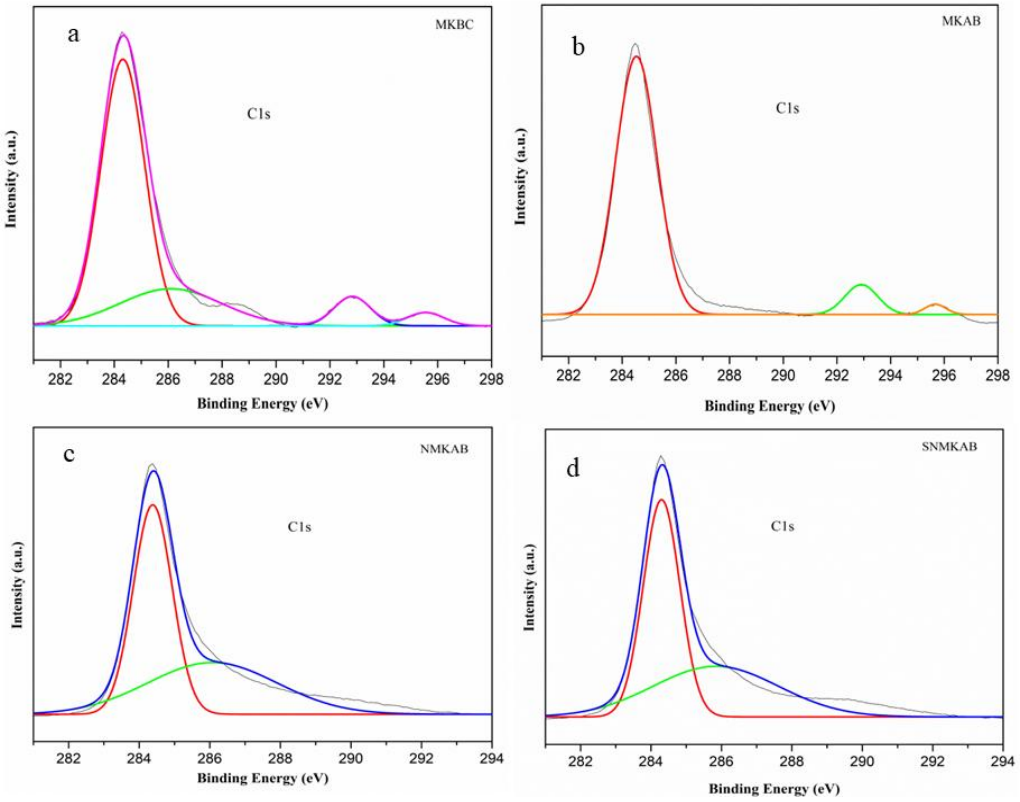

Figure 7.7(B): XPS spectra of C1s regions for (a) MKBC, (b) MKAB, (c) NMKAB and (d) SNMKAB.

Full Width at Half Maximum (FWHM) is a critical indicator of peak complexity and heterogeneity. SNMKAB consistently shows the broadest oxygen peaks (up to 4.26 eV), suggesting greater heterogeneity in oxygen functionalities and potentially better surface chemistry resulting from the surfactant-assisted approach. This broader distribution indicates more diverse oxygen coordination environments. The significant broadening observed in NMKAB (4.43 eV) and SNMKAB (4.3 eV) compared to MKBC (1.9 eV) indicates that urea

treatment creates more complex carbon environments with multiple oxidation states and bonding configurations.

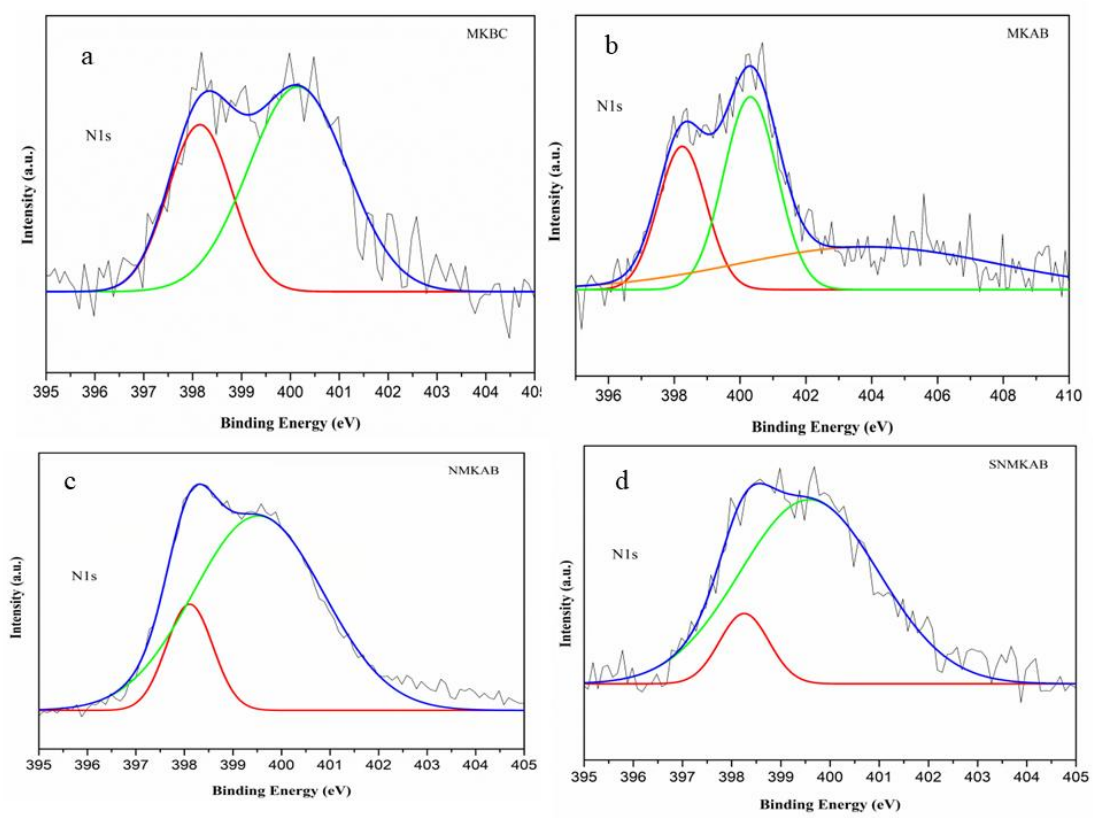

Figure 7.7 (C): XPS spectra of N1s regions for (a) MKBC, (b) MKAB, (c) NMKAB and (d) SNMKAB.

The transition from MKBC to MKAB shows changes in peak positions with slightly increased FWHM values, particularly in the O1s region (from 1.39 to 1.96 and from 2.43 to 2.84 eV for the two main peaks). This indicates that KOH activation creates additional oxygen functionalities, likely through oxidation during the activation process. The introduction of nitrogen via urea treatment produces significantly broadened carbon and nitrogen peaks. This dramatic increase in C1s FWHM (from 1.8 eV to 4.43 eV at the 284.5 eV peak) suggests that urea incorporation creates a more chemically diverse carbon matrix, possibly through formation of carbon-nitrogen bonds and increased surface oxidation. Surfactant-assisted treatment does not reduce overall FWHM values, it produces more uniform nitrogen

incorporation (narrowest N1s peak at 0.27 eV) and maintains good peak definition in the O1s region. Surfactant likely improves the distribution and homogeneity of nitrogen functional group [326] [327]. Furthermore, N-doped and surfactant modified material retain dominant pyrrolic-N groups which are believed to be additional efficient in attracting CO_2 molecule of acidic nature [328].

Table 7.1: BE and FWHM values for the respect samples.

Sample		BE (eV)	FWHM (eV)	Sample		BE (eV)	FWHM (eV)
MKBC	O1s	530.5	1.39	NMKAB	O1s	530.8	1.5
		532.4	2.43			532.6	2.49
	C1s	284.3	1.9			534.2	3.86
		286.1	4.43		C1s	284.4	1.3
		292.8	1.6			286.1	4.3
		295.5	1.6		N1s	398.1	1.13
	N1s	398.1	1.54			399.5	3.15
		400.1	2.37	SNMKAB	O1s	530.6	1.5
MKAB	O1s	531.1	1.96			532.7	2.8
		532.5	2.84			534.7	4.26
	C1s	284.5	1.8		C1s	284.3	1.22
		292.9	1.4			285.8	4.19
		295.6	0.94		N1s	398.2	1.17
	N1s	398.2	1.71			399.5	3.32
		400.3	1.91				
		403.9	9.27				

7.3.5 Field emission scanning electron microscope (FE-SEM) with EDX

The surface morphology of MK biochar activated biochar and surfactant modified biochar is shown in fig 7.8. MKBC exhibit compact surface with limited pores. This may be attributed to preparation of biochar by direct pyrolysis without activation, and surface appears to be less developed and less formation of pores as observed in Fig. 7.8(a). After KOH activation of biochar (MKAB), surface morphology was observed to be more porous than the prismatic MKBC as shown in Fig.7.8 (b). It may be due to activation process with KOH, which removes few atoms from carbon skeleton of prismatic biochar making collapsed or porous structure [329] [330] [331] [332]. These morphological changes observed are consistent with

the increase in BET surface area after activation and ensures the role of KOH in formation of porous carbon network. Furthermore, N-doped activated biochar (NMKAB) exhibits smooth surface with comparatively less visible cavities than that of MKAB (Fig.7.8 (c)). This may be attributed to addition of nitrogen within carbon matrix, nitrogen may occupy some portion of the pore mouth that may partially block entrance however the inner carbon matrix has smaller pores due to N-induced reaction that can be a reason for improvement in BET specific surface area after N-doping [333] [334] [335] [336]. After addition of surfactant (SNMKAB), surface seems to be more coated and compact along with reduced pore visibility (Fig.7.8 (d)) as compared to NMKAB. This may be attributed to filling of pores by surfactant molecules on the carbon surface within the framework and reduced BET surface area are consistent with this observation. Though, porous network shows that surface modification initially alters the surface chemistry rather than complete blocking of pores within the matrix.

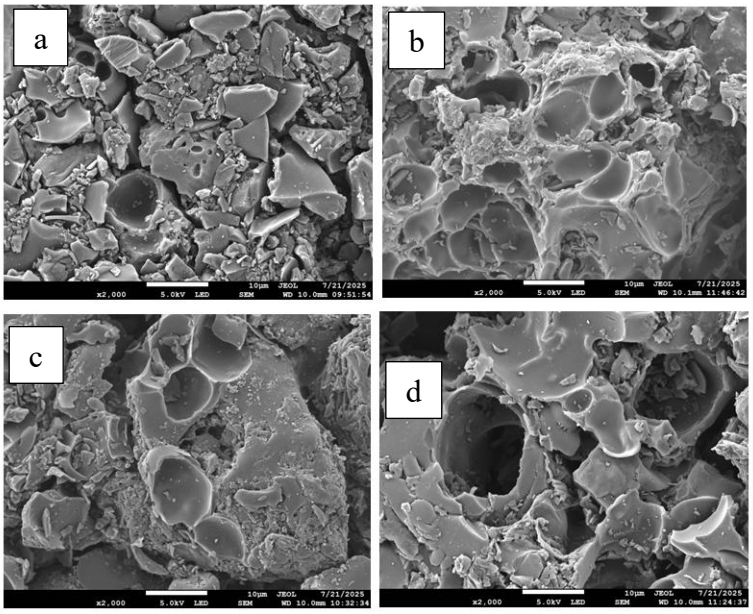

Figure 7.8: High resolution FE-SEM images for (a) MKBC, (b) MKAB, (c)NMKAB and (d) SNMKAB.

The EDX elemental maps of MKBC, MKAB, NMKAB and SNMKAB surfaces, have been shown in fig. 7.9(a) and 7.9(b). Initially, MKBC contains carbon and oxygen and increase in both was observed after KOH activated biochar (MKAB). While a significant increase in

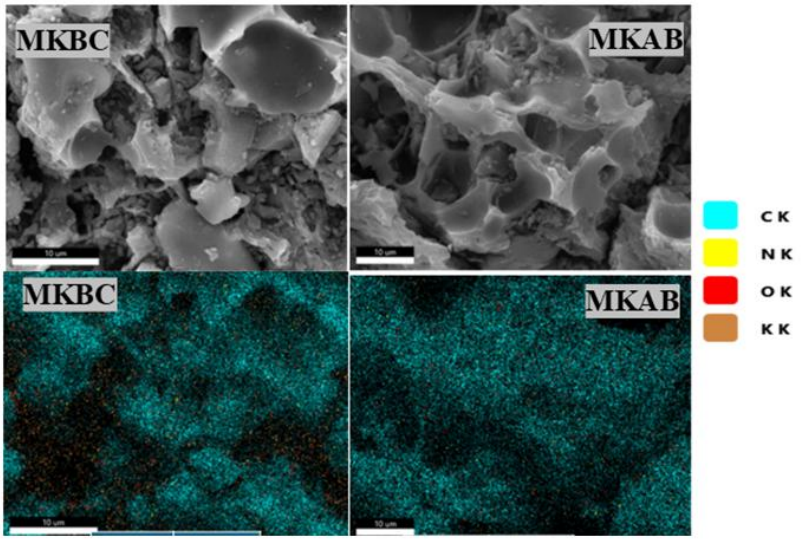

Figure 7.9 (a): Area mapping of Biochar and KOH activated biochar.

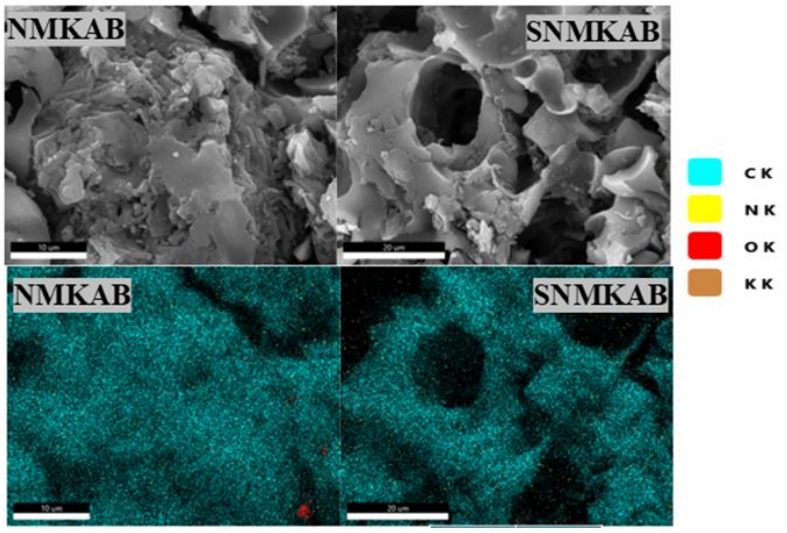

Figure 7.9 (b): Area mapping of N-doped and Surfactant modified sample.

Table 7.2: Elemental analysis of surface elements

Sample	C%	O%	N%
MKBC	77.7	8.8	10.4
MKAB	80.3	9.4	10.2
NMKAB	82.6	3.2	14.1
SNMKAB	81.6	4.7	13.7

nitrogen was observed for nitrogen doped activated biochar (NMKAB), which confirms successful doping of nitrogen as shown in table 7.2.

In addition to this, after surface modification (SNMKAB), nitrogen species were retained, which shows that nitrogen functionalities remain stable during the surface modification. Therefore, FESEM and EDX analysis indicates successful activation followed by nitrogen doping and surface modification alters surface morphology and elemental composition of mango kernel biochar, contribution to better CO_2 entrapment performance.

7.3.6 CO_2 entrapment performance by pressure decay studies

CO_2 entrapment performance of various biochar and activated biochar samples was evaluated by using pressure decay studies conducted under identical initial conditions as shown in figure 7.10. Error bars in the plots represent ±5% experimental uncertainty in the measured values. All the measurements were performed by charging the system with CO_2 to an initial pressure of 14 bar and pressure drop was monitored over time until equilibrium was reached. Larger pressure drop indicates strong CO_2 interaction and higher entrapment efficiency. Pristine biochar (MKBC) shows limited pressure drop with pressure decreasing from 14-12 bar approximately. This small pressure drop reflects weak CO_2 interaction and low entrapment efficiency, consistent with low BET surface area and poorly developed microporous structure. Thus, limited availability of pores restricts effective CO_2 confinement. In contrast, KOH activated biochar (MKAB) exhibit considerable drop in pressure, that is, from 14 - ~10 bar. This increase in pressure drop confirms enhanced CO_2 entrapment and may be attributed to

formation of highly porous structure with large surface area. Presence of abundant micropores facilitates rapid diffusion of CO_2 molecules as well as their retention within pore network. Further improvement was observed for NMKAB, where pressure drop was observed from 14- ~8.5 bar. Greater pressure reduction indicated strong CO_2-solid interaction as compared to MKAB.

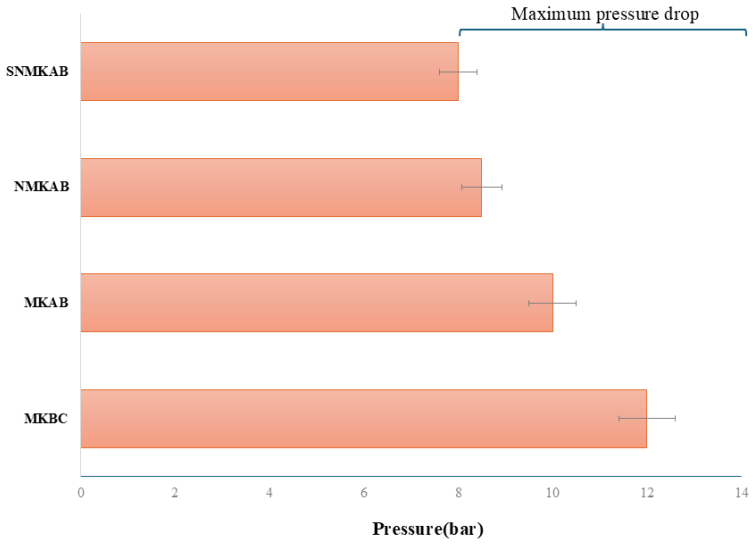

Figure 7.10: Pressure decay study results of CO_2 entrapment test.

This enhancement may be attributed to combined effect of increased microporosity as well as introduction of nitrogen containing functional groups, thereby provides basic sites that interact with CO_2 molecule and improve gas retention.

Lastly, SNMKAB demonstrates highest CO_2 entrapment performance, with pressure decreasing from 14- ~8 bar. Despite having low BET surface area than NMKAB, SNMKAB shows better pressure decay, highlighting the role of surface chemistry as well as interfacial effects. Surfactant molecules present on carbon surface and within the pores are likely to enhance CO_2 entrapment by stabilizing gas molecule and reducing their mobility within porous framework.

Overall, the trend observed in pressure decay studies clearly highlights the synergistic influence of chemical activation, nitrogen doping and surfactant modification on CO_2 entrapment. These findings confirm that CO_2 entrapment not only depends on surface area, but also on pore structure as well as surface functionality, making SNMKAB a promising material for carbon capture applications.

7.4. Conclusions

This study demonstrates a systematic strategy where mango kernel biomass was converted into high performance carbon material through KOH activation followed by nitrogen doping and surface modification with natural surfactant extracted from fenugreek seeds. KOH activation provides highly porous structure from prepared biochar and increases in BET surface area was observed from 21.6 m^2 g^{-1} (for pristine biochar; MKBC) to 188201 $m^2.g^{-1}$ (for activated biochar; MKAB). Further, nitrogen doping leads to enhancement in BET surface area to 2021.6 m^2 g^{-1}, which shows presence of chemically active nitrogen functionalities as confirmed by XPS and Raman analysis. Structural and surface characterization shows increase in defects, expanded carbon domain followed by enriched functionality. All of these are favourable for gas adsorption. As surface modification leads to decrease in BET surface area (1183.6 m^2 g^{-1}) due to occupied partial pores within carbon framework, the microporous framework was retained, and surface chemistry became favourable for CO_2 interaction. In addition to this, pressure decay studies show clear improvement in CO_2 entrapment across all prepared samples. Pressure drops progressively improved under identical conditions, confirming the positive effect of activation followed by nitrogen doping and surface modification. This clearly shows that CO_2 entrapment performance not only depends on surface area but also by surface chemistry and pore level interactions. In summary, this work presents sustainable and effective approach for CO_2 entrapment using agricultural waste derived

carbons and bio-based additives. This also offers low cost and environmentally friendly alternative to conventional materials.

CO_2 entrapment performance was monitored under static pressure decay condition, which may not fully represent dynamic gas flow environment. Therefore, future studies should focus on dynamic breakthrough experiments and multi cycle adsorption-desorption testing to access practical applicability. Investigation of different agricultural waste as well as bio-based surfactant and their optimization may lead to enhancement in CO_2 entrapment efficiency.

…… ***…….....

The next chapter summarizes the key conclusions of this thesis and proposes directions for future research.

CHAPTER 8

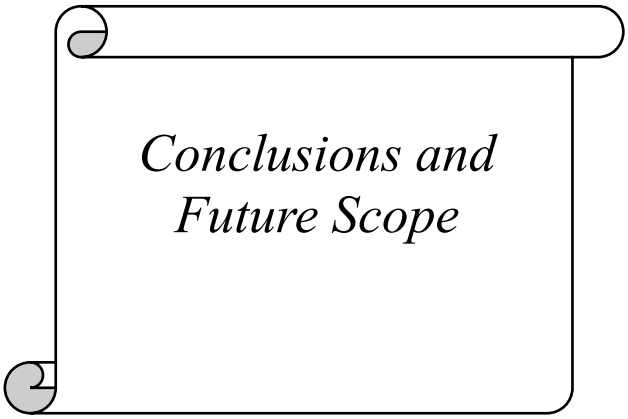

8.1. Conclusions from the thesis:

The following conclusions can be drawn from the thesis:

- Pyrolysis parameters significantly affect biochar yield, pore structure, and surface chemistry.
- The biochar obtained from pyrolysis of rice straw, sugarcane bagasse and its blend has excellent calorific value that can be utilized further for fuel or gasification to generate H_2 gas.
- The rice straw and sugarcane bagasse co-pyrolysis produced highest mass yield among all that indicates a positive synergistic effect.
- Powdered or loose biomass pyrolysis resulted in biochar with lower mass yield and slightly higher carbon content than pelletized samples. Also, mixing RS with SB improved pellet formation and produced stable biochar, suggesting that mixed-feed pellets are more suitable for further gasification applications.
- Pyrolysis and co-pyrolysis work of rice-straw (RS) and mustard de-oiled residue (MR) lower temperature favoured higher mass yield. When examining the individual feedstocks, MR produced the highest biochar mass yield, while RS yielded the least.
- Additionally, MR biochar exhibited the highest heating value, making it a promising fuel source.
- Combining RS and MR in a 7:3 ratio resulted in optimal outcomes, as it uses lower proportion of high valued mustard-oil biomass. The optimum was decided based on both biomasses' economical value, comparable properties such as mass yield, energy yield etc.
- Physical observation showed that MR particles contributed to binding the RS particles, enhancing the strength of the feedstock pellet, which may facilitate easier transport and storage.

- Overall, the pyrolysis of RS, MR, and their blend proves to be an effective method for producing biochar, with MR biochar particularly notable for its high energy potential as a sustainable fuel.
- Biochar obtained from rice straw pyrolysis was further used for composite preparation using graphene oxide (GO). Two composites with varying composition of GO were prepared: RS-GO-0.1 and RS-GO-1.
- Composites showed excellent adsorption potential of methylene blue dye from aqueous solution under batch adsorption conditions (with initial dye concentrations of 10, 20, and 30 ppm. It was observed that at the biochar-graphene oxide composites RS-GO-1 exhibited the best performance.
- The hydrothermal treatment during the synthesis process was done to ensure a strong bonding of graphene oxide over biochar surfaces. The adsorption of the low-concentration dye was almost 100% using the RS-GO-1 composite. The enhancement of adsorption by composites may be attributed to the increased surface area, as observed in the BET results, and the GO-induced interaction and functional groups over the biochar surface.
- The use of GO for the synthesis of biochar composite improved the adsorption capacity of raw biochar, so it could be a good alternative adsorbent for sustainable industrial uses.
- The biochar was further used to test its CO_2 entrapment potential. For this, biochar obtained from mango kernel was activated with KOH and doped with nitrogen for improved functionalities. Thereafter, surface modification was done with natural surfactant extracted from fenugreek seeds.
- Significant improvement in material properties as observed by characterization, supports favourable CO_2 interaction over the material surface.

- Pressure decay studied for testing CO_2 entrapment performance showed positive effect of activation, N-doping and surface modification with improvement results for each.

Agricultural biomass residues are proven sustainable raw materials for energy uses or producing value-added carbon materials through controlled pyrolysis and activation. Co-pyrolysis, activation and composite development substantially enhance materials performance and functional applications.

The study supports waste valorisation, reduction of biomass burning, and advancement of circular bioeconomy principles.

8.2. Future scope:

- Scale-up of pyrolysis and activation processes for pilot or industrial production can be done.
- Exploring additional feedstock combinations and catalytic co-pyrolysis for improved performance is recommended.
- Detailed thermogravimetric analysis of different biomass mixing ratios could be carried out to better understand the thermal degradation behaviour during co-pyrolysis.
- Advance functionalization and heteroatom doping of biochar for targeted applications such as supercapacitors, CO_2 capture, and sensors could be some area of study.
- Detailed adsorption mechanism studies and real wastewater / flue gas experiments, isotherm modelling and reaeration-cycle analysis can be done.
- Techno-economic analysis and life-cycle assessment for commercialization feasibility can be done.
- Development of hybrid carbon materials with polymers, metal oxides, or nanomaterials could be potentially beneficial.
- Field studies on long-term carbon sequestration and agricultural soil benefit from biochar application could be explored.

References

[1] A. Cherp and J. Jewell, “The concept of energy security: Beyond the four As,” *Energy Policy*, vol. 75, pp. 415–421, Dec. 2014, doi: 10.1016/j.enpol.2014.09.005.

[2] S. C. Bhattacharyya, *Energy Economics: Concepts, Issues, Markets and Governance*. London: Springer London, 2011. doi: 10.1007/978-0-85729-268-1.

[3] A. Kumar, N. Kumar, P. Baredar, and A. Shukla, “A review on biomass energy resources, potential, conversion and policy in India,” *Renew. Sustain. Energy Rev.*, vol. 45, pp. 530–539, May 2015, doi: 10.1016/j.rser.2015.02.007.

[4] T. Kan, V. Strezov, and T. J. Evans, “Lignocellulosic biomass pyrolysis: A review of product properties and effects of pyrolysis parameters,” *Renew. Sustain. Energy Rev.*, vol. 57, pp. 1126–1140, May 2016, doi: 10.1016/j.rser.2015.12.185.

[5] V. Vijay, R. Kapoor, P. Singh, M. Hiloidhari, and P. Ghosh, “Sustainable utilization of biomass resources for decentralized energy generation and climate change mitigation: A regional case study in India,” *Environ. Res.*, vol. 212, p. 113257, Sep. 2022, doi: 10.1016/j.envres.2022.113257.

[6] S. Babu *et al.*, “Biochar implications in cleaner agricultural production and environmental sustainability,” *Environ. Sci. Adv.*, vol. 2, no. 8, pp. 1042–1059, 2023, doi: 10.1039/D2VA00324D.

[7] E. Singh, R. Mishra, A. Kumar, S. K. Shukla, S.-L. Lo, and S. Kumar, “Circular economy-based environmental management using biochar: Driving towards sustainability,” *Process Saf. Environ. Prot.*, vol. 163, pp. 585–600, Jul. 2022, doi: 10.1016/j.psep.2022.05.056.

[8] N. Wen, J. Yang, and C. C. Xu, “Introduction to biomass,” in *Biomass Conversion and High-Value Utilization*, Elsevier, 2026, pp. 1–43. doi: 10.1016/B978-0-443-33339-2.00018-6.

[9] M.-A. Perea-Moreno, E. Samerón-Manzano, and A.-J. Perea-Moreno, “Biomass as Renewable Energy: Worldwide Research Trends,” *Sustainability*, vol. 11, no. 3, p. 863, Feb. 2019, doi: 10.3390/su11030863.

[10] L. Ge *et al.*, “A critical review on conversion technology for liquid biofuel production from lignocellulosic biomass,” *Renew. Sustain. Energy Rev.*, vol. 217, p. 115726, Jul. 2025, doi: 10.1016/j.rser.2025.115726.

[11] W. Deng *et al.*, “Catalytic conversion of lignocellulosic biomass into chemicals and fuels,” *Green Energy Environ.*, vol. 8, no. 1, pp. 10–114, Feb. 2023, doi: 10.1016/j.gee.2022.07.003.

[12] A. S. Reddy, V. P. Kasa, B. Samal, B. K. Dubey, V. Yadav, and D. S. Pandey, “Sustainable agricultural waste management in India: Innovations, challenges, and future perspectives,” *Biomass Bioenergy*, vol. 202, p. 108261, Nov. 2025, doi: 10.1016/j.biombioe.2025.108261.

[13] A. Deep Singh, B. Gajera, and A. K. Sarma, “Appraising the availability of biomass residues in India and their bioenergy potential,” *Waste Manag.*, vol. 152, pp. 38–47, Oct. 2022, doi: 10.1016/j.wasman.2022.08.001.

[14] A. Tursi, “A review on biomass: importance, chemistry, classification, and conversion,” *Biofuel Res. J.*, vol. 6, no. 2, pp. 962–979, Jun. 2019, doi: 10.18331/BRJ2019.6.2.3.

[15] Jaya Shankar Tumuluru, Christopher T Wright, Richard D Boardman, Neal A Yancey, and Shahab Sokhansanj, “A review on biomass classification and composition, co-firing issues and pretreatment methods,” in *2011 Louisville, Kentucky, August 7 - August 10, 2011*, American Society of Agricultural and Biological Engineers, 2011. doi: 10.13031/2013.37191.

[16] M. Mujtaba *et al.*, “Lignocellulosic biomass from agricultural waste to the circular economy: a review with focus on biofuels, biocomposites and bioplastics,” *J. Clean. Prod.*, vol. 402, p. 136815, May 2023, doi: 10.1016/j.jclepro.2023.136815.
[17] V. Pasangulapati, K. D. Ramachandriya, A. Kumar, M. R. Wilkins, C. L. Jones, and R. L. Huhnke, “Effects of cellulose, hemicellulose and lignin on thermochemical conversion characteristics of the selected biomass,” *Bioresour. Technol.*, vol. 114, pp. 663–669, Jun. 2012, doi: 10.1016/j.biortech.2012.03.036.
[18] J. Wang and Y. Yin, “Clostridium species for fermentative hydrogen production: An overview,” *Int. J. Hydrog. Energy*, vol. 46, no. 70, pp. 34599–34625, Oct. 2021, doi: 10.1016/j.ijhydene.2021.08.052.
[19] A. Zoghlami and G. Paës, “Lignocellulosic Biomass: Understanding Recalcitrance and Predicting Hydrolysis,” *Front. Chem.*, vol. 7, p. 874, Dec. 2019, doi: 10.3389/fchem.2019.00874.
[20] J. B. Sluiter, R. O. Ruiz, C. J. Scarlata, A. D. Sluiter, and D. W. Templeton, “Compositional Analysis of Lignocellulosic Feedstocks. 1. Review and Description of Methods,” *J. Agric. Food Chem.*, vol. 58, no. 16, pp. 9043–9053, Aug. 2010, doi: 10.1021/jf1008023.
[21] F. H. Isikgor and C. R. Becer, “Lignocellulosic biomass: a sustainable platform for the production of bio-based chemicals and polymers,” *Polym. Chem.*, vol. 6, no. 25, pp. 4497–4559, 2015, doi: 10.1039/C5PY00263J.
[22] A. K. Vuppaladadiyam *et al.*, “Bio-oil and biochar from the pyrolytic conversion of biomass: A current and future perspective on the trade-off between economic, environmental, and technical indicators,” *Sci. Total Environ.*, vol. 857, p. 159155, Jan. 2023, doi: 10.1016/j.scitotenv.2022.159155.
[23] M. Shahbaz *et al.*, “A comprehensive review of biomass based thermochemical conversion technologies integrated with CO2 capture and utilisation within BECCS networks,” *Resour. Conserv. Recycl.*, vol. 173, p. 105734, Oct. 2021, doi: 10.1016/j.resconrec.2021.105734.
[24] S. Yu, Q. Li, Y. Zhang, J. Yan, and H. Zhou, “Enhancing carbon-negative emission technologies through biomass integration,” *The Innovation*, vol. 6, no. 12, p. 101079, Dec. 2025, doi: 10.1016/j.xinn.2025.101079.
[25] P. McKendry, “Energy production from biomass (part 1): overview of biomass,” *Bioresour. Technol.*, vol. 83, no. 1, pp. 37–46, May 2002, doi: 10.1016/S0960-8524(01)00118-3.
[26] *Biomass Gasification and Pyrolysis*. Elsevier, 2010. doi: 10.1016/C2009-0-20099-7.
[27] A. Demirbaş, “Biomass resource facilities and biomass conversion processing for fuels and chemicals,” *Energy Convers. Manag.*, vol. 42, no. 11, pp. 1357–1378, Jul. 2001, doi: 10.1016/S0196-8904(00)00137-0.
[28] A. V. Bridgwater, “Review of fast pyrolysis of biomass and product upgrading,” *Biomass Bioenergy*, vol. 38, pp. 68–94, Mar. 2012, doi: 10.1016/j.biombioe.2011.01.048.
[29] M. Balat and H. Balat, “Recent trends in global production and utilization of bio-ethanol fuel,” *Appl. Energy*, vol. 86, no. 11, pp. 2273–2282, Nov. 2009, doi: 10.1016/j.apenergy.2009.03.015.
[30] L. Appels *et al.*, “Anaerobic digestion in global bio-energy production: Potential and research challenges,” *Renew. Sustain. Energy Rev.*, vol. 15, no. 9, pp. 4295–4301, Dec. 2011, doi: 10.1016/j.rser.2011.07.121.
[31] A. J. Ward, P. J. Hobbs, P. J. Holliman, and D. L. Jones, “Optimisation of the anaerobic digestion of agricultural resources,” *Bioresour. Technol.*, vol. 99, no. 17, pp. 7928–7940, Nov. 2008, doi: 10.1016/j.biortech.2008.02.044.

[32] C. Mao, Y. Feng, X. Wang, and G. Ren, “Review on research achievements of biogas from anaerobic digestion,” *Renew. Sustain. Energy Rev.*, vol. 45, pp. 540–555, May 2015, doi: 10.1016/j.rser.2015.02.032.
[33] P. Alvira, E. Tomás-Pejó, M. Ballesteros, and M. J. Negro, “Pretreatment technologies for an efficient bioethanol production process based on enzymatic hydrolysis: A review,” *Bioresour. Technol.*, vol. 101, no. 13, pp. 4851–4861, Jul. 2010, doi: 10.1016/j.biortech.2009.11.093.
[34] L. Brennan and P. Owende, “Biofuels from microalgae—A review of technologies for production, processing, and extractions of biofuels and co-products,” *Renew. Sustain. Energy Rev.*, vol. 14, no. 2, pp. 557–577, Feb. 2010, doi: 10.1016/j.rser.2009.10.009.
[35] Y. Chisti, “Biodiesel from microalgae,” *Biotechnol. Adv.*, vol. 25, no. 3, pp. 294–306, May 2007, doi: 10.1016/j.biotechadv.2007.02.001.
[36] R. Kapoore, T. Butler, J. Pandhal, and S. Vaidyanathan, “Microwave-Assisted Extraction for Microalgae: From Biofuels to Biorefinery,” *Biology*, vol. 7, no. 1, p. 18, Feb. 2018, doi: 10.3390/biology7010018.
[37] B. M. Jenkins, L. L. Baxter, T. R. Miles, and T. R. Miles, “Combustion properties of biomass,” *Fuel Process. Technol.*, vol. 54, no. 1–3, pp. 17–46, Mar. 1998, doi: 10.1016/S0378-3820(97)00059-3.
[38] J. Werther, M. Saenger, E.-U. Hartge, T. Ogada, and Z. Siagi, “Combustion of agricultural residues,” *Prog. Energy Combust. Sci.*, vol. 26, no. 1, pp. 1–27, Feb. 2000, doi: 10.1016/S0360-1285(99)00005-2.
[39] S. V. Vassilev, D. Baxter, L. K. Andersen, and C. G. Vassileva, “An overview of the chemical composition of biomass,” *Fuel*, vol. 89, no. 5, pp. 913–933, May 2010, doi: 10.1016/j.fuel.2009.10.022.
[40] J. Koppejan and S. Van Loo, Eds., *The Handbook of Biomass Combustion and Co-firing*, 0 ed. Routledge, 2012. doi: 10.4324/9781849773041.
[41] J. Qiu *et al.*, “Coal gasification in steam and air medium under plasma conditions: a preliminary study,” *Fuel Process. Technol.*, vol. 85, no. 8–10, pp. 969–982, Jul. 2004, doi: 10.1016/j.fuproc.2003.11.035.
[42] J. Gil, J. Corella, M. P. Aznar, and M. A. Caballero, “Biomass gasification in atmospheric and bubbling fluidized bed: Effect of the type of gasifying agent on the product distribution,” *Biomass Bioenergy*, vol. 17, no. 5, pp. 389–403, Nov. 1999, doi: 10.1016/S0961-9534(99)00055-0.
[43] M. Asadullah, “Barriers of commercial power generation using biomass gasification gas: A review,” *Renew. Sustain. Energy Rev.*, vol. 29, pp. 201–215, Jan. 2014, doi: 10.1016/j.rser.2013.08.074.
[44] Q. Zhou, Y. Shen, and X. Gu, “Progress in torrefaction pretreatment for biomass gasification,” *Green Chem.*, vol. 26, no. 18, pp. 9652–9670, 2024, doi: 10.1039/D4GC03243H.
[45] D. Mohan, C. U. Pittman, and P. H. Steele, “Pyrolysis of Wood/Biomass for Bio-oil: A Critical Review,” *Energy Fuels*, vol. 20, no. 3, pp. 848–889, May 2006, doi: 10.1021/ef0502397.
[46] H. Karami, M. Kazemeini, S. Soltanali, and M. Rashidzadeh, “Influence of adding a modified zeolite-Y onto the NiMo/Al2O3 catalyst utilized to produce a diesel fuel with highly reduced sulfur content,” *Microporous Mesoporous Mater.*, vol. 332, p. 111704, Feb. 2022, doi: 10.1016/j.micromeso.2022.111704.
[47] P. Zhang, Z. Chen, Q. Zhang, S. Zhang, X. Ning, and J. Zhou, “Co-pyrolysis characteristics and kinetics of low metamorphic coal and pine sawdust,” *RSC Adv.*, vol. 12, no. 34, pp. 21725–21735, 2022, doi: 10.1039/D2RA02461F.

[48] S. Kolb, T. Plankenbühler, K. Hofmann, J. Bergerson, and J. Karl, “Life cycle greenhouse gas emissions of renewable gas technologies: A comparative review,” *Renew. Sustain. Energy Rev.*, vol. 146, p. 111147, Aug. 2021, doi: 10.1016/j.rser.2021.111147.

[49] J. Lehmann, M. C. Rillig, J. Thies, C. A. Masiello, W. C. Hockaday, and D. Crowley, “Biochar effects on soil biota – A review,” *Soil Biol. Biochem.*, vol. 43, no. 9, pp. 1812–1836, Sep. 2011, doi: 10.1016/j.soilbio.2011.04.022.

[50] J. Shankar Tumuluru, S. Sokhansanj, J. R. Hess, C. T. Wright, and R. D. Boardman, “REVIEW: A review on biomass torrefaction process and product properties for energy applications,” *Ind. Biotechnol.*, vol. 7, no. 5, pp. 384–401, Oct. 2011, doi: 10.1089/ind.2011.7.384.

[51] A. Uslu, A. P. C. Faaij, and P. C. A. Bergman, “Pre-treatment technologies, and their effect on international bioenergy supply chain logistics. Techno-economic evaluation of torrefaction, fast pyrolysis and pelletisation,” *Energy*, vol. 33, no. 8, pp. 1206–1223, Aug. 2008, doi: 10.1016/j.energy.2008.03.007.

[52] Q. Zhou, Y. Shen, Q. Zhou, C. Zhang, and X. Gu, “Torrefaction integrated with steam gasification of agricultural biomass wastes for enhancing tar reduction and hydrogen-rich syngas production,” *Int. J. Hydrog. Energy*, vol. 94, pp. 474–484, Dec. 2024, doi: 10.1016/j.ijhydene.2024.11.144.

[53] A. R. K. Gollakota, N. Kishore, and S. Gu, “A review on hydrothermal liquefaction of biomass,” *Renew. Sustain. Energy Rev.*, vol. 81, pp. 1378–1392, Jan. 2018, doi: 10.1016/j.rser.2017.05.178.

[54] A. A. Peterson, F. Vogel, R. P. Lachance, M. Fröling, M. J. Antal, Jr., and J. W. Tester, “Thermochemical biofuel production in hydrothermal media: A review of sub- and supercritical water technologies,” *Energy Environ. Sci.*, vol. 1, no. 1, p. 32, 2008, doi: 10.1039/b810100k.

[55] Z. Li, S. Li, W. Shen, X. Wang, Z. Su, and M. Yang, “Investigating the adsorption behavior of NOx molecules on γ-Al2O3(1 0 0)-supported proximal Pt-Ba clusters using density functional theory,” *Fuel*, vol. 351, p. 128867, Nov. 2023, doi: 10.1016/j.fuel.2023.128867.

[56] S. K. Hoekman, A. Broch, and C. Robbins, “Hydrothermal Carbonization (HTC) of Lignocellulosic Biomass,” *Energy Fuels*, vol. 25, no. 4, pp. 1802–1810, Apr. 2011, doi: 10.1021/ef101745n.

[57] J. A. Libra *et al.*, “Hydrothermal carbonization of biomass residuals: a comparative review of the chemistry, processes and applications of wet and dry pyrolysis,” *Biofuels*, vol. 2, no. 1, pp. 71–106, Jan. 2011, doi: 10.4155/bfs.10.81.

[58] T. Wang, Y. Zhai, Y. Zhu, C. Li, and G. Zeng, “A review of the hydrothermal carbonization of biomass waste for hydrochar formation: Process conditions, fundamentals, and physicochemical properties,” *Renew. Sustain. Energy Rev.*, vol. 90, pp. 223–247, Jul. 2018, doi: 10.1016/j.rser.2018.03.071.

[59] S. Mukherjee, C. Mazumder, A. Biswas, A. Roy, A. Chatterjee, and S. Paul, “Biomass Energy Resource – Future of Global Power Production,” *J. Sci. Res.*, vol. 66, no. 05, pp. 16–23, 2022, doi: 10.37398/JSR.2022.660504.

[60] C. L. Williams, R. M. Emerson, and J. S. Tumuluru, “Biomass Compositional Analysis for Conversion to Renewable Fuels and Chemicals,” in *Biomass Volume Estimation and Valorization for Energy*, J. S. Tumuluru, Ed., InTech, 2017. doi: 10.5772/65777.

[61] A. Sertolli, Z. Gabnai, P. Lengyel, and A. Bai, “Biomass Potential and Utilization in Worldwide Research Trends—A Bibliometric Analysis,” *Sustainability*, vol. 14, no. 9, p. 5515, May 2022, doi: 10.3390/su14095515.

[62] E. Smith, “The Biomass Report: a review,” *Polar Rec.*, vol. 19, no. 119, pp. 204–206, May 1978, doi: 10.1017/S0032247400002059.
[63] M. Saleem, “Possibility of utilizing agriculture biomass as a renewable and sustainable future energy source,” *Heliyon*, vol. 8, no. 2, p. e08905, Feb. 2022, doi: 10.1016/j.heliyon.2022.e08905.
[64] J. A. Kumar *et al.*, “Agricultural waste biomass for sustainable bioenergy production: Feedstock, characterization and pre-treatment methodologies,” *Chemosphere*, vol. 331, p. 138680, Aug. 2023, doi: 10.1016/j.chemosphere.2023.138680.
[65] K. L. Kenney, W. A. Smith, G. L. Gresham, and T. L. Westover, “Understanding biomass feedstock variability,” *Biofuels*, vol. 4, no. 1, pp. 111–127, Jan. 2013, doi: 10.4155/bfs.12.83.
[66] “National Biomass Atlas of Inida,” NIBE, Technical report, 2024. [Online]. Available: ttps://nibe.res.in/english/biomass-atlas.php
[67] L. J. R. Nunes, T. P. Causer, and D. Ciolkosz, “Biomass for energy: A review on supply chain management models,” *Renew. Sustain. Energy Rev.*, vol. 120, p. 109658, Mar. 2020, doi: 10.1016/j.rser.2019.109658.
[68] Deepti, D. Awasthi, K. Pal, T. K. Patra, N. Gakkhar, and A. P. Toor, “Biomass densification pathways for India: An overview on technologies, characterization, testing, challenges and economics,” *Energy Sustain. Dev.*, vol. 90, p. 101878, Jan. 2026, doi: 10.1016/j.esd.2025.101878.
[69] N. Kumar *et al.*, “Crop residue management challenges, opportunities and way forward for sustainable food-energy security in India: A review,” *Soil Tillage Res.*, vol. 228, p. 105641, Apr. 2023, doi: 10.1016/j.still.2023.105641.
[70] R. K. Singh, D. Pandey, T. Patil, and A. N. Sawarkar, “Pyrolysis of banana leaves biomass: Physico-chemical characterization, thermal decomposition behavior, kinetic and thermodynamic analyses,” *Bioresour. Technol.*, vol. 310, p. 123464, Aug. 2020, doi: 10.1016/j.biortech.2020.123464.
[71] D. K. W. Gan *et al.*, “Kinetics and thermodynamic analysis in one-pot pyrolysis of rice hull using renewable calcium oxide based catalysts,” *Bioresour. Technol.*, vol. 265, pp. 180–190, Oct. 2018, doi: 10.1016/j.biortech.2018.06.003.
[72] J. O. Titiloye, M. S. Abu Bakar, and T. E. Odetoye, “Thermochemical characterisation of agricultural wastes from West Africa,” *Ind. Crops Prod.*, vol. 47, pp. 199–203, May 2013, doi: 10.1016/j.indcrop.2013.03.011.
[73] C. R. Cardoso, M. R. Miranda, K. G. Santos, and C. H. Ataíde, “Determination of kinetic parameters and analytical pyrolysis of tobacco waste and sorghum bagasse,” *J. Anal. Appl. Pyrolysis*, vol. 92, no. 2, pp. 392–400, Nov. 2011, doi: 10.1016/j.jaap.2011.07.013.
[74] M. Kumar, S. Sabbarwal, P. K. Mishra, and S. N. Upadhyay, “Thermal degradation kinetics of sugarcane leaves (Saccharum officinarum L) using thermo-gravimetric and differential scanning calorimetric studies,” *Bioresour. Technol.*, vol. 279, pp. 262–270, May 2019, doi: 10.1016/j.biortech.2019.01.137.
[75] S. Yorgun, S. Şensöz, and Ö. M. Koçkar, “Characterization of the pyrolysis oil produced in the slow pyrolysis of sunflower-extracted bagasse,” *Biomass Bioenergy*, vol. 20, no. 2, pp. 141–148, Feb. 2001, doi: 10.1016/S0961-9534(00)00064-7.
[76] K. Midhun Prasad and S. Murugavelh, “Experimental investigation and kinetics of tomato peel pyrolysis: Performance, combustion and emission characteristics of bio-oil blends in diesel engine,” *J. Clean. Prod.*, vol. 254, p. 120115, May 2020, doi: 10.1016/j.jclepro.2020.120115.
[77] G. Özsin and A. E. Pütün, “Kinetics and evolved gas analysis for pyrolysis of food processing wastes using TGA/MS/FT-IR,” *Waste Manag.*, vol. 64, pp. 315–326, Jun. 2017, doi: 10.1016/j.wasman.2017.03.020.

[78] M. Kumar, S. N. Upadhyay, and P. K. Mishra, “A comparative study of thermochemical characteristics of lignocellulosic biomasses,” *Bioresour. Technol. Rep.*, vol. 8, p. 100186, Dec. 2019, doi: 10.1016/j.biteb.2019.100186.
[79] N. Şen and Y. Kar, “Pyrolysis of black cumin seed cake in a fixed-bed reactor,” *Biomass Bioenergy*, vol. 35, no. 10, pp. 4297–4304, Oct. 2011, doi: 10.1016/j.biombioe.2011.07.019.
[80] E. Pütün, B. B. Uzun, and A. E. Pütün, “Fixed-bed catalytic pyrolysis of cotton-seed cake: Effects of pyrolysis temperature, natural zeolite content and sweeping gas flow rate,” *Bioresour. Technol.*, vol. 97, no. 5, pp. 701–710, Mar. 2006, doi: 10.1016/j.biortech.2005.04.005.
[81] C. Acikgoz and O. M. Kockar, “Characterization of slow pyrolysis oil obtained from linseed (Linum usitatissimum L.),” *J. Anal. Appl. Pyrolysis*, vol. 85, no. 1–2, pp. 151–154, May 2009, doi: 10.1016/j.jaap.2008.08.011.
[82] S. Uçar and S. Karagöz, “The slow pyrolysis of pomegranate seeds: The effect of temperature on the product yields and bio-oil properties,” *J. Anal. Appl. Pyrolysis*, vol. 84, no. 2, pp. 151–156, Mar. 2009, doi: 10.1016/j.jaap.2009.01.005.
[83] O. Onay, “Influence of pyrolysis temperature and heating rate on the production of bio-oil and char from safflower seed by pyrolysis, using a well-swept fixed-bed reactor,” *Fuel Process. Technol.*, vol. 88, no. 5, pp. 523–531, May 2007, doi: 10.1016/j.fuproc.2007.01.001.
[84] M. H. Tahir, G. Çakman, J. L. Goldfarb, Y. Topcu, S. R. Naqvi, and S. Ceylan, “Demonstrating the suitability of canola residue biomass to biofuel conversion via pyrolysis through reaction kinetics, thermodynamics and evolved gas analyses,” *Bioresour. Technol.*, vol. 279, pp. 67–73, May 2019, doi: 10.1016/j.biortech.2019.01.106.
[85] C. L. Yiin, S. Yusup, A. T. Quitain, Y. Uemura, M. Sasaki, and T. Kida, “Thermogravimetric analysis and kinetic modeling of low-transition-temperature mixtures pretreated oil palm empty fruit bunch for possible maximum yield of pyrolysis oil,” *Bioresour. Technol.*, vol. 255, pp. 189–197, May 2018, doi: 10.1016/j.biortech.2018.01.132.
[86] A. E. Pütün, B. B. Uzun, E. Apaydin, and E. Pütün, “Bio-oil from olive oil industry wastes: Pyrolysis of olive residue under different conditions,” *Fuel Process. Technol.*, vol. 87, no. 1, pp. 25–32, Dec. 2005, doi: 10.1016/j.fuproc.2005.04.003.
[87] S. W. Kim *et al.*, “Bio-oil from the pyrolysis of palm and Jatropha wastes in a fluidized bed,” *Fuel Process. Technol.*, vol. 108, pp. 118–124, Apr. 2013, doi: 10.1016/j.fuproc.2012.05.002.
[88] G. Özsin and A. E. Pütün, “Insights into pyrolysis and co-pyrolysis of biomass and polystyrene: Thermochemical behaviors, kinetics and evolved gas analysis,” *Energy Convers. Manag.*, vol. 149, pp. 675–685, Oct. 2017, doi: 10.1016/j.enconman.2017.07.059.
[89] X. Huang *et al.*, “Pyrolysis kinetics of soybean straw using thermogravimetric analysis,” *Fuel*, vol. 169, pp. 93–98, Apr. 2016, doi: 10.1016/j.fuel.2015.12.011.
[90] M. S. Ahmad *et al.*, “Kinetic analyses and pyrolytic behavior of Para grass (Urochloa mutica) for its bioenergy potential,” *Bioresour. Technol.*, vol. 224, pp. 708–713, Jan. 2017, doi: 10.1016/j.biortech.2016.10.090.
[91] M. Kumar, P. K. Mishra, and S. N. Upadhyay, “Pyrolysis of Saccharum munja: Optimization of process parameters using response surface methodology (RSM) and evaluation of kinetic parameters,” *Bioresour. Technol. Rep.*, vol. 8, p. 100332, Dec. 2019, doi: 10.1016/j.biteb.2019.100332.

[92] S. Naik, V. V. Goud, P. K. Rout, K. Jacobson, and A. K. Dalai, "Characterization of Canadian biomass for alternative renewable biofuel," *Renew. Energy*, vol. 35, no. 8, pp. 1624–1631, Aug. 2010, doi: 10.1016/j.renene.2009.08.033.
[93] D. Li, L. Chen, X. Zhang, N. Ye, and F. Xing, "Pyrolytic characteristics and kinetic studies of three kinds of red algae," *Biomass Bioenergy*, vol. 35, no. 5, pp. 1765–1772, May 2011, doi: 10.1016/j.biombioe.2011.01.011.
[94] S. Ceylan, Y. Topcu, and Z. Ceylan, "Thermal behaviour and kinetics of alga Polysiphonia elongata biomass during pyrolysis," *Bioresour. Technol.*, vol. 171, pp. 193–198, Nov. 2014, doi: 10.1016/j.biortech.2014.08.064.
[95] M. S. Ahmad *et al.*, "Bioenergy potential of Wolffia arrhiza appraised through pyrolysis, kinetics, thermodynamics parameters and TG-FTIR-MS study of the evolved gases," *Bioresour. Technol.*, vol. 253, pp. 297–303, Apr. 2018, doi: 10.1016/j.biortech.2018.01.033.
[96] C. T. Chong *et al.*, "Pyrolysis characteristics and kinetic studies of horse manure using thermogravimetric analysis," *Energy Convers. Manag.*, vol. 180, pp. 1260–1267, Jan. 2019, doi: 10.1016/j.enconman.2018.11.071.
[97] F. Sotoudehnia, A. Baba Rabiu, A. Alayat, and A. G. McDonald, "Characterization of bio-oil and biochar from pyrolysis of waste corrugated cardboard," *J. Anal. Appl. Pyrolysis*, vol. 145, p. 104722, Jan. 2020, doi: 10.1016/j.jaap.2019.104722.
[98] S. Luo, B. Xiao, Z. Hu, and S. Liu, "Effect of particle size on pyrolysis of single-component municipal solid waste in fixed bed reactor," *Int. J. Hydrog. Energy*, vol. 35, no. 1, pp. 93–97, Jan. 2010, doi: 10.1016/j.ijhydene.2009.10.048.
[99] S. Gu, J. Zhou, Z. Luo, Q. Wang, and M. Ni, "A detailed study of the effects of pyrolysis temperature and feedstock particle size on the preparation of nanosilica from rice husk," *Ind. Crops Prod.*, vol. 50, pp. 540–549, Oct. 2013, doi: 10.1016/j.indcrop.2013.08.004.
[100] S. V. Vassilev, D. Baxter, L. K. Andersen, C. G. Vassileva, and T. J. Morgan, "An overview of the organic and inorganic phase composition of biomass," *Fuel*, vol. 94, pp. 1–33, Apr. 2012, doi: 10.1016/j.fuel.2011.09.030.
[101] N. Tröger, D. Richter, and R. Stahl, "Effect of feedstock composition on product yields and energy recovery rates of fast pyrolysis products from different straw types," *J. Anal. Appl. Pyrolysis*, vol. 100, pp. 158–165, Mar. 2013, doi: 10.1016/j.jaap.2012.12.012.
[102] L. Wei *et al.*, "Characteristics of fast pyrolysis of biomass in a free fall reactor," *Fuel Process. Technol.*, vol. 87, no. 10, pp. 863–871, Oct. 2006, doi: 10.1016/j.fuproc.2006.06.002.
[103] I. Díaz, M. Rodríguez, C. Arnaiz, G. San Miguel, and M. Domínguez, "Biomass pyrolysis kinetics through thermogravimetric analysis," in *Computer Aided Chemical Engineering*, vol. 32, Elsevier, 2013, pp. 1–6. doi: 10.1016/B978-0-444-63234-0.50001-4.
[104] J. Chen, Y. Wang, X. Lang, X. Ren, and S. Fan, "Evaluation of agricultural residues pyrolysis under non-isothermal conditions: Thermal behaviors, kinetics, and thermodynamics," *Bioresour. Technol.*, vol. 241, pp. 340–348, Oct. 2017, doi: 10.1016/j.biortech.2017.05.036.
[105] F. Ateş and M. A. Işıkdağ, "Evaluation of the Role of the Pyrolysis Temperature in Straw Biomass Samples and Characterization of the Oils by GC/MS," *Energy Fuels*, vol. 22, no. 3, pp. 1936–1943, May 2008, doi: 10.1021/ef7006276.
[106] G. Duman, C. Okutucu, S. Ucar, R. Stahl, and J. Yanik, "The slow and fast pyrolysis of cherry seed," *Bioresour. Technol.*, vol. 102, no. 2, pp. 1869–1878, Jan. 2011, doi: 10.1016/j.biortech.2010.07.051.

[107] H. H. Sait, A. Hussain, A. A. Salema, and F. N. Ani, “Pyrolysis and combustion kinetics of date palm biomass using thermogravimetric analysis,” *Bioresour. Technol.*, vol. 118, pp. 382–389, Aug. 2012, doi: 10.1016/j.biortech.2012.04.081.
[108] F. C. R. Lopes, J. C. Pereira, and K. Tannous, “Thermal decomposition kinetics of guarana seed residue through thermogravimetric analysis under inert and oxidizing atmospheres,” *Bioresour. Technol.*, vol. 270, pp. 294–302, Dec. 2018, doi: 10.1016/j.biortech.2018.09.021.
[109] K. Murata, P. Somwongsa, S. Larpkiattaworn, Y. Liu, M. Inaba, and I. Takahara, “Analyses of Liquid Products from Catalytic Pyrolysis of Jatropha Seed Cakes,” *Energy Fuels*, vol. 25, no. 11, pp. 5429–5437, Nov. 2011, doi: 10.1021/ef201237s.
[110] R. K. Mishra and K. Mohanty, “Pyrolysis kinetics and thermal behavior of waste sawdust biomass using thermogravimetric analysis,” *Bioresour. Technol.*, vol. 251, pp. 63–74, Mar. 2018, doi: 10.1016/j.biortech.2017.12.029.
[111] N. K. Nayan, S. Kumar, and R. K. Singh, “Production of the liquid fuel by thermal pyrolysis of neem seed,” *Fuel*, vol. 103, pp. 437–443, Jan. 2013, doi: 10.1016/j.fuel.2012.08.058.
[112] O. Onay and O. Kockar, “Pyrolysis of rapeseed in a free fall reactor for production of bio-oil,” *Fuel*, vol. 85, no. 12–13, pp. 1921–1928, Sep. 2006, doi: 10.1016/j.fuel.2006.03.009.
[113] S. Şensöz and D. Angın, “Pyrolysis of safflower (Charthamus tinctorius L.) seed press cake in a fixed-bed reactor: Part 2. Structural characterization of pyrolysis bio-oils,” *Bioresour. Technol.*, vol. 99, no. 13, pp. 5498–5504, Sep. 2008, doi: 10.1016/j.biortech.2007.11.004.
[114] R. Kaur, P. Gera, M. K. Jha, and T. Bhaskar, “Pyrolysis kinetics and thermodynamic parameters of castor (Ricinus communis) residue using thermogravimetric analysis,” *Bioresour. Technol.*, vol. 250, pp. 422–428, Feb. 2018, doi: 10.1016/j.biortech.2017.11.077.
[115] S. Sfakiotakis and D. Vamvuka, “Study of co-pyrolysis of olive kernel with waste biomass using TGA/DTG/MS,” *Thermochim. Acta*, vol. 670, pp. 44–54, Dec. 2018, doi: 10.1016/j.tca.2018.10.006.
[116] Ö. Çepelioğullar and A. E. Pütün, “Thermal and kinetic behaviors of biomass and plastic wastes in co-pyrolysis,” *Energy Convers. Manag.*, vol. 75, pp. 263–270, Nov. 2013, doi: 10.1016/j.enconman.2013.06.036.
[117] A. M. Cortés and A. V. Bridgwater, “Kinetic study of the pyrolysis of miscanthus and its acid hydrolysis residue by thermogravimetric analysis,” *Fuel Process. Technol.*, vol. 138, pp. 184–193, Oct. 2015, doi: 10.1016/j.fuproc.2015.05.013.
[118] T. G. Bridgeman *et al.*, “Influence of particle size on the analytical and chemical properties of two energy crops,” *Fuel*, vol. 86, no. 1–2, pp. 60–72, Jan. 2007, doi: 10.1016/j.fuel.2006.06.022.
[119] K. Kirtania and S. Bhattacharya, “Pyrolysis kinetics and reactivity of algae–coal blends,” *Biomass Bioenergy*, vol. 55, pp. 291–298, Aug. 2013, doi: 10.1016/j.biombioe.2013.02.019.
[120] M. M. Phukan, R. S. Chutia, B. K. Konwar, and R. Kataki, “Microalgae Chlorella as a potential bio-energy feedstock,” *Appl. Energy*, vol. 88, no. 10, pp. 3307–3312, Oct. 2011, doi: 10.1016/j.apenergy.2010.11.026.
[121] J. Li, Y. Qiao, P. Zong, S. Qin, C. Wang, and Y. Tian, “Fast pyrolysis characteristics of two typical coastal zone biomass fuels by thermal gravimetric analyzer and down tube reactor,” *Bioresour. Technol.*, vol. 283, pp. 96–105, Jul. 2019, doi: 10.1016/j.biortech.2019.02.097.

[122] X. Ming *et al.*, "Thermal degradation of food waste by TG-FTIR and Py-GC/MS: Pyrolysis behaviors, products, kinetic and thermodynamic analysis," *J. Clean. Prod.*, vol. 244, p. 118713, Jan. 2020, doi: 10.1016/j.jclepro.2019.118713.
[123] S. Wen, Y. Yan, J. Liu, M. Buyukada, and F. Evrendilek, "Pyrolysis performance, kinetic, thermodynamic, product and joint optimization analyses of incense sticks in N2 and CO2 atmospheres," *Renew. Energy*, vol. 141, pp. 814–827, Oct. 2019, doi: 10.1016/j.renene.2019.04.040.
[124] Z. Chen, Q. Zhu, X. Wang, B. Xiao, and S. Liu, "Pyrolysis behaviors and kinetic studies on Eucalyptus residues using thermogravimetric analysis," *Energy Convers. Manag.*, vol. 105, pp. 251–259, Nov. 2015, doi: 10.1016/j.enconman.2015.07.077.
[125] L. Chen, Z. Yu, J. Liang, Y. Liao, and X. Ma, "Co-pyrolysis of chlorella vulgaris and kitchen waste with different additives using TG-FTIR and Py-GC/MS," *Energy Convers. Manag.*, vol. 177, pp. 582–591, Dec. 2018, doi: 10.1016/j.enconman.2018.10.010.
[126] H. Yang, G. Ji, P. T. Clough, X. Xu, and M. Zhao, "Kinetics of catalytic biomass pyrolysis using Ni-based functional materials," *Fuel Process. Technol.*, vol. 195, p. 106145, Dec. 2019, doi: 10.1016/j.fuproc.2019.106145.
[127] A. Sriram and G. Swaminathan, "Pyrolysis of Musa balbisiana flower petal using thermogravimetric studies," *Bioresour. Technol.*, vol. 265, pp. 236–246, Oct. 2018, doi: 10.1016/j.biortech.2018.05.043.
[128] N. Kongkaew, W. Pruksakit, and S. Patumsawad, "Thermogravimetric Kinetic Analysis of the Pyrolysis of Rice Straw," *Energy Procedia*, vol. 79, pp. 663–670, Nov. 2015, doi: 10.1016/j.egypro.2015.11.552.
[129] D. Li, L. Chen, S. Chen, X. Zhang, F. Chen, and N. Ye, "Comparative evaluation of the pyrolytic and kinetic characteristics of a macroalga (Sargassum thunbergii) and a freshwater plant (Potamogeton crispus)," *Fuel*, vol. 96, pp. 185–191, Jun. 2012, doi: 10.1016/j.fuel.2012.01.005.
[130] R. Kumar Singh, T. Patil, D. Pandey, and A. N. Sawarkar, "Pyrolysis of mustard oil residue: A kinetic and thermodynamic study," *Bioresour. Technol.*, vol. 339, p. 125631, Nov. 2021, doi: 10.1016/j.biortech.2021.125631.
[131] R. K. Mishra, Q. Lu, and K. Mohanty, "Thermal behaviour, kinetics and fast pyrolysis of Cynodon dactylon grass using Py-GC/MS and Py-FTIR analyser," *J. Anal. Appl. Pyrolysis*, vol. 150, p. 104887, Sep. 2020, doi: 10.1016/j.jaap.2020.104887.
[132] R. K. Singh, T. Patil, A. Verma, S. P. Tekade, and A. N. Sawarkar, "Insights into kinetics, reaction mechanism, and thermodynamic analysis of pyrolysis of rice straw from rice bowl of India," *Bioresour. Technol. Rep.*, vol. 13, p. 100639, Feb. 2021, doi: 10.1016/j.biteb.2021.100639.
[133] A. O. Aboyade *et al.*, "Non-isothermal kinetic analysis of the devolatilization of corn cobs and sugar cane bagasse in an inert atmosphere," *Thermochim. Acta*, vol. 517, no. 1–2, pp. 81–89, Apr. 2011, doi: 10.1016/j.tca.2011.01.035.
[134] S. R. Naqvi *et al.*, "Pyrolysis of high ash sewage sludge: Kinetics and thermodynamic analysis using Coats-Redfern method," *Renew. Energy*, vol. 131, pp. 854–860, Feb. 2019, doi: 10.1016/j.renene.2018.07.094.
[135] M. H. Tahir, Z. Zhao, J. Ren, T. Rasool, and S. R. Naqvi, "Thermo-kinetics and gaseous product analysis of banana peel pyrolysis for its bioenergy potential," *Biomass Bioenergy*, vol. 122, pp. 193–201, Mar. 2019, doi: 10.1016/j.biombioe.2019.01.009.
[136] P. Kumar, P. Chaunsali, and R. Vinu, "Pyrolysis of rice husk, bagasse and wood chips blends: Distributed activation energy modelling and pyrolysate composition analysis," *Fuel*, vol. 404, p. 136116, Jan. 2026, doi: 10.1016/j.fuel.2025.136116.
[137] B. Biswas, P. Balla, B. B. Krishna, Sushil Adhikari, and T. Bhaskar, "Physiochemical characteristics of bio-char derived from pyrolysis of rice straw under different

temperatures," *Biomass Convers. Biorefinery*, vol. 14, no. 12, pp. 12775–12783, Jun. 2024, doi: 10.1007/s13399-022-03261-y.
[138] L. Kapoor, N. Agarwal, and S. Garg, "Evaluating the blending potential of two different biomass via co-pyrolysis as sustainable pathway using RSM optimization for bioenergy and bio char production," *Biofuels*, vol. 15, no. 9, pp. 1159–1171, Oct. 2024, doi: 10.1080/17597269.2024.2341499.
[139] G. K. Gupta, P. K. Gupta, and M. K. Mondal, "Experimental process parameters optimization and in-depth product characterizations for teak sawdust pyrolysis," *Waste Manag.*, vol. 87, pp. 499–511, Mar. 2019, doi: 10.1016/j.wasman.2019.02.035.
[140] C. Diblasi, "Modeling chemical and physical processes of wood and biomass pyrolysis," *Prog. Energy Combust. Sci.*, vol. 34, no. 1, pp. 47–90, Feb. 2008, doi: 10.1016/j.pecs.2006.12.001.
[141] D. K. Shen and S. Gu, "The mechanism for thermal decomposition of cellulose and its main products," *Bioresour. Technol.*, vol. 100, no. 24, pp. 6496–6504, Dec. 2009, doi: 10.1016/j.biortech.2009.06.095.
[142] D. Chen *et al.*, "Insight into biomass pyrolysis mechanism based on cellulose, hemicellulose, and lignin: Evolution of volatiles and kinetics, elucidation of reaction pathways, and characterization of gas, biochar and bio-oil," *Combust. Flame*, vol. 242, p. 112142, Aug. 2022, doi: 10.1016/j.combustflame.2022.112142.
[143] A. Bhatnagar, R. Barthen, H. Tolvanen, and J. Konttinen, "Bio-oil stability through stepwise pyrolysis of groundnut shells: Role of chemical composition, alkali and alkaline earth metals, and storage conditions," *J. Anal. Appl. Pyrolysis*, vol. 157, p. 105219, Aug. 2021, doi: 10.1016/j.jaap.2021.105219.
[144] S. Ren and X. P. Ye, "Stability of crude bio-oil and its water-extracted fractions," *J. Anal. Appl. Pyrolysis*, vol. 132, pp. 151–162, Jun. 2018, doi: 10.1016/j.jaap.2018.03.005.
[145] Y. Wu *et al.*, "Effect of pyrolysis atmospheres on gaseous products evolution of coal pyrolysis at high temperature," *Fuel*, vol. 366, p. 131336, Jun. 2024, doi: 10.1016/j.fuel.2024.131336.
[146] H. Wang, M. Liu, Y. Zheng, and Y. Zeng, "H2-rich syngas production from biowastes: Steam gasification and supercritical water gasification," *Biomass Bioenergy*, vol. 206, p. 108648, Mar. 2026, doi: 10.1016/j.biombioe.2025.108648.
[147] Y. Trivedi *et al.*, "Biochar potential for pollutant removal during wastewater treatment: A comprehensive review of separation mechanisms, technological integration, and process analysis," *Desalination*, vol. 600, p. 118509, May 2025, doi: 10.1016/j.desal.2024.118509.
[148] A. Mukherjee, B. R. Patra, J. Podder, and A. K. Dalai, "Synthesis of Biochar From Lignocellulosic Biomass for Diverse Industrial Applications and Energy Harvesting: Effects of Pyrolysis Conditions on the Physicochemical Properties of Biochar," *Front. Mater.*, vol. 9, p. 870184, Jun. 2022, doi: 10.3389/fmats.2022.870184.
[149] S. P. Singh Yadav *et al.*, "Biochar application: A sustainable approach to improve soil health," *J. Agric. Food Res.*, vol. 11, p. 100498, Mar. 2023, doi: 10.1016/j.jafr.2023.100498.
[150] S. Shyam, J. Arun, K. P. Gopinath, G. Ribhu, M. Ashish, and S. Ajay, "Biomass as source for hydrochar and biochar production to recover phosphates from wastewater: A review on challenges, commercialization, and future perspectives," *Chemosphere*, vol. 286, p. 131490, Jan. 2022, doi: 10.1016/j.chemosphere.2021.131490.
[151] M. Kamali, N. Sweygers, S. Al-Salem, L. Appels, T. M. Aminabhavi, and R. Dewil, "Biochar for soil applications-sustainability aspects, challenges and future prospects," *Chem. Eng. J.*, vol. 428, p. 131189, Jan. 2022, doi: 10.1016/j.cej.2021.131189.

[152] M. Raza *et al.*, “Progress of the Pyrolyzer Reactors and Advanced Technologies for Biomass Pyrolysis Processing,” *Sustainability*, vol. 13, no. 19, p. 11061, Oct. 2021, doi: 10.3390/su131911061.
[153] A. T. Tag, G. Duman, S. Ucar, and J. Yanik, “Effects of feedstock type and pyrolysis temperature on potential applications of biochar,” *J. Anal. Appl. Pyrolysis*, vol. 120, pp. 200–206, Jul. 2016, doi: 10.1016/j.jaap.2016.05.006.
[154] R. Kumar Mishra, D. Jaya Prasanna Kumar, A. Narula, S. Minnat Chistie, and S. Ullhas Naik, “Production and beneficial impact of biochar for environmental application: A review on types of feedstocks, chemical compositions, operating parameters, techno-economic study, and life cycle assessment,” *Fuel*, vol. 343, p. 127968, Jul. 2023, doi: 10.1016/j.fuel.2023.127968.
[155] X. Gai *et al.*, “Effects of Feedstock and Pyrolysis Temperature on Biochar Adsorption of Ammonium and Nitrate,” *PLoS ONE*, vol. 9, no. 12, p. e113888, Dec. 2014, doi: 10.1371/journal.pone.0113888.
[156] A. Al-Rumaihi, M. Shahbaz, G. Mckay, H. Mackey, and T. Al-Ansari, “A review of pyrolysis technologies and feedstock: A blending approach for plastic and biomass towards optimum biochar yield,” *Renew. Sustain. Energy Rev.*, vol. 167, p. 112715, Oct. 2022, doi: 10.1016/j.rser.2022.112715.
[157] M. Tripathi, J. N. Sahu, and P. Ganesan, “Effect of process parameters on production of biochar from biomass waste through pyrolysis: A review,” *Renew. Sustain. Energy Rev.*, vol. 55, pp. 467–481, Mar. 2016, doi: 10.1016/j.rser.2015.10.122.
[158] T. T. Mengesha, V. R. Ancha, L. S. Sundar, and A. Pollex, “Review on the influence of pyrolysis process parameters for biochar production with minimized polycyclic aromatic hydrocarbon content,” *J. Anal. Appl. Pyrolysis*, vol. 182, p. 106699, Sep. 2024, doi: 10.1016/j.jaap.2024.106699.
[159] A. E. Pütün, A. Özcan, and E. Pütün, “Pyrolysis of hazelnut shells in a fixed-bed tubular reactor: yields and structural analysis of bio-oil,” *J. Anal. Appl. Pyrolysis*, vol. 52, no. 1, pp. 33–49, Sep. 1999, doi: 10.1016/S0165-2370(99)00044-3.
[160] F. Ateş, E. Pütün, and A. E. Pütün, “Fast pyrolysis of sesame stalk: yields and structural analysis of bio-oil,” *J. Anal. Appl. Pyrolysis*, vol. 71, no. 2, pp. 779–790, Jun. 2004, doi: 10.1016/j.jaap.2003.11.001.
[161] P. T. Williams and N. Nugranad, “Comparison of products from the pyrolysis and catalytic pyrolysis of rice husks,” *Energy*, vol. 25, no. 6, pp. 493–513, Jun. 2000, doi: 10.1016/S0360-5442(00)00009-8.
[162] A. K. Sakhiya, V. K. Vijay, and P. Kaushal, “Efficacy of rice straw derived biochar for removal of Pb+2 and Zn+2 from aqueous: Adsorption, thermodynamic and cost analysis,” *Bioresour. Technol. Rep.*, vol. 17, p. 100920, Feb. 2022, doi: 10.1016/j.biteb.2021.100920.
[163] M. G. P. Valenga, A. Gevaerd, L. H. Marcolino-Junior, and M. F. Bergamini, “Biochar from sugarcane bagasse: Synthesis, characterization, and application in an electrochemical sensor for copper (II) determination,” *Biomass Bioenergy*, vol. 184, p. 107206, May 2024, doi: 10.1016/j.biombioe.2024.107206.
[164] P. T. Williams and S. Besler, “The influence of temperature and heating rate on the slow pyrolysis of biomass,” *Renew. Energy*, vol. 7, no. 3, pp. 233–250, Mar. 1996, doi: 10.1016/0960-1481(96)00006-7.
[165] D. Angın, “Effect of pyrolysis temperature and heating rate on biochar obtained from pyrolysis of safflower seed press cake,” *Bioresour. Technol.*, vol. 128, pp. 593–597, Jan. 2013, doi: 10.1016/j.biortech.2012.10.150.
[166] F. Amalina, A. Syukor Abd Razak, S. Krishnan, H. Sulaiman, A. W. Zularisam, and M. Nasrullah, “Advanced techniques in the production of biochar from lignocellulosic

biomass and environmental applications," *Clean. Mater.*, vol. 6, p. 100137, Dec. 2022, doi: 10.1016/j.clema.2022.100137.
[167] M.-S. Safdari, E. Amini, D. R. Weise, and T. H. Fletcher, "Heating rate and temperature effects on pyrolysis products from live wildland fuels," *Fuel*, vol. 242, pp. 295–304, Apr. 2019, doi: 10.1016/j.fuel.2019.01.040.
[168] T. Aysu and M. M. Küçük, "Biomass pyrolysis in a fixed-bed reactor: Effects of pyrolysis parameters on product yields and characterization of products," *Energy*, vol. 64, pp. 1002–1025, Jan. 2014, doi: 10.1016/j.energy.2013.11.053.
[169] S. Şensöz and D. Angın, "Pyrolysis of safflower (Charthamus tinctorius L.) seed press cake: Part 1. The effects of pyrolysis parameters on the product yields," *Bioresour. Technol.*, vol. 99, no. 13, pp. 5492–5497, Sep. 2008, doi: 10.1016/j.biortech.2007.10.046.
[170] A. Demirbas, "Determination of calorific values of bio-chars and pyro-oils from pyrolysis of beech trunkbarks," *J. Anal. Appl. Pyrolysis*, vol. 72, no. 2, pp. 215–219, Nov. 2004, doi: 10.1016/j.jaap.2004.06.005.
[171] Z. Wang, K. Liu, L. Xie, H. Zhu, S. Ji, and X. Shu, "Effects of residence time on characteristics of biochars prepared via co-pyrolysis of sewage sludge and cotton stalks," *J. Anal. Appl. Pyrolysis*, vol. 142, p. 104659, Sep. 2019, doi: 10.1016/j.jaap.2019.104659.
[172] B. Zhao *et al.*, "Effect of pyrolysis temperature, heating rate, and residence time on rapeseed stem derived biochar," *J. Clean. Prod.*, vol. 174, pp. 977–987, Feb. 2018, doi: 10.1016/j.jclepro.2017.11.013.
[173] K. K. B. Suresh Babu, M. Nataraj, M. Tayappa, Y. Vyas, R. K. Mishra, and B. Acharya, "Production of biochar from waste biomass using slow pyrolysis: Studies of the effect of pyrolysis temperature and holding time on biochar yield and properties," *Mater. Sci. Energy Technol.*, vol. 7, pp. 318–334, 2024, doi: 10.1016/j.mset.2024.05.002.
[174] S. Chandra and J. Bhattacharya, "Influence of temperature and duration of pyrolysis on the property heterogeneity of rice straw biochar and optimization of pyrolysis conditions for its application in soils," *J. Clean. Prod.*, vol. 215, pp. 1123–1139, Apr. 2019, doi: 10.1016/j.jclepro.2019.01.079.
[175] J. M. Encinar, J. F. González, and J. González, "Fixed-bed pyrolysis of Cynara cardunculus L. Product yields and compositions," *Fuel Process. Technol.*, vol. 68, no. 3, pp. 209–222, Dec. 2000, doi: 10.1016/S0378-3820(00)00125-9.
[176] A. Demirbas, "Effects of temperature and particle size on bio-char yield from pyrolysis of agricultural residues," *J. Anal. Appl. Pyrolysis*, vol. 72, no. 2, pp. 243–248, Nov. 2004, doi: 10.1016/j.jaap.2004.07.003.
[177] H. Zhang, R. Xiao, H. Huang, and G. Xiao, "Comparison of non-catalytic and catalytic fast pyrolysis of corncob in a fluidized bed reactor," *Bioresour. Technol.*, vol. 100, no. 3, pp. 1428–1434, Feb. 2009, doi: 10.1016/j.biortech.2008.08.031.
[178] T. Mani, P. Murugan, J. Abedi, and N. Mahinpey, "Pyrolysis of wheat straw in a thermogravimetric analyzer: Effect of particle size and heating rate on devolatilization and estimation of global kinetics," *Chem. Eng. Res. Des.*, vol. 88, no. 8, pp. 952–958, Aug. 2010, doi: 10.1016/j.cherd.2010.02.008.
[179] S. Şensöz, D. Angın, and S. Yorgun, "Influence of particle size on the pyrolysis of rapeseed (Brassica napus L.): fuel properties of bio-oil," *Biomass Bioenergy*, vol. 19, no. 4, pp. 271–279, Oct. 2000, doi: 10.1016/S0961-9534(00)00041-6.
[180] S. Şensöz and İ. Kaynar, "Bio-oil production from soybean (Glycine max L.); fuel properties of Bio-oil," *Ind. Crops Prod.*, vol. 23, no. 1, pp. 99–105, Jan. 2006, doi: 10.1016/j.indcrop.2005.04.005.

[181] O. Onay and O. M. Kockar, “Slow, fast and flash pyrolysis of rapeseed,” *Renew. Energy*, vol. 28, no. 15, pp. 2417–2433, Dec. 2003, doi: 10.1016/S0960-1481(03)00137-X.
[182] M. Troiano, V. Ianzito, R. Solimene, E. T. Ganda, and P. Salatino, “Fluidized Bed Pyrolysis of Biomass: A Model-Based Assessment of the Relevance of Heterogeneous Secondary Reactions and Char Loading,” *Energy Fuels*, vol. 36, no. 17, pp. 9660–9671, Sep. 2022, doi: 10.1021/acs.energyfuels.2c01483.
[183] F. R. Vieira, C. M. Romero Luna, G. L. A. F. Arce, and I. Ávila, “Optimization of slow pyrolysis process parameters using a fixed bed reactor for biochar yield from rice husk,” *Biomass Bioenergy*, vol. 132, p. 105412, Jan. 2020, doi: 10.1016/j.biombioe.2019.105412.
[184] Y. Choi *et al.*, “Sustainable strategy for converting plastic waste into energy over pyrolysis: A comparative study of fluidized-bed and fixed-bed reactors,” *Energy*, vol. 286, p. 129564, Jan. 2024, doi: 10.1016/j.energy.2023.129564.
[185] “Design of bench–scale auger pyrolysis reactor: Experimental investigation on rice husk biomass,” *Indian J. Chem. Technol.*, 2025, doi: 10.56042/ijct.v32i4.8520.
[186] P. Brassard, S. Godbout, and V. Raghavan, “Pyrolysis in auger reactors for biochar and bio-oil production: A review,” *Biosyst. Eng.*, vol. 161, pp. 80–92, Sep. 2017, doi: 10.1016/j.biosystemseng.2017.06.020.
[187] C. Guizani, F. J. Escudero Sanz, and S. Salvador, “Effects of CO2 on biomass fast pyrolysis: Reaction rate, gas yields and char reactive properties,” *Fuel*, vol. 116, pp. 310–320, Jan. 2014, doi: 10.1016/j.fuel.2013.07.101.
[188] E. Pütün, F. Ateş, and A. E. Pütün, “Catalytic pyrolysis of biomass in inert and steam atmospheres,” *Fuel*, vol. 87, no. 6, pp. 815–824, May 2008, doi: 10.1016/j.fuel.2007.05.042.
[189] F. L. P. Resende, “Recent advances on fast hydropyrolysis of biomass,” *Catal. Today*, vol. 269, pp. 148–155, Jul. 2016, doi: 10.1016/j.cattod.2016.01.004.
[190] D. S. Chandler, G. V. S. Seufitelli, and F. L. P. Resende, “Catalytic Route for the Production of Alkanes from Hydropyrolysis of Biomass,” *Energy Fuels*, vol. 34, no. 10, pp. 12573–12585, Oct. 2020, doi: 10.1021/acs.energyfuels.0c01548.
[191] B. Balagurumurthy *et al.*, “Effect of pressure and temperature on the hydropyrolysis of cotton residue,” *J. Mater. Cycles Waste Manag.*, vol. 16, no. 3, pp. 442–448, Jul. 2014, doi: 10.1007/s10163-014-0250-1.
[192] P. Premchand, F. Demichelis, D. Chiaramonti, S. Bensaid, and D. Fino, “Biochar production from slow pyrolysis of biomass under CO2 atmosphere: A review on the effect of CO2 medium on biochar production, characterisation, and environmental applications,” *J. Environ. Chem. Eng.*, vol. 11, no. 3, p. 110009, Jun. 2023, doi: 10.1016/j.jece.2023.110009.
[193] R. Maggi and B. Delmon, “Comparison between ‘slow’ and ‘flash’ pyrolysis oils from biomass,” *Fuel*, vol. 73, no. 5, pp. 671–677, May 1994, doi: 10.1016/0016-2361(94)90007-8.
[194] B. B. Uzun, A. E. Pütün, and E. Pütün, “Fast pyrolysis of soybean cake: Product yields and compositions,” *Bioresour. Technol.*, vol. 97, no. 4, pp. 569–576, Mar. 2006, doi: 10.1016/j.biortech.2005.03.026.
[195] M. Somerville and A. Deev, “The effect of heating rate, particle size and gas flow on the yield of charcoal during the pyrolysis of radiata pine wood,” *Renew. Energy*, vol. 151, pp. 419–425, May 2020, doi: 10.1016/j.renene.2019.11.036.
[196] W. Buss, M. C. Graham, G. MacKinnon, and O. Mašek, “Strategies for producing biochars with minimum PAH contamination,” *J. Anal. Appl. Pyrolysis*, vol. 119, pp. 24–30, May 2016, doi: 10.1016/j.jaap.2016.04.001.

[197] P. Shrivastava, A. Kumar, P. Tekasakul, S. S. Lam, and A. Palamanit, “Comparative Investigation of Yield and Quality of Bio-Oil and Biochar from Pyrolysis of Woody and Non-Woody Biomasses,” *Energies*, vol. 14, no. 4, p. 1092, Feb. 2021, doi: 10.3390/en14041092.
[198] B. C. Smith, *Fundamentals of Fourier Transform Infrared Spectroscopy*, 0 ed. CRC Press, 2011. doi: 10.1201/b10777.
[199] B. H. Stuart, *Infrared Spectroscopy: Fundamentals and Applications*, 1st ed. in Analytical Techniques in the Sciences. Wiley, 2004. doi: 10.1002/0470011149.
[200] J. Epp, “X-ray diffraction (XRD) techniques for materials characterization,” in *Materials Characterization Using Nondestructive Evaluation (NDE) Methods*, Elsevier, 2016, pp. 81–124. doi: 10.1016/B978-0-08-100040-3.00004-3.
[201] S. Hüfner, *Photoelectron Spectroscopy*. in Advanced Texts in Physics. Berlin, Heidelberg: Springer Berlin Heidelberg, 2003. doi: 10.1007/978-3-662-09280-4.
[202] E. Smith and G. Dent, *Modern Raman Spectroscopy – A Practical Approach*, 1st ed. Wiley, 2004. doi: 10.1002/0470011831.
[203] Indian Institute of Science (IISC)-INUP & VVIT *et al.*, “SEM Imaging for Advanced Bio Materials,” *Radiol. Res. Diagn. Imaging*, vol. 2, no. 2, Feb. 2023, doi: 10.58489/2836-5127/011.
[204] I. Chakraborty *et al.*, “An insight into microscopy and analytical techniques for morphological, structural, chemical, and thermal characterization of cellulose,” *Microsc. Res. Tech.*, vol. 85, no. 5, pp. 1990–2015, May 2022, doi: 10.1002/jemt.24057.
[205] S. Jung, Y.-K. Park, and E. E. Kwon, “Strategic use of biochar for CO2 capture and sequestration,” *J. CO2 Util.*, vol. 32, pp. 128–139, Jul. 2019, doi: 10.1016/j.jcou.2019.04.012.
[206] A. T. Irewale, E. E. Elemike, A. M. Shaik, C. O. Dimkpa, and E. E. Oguzie, “Theoretical and experimental insights into BET surface area and pore analysis of water hyacinth biochar: Prospects for efficient bio-nanofertilizer development,” *MRS Adv.*, vol. 10, no. 9, pp. 1029–1035, Jul. 2025, doi: 10.1557/s43580-025-01248-1.
[207] K. Y. Foo and B. H. Hameed, “Insights into the modeling of adsorption isotherm systems,” *Chem. Eng. J.*, vol. 156, no. 1, pp. 2–10, Jan. 2010, doi: 10.1016/j.cej.2009.09.013.
[208] G. Crini, “Non-conventional low-cost adsorbents for dye removal: A review,” *Bioresour. Technol.*, vol. 97, no. 9, pp. 1061–1085, Jun. 2006, doi: 10.1016/j.biortech.2005.05.001.
[209] L. Matović, J. Lađarević, Ž. Vitnik, V. Vitnik, and D. Mijin, “A detailed UV–Vis spectral investigation of six azo dyes derived from benzoic- and cinnamic acids: experimental and theoretical insight,” *Comptes Rendus Chim.*, vol. 24, no. 2, pp. 267–280, Jun. 2021, doi: 10.5802/crchim.85.
[210] J. Chen *et al.*, “A review of biomass burning: Emissions and impacts on air quality, health and climate in China,” *Sci. Total Environ.*, vol. 579, pp. 1000–1034, Feb. 2017, doi: 10.1016/j.scitotenv.2016.11.025.
[211] R. Rauch, J. Hrbek, and H. Hofbauer, “Biomass gasification for synthesis gas production and applications of the syngas,” *WIREs Energy Environ.*, vol. 3, no. 4, pp. 343–362, Jul. 2014, doi: 10.1002/wene.97.
[212] A. L. Robinson, J. S. Rhodes, and D. W. Keith, “Assessment of Potential Carbon Dioxide Reductions Due to Biomass−Coal Cofiring in the United States,” *Environ. Sci. Technol.*, vol. 37, no. 22, pp. 5081–5089, Nov. 2003, doi: 10.1021/es034367q.
[213] C. Jaroenkhasemmeesuk and N. Tippayawong, “Technical and Economic Analysis of A Biomass Pyrolysis Plant,” *Energy Procedia*, vol. 79, pp. 950–955, Nov. 2015, doi: 10.1016/j.egypro.2015.11.592.

[214] D. Klinar, “Universal model of slow pyrolysis technology producing biochar and heat from standard biomass needed for the techno-economic assessment,” *Bioresour. Technol.*, vol. 206, pp. 112–120, Apr. 2016, doi: 10.1016/j.biortech.2016.01.053.
[215] M. B. Ahmed, J. L. Zhou, H. H. Ngo, and W. Guo, “Insight into biochar properties and its cost analysis,” *Biomass Bioenergy*, vol. 84, pp. 76–86, Jan. 2016, doi: 10.1016/j.biombioe.2015.11.002.
[216] A. Veksha, H. McLaughlin, D. B. Layzell, and J. M. Hill, “Pyrolysis of wood to biochar: Increasing yield while maintaining microporosity,” *Bioresour. Technol.*, vol. 153, pp. 173–179, Feb. 2014, doi: 10.1016/j.biortech.2013.11.082.
[217] N. H. Leibbrandt, A. O. Aboyade, J. H. Knoetze, and J. F. Görgens, “Process efficiency of biofuel production via gasification and Fischer–Tropsch synthesis,” *Fuel*, vol. 109, pp. 484–492, Jul. 2013, doi: 10.1016/j.fuel.2013.03.013.
[218] J. Alvarez, G. Lopez, M. Amutio, J. Bilbao, and M. Olazar, “Kinetic Study of Carbon Dioxide Gasification of Rice Husk Fast Pyrolysis Char,” *Energy Fuels*, vol. 29, no. 5, pp. 3198–3207, May 2015, doi: 10.1021/acs.energyfuels.5b00318.
[219] P. R. Yaashikaa, P. S. Kumar, S. Varjani, and A. Saravanan, “A critical review on the biochar production techniques, characterization, stability and applications for circular bioeconomy,” *Biotechnol. Rep.*, vol. 28, p. e00570, Dec. 2020, doi: 10.1016/j.btre.2020.e00570.
[220] K.-Q. Tran, H.-H. Bui, A. Luengnaruemitchai, L. Wang, and Ø. Skreiberg, “Isothermal and non-isothermal kinetic study on CO2 gasification of torrefied forest residues,” *Biomass Bioenergy*, vol. 91, pp. 175–185, Aug. 2016, doi: 10.1016/j.biombioe.2016.05.024.
[221] B. Yao *et al.*, “Co-pyrolysis of dyeing sludge and pine sawdust in a fluidized bed: Characterization and analysis of pyrolytic products and investigation of synergetic effects,” *Waste Manag.*, vol. 167, pp. 122–134, Jul. 2023, doi: 10.1016/j.wasman.2023.05.030.
[222] S. Xie, S. Kumagai, N. Takahashi, T. Kameda, Y. Saito, and T. Yoshioka, “A novel strategy for rapid identification of pyrolytic synergy and prediction of product yield: Insight into co-pyrolysis of xylan and polyethylene,” *Chem. Eng. J.*, vol. 453, p. 139958, Feb. 2023, doi: 10.1016/j.cej.2022.139958.
[223] J. Park, Y. Lee, C. Ryu, and Y.-K. Park, “Slow pyrolysis of rice straw: Analysis of products properties, carbon and energy yields,” *Bioresour. Technol.*, vol. 155, pp. 63–70, Mar. 2014, doi: 10.1016/j.biortech.2013.12.084.
[224] A. W. Coats and J. P. Redfern, “Kinetic Parameters from Thermogravimetric Data,” *Nature*, vol. 201, no. 4914, pp. 68–69, Jan. 1964, doi: 10.1038/201068a0.
[225] T. Emiola-Sadiq, L. Zhang, and A. K. Dalai, “Thermal and Kinetic Studies on Biomass Degradation *via* Thermogravimetric Analysis: A Combination of Model-Fitting and Model-Free Approach,” *ACS Omega*, vol. 6, no. 34, pp. 22233–22247, Aug. 2021, doi: 10.1021/acsomega.1c02937.
[226] J. Zhang, J. Liu, and R. Liu, “Effects of pyrolysis temperature and heating time on biochar obtained from the pyrolysis of straw and lignosulfonate,” *Bioresour. Technol.*, vol. 176, pp. 288–291, Jan. 2015, doi: 10.1016/j.biortech.2014.11.011.
[227] E. Santoso, R. Ediati, Y. Kusumawati, H. Bahruji, D. O. Sulistiono, and D. Prasetyoko, “Review on recent advances of carbon based adsorbent for methylene blue removal from waste water,” *Mater. Today Chem.*, vol. 16, p. 100233, Jun. 2020, doi: 10.1016/j.mtchem.2019.100233.
[228] A. K. Sakhiya, A. Anand, V. K. Vijay, and P. Kaushal, “Thermal decomposition of rice straw from rice basin of India to improve energy-pollution nexus: Kinetic modeling and

thermodynamic analysis," *Energy Nexus*, vol. 4, p. 100026, Dec. 2021, doi: 10.1016/j.nexus.2021.100026.
[229] P. Azadi, O. R. Inderwildi, R. Farnood, and D. A. King, "Liquid fuels, hydrogen and chemicals from lignin: A critical review," *Renew. Sustain. Energy Rev.*, vol. 21, pp. 506–523, May 2013, doi: 10.1016/j.rser.2012.12.022.
[230] S. De, S. Mishra, E. Poonguzhali, M. Rajesh, and K. Tamilarasan, "Fractionation and characterization of lignin from waste rice straw: Biomass surface chemical composition analysis," *Int. J. Biol. Macromol.*, vol. 145, pp. 795–803, Feb. 2020, doi: 10.1016/j.ijbiomac.2019.10.068.
[231] W. Jonglertjunya, T. Juntong, N. Pakkang, N. Srimarut, and C. Sakdaronnarong, "Properties of lignin extracted from sugarcane bagasse and its efficacy in maintaining postharvest quality of limes during storage," *LWT - Food Sci. Technol.*, vol. 57, no. 1, pp. 116–125, Jun. 2014, doi: 10.1016/j.lwt.2013.11.042.
[232] T. Wang, D. Meng, J. Zhu, and X. Chen, "Effects of pelletizing conditions on the structure of rice straw-pellet pyrolysis char," *Fuel*, vol. 264, p. 116909, Mar. 2020, doi: 10.1016/j.fuel.2019.116909.
[233] N. Manic, B. Jankovic, D. Stojiljkovic, V. Jovanovic, and M. Radojevic, "TGA-DSC-MS analysis of pyrolysis process of various agricultural residues," *Therm. Sci.*, vol. 23, no. Suppl. 5, pp. 1457–1472, 2019, doi: 10.2298/TSCI180118182M.
[234] R. K. Mishra and K. Mohanty, "Fuel properties and compositional analysis of Areca catechu sawdust over MgO and ZSM-5 catalysts," *J. Energy Inst.*, vol. 94, pp. 252–262, Feb. 2021, doi: 10.1016/j.joei.2020.09.009.
[235] S. Kant Bhatia *et al.*, "Trends in renewable energy production employing biomass-based biochar," *Bioresour. Technol.*, vol. 340, p. 125644, Nov. 2021, doi: 10.1016/j.biortech.2021.125644.
[236] C. C. Seah *et al.*, "Co-pyrolysis of biomass and plastic: Circularity of wastes and comprehensive review of synergistic mechanism," *Results Eng.*, vol. 17, p. 100989, Mar. 2023, doi: 10.1016/j.rineng.2023.100989.
[237] S. Janaswamy, M. P. Yadav, M. Hoque, S. Bhattarai, and S. Ahmed, "Cellulosic fraction from agricultural biomass as a viable alternative for plastics and plastic products," *Ind. Crops Prod.*, vol. 179, p. 114692, May 2022, doi: 10.1016/j.indcrop.2022.114692.
[238] P. V. Gokul, P. Singh, V. P. Singh, and A. N. Sawarkar, "Thermal behavior and kinetics of pyrolysis of areca nut husk," *Energy Sources Part Recovery Util. Environ. Eff.*, vol. 41, no. 23, pp. 2906–2916, Dec. 2019, doi: 10.1080/15567036.2019.1582733.
[239] F. Trajkova, S. Arsov, and L. Koleva Gudeva, "THE ROLE AND IMPORTANCE OF AGROBIODIVERSITY FOR AGRICULTURE," *J. Agric. Plant Sci.*, vol. 19, no. 2, pp. 47–64, 2021, doi: 10.46763/JAPS21192047t.
[240] N. Worasuwannarak, T. Sonobe, and W. Tanthapanichakoon, "Pyrolysis behaviors of rice straw, rice husk, and corncob by TG-MS technique," *J. Anal. Appl. Pyrolysis*, vol. 78, no. 2, pp. 265–271, Mar. 2007, doi: 10.1016/j.jaap.2006.08.002.
[241] S. Jha, S. Nanda, B. Acharya, and A. K. Dalai, "A Review of Thermochemical Conversion of Waste Biomass to Biofuels," *Energies*, vol. 15, no. 17, p. 6352, Aug. 2022, doi: 10.3390/en15176352.
[242] P. K. Sadh, S. Duhan, and J. S. Duhan, "Agro-industrial wastes and their utilization using solid state fermentation: a review," *Bioresour. Bioprocess.*, vol. 5, no. 1, p. 1, Dec. 2018, doi: 10.1186/s40643-017-0187-z.
[243] L. Yafetto, G. T. Odamtten, and M. Wiafe-Kwagyan, "Valorization of agro-industrial wastes into animal feed through microbial fermentation: A review of the global and Ghanaian case," *Heliyon*, vol. 9, no. 4, p. e14814, Apr. 2023, doi: 10.1016/j.heliyon.2023.e14814.

[244] K. Shekhawat, S. S. Rathore, O. P. Premi, B. K. Kandpal, and J. S. Chauhan, “Advances in Agronomic Management of Indian Mustard (*Brassica juncea* (L.) Czernj. Cosson): An Overview,” *Int. J. Agron.*, vol. 2012, pp. 1–14, 2012, doi: 10.1155/2012/408284.
[245] F. Karaosmanoglu, “Vegetable Oil Fuels: A Review,” *Energy Sources*, vol. 21, no. 3, pp. 221–231, Feb. 1999, doi: 10.1080/00908319950014858.
[246] S. G. C. De Almeida, L. A. C. Tarelho, T. Hauschild, M. A. M. Costa, and K. J. Dussán, “Biochar production from sugarcane biomass using slow pyrolysis: Characterization of the solid fraction,” *Chem. Eng. Process. - Process Intensif.*, vol. 179, p. 109054, Sep. 2022, doi: 10.1016/j.cep.2022.109054.
[247] A. A. Boateng, C. A. Mullen, and N. M. Goldberg, “Producing Stable Pyrolysis Liquids from the Oil-Seed Presscakes of Mustard Family Plants: Pennycress (Thlaspi arvense L.) and Camelina (Camelina sativa)†,” *Energy Fuels*, vol. 24, no. 12, pp. 6624–6632, Dec. 2010, doi: 10.1021/ef101223a.
[248] A. Sarkar and R. Chowdhury, “Co-pyrolysis of paper waste and mustard press cake in a semi-batch pyrolyzer—optimization and bio-oil characterization,” *Int. J. Green Energy*, vol. 13, no. 4, pp. 373–382, Mar. 2016, doi: 10.1080/15435075.2014.952423.
[249] J. Yoder, S. Galinato, D. Granatstein, and M. Garcia-Pérez, “Economic tradeoff between biochar and bio-oil production via pyrolysis,” *Biomass Bioenergy*, vol. 35, no. 5, pp. 1851–1862, May 2011, doi: 10.1016/j.biombioe.2011.01.026.
[250] M. Ahmad *et al.*, “Effects of pyrolysis temperature on soybean stover- and peanut shell-derived biochar properties and TCE adsorption in water,” *Bioresour. Technol.*, vol. 118, pp. 536–544, Aug. 2012, doi: 10.1016/j.biortech.2012.05.042.
[251] C.-C. Lo, Y.-W. Chang, Y.-L. Chen, Y.-L. Liu, H.-S. Wu, and Y.-M. Sun, “Lignin recovery from rice straw biorefinery solid waste by soda process with ethylene glycol as co-solvent,” *J. Taiwan Inst. Chem. Eng.*, vol. 126, pp. 50–57, Sep. 2021, doi: 10.1016/j.jtice.2021.07.030.
[252] J. M. Novak, W. J. Busscher, D. L. Laird, M. Ahmedna, D. W. Watts, and M. A. S. Niandou, “Impact of Biochar Amendment on Fertility of a Southeastern Coastal Plain Soil,” *Soil Sci.*, vol. 174, no. 2, pp. 105–112, Feb. 2009, doi: 10.1097/SS.0b013e3181981d9a.
[253] L. Rodier, K. Bilba, C. Onésippe, and M.-A. Arsène, “Utilization of bio-chars from sugarcane bagasse pyrolysis in cement-based composites,” *Ind. Crops Prod.*, vol. 141, p. 111731, Dec. 2019, doi: 10.1016/j.indcrop.2019.111731.
[254] A. Selvarajoo, Y. L. Wong, K. S. Khoo, W.-H. Chen, and P. L. Show, “Biochar production via pyrolysis of citrus peel fruit waste as a potential usage as solid biofuel,” *Chemosphere*, vol. 294, p. 133671, May 2022, doi: 10.1016/j.chemosphere.2022.133671.
[255] A. A. Siyal *et al.*, “Pyrolysis of pellets prepared from pure and blended biomass feedstocks: Characterization and analysis of pellets quality,” *J. Anal. Appl. Pyrolysis*, vol. 161, p. 105422, Jan. 2022, doi: 10.1016/j.jaap.2021.105422.
[256] H.-S. Tai and C.-Y. Chen, “Analyzing the pyrolysis kinetics of rice straw, bagasse, and mixtures thereof and product energy yield,” *J. Chin. Inst. Eng.*, vol. 39, no. 3, pp. 381–389, Apr. 2016, doi: 10.1080/02533839.2015.1112249.
[257] Y. Zhang, A. Yao, and K. Song, “Torrefaction of cultivation residue of Auricularia auricula-judae to obtain biochar with enhanced fuel properties,” *Bioresour. Technol.*, vol. 206, pp. 211–216, Apr. 2016, doi: 10.1016/j.biortech.2016.01.099.
[258] S.-W. Park, C.-H. Jang, K.-R. Baek, and J.-K. Yang, “Torrefaction and low-temperature carbonization of woody biomass: Evaluation of fuel characteristics of the products,” *Energy*, vol. 45, no. 1, pp. 676–685, Sep. 2012, doi: 10.1016/j.energy.2012.07.024.

[259] J. Pena, A. Villot, and C. Gerente, “Pyrolysis chars and physically activated carbons prepared from buckwheat husks for catalytic purification of syngas,” *Biomass Bioenergy*, vol. 132, p. 105435, Jan. 2020, doi: 10.1016/j.biombioe.2019.105435.
[260] P. Subramanian, K. Nithiya, K. Chandrakumar, and V. Karuppasamy Vikraman, “Assessing the pyrolysis potential of redgram stalk: Thermo-kinetic study, empirical modelling and product characterization,” *Results Eng.*, vol. 14, p. 100426, Jun. 2022, doi: 10.1016/j.rineng.2022.100426.
[261] W. Wu *et al.*, “Chemical characterization of rice straw-derived biochar for soil amendment,” *Biomass Bioenergy*, vol. 47, pp. 268–276, Dec. 2012, doi: 10.1016/j.biombioe.2012.09.034.
[262] J. Ouyang, L. Zhou, Z. Liu, J. Y. Y. Heng, and W. Chen, “Biomass-derived activated carbons for the removal of pharmaceutical mircopollutants from wastewater: A review,” *Sep. Purif. Technol.*, vol. 253, p. 117536, Dec. 2020, doi: 10.1016/j.seppur.2020.117536.
[263] B. Qiu, Q. Shao, J. Shi, C. Yang, and H. Chu, “Application of biochar for the adsorption of organic pollutants from wastewater: Modification strategies, mechanisms and challenges,” *Sep. Purif. Technol.*, vol. 300, p. 121925, Nov. 2022, doi: 10.1016/j.seppur.2022.121925.
[264] J. Wei, Y. Liu, J. Li, Y. Zhu, H. Yu, and Y. Peng, “Adsorption and co-adsorption of tetracycline and doxycycline by one-step synthesized iron loaded sludge biochar,” *Chemosphere*, vol. 236, p. 124254, Dec. 2019, doi: 10.1016/j.chemosphere.2019.06.224.
[265] F. De Felice, A. G. Fareed, A. Zahid, M. E. Nenni, and A. Petrillo, “Circular economy practices in the textile industry for sustainable future: A systematic literature review,” *J. Clean. Prod.*, vol. 486, p. 144547, Jan. 2025, doi: 10.1016/j.jclepro.2024.144547.
[266] S. A. AL-Hammadi, A. A. Al-Absi, O. A. Bin-Dahman, and T. A. Saleh, “Poly(trimesoyl chloride-melamine) grafted on palygorskite for simultaneous ultra-trace removal of methylene blue and toxic metals,” *J. Environ. Manage.*, vol. 226, pp. 358–364, Nov. 2018, doi: 10.1016/j.jenvman.2018.08.025.
[267] S. Gao, W. Zhang, Z. An, S. Kong, and D. Chen, “Adsorption of anionic dye onto magnetic Fe_3O_4 /CeO_2 nanocomposite: Equilibrium, kinetics, and thermodynamics,” *Adsorpt. Sci. Technol.*, vol. 37, no. 3–4, pp. 185–204, May 2019, doi: 10.1177/0263617418819164.
[268] J. Guo, Y. Fan, X. Dong, X. Ma, S. Yao, and H. Xing, “Modified coal tailings with TiO2 nanotubes and their application for methylene blue removal,” *Colloids Surf. Physicochem. Eng. Asp.*, vol. 627, p. 127211, Oct. 2021, doi: 10.1016/j.colsurfa.2021.127211.
[269] D. H. Nguyen, H. N. Tran, H.-P. Chao, and C.-C. Lin, “Effect of nitric acid oxidation on the surface of hydrochars to sorb methylene blue: An adsorption mechanism comparison,” *Adsorpt. Sci. Technol.*, vol. 37, no. 7–8, pp. 607–622, Oct. 2019, doi: 10.1177/0263617419867519.
[270] L. Dai *et al.*, “Tuning oxygenated functional groups on biochar for water pollution control: A critical review,” *J. Hazard. Mater.*, vol. 420, p. 126547, Oct. 2021, doi: 10.1016/j.jhazmat.2021.126547.
[271] J. Fito *et al.*, “Adsorption of methylene blue from textile industrial wastewater using activated carbon developed from Rumex abyssinicus plant,” *Sci. Rep.*, vol. 13, no. 1, p. 5427, Apr. 2023, doi: 10.1038/s41598-023-32341-w.
[272] M. B. Ahmed, J. L. Zhou, H. H. Ngo, W. Guo, and M. Chen, “Progress in the preparation and application of modified biochar for improved contaminant removal from water and wastewater,” *Bioresour. Technol.*, vol. 214, pp. 836–851, Aug. 2016, doi: 10.1016/j.biortech.2016.05.057.

[273] B. Cabal, T. Budinova, C. O. Ania, B. Tsyntsarski, J. B. Parra, and B. Petrova, “Adsorption of naphthalene from aqueous solution on activated carbons obtained from bean pods,” *J. Hazard. Mater.*, vol. 161, no. 2–3, pp. 1150–1156, Jan. 2009, doi: 10.1016/j.jhazmat.2008.04.108.
[274] P. Regkouzas and E. Diamadopoulos, “Adsorption of selected organic micro-pollutants on sewage sludge biochar,” *Chemosphere*, vol. 224, pp. 840–851, Jun. 2019, doi: 10.1016/j.chemosphere.2019.02.165.
[275] L. Dai *et al.*, “Calcium-rich biochar from crab shell: An unexpected super adsorbent for dye removal,” *Bioresour. Technol.*, vol. 267, pp. 510–516, Nov. 2018, doi: 10.1016/j.biortech.2018.07.090.
[276] G. Abdul, X. Zhu, and B. Chen, “Structural characteristics of biochar-graphene nanosheet composites and their adsorption performance for phthalic acid esters,” *Chem. Eng. J.*, vol. 319, pp. 9–20, Jul. 2017, doi: 10.1016/j.cej.2017.02.074.
[277] V. Chakraborty, P. Das, and P. K. Roy, “Graphene oxide–coated pyrolysed biochar from waste sawdust and its application for treatment of cadmium-containing solution: batch, fixed-bed column, regeneration, and mathematical modelling,” *Biomass Convers. Biorefinery*, vol. 13, no. 2, pp. 867–878, Jan. 2023, doi: 10.1007/s13399-020-01153-7.
[278] Y. Shen, Q. Fang, and B. Chen, “Environmental Applications of Three-Dimensional Graphene-Based Macrostructures: Adsorption, Transformation, and Detection,” *Environ. Sci. Technol.*, vol. 49, no. 1, pp. 67–84, Jan. 2015, doi: 10.1021/es504421y.
[279] L. Xiong *et al.*, “Adsorption behavior of methylene blue onto titanate nanotubes,” *Chem. Eng. J.*, vol. 156, no. 2, pp. 313–320, Jan. 2010, doi: 10.1016/j.cej.2009.10.023.
[280] H. Pandey, A. Pandey, and G. K. Agrahari, “Pyrolysis of rice-straw and mustard-oil residue blend: evaluation of biochar properties for its sustainable use,” *Biofuels*, vol. 16, no. 9, pp. 1045–1053, Oct. 2025, doi: 10.1080/17597269.2025.2484075.
[281] H. Pandey, A. Pandey, A. S. K. Sinha, G. K. Agrahari, and Pyrolysis, Gasification Research Group, “Conversion of rice straw and sugarcane bagasse waste to biochar through pyrolysis: influence of feedstock and process conditions,” *J. Mater. Cycles Waste Manag.*, vol. 27, no. 5, pp. 3603–3618, Sep. 2025, doi: 10.1007/s10163-025-02329-x.
[282] Sh. H. Hegazy and S. K. Mohamed, “Starch-graft-polyacrylamide copolymer /Fe3O4 /graphene oxide nanocomposite: synthesis, characterization, and application as a low-cost adsorbent for Ni (II) from aqueous solutions,” *J. Polym. Res.*, vol. 28, no. 2, p. 49, Feb. 2021, doi: 10.1007/s10965-020-02275-2.
[283] C. A. Mullen and A. A. Boateng, “Catalytic pyrolysis-GC/MS of lignin from several sources,” *Fuel Process. Technol.*, vol. 91, no. 11, pp. 1446–1458, Nov. 2010, doi: 10.1016/j.fuproc.2010.05.022.
[284] S. Xiong, Z. Wu, and Z. Li, “Facile fabrication of robust, versatile, and recyclable biochar-graphene oxide composite monoliths for efficient removal of different contaminants in water,” *Chemosphere*, vol. 287, p. 132418, Jan. 2022, doi: 10.1016/j.chemosphere.2021.132418.
[285] A. Allahbakhsh, “PVC/rice straw/SDBS-modified graphene oxide sustainable Nanocomposites: Melt mixing process and electrical insulation characteristics,” *Compos. Part Appl. Sci. Manuf.*, vol. 134, p. 105902, Jul. 2020, doi: 10.1016/j.compositesa.2020.105902.
[286] B. Feng, R. Jin, J. Wang, W. Chen, D. Qi, and S. Zhai, “Application of biochar from desorption perspective: Targeting adsorption properties of biochar and its desorption-recovery ability,” *Chem. Eng. Res. Des.*, vol. 218, pp. 674–681, Jun. 2025, doi: 10.1016/j.cherd.2025.05.026.

[287] T. S. Anirudhan and M. Ramachandran, “Adsorptive removal of basic dyes from aqueous solutions by surfactant modified bentonite clay (organoclay): Kinetic and competitive adsorption isotherm,” *Process Saf. Environ. Prot.*, vol. 95, pp. 215–225, May 2015, doi: 10.1016/j.psep.2015.03.003.
[288] S. Senapati *et al.*, “Rapid adsorption of industrial cationic dye pollutant using base-activated rice straw biochar: performance, isotherm, kinetic and thermodynamic evaluation,” *Discov. Sustain.*, vol. 6, no. 1, p. 46, Jan. 2025, doi: 10.1007/s43621-025-00835-4.
[289] L. Ai, M. Li, and L. Li, “Adsorption of Methylene Blue from Aqueous Solution with Activated Carbon/Cobalt Ferrite/Alginate Composite Beads: Kinetics, Isotherms, and Thermodynamics,” *J. Chem. Eng. Data*, vol. 56, no. 8, pp. 3475–3483, Aug. 2011, doi: 10.1021/je200536h.
[290] J. Ma *et al.*, “Enhanced Adsorptive Removal of Methyl Orange and Methylene Blue from Aqueous Solution by Alkali-Activated Multiwalled Carbon Nanotubes,” *ACS Appl. Mater. Interfaces*, vol. 4, no. 11, pp. 5749–5760, Nov. 2012, doi: 10.1021/am301053m.
[291] A. Acharya *et al.*, “Adsorption of arsenic and fluoride: Modeling of single and competitive adsorption systems,” *Heliyon*, vol. 10, no. 11, p. e31967, Jun. 2024, doi: 10.1016/j.heliyon.2024.e31967.
[292] X. Jin, M. Jiang, X. Shan, Z. Pei, and Z. Chen, “Adsorption of methylene blue and orange II onto unmodified and surfactant-modified zeolite,” *J. Colloid Interface Sci.*, vol. 328, no. 2, pp. 243–247, Dec. 2008, doi: 10.1016/j.jcis.2008.08.066.
[293] S. Radoor, J. Karayil, A. Jayakumar, J. Parameswaranpillai, and S. Siengchin, “Removal of Methylene Blue Dye from Aqueous Solution using PDADMAC Modified ZSM-5 Zeolite as a Novel Adsorbent,” *J. Polym. Environ.*, vol. 29, no. 10, pp. 3185–3198, Oct. 2021, doi: 10.1007/s10924-021-02111-8.
[294] A. Aygün, S. Yenisoy-Karakaş, and I. Duman, “Production of granular activated carbon from fruit stones and nutshells and evaluation of their physical, chemical and adsorption properties,” *Microporous Mesoporous Mater.*, vol. 66, no. 2–3, pp. 189–195, Dec. 2003, doi: 10.1016/j.micromeso.2003.08.028.
[295] S. Deng, H. Wei, T. Chen, B. Wang, J. Huang, and G. Yu, “Superior CO2 adsorption on pine nut shell-derived activated carbons and the effective micropores at different temperatures,” *Chem. Eng. J.*, vol. 253, pp. 46–54, Oct. 2014, doi: 10.1016/j.cej.2014.04.115.
[296] A. Mohd, W. A. W. Ab Karim Ghani, N. Z. Resitanim, and L. Sanyang, “A Review: Carbon Dioxide Capture: Biomass-Derived-Biochar and Its Applications,” *J. Dispers. Sci. Technol.*, vol. 34, no. 7, pp. 974–984, Jul. 2013, doi: 10.1080/01932691.2012.704753.
[297] M. Kacem, M. Pellerano, and A. Delebarre, “Pressure swing adsorption for CO 2 /N 2 and CO 2 /CH 4 separation: Comparison between activated carbons and zeolites performances,” *Fuel Process. Technol.*, vol. 138, pp. 271–283, Oct. 2015, doi: 10.1016/j.fuproc.2015.04.032.
[298] N. Kaya and Z. Y. Uzun, “Investigation of effectiveness of pine cone biochar activated with KOH for methyl orange adsorption and CO2 capture,” *Biomass Convers. Biorefinery*, vol. 11, no. 3, pp. 1067–1083, Jun. 2021, doi: 10.1007/s13399-020-01063-8.
[299] Z. Rouzitalab, D. Mohammady Maklavany, A. Rashidi, and S. Jafarinejad, “Synthesis of N-doped nanoporous carbon from walnut shell for enhancing CO2 adsorption capacity and separation,” *J. Environ. Chem. Eng.*, vol. 6, no. 5, pp. 6653–6663, Oct. 2018, doi: 10.1016/j.jece.2018.10.035.

[300] J. Sreńscek-Nazzal, A. Kamińska, J. Serafin, and B. Michalkiewicz, “Chemical Activation of Banana Peel Waste-Derived Biochar Using KOH and Urea for CO2 Capture,” *Materials*, vol. 17, no. 4, p. 872, Feb. 2024, doi: 10.3390/ma17040872.
[301] J. Zhang *et al.*, “Prediction of CO2 adsorption of biochar under KOH activation via machine learning,” *Carbon Capture Sci. Technol.*, vol. 13, p. 100309, Dec. 2024, doi: 10.1016/j.ccst.2024.100309.
[302] A. Singh, M. M. S. Abdullah, S. Iglauer, A. Keshavarz, and T. Sharma, “Sustainable biomass derived natural surfactant of soybean seeds in fly ash industrial waste utilization for carbon storage: Evaluation of environmental impact,” *J. Environ. Chem. Eng.*, vol. 12, no. 6, p. 114530, Dec. 2024, doi: 10.1016/j.jece.2024.114530.
[303] M. Keiluweit, P. S. Nico, M. G. Johnson, and M. Kleber, “Dynamic Molecular Structure of Plant Biomass-Derived Black Carbon (Biochar),” *Environ. Sci. Technol.*, vol. 44, no. 4, pp. 1247–1253, Feb. 2010, doi: 10.1021/es9031419.
[304] M. Gale, T. Nguyen, M. Moreno, and K. L. Gilliard-AbdulAziz, “Physiochemical Properties of Biochar and Activated Carbon from Biomass Residue: Influence of Process Conditions to Adsorbent Properties,” *ACS Omega*, vol. 6, no. 15, pp. 10224–10233, Apr. 2021, doi: 10.1021/acsomega.1c00530.
[305] Z. Guo *et al.*, “Revisiting potassium intercalation in graphite: an *operando* characterisation and computational approach,” *EES Batter.*, p. 10.1039.D5EB00184F, 2026, doi: 10.1039/D5EB00184F.
[306] N. Yoshizawa *et al.*, “XRD evaluation of KOH activation process and influence of coal rank,” *Fuel*, vol. 81, no. 13, pp. 1717–1722, Aug. 2002, doi: 10.1016/S0016-2361(02)00101-1.
[307] *Activated Carbon*. Elsevier, 2006. doi: 10.1016/B978-0-08-044463-5.X5013-4.
[308] H. Jedli, M. Almonnef, R. Rabhi, M. Mbarek, J. Abdessalem, and K. Slimi, “Activated Carbon as an Adsorbent for CO_2 Capture: Adsorption, Kinetics, and RSM Modeling,” *ACS Omega*, vol. 9, no. 2, pp. 2080–2087, Jan. 2024, doi: 10.1021/acsomega.3c02476.
[309] L. Deng *et al.*, “Straw-based biochar prepared from multi-step KOH activation and its structure-effect relationship of CO2 capture under atmospheric/pressurized conditions via experimental analysis and MD/DFT calculations,” *Chem. Eng. J.*, vol. 495, p. 153403, Sep. 2024, doi: 10.1016/j.cej.2024.153403.
[310] K. Skic, A. Adamczuk, A. Gryta, P. Boguta, T. Tóth, and G. Jozefaciuk, “Surface areas and adsorption energies of biochars estimated from nitrogen and water vapour adsorption isotherms,” *Sci. Rep.*, vol. 14, no. 1, p. 30362, Dec. 2024, doi: 10.1038/s41598-024-81030-9.
[311] O. Gotore, R. Rameshprabu, and T. Itayama, “Adsorption performances of corn cob-derived biochar in saturated and semi-saturated vertical-flow constructed wetlands for nutrient removal under erratic oxygen supply,” *Environ. Chem. Ecotoxicol.*, vol. 4, pp. 155–163, 2022, doi: 10.1016/j.enceco.2022.05.001.
[312] S. Fan *et al.*, “Biochar derived from corn stalk and polyethylene co-pyrolysis: characterization and Pb(II) removal potential,” *RSC Adv.*, vol. 10, no. 11, pp. 6362–6376, 2020, doi: 10.1039/C9RA09487C.
[313] F. Ambroz, T. J. Macdonald, V. Martis, and I. P. Parkin, “Evaluation of the BET Theory for the Characterization of Meso and Microporous MOFs,” *Small Methods*, vol. 2, no. 11, p. 1800173, Nov. 2018, doi: 10.1002/smtd.201800173.
[314] J. Díaz-Terán, D. M. Nevskaia, J. L. G. Fierro, A. J. López-Peinado, and A. Jerez, “Study of chemical activation process of a lignocellulosic material with KOH by XPS and XRD,” *Microporous Mesoporous Mater.*, vol. 60, no. 1–3, pp. 173–181, Jun. 2003, doi: 10.1016/S1387-1811(03)00338-X.

[315] Y. Shen and Y. Fu, “KOH-activated rice husk char via CO2 pyrolysis for phenol adsorption,” *Mater. Today Energy*, vol. 9, pp. 397–405, Sep. 2018, doi: 10.1016/j.mtener.2018.07.005.
[316] T. Jiang *et al.*, “Nitrogen-doped porous graphene electrodes for highly efficient capacitive deionization,” *Int. J. Electrochem. Sci.*, vol. 19, no. 1, p. 100434, Jan. 2024, doi: 10.1016/j.ijoes.2023.100434.
[317] S. Liu *et al.*, “Urea-assisted one-step fabrication of a novel nitrogen-doped carbon fiber aerogel from cotton as metal-free catalyst in peroxymonosulfate activation for efficient degradation of carbamazepine,” *Chem. Eng. J.*, vol. 386, p. 124015, Apr. 2020, doi: 10.1016/j.cej.2020.124015.
[318] D. Hisse *et al.*, “Microporous Nitrogen-Doped Activated Biochars Derived from Corn: Use of Husk Waste and Urea for CO2 Capture,” *J. Braz. Chem. Soc.*, 2024, doi: 10.21577/0103-5053.20240034.
[319] A. B. Fuertes *et al.*, “Chemical and structural properties of carbonaceous products obtained by pyrolysis and hydrothermal carbonisation of corn stover,” *Soil Res.*, vol. 48, no. 7, pp. 618–626, Sep. 2010, doi: 10.1071/SR10010.
[320] A. C. Ferrari, “Raman spectroscopy of graphene and graphite: Disorder, electron–phonon coupling, doping and nonadiabatic effects,” *Solid State Commun.*, vol. 143, no. 1–2, pp. 47–57, Jul. 2007, doi: 10.1016/j.ssc.2007.03.052.
[321] J. Xu *et al.*, “Raman spectroscopy of biochar from the pyrolysis of three typical Chinese biomasses: A novel method for rapidly evaluating the biochar property,” *Energy*, vol. 202, p. 117644, Jul. 2020, doi: 10.1016/j.energy.2020.117644.
[322] X. Chen *et al.*, “Enhancing sulfacetamide degradation by peroxymonosulfate activation with N-doped graphene produced through delicately-controlled nitrogen functionalization via tweaking thermal annealing processes,” *Appl. Catal. B Environ.*, vol. 225, pp. 243–257, Jun. 2018, doi: 10.1016/j.apcatb.2017.11.071.
[323] R. Han *et al.*, “N-Doped Biochar as a New Metal-Free Activator of Peroxymonosulfate for Singlet Oxygen-Dominated Catalytic Degradation of Acid Orange 7,” *Nanomaterials*, vol. 11, no. 9, p. 2288, Sep. 2021, doi: 10.3390/nano11092288.
[324] M. Sevilla and A. B. Fuertes, “Sustainable porous carbons with a superior performance for CO2 capture,” *Energy Environ. Sci.*, vol. 4, no. 5, p. 1765, 2011, doi: 10.1039/c0ee00784f.
[325] Y. Mao, B. Cai, M. Huang, X. Liu, W. Zhang, and Z. Ma, “A sustainable preparation strategy for the nitrogen-doped hierarchical biochar with high surface area for the enhanced removal of organic dye,” *Biochar*, vol. 5, no. 1, p. 70, Nov. 2023, doi: 10.1007/s42773-023-00269-z.
[326] Z. Ma *et al.*, “Oxygen migration characteristics during bamboo torrefaction process based on the properties of torrefied solid, gaseous, and liquid products,” *Biomass Bioenergy*, vol. 128, p. 105300, Sep. 2019, doi: 10.1016/j.biombioe.2019.105300.
[327] Y. Yamada, J. Kim, S. Matsuo, and S. Sato, “Nitrogen-containing graphene analyzed by X-ray photoelectron spectroscopy,” *Carbon*, vol. 70, pp. 59–74, Apr. 2014, doi: 10.1016/j.carbon.2013.12.061.
[328] Mr. G. Singh, K. S. Lakhi, D. Park, P. Srivastava, R. Naidu, and A. Vinu, “Facile One-Pot Synthesis of Activated Porous Biocarbons with a High Nitrogen Content for CO_2 Capture,” *ChemNanoMat*, vol. 4, no. 3, pp. 281–290, Mar. 2018, doi: 10.1002/cnma.201700348.
[329] N. E. Williams, O. A. Oba, and N. P. Aydinlik, “Modification, Production, and Methods of KOH-Activated Carbon,” *ChemBioEng Rev.*, vol. 9, no. 2, pp. 164–189, Apr. 2022, doi: 10.1002/cben.202100030.

[330] S. Li, K. Han, J. Li, M. Li, and C. Lu, “Preparation and characterization of super activated carbon produced from gulfweed by KOH activation,” *Microporous Mesoporous Mater.*, vol. 243, pp. 291–300, May 2017, doi: 10.1016/j.micromeso.2017.02.052.
[331] T. Yang, X. Xin, J. Jiang, Z. Yin, and L. Meng, “Nitrogen-doped biochar as an efficient sensing material for the electrochemical detection of heavy metal ion Pb^{2+} and Cd^{2+},” *Asia-Pac. J. Chem. Eng.*, vol. 18, no. 5, p. e2962, Sep. 2023, doi: 10.1002/apj.2962.
[332] J. Wang, F. Lou, M. Zhang, and J. Yuan, “Recent progress in nitrogen-doped activated carbon: Microstructural regulation and enhanced gas adsorption,” *J. Environ. Chem. Eng.*, vol. 13, no. 5, p. 118107, Oct. 2025, doi: 10.1016/j.jece.2025.118107.
[333] E. Z. Piña-Salazar *et al.*, “Pore-Mouth Structure of Highly Agglomerated Detonation Nanodiamonds,” *Nanomaterials*, vol. 11, no. 11, p. 2772, Oct. 2021, doi: 10.3390/nano11112772.
[334] J. Shi, H. Cui, J. Xu, N. Yan, and S. You, “Synthesis of N-doped hierarchically ordered micro-mesoporous carbons for CO2 adsorption,” *J. CO2 Util.*, vol. 62, p. 102081, Aug. 2022, doi: 10.1016/j.jcou.2022.102081.
[335] F. Huang *et al.*, “Rational introduction of nitridizing agent to hydrothermal carbonization for enhancing CO2 capture performance of tobacco stalk-based porous carbons,” *J. Anal. Appl. Pyrolysis*, vol. 157, p. 105047, Aug. 2021, doi: 10.1016/j.jaap.2021.105047.
[336] M. Vorokhta, M. I. M. Kusdhany, D. Vöröš, M. Nishihara, K. Sasaki, and S. M. Lyth, “Microporous carbon foams: The effect of nitrogen-doping on CO2 capture and separation via pressure swing adsorption,” *Chem. Eng. J.*, vol. 471, p. 144524, Sep. 2023, doi: 10.1016/j.cej.2023.144524.

List of Publications

1. **Pandey, H**., Pandey, A., Sinha, A.S.K., Agrahari, G.K. et al. Conversion of rice straw and sugarcane bagasse waste to biochar through pyrolysis: influence of feedstock and process conditions. J Mater Cycles Waste Manag (2025). https://doi.org/10.1007/s10163-025-02329-x
2. **Pandey, H**., Pandey, A., & Agrahari, G. K. (2025). Pyrolysis of rice-straw and mustard-oil residue blend: evaluation of biochar properties for its sustainable use. Biofuels, 1–9. https://doi.org/10.1080/17597269.2025.2484075
3. Green Synthesis of Biochar-Graphene Oxide Composite via Hydrothermal Route for Superior Adsorption of Dye from Aqueous Phase. (Submitted to the journal)
4. Synthesis of surfactant modified N-doped activated biochar using mango kernel for sustainable utilization in CO_2 entrapment. (Submitted to the journal).

Patent

Sujeet Kumar Pandey. Aash Mohammad, **Harikeshvar Pandey** Rohit Kumar Singh, Siddharth Atal, Indian Design Patent, Patent No. 442388-001,2024 (Granted)

…… ***…….

Conferences

1. Densification of Rice-Straw Biomass: Evaluation and Characterization of Pyrolysis Char (*Presented at N0ET-2022 at IIT-ISM on 12-13 Dec 2022*).
2. Studying the physical and chemical properties of rice Straw pellets with and without binder (*Presented at ENT-2023 at NIT-Puducherry; Feb 2-4, 2023*).
3. Pelletization of agricultural biomass for storage, transportation, and energy applications using plant-extracted polysaccharides as binders to provide strength and durability. (*Presented at CHEM TECHNOVA 2025, HBTU, Kanpur, 3-5 April 2025*)

…… ***…….

Brief about the supervisor **Dr. Gunjan Kumar Agrahari**

Education and Experience:

Faculty	2016-till date	Rajiv Gandhi Institute of Petroleum Technology, Jais, Amethi
Post-doc	2013-15	Post-Doctoral Fellow, Katholieke University Leuven, (KU Leuven), Belgium
PhD	2013	Indian Institute of Technology, Kanpur

Area of Research Interest:

Membrane Process, Microbial fuel cell, waste utilization, water treatment, pyrolysis and gasification of biomass.

Contact:

:gagrahari@rgipt.ac.in

: +91 9775885136

Brief about the author **HARIKESHVAR PANDEY**

Personal information

Name	Harikeshvar Pandey
DOB	26 February, 1995
Mother's name	Smt. Vindhyavasini Pandey
Father's name	Sri. Krishnamohan Pandey
Place of birth	Village- Ekauna, Deoria, Uttar-Pradesh, India

Educational Qualifications:

Ph.D.	Rajiv Gandhi Institute of Petroleum Technology, Amethi, Uttar-Pradesh	2020-2025
M.Tech	Indian Institute of Technology (IIT-BHU), Varanasi, Uttar-Pradesh	2018-2020
B.Tech	Babu Banarasi Das University, Lucknow, Uttar Pradesh	2012-2016

Contact:

: 20ce0007@rgipt.ac.in, harikeshvarpandey.cer18@itbhu.ac.in